UNIVERSIDAD DE SALAMANCA

CENTRO DE INVESTIGACIÓN DEL CÁNCER

C3G in chronic myeloid leukemia

Linking disease progression in mouse models with cellular leukemogenic mechanisms

MEMORIA PARA OPTAR AL GRADO DE DOCTOR

PRESENTADA POR

Pablo Berrocal Navarro

Bajo la dirección de la Doctora:

Carmen Guerrero Arroyo

Cofinanciado por la Unión Europea

Salamanca, 2026

Dra. CARMEN GUERRERO ARROYO, Catedrática de Universidad del Departamento de Medicina en el Centro de Investigación del Cáncer (CIC, CSIC-Universidad de Salamanca).

CERTIFICA:

Que D. Pablo Berrocal Navarro, graduado en Biotecnología por la Universidad de Salamanca y Máster Universitario en Biotecnología Biomédica por la Universitat Politècnica de València, ha realizado bajo su dirección el trabajo de Tesis Doctoral que lleva por título "***C3G in Chronic Myeloid Leukemia: Linking Disease Progression in Mouse Models with Cellular Leukemogenic Mechanisms"***, y considera que éste reúne originalidad y contenidos suficientes para que sea presentada ante el Tribunal correspondiente y optar al Grado de Doctor por la Universidad de Salamanca.

Y para que así conste a los efectos oportunos, expide el presente certificado en Salamanca a 2 de febrero de 2026.

Dra. Carmen Guerrero Arroyo
Directora

Pablo Berrocal Navarro ha realizado esta Tesis Doctoral siendo beneficiario de un contrato predoctoral de personal investigador de la convocatoria del año 2022 (Orden de 26 de agosto de 2022) cofinanciado por la Consejería de Educación de la Junta de Castilla y León (JCyL) y el Fondo Social Europeo Plus (FSE+) durante el periodo de enero de 2023 a diciembre de 2026.

Este trabajo se ha enmarcado dentro de los proyectos del Plan Nacional I+D+i: "*New functions for C3G in tumor progression, liver physiology and megakaryocyte and platelet biology. Contribution of platelet C3G to pathological neoangiogenesis and liver damage*" (PID2019-104143RB-C21) y "*C3G as a multitasking protein: defining new roles for C3G in liver pathophysiology, cancer, hematopoiesis and immune response. Contribution of platelet C3G*" (PID2022-137717OB-C22) financiados por la Agencia Estatal de Investigación (Ministerio de Ciencia, Innovación y Universidades, MCIN/AEI10.13039/501100011033) y el Fondo Europeo de Desarrollo Regional (FEDER) "Una forma de hacer Europa"; del proyecto del Programa de Apoyo a Proyectos de Investigación de la Consejería de Educación de la JCyL: "*Papel de C3G en tumores hematopoyéticos y en angiogénesis mediada por plaquetas. Evaluación de su uso como diana terapéutica*" (SA078P20), cofinanciados por FEDER "Una forma de hacer Europa"; y del proyecto del programa de Subvenciones destinadas al apoyo a Grupos de Investigación Reconocidos (GIR) de las Universidades Públicas de Castilla y León (SA064G24) financiado por la JCyL. El Centro de Investigación del Cáncer (CIC), donde se ha realizado este trabajo, ha recibido financiación del Programa de Apoyo a Planes Estratégicos de Investigación de Estructuras de Investigación de Excelencia, cofinanciado por la JCyL y FEDER (CLC-2017-01 y CLU-2O23-2-01) y por la Fundación Científica de la Asociación Española Contra el Cáncer (AECC, Programa Excelencia 2022, EPAEC222641CICS).

Durante el desarrollo de la Tesis Doctoral, Pablo Berrocal Navarro realizó una estancia de tres meses de duración en el laboratorio de la Dra. Karoline Kollmann en el Department of Biological Sciences and Pathobiology, Pharmacology and Toxicology. Veterinary Medicine University of Vienna (Viena, Austria). La estancia estuvo parcialmente financiada por la JCyL y el FSE+.

Abstract

ABSTRACT

Chronic myeloid leukemia (CML) is a myeloproliferative neoplasm caused by the formation of the Philadelphia chromosome in hematopoietic stem and progenitor cells (HSPCs), where a reciprocal translocation generates the *BCR::ABL1* fusion oncogene. The main isoform present in CML is BCR::ABL1 p210, a constitutively active kinase that drives the leukemogenic transformation of HSPCs into leukemic stem cells (LSCs). These CML LSCs are largely responsible for disease initiation, maintenance, and resistance to therapy, as they can self-renew and persist despite tyrosine kinase inhibitor (TKI) therapy, which specifically targets BCR::ABL1. CML is typically a triphasic disease, beginning with a chronic phase characterized by the gradual expansion of mature neutrophils in circulation, followed by an accelerated phase marked by increased myeloid proliferation and genetic instability, and ultimately progressing into a blast crisis, which resembles acute leukemia with high numbers of immature blasts and poor prognosis if not treated.

Rap1 small GTPase deregulation in mouse models has been associated with myeloid neoplasms resembling human CML, highlighting the importance of its regulation for proper hematopoietic homeostasis. C3G, a guanine nucleotide exchange factor (GEF) for Rap1, interacts with BCR::ABL1, forming signaling complexes involved in adhesion and cytoskeletal regulation, but its potential role in disease onset and progression remains unexplored. In the K562 CML-derived cell line, C3G exerts a dual effect by modulating downstream BCR::ABL1 signaling and promoting the aberrant adhesion properties characteristic of leukemic cells. Additionally, C3G has been shown to modulate imatinib-induced apoptosis in a non-linear manner in this cell line. Recent evidence also identifies C3G as a key regulator of hematopoiesis, as altered C3G activity disrupts hematopoietic stem cell (HSC) fate. Increased C3G activity in HSCs promotes premature progenitor exhaustion and impairs long-term hematopoiesis, while C3G also regulates megakaryocytic lineage by modulating HSC interactions with the bone marrow (BM) niche to promote myeloid reconstitution after hematopoietic stress.

Despite the well-documented functional relationship between BCR::ABL1 and C3G, the specific role of C3G in CML development has not been fully addressed. To explore this, we used a transgenic BCR::ABL1 p210 (hereinafter p210) mouse model presenting a time-controlled deficiency of C3G in HSCs.

BCR::ABL1-expressing mice develop a myeloproliferative disease resembling the chronic phase of CML, characterized by massive expansion of mature neutrophils in peripheral blood and myeloid infiltration in medullary and extramedullary tissues. In the absence of hematopoietic C3G from the first month of life, p210 mice develop an attenuated CML course, characterized by lower neutrophil levels in peripheral blood at late disease stages,

delayed leukemia onset, and increased survival, specifically in female C3G-deficient p210 mice. Additionally, at terminal disease stages, C3G-knockout p210 mice display reduced leukemic infiltration, including decreased neutrophil presence in BM and thymus and increased B lymphocyte levels in BM and spleen, suggesting a partial restoration of hematopoietic tissue balance. Consistently, C3G deletion at later stages, coinciding with average disease onset, led to a more modest attenuation of the myeloproliferative phenotype, supporting a time-dependent effect of C3G deficiency on CML progression.

Analysis of BM HSPC subpopulations at CML onset in mice in which C3G was deleted during the first month of life revealed significant alterations, predominantly affecting myeloid-committed progenitors. C3G-deficient mice displayed increased levels of immature BM cells, with a notable accumulation of granulocyte-monocyte progenitors (GMP), the immediate precursors of circulating neutrophils. Moreover, BM neutrophils from C3G-deficient p210 mice exhibited impaired migratory capacity in response to chemotactic stimulus. Altogether, these findings indicate that early C3G deletion disrupts proper neutrophil differentiation and function, leading to accumulation of intermediate progenitors in the BM together with reduced numbers and functionality of mature neutrophils, potentially explaining the lower neutrophil levels observed in circulation.

In vivo results therefore suggested that C3G deficiency could act as an attenuating factor of CML. To further investigate the underlying leukemogenic mechanisms, we studied the role of C3G in BCR::ABL1-expressing cell lines using the Ba/F3 cell line expressing the *BCR::ABL1 p210* oncogene (hereinafter Ba/F3-p210).

Interestingly, BCR::ABL1 expression in Ba/F3 cells correlated with decreased C3G levels, suggesting signaling crosstalk between both proteins. To further investigate the contribution of C3G in a BCR::ABL1-expressing setting, overexpression and knockdown cell lines were generated. While modulation of C3G expression did not affect the proliferation rate of Ba/F3-p210 cells, it substantially modified their sensitivity to imatinib, the main TKI used for CML treatment. Both C3G-overexpressing and C3G-knockdown Ba/F3-p210 cells displayed lower viability and increased apoptosis upon imatinib exposure compared with control cells.

Leukemogenic pathways were also affected by changes in C3G expression. Phosphorylation of the BCR::ABL1 kinase domain, indicative of its oncogenic activity, was moderately attenuated in both C3G-overexpressing and knockdown lines. However, downstream targets such as CrkL remained unchanged, suggesting the involvement of additional regulatory mechanisms. Remarkably, JAK/STAT signaling, a major leukemogenic axis in CML, was disrupted upon both C3G overexpression and knockdown, as reflected by a concomitant

reduction in p-JAK2, p-STAT3, and p-STAT5 levels. In contrast, ERK1/2 and PI3K/AKT pathway activation was comparable among all lines.

The observation that tightly regulated C3G expression in a BCR::ABL1 context is required for proper JAK/STAT signaling prompted us to investigate its impact on hematopoietic differentiation, particularly given our prior findings of disrupted neutropoiesis in p210 mice. To this end, we performed additional experiments using the 32D myeloblast-like cell line, in which C3G expression was engineered to generate overexpression and knockdown models, following the same strategy used for Ba/F3-p210 cells.

32D cells were stimulated with granulocyte colony-stimulating factor (G-CSF), a cytokine that induces neutrophil differentiation in myeloid-committed HSPCs through activation of the JAK/STAT pathway, with STAT3 acting as a principal mediator. Notably, C3G-knockdown 32D cells exhibited reduced STAT3 activation upon G-CSF stimulation, suggesting that low C3G levels compromise JAK/STAT3 signaling and thereby impair the neutrophilic differentiation program. Furthermore, both C3G-overexpressing and C3G-knockdown 32D cell lines displayed cytokine-induced alterations in the ERK1/2 pathway, which may further contribute to the observed signaling dysregulation.

Overall, these data support a role for C3G in regulating chronic-phase CML progression, likely by modulating key leukemogenic pathways such as JAK/STAT. Disruption of this axis may impair neutrophil differentiation, attenuate the myeloproliferative phenotype, and alter myeloid-committed HSPC populations, ultimately reducing the number of mature neutrophils in circulation. C3G thus supports physiological neutrophil differentiation, and its loss may limit BCR::ABL1-driven myeloproliferation, as also observed in non-oncogenic models such as the 32D cells.

Furthermore, altered JAK/STAT signaling in CML cells upon C3G modulation may increase sensitivity to imatinib, consistent with the pathway’s known role in TKI resistance. These results highlight C3G as a promising therapeutic target in CML, both for controlling the myeloproliferative phenotype and for potentially sensitizing LSCs through combined C3G inhibition and TKI treatment, addressing a key challenge in current CML research.

Resumen

RESUMEN

La leucemia mieloide crónica (LMC) es una neoplasia mieloproliferativa causada por la formación del cromosoma Filadelfia en células madre y progenitoras hematopoyéticas (HSPC), donde una translocación recíproca genera el oncogén de fusión *BCR::ABL1*. La principal isoforma presente en la LMC es BCR::ABL1 p210, una quinasa constitutivamente activa que promueve la transformación leucemogénica de las HSPC en células madre leucémicas (LSC). Las LSC en la LMC son en gran medida responsables del inicio, mantenimiento y resistencia a la terapia, ya que pueden autorrenovarse y persistir a pesar del tratamiento con inhibidores de tirosina quinasa (TKI), dirigidos específicamente a BCR::ABL1. La LMC es típicamente una enfermedad trifásica, que comienza con una fase crónica caracterizada por la expansión gradual de neutrófilos maduros en circulación, seguida de una fase acelerada marcada por un aumento de la proliferación mieloide e inestabilidad genética, y progresando finalmente a crisis blástica, similar a una leucemia aguda, caracterizada por un alto número de blastos inmaduros y, un pronóstico desfavorable si no se trata adecuadamente.

La desregulación de la GTPasa Rap1 en modelos murinos se ha asociado con neoplasias mieloides similares a la LMC humana, lo que resalta la importancia de su regulación para el mantenimiento adecuado de la homeostasis hematopoyética. C3G, un factor de intercambio de nucleótidos de guanina (GEF) de Rap1, interactúa con BCR::ABL1 formando complejos de señalización implicados en la adhesión y la regulación del citoesqueleto celular, aunque su posible papel en la aparición y progresión de la enfermedad aún no ha sido explorado. En células K562, una línea celular derivada de LMC, C3G ejerce un efecto dual al modular la señalización oncogénica de BCR::ABL1 y promover las propiedades de adhesión aberrantes características de las células leucémicas. Además, se ha demostrado que C3G modula la apoptosis inducida por imatinib de manera no lineal en esta línea celular. Estudios recientes también identifican a C3G como un regulador clave de la hematopoyesis, ya que su actividad alterada afecta la diferenciación de las células madre hematopoyéticas (HSC). El aumento de la actividad de C3G en las HSC promueve el agotamiento prematuro de progenitores e impide la hematopoyesis a largo plazo, mientras que también regula, a nivel de linaje megacariocítico, las interacciones de las HSC con el nicho de médula ósea (MO) para favorecer la reconstitución mieloide tras estrés hematopoyético.

A pesar de la demostrada relación funcional entre BCR::ABL1 y C3G, el papel específico de C3G en el desarrollo de LMC no ha sido completamente abordado. Para explorarlo, hemos utilizado un modelo murino transgénico BCR::ABL1 p210 (en adelante p210) con deficiencia controlada en el tiempo de C3G en las HSC.

Resumen

Los ratones que expresan BCR::ABL1 desarrollan una enfermedad mieloproliferativa similar a la fase crónica de la LMC, caracterizada por la expansión masiva de neutrófilos maduros en sangre periférica y la infiltración mieloide en tejidos medulares y extramedulares. En ausencia de C3G en el linaje hematopoyético desde el primer mes de vida, los ratones p210 desarrollan un curso atenuado de LMC, caracterizado por niveles más bajos de neutrófilos en sangre periférica en etapas tardías de la enfermedad, inicio retardado de la leucemia y mayor supervivencia específicamente en hembras. Además, en las etapas terminales de la enfermedad, los ratones p210 sin C3G presentan una infiltración leucémica reducida, incluyendo menor presencia de neutrófilos en MO y timo y aumento de linfocitos B en MO y bazo, sugiriendo una restauración parcial del balance celular de los tejidos hematopoyéticos. De igual manera, la deleción de C3G en etapas más tardías, coincidiendo con el inicio promedio de la enfermedad, condujo a una atenuación más modesta del fenotipo mieloproliferativo, apoyando un efecto dependiente del tiempo de la deficiencia de C3G en la progresión de la LMC.

El análisis de las subpoblaciones de HSPC de la MO al inicio de LMC en ratones en los que C3G fue delecionado durante el primer mes de vida reveló alteraciones significativas, afectando predominantemente a los progenitores comprometidos con la línea mieloide. Los ratones deficientes en C3G mostraron niveles aumentados de células inmaduras en MO, con una notable acumulación de progenitores granulocito-monocito (GMP), precursores inmediatos de los neutrófilos circulantes. Además, los neutrófilos de MO de ratones p210 deficientes en C3G presentaron una capacidad migratoria reducida en respuesta a estímulos quimiotácticos. En conjunto, estos hallazgos indican que la eliminación temprana de C3G altera la diferenciación y función adecuadas de los neutrófilos, llevando a la acumulación de progenitores intermedios en BM junto con la reducción en número y funcionalidad de neutrófilos maduros, lo que podría explicar los niveles más bajos de neutrófilos observados en circulación.

Los resultados *in vivo* sugieren, por tanto, que la deficiencia de C3G podría actuar como un factor atenuante de la LMC. Para investigar más a fondo los mecanismos leucemogénicos subyacentes, hemos estudiado el papel de C3G en líneas celulares que expresan BCR::ABL1, utilizando para ello la línea Ba/F3 que expresa el oncogén *BCR::ABL1 p210* (en adelante Ba/F3-p210).

De forma notable, la expresión de BCR::ABL1 en células Ba/F3 se correlacionó con niveles disminuidos de C3G, sugiriendo una interacción funcional en sus vías de señalización. Para explorar la contribución de C3G en un contexto de expresión de BCR::ABL1, se generaron líneas celulares con sobreexpresión y silenciamiento de C3G. Si bien la modulación de C3G no afectó a la tasa de proliferación de las células Ba/F3-p210, sí modificó sustancialmente su sensibilidad a imatinib, el principal TKI utilizado en el tratamiento de la LMC. Tanto las

células Ba/F3-p210 con sobreexpresión como con silenciamiento de C3G mostraron menor viabilidad y mayor apoptosis tras la exposición a imatinib en comparación con las células control.

La señalización leucemogénica también se vio afectada por los cambios en la expresión de C3G. La fosforilación del dominio quinasa de BCR::ABL1, indicativa de su actividad oncogénica, mostró una moderada disminución en ambas líneas con sobreexpresión y silenciamiento de C3G. Sin embargo, los niveles de fosforilación de CrkL, la principal diana de BCR::ABL1, permanecieron sin cambios, sugiriendo la participación de mecanismos reguladores adicionales. De manera notable, la señalización JAK/STAT, un eje leucemogénico principal en LMC, se vio alterada tanto por la sobreexpresión como por la deleción de C3G, reflejándose en una reducción concomitante de los niveles de p-JAK2, p-STAT3 y p-STAT5. En contraste, la activación de las vías ERK1/2 y PI3K/AKT no mostraron cambios en todas las líneas.

La observación de que la regulación precisa de C3G en un contexto de BCR::ABL1 es necesaria para la señalización adecuada de JAK/STAT nos llevó a investigar su impacto en la diferenciación hematopoyética, particularmente a la luz de nuestros hallazgos previos de alteraciones en la neutropoyesis en ratones p210. Para ello, realizamos experimentos adicionales en la línea celular mieloblástica 32D, en la que se generaron modelos de sobreexpresión y deleción de C3G, siguiendo la misma estrategia utilizada para las células Ba/F3-p210.

Las células 32D se estimularon con factor estimulante de colonias de granulocitos (G-CSF), una citoquina que induce la diferenciación de neutrófilos en HSPCs comprometidas con la línea mieloide mediante activación de la vía JAK/STAT, con STAT3 actuando como mediador principal. De forma notable, las células 32D con silenciamiento de C3G mostraron una activación reducida de STAT3 tras la estimulación con G-CSF, sugiriendo que niveles bajos de C3G comprometen la señalización JAK/STAT3 y, por tanto, la diferenciación neutrofílica. Además, tanto las líneas celulares 32D con sobreexpresión como con silenciamiento de C3G mostraron alteraciones en la vía ERK1/2 tras la estimulación con citoquinas, lo que podría contribuir adicionalmente a la disfunción de la señalización observada.

En conjunto, estos datos respaldan un papel de C3G en la regulación de la progresión de la LMC en fase crónica, probablemente mediante la modulación de vías leucemogénicas clave como JAK/STAT. La alteración de este eje puede afectar a la diferenciación de neutrófilos, atenuar el fenotipo mieloproliferativo y modificar las poblaciones de HSPC dirigidas hacia la línea mieloide, lo que en última instancia reduciría el número de neutrófilos maduros en circulación. Así, C3G sostendría la diferenciación fisiológica de neutrófilos, y su ausencia

podría limitar la mieloproliferación inducida por BCR::ABL1, como también se observa en modelos no oncogénicos, como las células 32D.

Además, la alteración de la señalización JAK/STAT en células de LMC tras la modulación de C3G podría aumentar la sensibilidad al imatinib, lo que concuerda con el papel conocido de esta vía en la resistencia a los TKI. Estos resultados destacan a C3G como una posible diana terapéutica en LMC, tanto para controlar el fenotipo mieloproliferativo como para potencialmente sensibilizar a las LSC mediante la combinación de inhibición de C3G y tratamiento con TKI, abordando uno de los principales retos actuales en la investigación de la LMC.

TABLE OF CONTENTS

Introduction

INTRODUCTION

1. Chronic myeloid leukemia: a myeloproliferative neoplasm

1.1. Overview

1.1.1. Definition and classification

Under normal conditions, cell proliferation is tightly regulated to maintain tissue homeostasis. Cancer arises when this control is lost, leading to uncontrolled cell growth. Cancerous cells can originate from almost any tissue and, in some cases, are able to acquire metastatic potential, which allows their dissemination to distant sites. Leukemia is a type of cancer that develops when a blood progenitor cell in the bone marrow (BM) undergoes malignant transformation, leading to an excessive production of abnormal leukocytes (National Cancer Institute, 2007).

Leukemic cells generally fail to mature and function properly. Instead, they proliferate rapidly and avoid programmed cell death, a process also known as apoptosis. Over time, these dysfunctional cells accumulate in the bloodstream, increasing leukocyte counts and potentially infiltrating other organs, thereby disrupting their normal physiological functions (Koolivand *et al.*, 2025).

Leukemias are classified as acute or chronic primarily according to disease kinetics and clinical course. Acute leukemias typically show rapid progression with accumulation of blast-like cells, whereas chronic leukemias evolve more slowly and are characterized by expansion of cells with more differentiated phenotypes that often retain partial functional properties (Arber *et al.*, 2022). In chronic leukemias, malignant cells fail to perform essential immune functions but exhibit extended survival, leading to their accumulation in hematopoietic tissues, therefore causing the displacement of healthy cells. While chronic leukemias progress more gradually than acute forms, they are generally more challenging to cure (Faderl *et al.*, 1999).

Leukemias can be myeloid or lymphoid, depending on the hematopoietic lineage from which they originate:

- **Myeloid leukemias** arise from myeloid progenitors, which normally give rise to granulocytes, monocytes, erythrocytes, and megakaryocytes (MK) (Arber *et al.*, 2022).
- **Lymphoid leukemias** originate from lymphoid progenitors, which differentiate into lymphocytes. It is important to distinguish lymphoid leukemias from lymphomas, as both malignancies affect lymphoid cells but differ in their primary sites of development. Leukemia primarily originates in the BM, whereas lymphoma arise mainly in the lymph nodes or other lymphoid tissues (Swerdlow *et al.*, 2016).

Thus, although numerous subtypes exist, leukemias are mainly divided according to two parameters: disease progression (acute or chronic) and cell lineage (myeloid or lymphoid) (Swerdlow *et al.*, 2016; Arber *et al.*, 2022):

- **Acute lymphoid leukemia (ALL)** is characterized by the fast proliferation of immature lymphoid cells (also termed lymphoblasts). As an acute disease, ALL progresses rapidly and is fatal within weeks or months if left untreated. Although it can occur in adults, it is most common in children aged 2 to 5 years.
- **Chronic lymphoid leukemia (CLL)** is typically characterized by the gradual accumulation of abnormal, mature B lymphocytes. Unlike ALL, CLL progresses slowly and often remains asymptomatic until advanced stages. It primarily affects older adults.
- **Acute myeloid leukemia (AML)** is defined by the uncontrolled growth of immature myeloid cells. Like ALL, AML progresses rapidly and requires urgent treatment. It predominantly affects adults.
- **Chronic myeloid leukemia (CML)** is characterized by the excessive proliferation of abnormal myeloid cells and belongs to a group of diseases known as myeloproliferative neoplasms (MPN). MPNs are clonal hematologic disorders marked by the overproduction of myeloid cells in the BM. In addition to CML, this group includes polycythemia vera (PV), essential thrombocythemia (ET), and primary myelofibrosis (PMF). Unlike AML, CML typically follows a gradual progression before potentially transforming into an acute phase. It is most commonly diagnosed in adults and is strongly associated with a well-defined genetic abnormality.

1.1.2. Background of CML

CML is likely the first type of leukemia to be formally described. In the 1840s, patients experiencing fever, splenomegaly, and unusually high leukocyte counts were first recognized and documented (Bennett, 1845). Early attempts to determine the cause of death in these patients led to the hypothesis that they had died from an abnormal accumulation of white blood cells (WBC). These early cases were probable examples of this neoplasm, which was initially referred to as chronic granulocytic leukemia (Goldman, 2010).

A major milestone in CML research occurred a century later, in the 1960s, when Nowell and Hungerford identified an abnormally small chromosome in the blood cells of patients diagnosed with chronic granulocytic leukemia. They also observed that these patients had lost the distal segment of the long arm of chromosome 22 (Nowell and Hungerford, 1960). This was a groundbreaking discovery as it represented the first known genetic abnormality linked to cancer. Years later, with the advancement of cytogenetic techniques, Janet Rowley demonstrated that this abnormal chromosome 22 resulted from a reciprocal translocation between the long arms of chromosomes 9 and 22 (**Figure 1**) (Rowley, 1973).

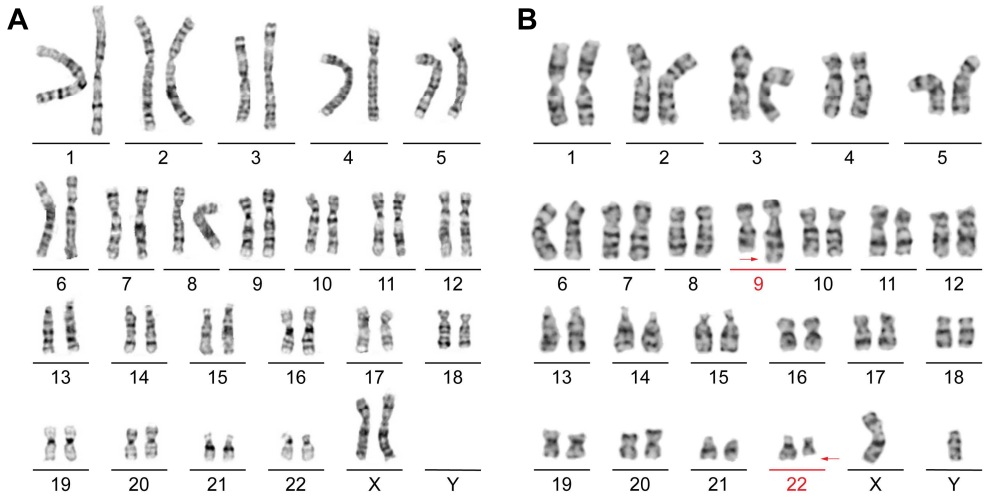

Figure 1. Karyotype illustrating the chromosomal abnormality found in patients with chronic myeloid leukemia (CML). (**A**) Normal XX karyotype from a healthy individual (adapted from Chen *et al*., 2012). (**B**) XY karyotype from a CML patient showing the reciprocal translocation between chromosomes 9 and 22 (pointed in red) (adapted from Atlas of Haematological Cytology).

This abnormally small chromosome 22 was eventually named the Philadelphia (Ph) chromosome, after the city where it was discovered (Koretzky, 2007). The identification of the Ph chromosome was the first description of a clonal cytogenetic abnormality in leukemia. Its presence in myeloid, megakaryocytic, and erythroid lineages suggested that the disease originated at a pluripotent stem cell stage (Fialkow *et al.*, 1977).

Subsequent research aimed to further understand the genetic features of the Ph translocation and its role in the CML phenotype. In 1975, Lozzio and Lozzio generated a leukemic cell line, later known as K562, from the pleural effusion of a 53-year-old woman who had been suffering from CML for almost 4 years. These cells could grow indefinitely in culture and exhibited typical CML characteristics, such as abnormal cell size and high enzymatic activity, two hallmark features of CML pathogenesis (Lozzio and Lozzio, 1975).

In-depth studies of the genomic structure of the Ph translocation revealed that the breakpoints occur in chromosome 9 upstream of the *ABL1* gene, a proto-oncogene encoding a non-receptor tyrosine kinase protein (Heisterkamp *et al.*, 1983). The translocation involves a region on chromosome 22 that was first called the "breakpoint cluster region" because breaks frequently occurred there. This region was later identified as a gene, which was named *BCR* after this original description (Groffen *et al.*, 1984). This finding raised the possibility that the *BCR* and *ABL1* genes were fused, leading to the constitutive activation of ABL1 (Shtivelman *et al.*, 1985).

Successive studies further explored the oncogenic properties of this *BCR::ABL1* fusion gene by demonstrating its ability to initiate malignant disease in transgenic mouse models, confirming its central role in the pathogenesis of CML (Daley *et al.*, 1990; Elefanty *et al.*, 1990; Heisterkamp *et al.*, 1990; Kelliher *et al.*, 1990).

1.1.3. Epidemiology

CML accounts for approximately 15-20% of all adult leukemia cases, with an annual incidence of 2 per 100,000 individuals (Jabbour and Kantarjian, 2024). Historically, the mortality rate for CML was approximately 10–20%, but with the introduction of tyrosine kinase inhibitor (TKI) therapies in 2000, this rate has significantly decreased to 1-2% (Sasaki *et al.*, 2023).

In the United States (US), the estimated prevalence of CML was around 30,000 cases in the year 2000 and has been increasing by approximately 9,000 cases each year, reaching over 150,000 cases by 2024 (Jabbour and Kantarjian, 2024). Early projections estimated that the prevalence of CML would reach a plateau of approximately 180,000 cases between 2030 and 2040, as a consequence of a balance between disease incidence and mortality following the widespread adoption of long-term TKI therapy (Huang *et al.*, 2012).

On a global scale, with a population of 8 billion and optimal CML management through widespread access to affordable TKIs, the global prevalence of CML could possibly rise above 10 million cases. However, these projections depend on multiple factors, including global population growth, as well as the accessibility, optimization, and affordability of TKI therapy (Hehlmann *et al.*, 2017).

The introduction of TKIs has significantly improved long-term outcomes, raising the 10-year survival rate from roughly 20% to 80-90% over 20 years of follow-up (Sasaki *et al.*, 2023). Disease-related mortality is around 10%, and the incidence of malignant transformation remains low, at 5-6% over 10 years. Although the overall 10-year survival rate is about 85%, many patients now normally die to causes unrelated to CML, such as aging or secondary malignancies (Hochhaus *et al.*, 2017; Jabbour and Kantarjian, 2024).

1.2. Molecular pathogenesis

1.2.1. Philadelphia chromosome formation

CML results from a reciprocal translocation between chromosomes 9 and 22 in a hematopoietic precursor cell (Rowley, 1973) (**Figure 2**). This specific genetic rearrangement, t(9;22)(q34;q11), generates an abnormally short chromosome 22, known as the Ph chromosome, which harbors the *BCR::ABL1* fusion oncogene. The fusion results from translocation of the *ABL1* locus on chromosome 9 to the *BCR* region on chromosome 22, producing a constitutively active tyrosine kinase (Kurzrock *et al.*, 1988). Persistent

kinase activation usually disrupts genomic integrity and main regulatory pathways, resulting in uncontrolled proliferation. Through this dysregulation, cells acquire the ability to proliferate independently of cytokines, while evading apoptosis under absence of growth factors (Mandanas *et al.*, 1993).

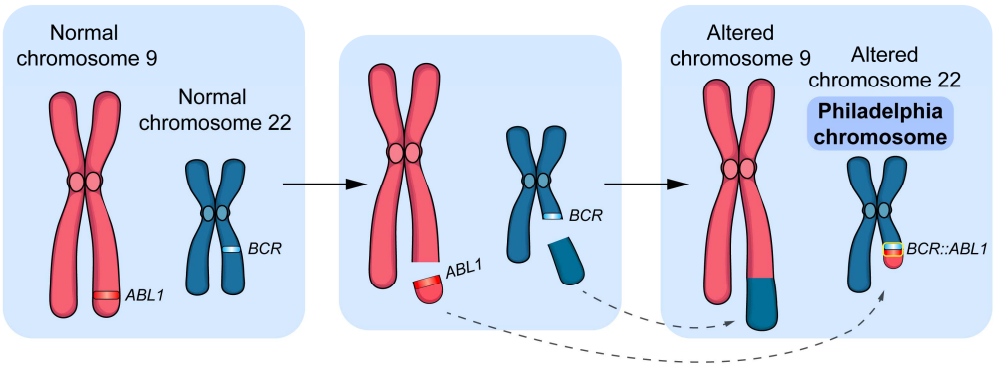

Figure 2. Philadelphia (Ph) chromosome formation. Chromosomes 9 and 22, which harbor the *ABL1* and *BCR* genes respectively, undergo a reciprocal translocation that juxtaposes them on chromosome 22, forming the Ph chromosome. This genetic rearrangement generates the *BCR::ABL1* fusion oncogene, whose product drives CML through its aberrant tyrosine kinase activity.

The Ph translocation is not exclusively linked to CML but is also observed in other leukemia subtypes. For instance, it occurs in approximately 2-5% of pediatric and 10-20% of adult cases of B-cell ALL (B-ALL). Additionally, patients with chronic neutrophilic leukemia (CNL) also harbor this translocation. To a lesser extent, the presence of the Ph chromosome has also been reported in certain cases of AML, lymphoma, and multiple myeloma (Melo, 1996). Clinical outcome varies according to the breakpoint within the *ABL1* gene, as discussed below.

1.2.2. The BCR::ABL1 fusion protein

At the genomic level, the Ph translocation results from the juxtaposition of the 5′ region of the *BCR* gene with the 3′ region of the *ABL1* gene. The specific chromosomal breakpoint locations determine the extent of the genomic fragments incorporated into the fusion oncogene (**Figure 3**) (Pane *et al.*, 2002).

In the majority of CML cases, breakpoints occur within a specific region in the central part of the *BCR* gene, known as the major breakpoint cluster region (*M-BCR*). This region spans between exons e13 (b2) and e14 (b3) (Groffen *et al.*, 1984). Alongside the primary breakpoint, several alternative breakpoints have been identified: the minor breakpoint cluster region (*m-BCR*), which is located between exons e1 and e2 and is primarily associated with B-ALL; and the micro breakpoint cluster region (*μ-BCR*), situated

downstream of exon e19 and linked to CNL. These three breakpoints (*M-BCR*, *m-BCR*, and *μ-BCR*) result in the generation of different isoforms of the BCR::ABL1 fusion protein, which are named according to their approximate molecular weight as p210, p190, and p230, respectively. Additionally, less frequent breakpoints within the *BCR* gene have been described, leading to the formation of atypical BCR::ABL1 fusion proteins, including p195, p200, and p225 (Weerkamp *et al.*, 2009).

Conversely, the breakpoint within the *ABL1* gene can occur at any location within a segment of approximately 300 kb at the 5' end of the gene (Melo, 1996). The breakpoints happen either upstream of the first alternative exon 1 (b1), downstream of the second alternative exon 1 (a1), or, more frequently, between the two. Regardless of the exact breakpoint location, the resulting transcript typically contains *BCR* sequences fused to exon a2 of *ABL1* (Izzo *et al.*, 2019).

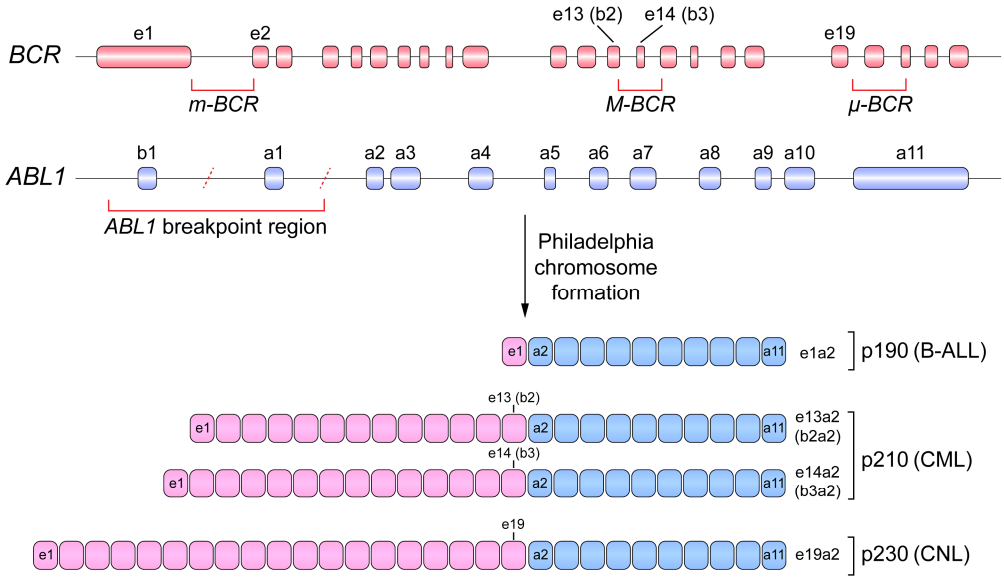

Figure 3. Genomic breakpoints in the Philadelphia chromosome generate diverse *BCR::ABL1* transcripts. Three genomic breakpoints have been described in the *BCR* gene: *m-BCR* (between exons e1 and e2), *M-BCR* (between e13 and e14) and *μ-BCR* (downstream of e19), generating the BCR::ABL1 p190, p210 and p230 isoforms, respectively. These isoforms are associated with different leukemia subtypes: p190 with B-cell acute lymphoid leukemia (B-ALL), p210 with chronic myeloid leukemia (CML), and p230 with chronic neutrophilic leukemia (CNL). Breakpoints on *ABL1* gene typically occur at the 5' end of the gene, upstream of exon b1, downstream of exon a1, or between them.

In CML, the *BCR::ABL1* fusion gene generally results from breakpoints occurring after exon e13, giving rise to the e13a2 (b2a2) fusion, or after exon e14, resulting in the e14a2 (b3a2) fusion. Both fusion transcripts are translated into the p210 isoform of the

BCR::ABL1 protein (Melo, 1996). Baccarani *et al.* reported that the distribution of these fusion transcripts in CML patients was as follows: 37.9% of cases harbored the e13a2 (b2a2) fusion, while 62.1% presented the e14a2 (b3a2) fusion. Additionally, unusual *BCR::ABL1* fusion transcripts, including e1a1, e8a1, e8a3, e15a2, and e23a1, were identified in 1.93% of the CML patients (Baccarani *et al.*, 2019).

Different aspects of CML pathogenesis can be attributed to the altered functions of BCR and ABL1 proteins (Deininger *et al.*, 2000). Therefore, a clear understanding of their physiological roles is crucial for assessing their impact on CML development.

The *BCR* gene encodes a ubiquitously expressed 160-kDa protein that contains multiple structural domains with different functional properties (**Figure 4A**). Its N-terminal domain (NTD) presents serine-threonine kinase activity, with identified substrates including BAP-1, VAV1 and potentially BCR itself (Reuther *et al.*, 1994). The C-terminal domain possesses GTPase activity for Rac, thereby regulating actin polymerization and the function of NADPH oxidase in phagocytic cells (Diekmann *et al.*, 1991). Moreover, it contains a DH-PH domain, acting as activator of Rho GTPases (Reckel *et al.*, 2017). Additionally, phosphorylation of BCR facilitates its interaction with Grb2, leading to the activation of the Ras signaling pathway (Ma *et al.*, 1997). Despite these roles in intracellular signaling, the specific biological function of BCR remains incompletely understood, as *Bcr*-deficient mice are viable and exhibit only minor immune abnormalities (Voncken *et al.*, 1995).

The *ABL1* gene was first identified as the human homolog of the v-*Abl* oncogene, originally discovered in the Abelson murine leukemia virus (Abelson and Rabstein, 1970). It encodes a 140-kDa protein composed of multiple functional domains (**Figure 4B**). In its NTD, ABL1 undergoes N-myristoylation, a modification essential for autoinhibiting kinase activity by facilitating the interaction between the myristoyl group and a specific pocket located in the kinase domain itself. Mutations that prevent access to the myristoyl pocket lead to a significant increase in kinase activity (Hantschel *et al.*, 2003). The NTD also contains several Src homology (SH) domains, including SH3 and SH2, which mediate protein-protein interactions; and SH1, which harbors the catalytic kinase activity (Woodring *et al.*, 2003). In the central region of the protein, proline-rich motifs enable interactions with SH3 domains of other proteins, including members of the Crk family, which can be phosphorylated by ABL1 (Feller *et al.*, 1994). The ABL1 protein plays a complex role in cellular biology, integrating extracellular and intracellular signals to regulate critical processes such as cell cycle progression and apoptosis (Van Etten, 1999). Mice deficient in the *Abl1* gene exhibit increased perinatal mortality and frequently present thymic and splenic atrophy, as well as T and B cell lymphopenia, among other complications. These findings highlight the essential role of ABL1 in the hematopoietic system (Tybulewicz *et al.*, 1991).

At the protein level, the formation of BCR::ABL1 results in the removal of certain domains (**Figure 4C**). For instance, the N-terminal myristoyl group of ABL1 is lost, impairing its autoinhibitory function and leading to the constitutive phosphorylation of multiple substrate proteins. Additionally, the BCR-derived region incorporated into the fusion protein provides critical domains and sequence motifs that further increase the activation of downstream signaling pathways (Hantschel, 2012). One key example is tyrosine 177 (Y177), which becomes phosphorylated and serves as a critical docking site for adaptor proteins, thereby amplifying the oncogenic signaling (Pendergast *et al.*, 1993). Additionally, a coiled-coil domain at the NTD of BCR promotes the dimerization of BCR::ABL1, an event that further facilitates strong autophosphorylation of the protein itself, reinforcing its oncogenic activity (Hantschel, 2012).

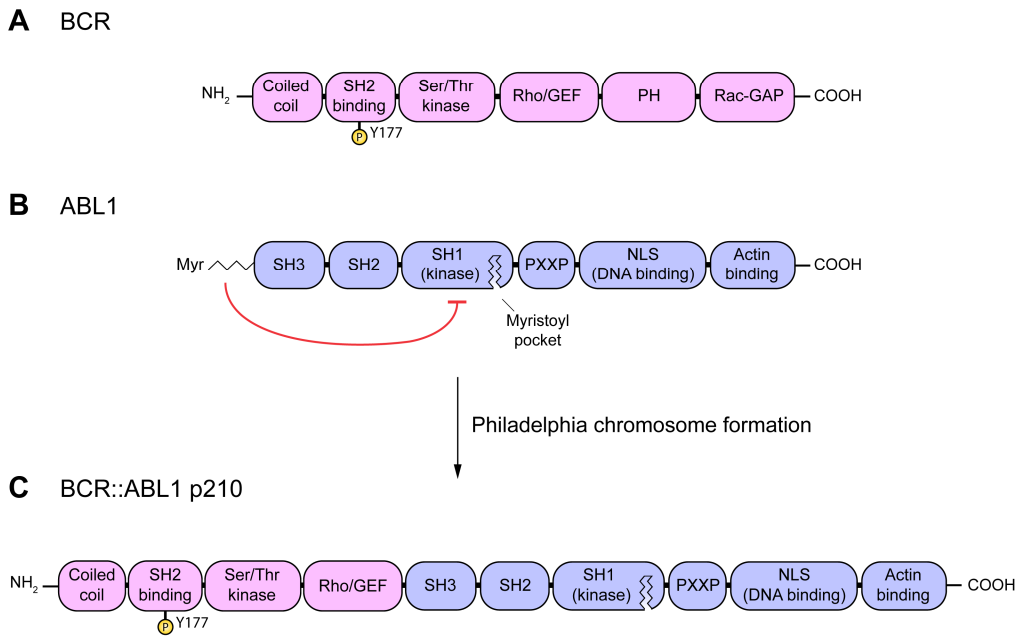

Figure 4. Protein domains of BCR, ABL1, and the resulting fusion protein BCR::ABL1 p210. (**A**) Structural domains of BCR. The tyrosine residue 177 (Y177), located in the SH2-binding domain and essential for recruitment of downstream effectors, is highlighted. (**B**) Structural domains of ABL1. The N-terminal myristoyl group (Myr) plays a critical role in its autoinhibitory mechanism by binding to the SH1 kinase domain and maintaining the kinase in an inactive conformation. (**C**) Structural domains of the BCR::ABL1 fusion. The myristoylation site is lost and replaced by the BCR coiled-coil domain, disrupting the autoinhibitory mechanism and promoting oligomerization, which locks the kinase in a constitutively active state. SH: Src homology domain, GEF: guanine nucleotide exchange factor, PH: pleckstrin homology domain, GAP: GTPase activating protein, NLS: nuclear localization sequence.

1.2.3. Oncogenic signaling

BCR::ABL1 activates multiple intracellular signaling cascades, directly or indirectly influencing critical pathways involved in cell survival, proliferation, and inhibition of apoptosis (McCubrey *et al.*, 2008). Moreover, while ABL1 is mainly localized in the nucleus under physiological conditions, the BCR::ABL1 fusion protein is retained in the cytosol. As a result, its tyrosine kinase activity is no longer subject to spatial regulation, allowing it to constitutively activate several signaling pathways (Hazlehurst *et al.*, 2009).

Co-immunoprecipitation assays conducted in the K562 cell line have uncovered the widespread and functionally significant interactome of BCR::ABL1, which includes key potentially oncogenic signaling proteins such as Grb2, Crk, c-Cbl, PI3K, SHC1, STS-1, and SHIP-2 (Brehme *et al.*, 2009). These proteins, along with other binding partners, enable the recruitment of intermediary and effector molecules, thereby initiating a extensive spectrum of signaling cascades (**Figure 5**), including Ras-ERK1/2, PI3K/AKT, JAK/STAT, Wnt/β-catenin, and apoptotic pathways, all of which play crucial roles in leukemogenesis (Amarante-Mendes *et al.*, 2022).

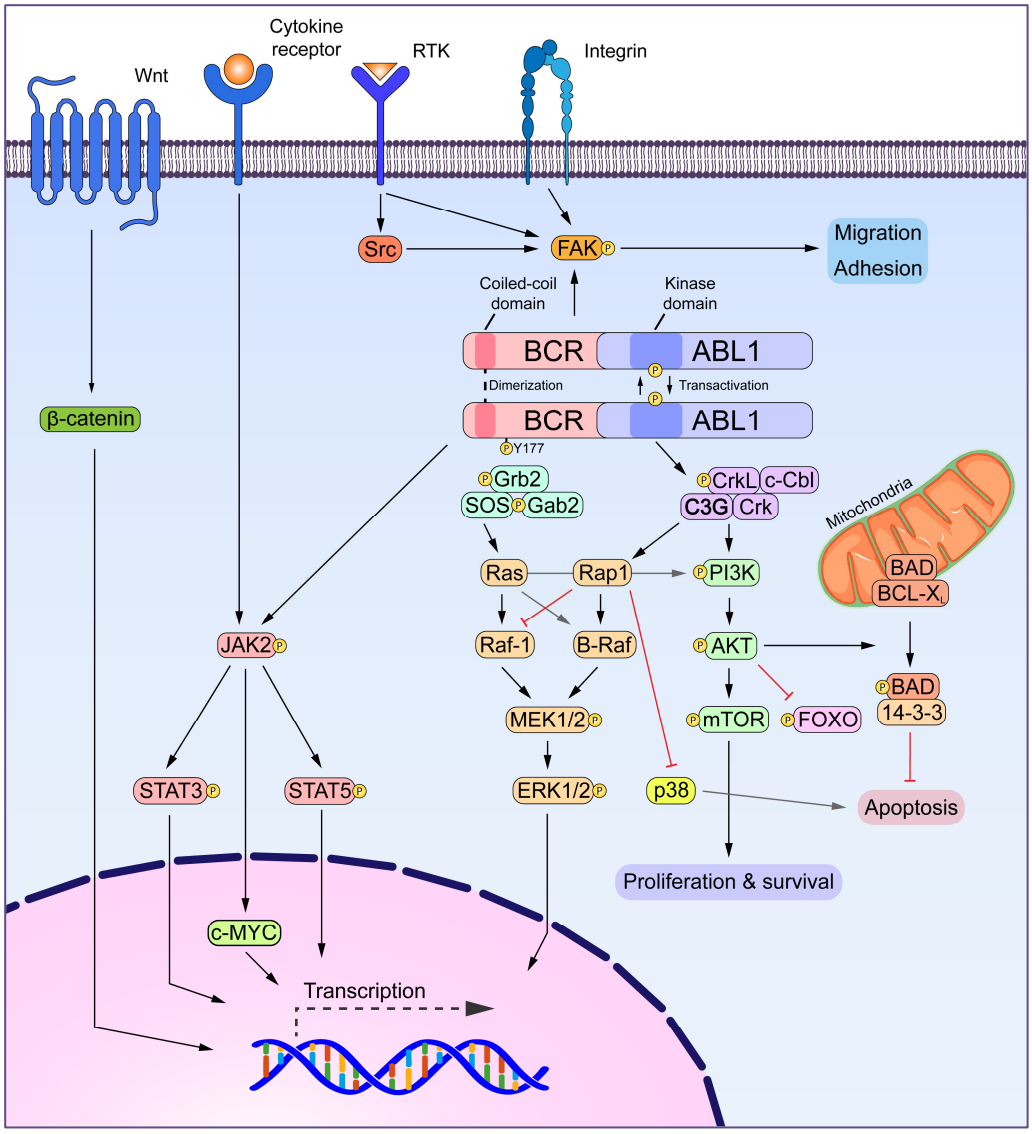

Figure 5. Major cellular signaling pathways activated by BCR::ABL1 oncoprotein. BCR::ABL1 completely rewires the cellular signaling landscape, constitutively phosphorylating numerous substrates and adaptor proteins that link to multiple downstream cascades. Through Grb2/SOS, it activates the Ras/Raf-1/MEK/ERK pathway, promoting proliferation. Activation of Ras proteins, in turn, stimulates the PI3K/AKT/mTOR axis, enhancing survival by inhibiting the intrinsic apoptotic pathway and increasing metabolic activity. AKT activation also downregulates FOXO transcription factors, further contributing to leukemogenesis. BCR::ABL1 can also trigger β-catenin signaling, further contributing to the proliferative phenotype. In parallel, it constitutively activates JAK2, thereby engaging the JAK/STAT pathways, where STATs, particularly STAT5, induce transcription of anti-apoptotic and self-renewal genes. Additionally, BCR::ABL1 perturbs cell adhesion by activating FAK and other cytoskeletal regulators, contributing to the loss of adhesion and increased motility characteristic of leukemic cells. RTK: Receptor tyrosine kinase.

The activation of the Ras/Raf/MEK/ERK cascade is initiated by the recruitment of Gab2 and SOS, the main guanine nucleotide exchange factor (GEF) of Ras, to BCR::ABL1 through the phosphorylated Y177 located in the BCR region (Sattler *et al.*, 2002). This interaction facilitates Ras activation, leading to the sequential activation of Raf-1, MEK1/2, and ERK1/2 signaling cascades, which play a fundamental role in regulating cell proliferation, differentiation, and survival (Chu *et al.*, 2007). BCR::ABL1 also activates C3G (Gutiérrez-Berzal *et al.*, 2006), a Rap1 GEF, leading to Rap1 activation. Activated Rap1 can either enhance or inhibit the ERK1/2 signaling pathway, depending on the relative balance of Raf-1 and B-Raf proteins within the cell. This selective activation contributes to the fine-tuning of ERK1/2 signaling, as Raf-1 and B-Raf have distinct expression patterns, activities, and functional roles across different tissues, a situation that is particularly relevant in certain cancers (Peyssonnaux and Eychène, 2001). In the context of BCR::ABL1 expression, the C3G-Rap1 axis may promote pro-survival pathways such as the ERK1/2 and PI3K/AKT cascades, while simultaneously inhibiting pro-apoptotic signaling, including the p38-MAPK pathway (Maia *et al.*, 2009). Importantly, activation of the C3G–Rap1 axis can also disrupt proper adhesion of leukemic cells (Maia *et al.*, 2013).

BCR::ABL1 also activates the PI3K/AKT/mTOR signaling cascade through both direct and indirect mechanisms. It interacts with PI3K via multiple proteins, including Ras, Rap1, c-Cbl, and CrkL, ultimately leading to the activation of AKT (Cho *et al.*, 2005; Ren, 2005). Once activated, AKT plays a critical role in promoting cell survival by phosphorylating key substrates involved in apoptosis inhibition. Additionally, AKT activation initiates downstream signaling through mTOR, which functions within the mTORC1 and mTORC2 complexes. While mTORC1 regulates cell cycle progression, proliferation, and angiogenesis, mTORC2 is predominantly involved in cytoskeletal organization and cell growth (Bertacchini *et al.*, 2015). Furthermore, AKT-driven mTOR activation modulates the expression of transcription factors, like the FOXO family, contributing to leukemogenesis (Pellicano *et al.*, 2014).

The JAK/STAT pathway plays a central role in CML, including growth factor independence and apoptosis resistance. In CML cell lines, JAK2 and STATs proteins are constitutively activated (Chai *et al.*, 1997). BCR::ABL1 can phosphorylate JAK2, thereby initiating the activation of multiple downstream effectors, including STAT3 and STAT5 (Xie *et al.*, 2001). STAT5 is particularly critical in CML, being essential for leukemogenesis (Ye *et al.*, 2006) and mediating resistance of BCR::ABL1-expressing cells to TKIs (Warsch *et al.*, 2011). JAK2 also activates c-MYC, a transcription factor essential for cell proliferation, differentiation, and apoptosis, which is necessary for BCR::ABL1-driven leukemogenesis (Sawyers *et al.*, 1992). Interestingly, Ph-negative MPNs, which include PV, ET and PMF,

are strongly associated with *JAK2* mutations, leading also to dysregulated JAK/STAT signaling (Coltro *et al.*, 2021).

In addition, dysregulation of the Wnt/β-catenin signaling pathway is a common feature in various leukemia subtypes, including CML (Fetisov *et al.*, 2018). Wnt signaling is initiated upon Wnt ligand binding to its extracellular receptor, triggering either the canonical or non-canonical pathway. The main distinction between these Wnt pathways lies in the involvement of β-catenin, which functions exclusively in the canonical pathway. In the absence of Wnt, β-catenin is continuously targeted for ubiquitination and proteasomal degradation (Rao and Kühl, 2010). However, in CML, BCR::ABL1 indirectly prevents β-catenin degradation, enabling its nuclear translocation. Once in the nucleus, β-catenin acts as a transcriptional regulator, promoting the expression of genes involved in leukemic cell proliferation and survival (Coluccia *et al.*, 2007).

A key characteristic of BCR::ABL1-expressing cells is their increased resistance to apoptosis (Cortez *et al.*, 1995). Cellular stress typically triggers the mitochondrial apoptosis pathway, which is regulated by members of the BCL-2 family. This family consists of both anti-apoptotic proteins (such as BCL-2, BCL-X_L, and MCL-1) and pro-apoptotic proteins (such as BAX and BAK). Under normal conditions, a balance between pro-apoptotic and anti-apoptotic BCL-2 family members maintains cellular survival. However, in response to apoptotic stimuli, this balance shifts in favor of pro-apoptotic factors since anti-apoptotic proteins are neutralized by BH3-only pro-apoptotic proteins, such as BAD and BID. This leads to the activation of BAX and BAK, which in turn foster the release of several pro-apoptotic factors from the mitochondria into the cytosol (Czabotar *et al.*, 2014). BCR::ABL1 promotes the sequestration of BAD by 14-3-3 proteins in the cytosol. This prevents BAD from antagonizing BCL-2 family anti-apoptotic members, thereby increasing their ability to sequester BAX/BAK and inhibit apoptosis (Neshat *et al.*, 2000). Consequently, BCR::ABL1 overexpression confers pronounced resistance to apoptosis, even in the presence of death-inducing stimuli, suggesting that BCR::ABL1 harbors even greater anti-apoptotic activity than BCL-2 or BCL-X_L proteins (Brumatti *et al.*, 2003).

1.3. Pathophysiological features

1.3.1. Normal hematopoiesis

Hematopoiesis refers to the process of blood cell production. To maintain homeostasis, the human body constantly generates new blood cells to replace aged or damaged ones, producing around 7×10^9 new blood cells per hour (Lew and Tiffert, 2017). These cells are generated in the BM from a rare population of cells known as hematopoietic stem and progenitor cells (HSPC). HSPCs can be divided based on their pluripotency and self-renewal capability into hematopoietic stem cells (HSC) and hematopoietic progenitor cells (HPC).

HSCs, which constitute approximately 0.01% of nucleated cells in the BM (Rossi *et al.*, 2011), exhibit self-renewal capacity and undergo asymmetric cell division, producing one daughter cell that retains stem cell properties and another that progresses toward differentiation. In contrast, HPCs have limited potency and lack self-renewal capacity, gradually giving rise to more lineage-committed progenitors that in due course generate all blood cell types (Gao *et al.*, 2023).

The gold-standard procedure for assessing HSPC potential has traditionally been defined by the transplantation of donor cells into lethally irradiated recipients lacking a functional endogenous hematopoietic system (Cheng *et al.*, 2020). The first evidence supporting the existence of HSPCs came from experiments demonstrating the rescue of lethally irradiated recipient mice through BM transplantation (BMT), leading to the formation of hematopoietic colonies in the spleens of the recipient mice (Till and McCulloch, 1961). These BMT studies allowed the distinction between HSCs and HPCs based on their multipotency, that is, their ability to produce all blood cell lineages (Orkin, 2000). Consequently, there has been growing interest in purifying these HSPCs from BM to further study their characteristics, functions, and role in hematopoiesis.

The isolation of HSPCs was first achieved through fluorescence-activated cell sorting (FACS) using antibodies targeting specific surface markers (Spangrude *et al.*, 1988). Over the past four decades, significant efforts have been made to identify novel surface markers and refine antibody combinations, allowing for the isolation and characterization of distinct subpopulations within the hematopoietic hierarchy (Challen *et al.*, 2009). Historically, commonly used markers for HSC isolation include CD34, Sca-1, c-Kit, and signaling lymphocyte activation molecule (SLAM) family proteins, among others (Cheng *et al.*, 2020).

The first model of the hematopoietic hierarchy, based on the immunophenotypic characterization of surface markers, was developed to classify and better understand the sequential steps of hematopoiesis (**Figure 6A**). In this tree-like model, HSCs are categorized into long-term HSCs (LT-HSC) and short-term HSCs (ST-HSC), depending on their ability to sustain hematopoiesis for prolonged or limited periods in lethally irradiated recipients, respectively. LT-HSCs give rise to ST-HSCs, which subsequently differentiate into multipotent progenitors (MPP). Unlike HSCs, MPPs lack self-renewal capacity and are therefore classified as HPCs. These MPPs can further differentiate into the two main hematopoietic branches: myeloid and lymphoid (Morrison *et al.*, 1997; Cheng *et al.*, 2020).

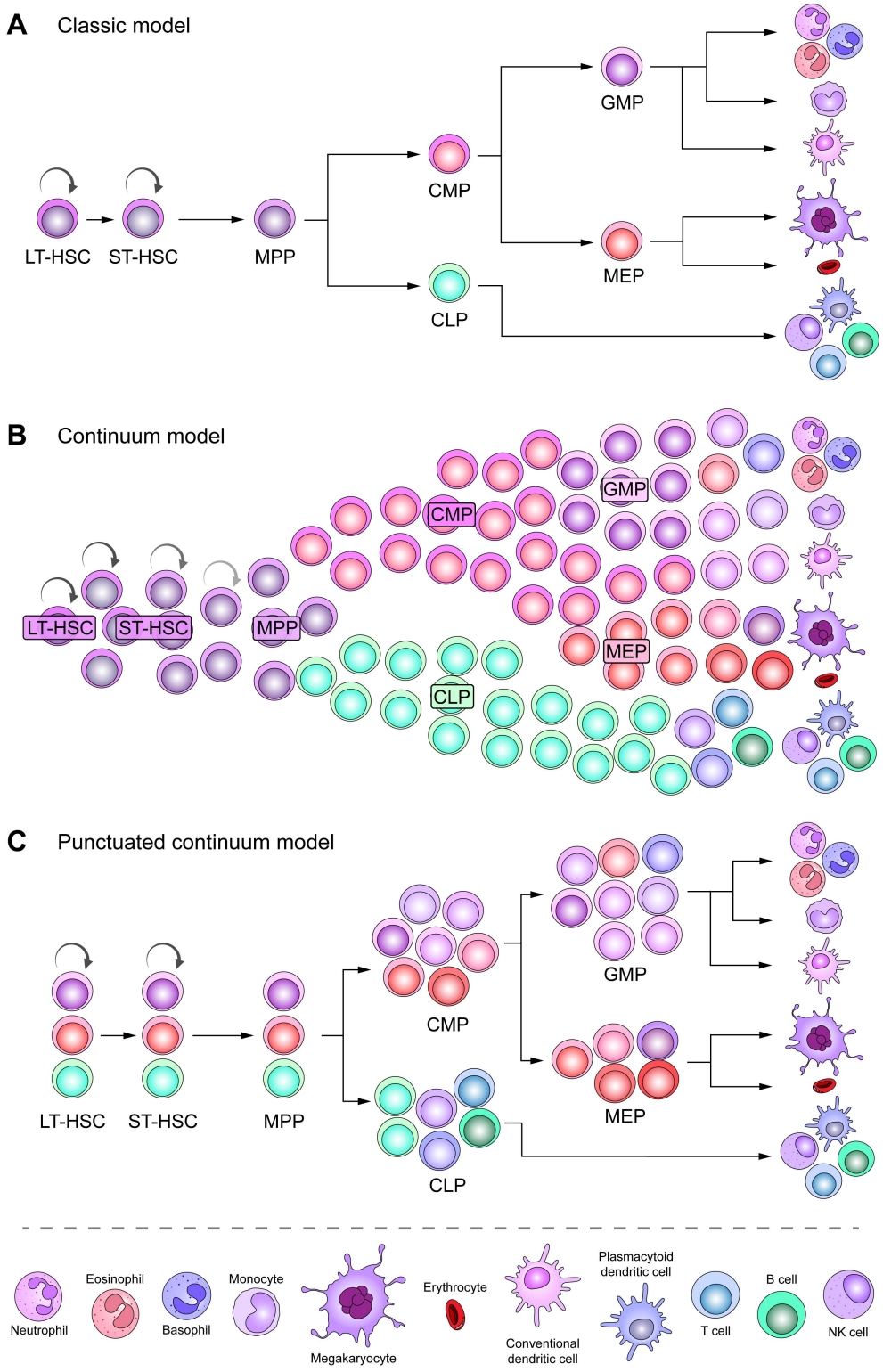
A Classic model
LT-HSC
ST-HSC
MPP
CMP
GMP
MEP
CLP
B Continuum model
LT-HSC
ST-HSC
MPP
CMP
GMP
MEP
CLP
C Punctuated continuum model
LT-HSC
ST-HSC
MPP
CMP
GMP
MEP
CLP
Neutrophil
Eosinophil
Basophil
Monocyte
Megakaryocyte
Erythrocyte
Conventional dendritic cell
Plasmacytoid dendritic cell
T cell
B cell
NK cell

◄ **Figure 6. Models of hematopoiesis.** (**A**) The classic model considers hematopoiesis as a stepwise, hierarchical process in which cells possess fixed identities and potentials, progressing through discrete stages where binary fate decisions determine lineage commitment. (**B**) The continuum model challenges this rigid hierarchy, proposing that differentiation is a smooth and gradual process in which individual cells display varying degrees of lineage bias without sharp boundaries between states. (**C**) The punctuated continuum model integrates both views. In this model, hematopoietic states are heterogeneous groups of variable primed cells, while still allowing critical transition points where differentiation decisions become reinforced. Each compartment contains a spectrum of cells already biased toward specific lineages. LT/ST-HSC: long-term/short-term hematopoietic stem cell, MPP: multipotent progenitor, CMP: common myeloid progenitor, CLP: common lymphoid progenitor, GMP: granulocyte-monocyte progenitor, MEP: megakaryocyte-erythrocyte progenitor.

The myeloid lineage is derived from the differentiation of MPPs into common myeloid progenitors (CMP). CMPs can further differentiate into granulocyte-monocyte progenitors (GMP) and megakaryocyte-erythrocyte progenitors (MEP). GMPs give rise to granulocytes (including neutrophils, eosinophils, and basophils) and monocytes, and have also the ability to generate a population of conventional dendritic cells (cDCs). In contrast, MEPs differentiate into MKs and erythrocytes (Akashi *et al.*, 2000). These mature myeloid cells play distinct physiological roles: granulocytes and monocytes contribute to innate immunity by defending against pathogens and initiating the adaptive immune response, which is mediated by antigen-presenting cDCs; MKs produce platelets, which are indispensable for hemostasis; and erythrocytes transport oxygen throughout the body (Liggett and Sankaran, 2020).

On the other hand, the lymphoid lineage arises when MPPs differentiate into common lymphoid progenitors (CLP), which ultimately give rise to mature T cells, B cells, natural killer (NK) cells, and plasmacytoid dendritic cells (pDCs) (Kondo *et al.*, 1997). Lymphoid cells predominantly mediate adaptive immunity, with T and B cells orchestrating antigen-specific immune responses. NK cells provide innate cytotoxicity, while pDCs play crucial roles in antiviral immunity and immune regulation (Liggett and Sankaran, 2020).

The classical model of hematopoiesis (**Figure 6A**) suggests that at each differentiation stage, cells become irreversibly committed to a precise lineage, with their fate determined through a series of binary decisions at specific stages, gradually limiting their developmental potential (Liggett and Sankaran, 2020). However, this model relies on the existence of distinct stages consisting of well-defined cell populations characterized by specific surface markers and assumes that lineage decisions happen within uniform cell pools. As a result, it oversimplifies what is actually a more complex process. The discovery of additional cellular markers has allowed researchers to identify more subpopulations, revising the timing of lineage commitment and further dividing cell stages into more subgroups (Adolfsson *et al.*, 2005; Görgens *et al.*, 2013; Yamamoto *et al.*, 2013). This, however, has led to more inconsistencies in defining new cell populations, making this model less clear. Recent advances in single-cell technologies have helped overcome these challenges, enabling more

precise identification and definition of cell populations, and leading to more accurate models of hematopoiesis (Laurenti and Göttgens, 2018).

Although the classical model provides a simple but powerful framework for understanding blood cell development, recent single-cell transcriptomic analyses have suggested that lineage commitment may follow a continuous process (**Figure 6B**). In this model, unilineage-restricted cells arise directly from a continuum of minimally committed, undifferentiated HSPCs, rather than progressing through distinct multipotent and bipotent stages (Macaulay *et al.*, 2016; Velten *et al.*, 2017; Karamitros *et al.*, 2018). Contrary to the discrete hierarchical structure proposed by the classical model, these findings indicate a lack of clear boundaries between HSCs and HPCs.

In addition, situated between these classical and continuum models lies the punctuated continuum model. It describes hematopoietic differentiation as a continuous process also regulated by critical checkpoints that support lineage commitment (**Figure 6C**). In this framework, HSPCs progressively acquire lineage biases while retaining some plasticity, with transcriptional, epigenetic, and signaling cues acting as regulatory "punctuations" that guide differentiation (Liggett and Sankaran, 2020). This model is supported by single-cell analyses, which reveal substantial heterogeneity among progenitor stages while still maintaining structured lineage outcomes (Giladi *et al.*, 2018).

1.3.2. Leukemic hematopoiesis and disease progression

HSCs maintain hemostasis and undergo continuous self-renewal and differentiation to generate blood cells. This constant activity, added to events of infection, aging, or inflammation, places them under replicative stress, which increases the likelihood of DNA damage. Over time, this stress can lead to accumulative mutations in the HSCs. These mutations can compromise their normal function and, in some cases, eventually lead to the generation of a potentially malignant population of cells known as leukemic stem cells (LSC) (Yamashita *et al.*, 2020).

Somatic mutations in HSCs can drive the expansion of a mutant clone without initially progressing to a hematological malignancy. This condition, known as clonal hematopoiesis of indeterminate potential (CHIP), is asymptomatic, but usually confers an increased risk of suffering hematological malignancies such as leukemia (Genovese *et al.*, 2014). CHIP is most commonly associated with mutations in genes regulating epigenetic modifications (*DNMT3A*, *TET2*, *ASXL1*), DNA repair (*PPM1D*, *TP53*), mRNA splicing (*SF3B1*, *SRSF2*), and kinase signaling (*JAK2*) (Marnell *et al.*, 2021). In some cases of CML, the *BCR::ABL1* fusion has been reported to arise within a pre-existing Ph-negative clonal population carrying CHIP-associated mutations, referred to as a preleukemic clone (Steensma *et al.*, 2015). This observation suggests that the presence of *BCR::ABL1* alone may not be

sufficient to initiate CML. Instead, certain CHIP mutations may confer a selective advantage, enhancing self-renewal capacity and creating a cellular environment in which the acquisition of *BCR::ABL1* more effectively drives leukemic transformation (Walter, 2017).

Similar to normal hematopoiesis (**Figure 7A**), leukemia follows a hierarchical organization, with LSCs at the apex. LSCs are responsible for disease initiation, as well as the maintenance and continuous production of malignant cells (Bonnet and Dick, 1997). LSCs share many characteristics with HSCs, including quiescence, pluripotency, and self-renewal. However, LSCs usually present a dysregulated activation of key signaling pathways that control proliferation, survival, and their ability to invade and disseminate, contributing to malignant progression. From a clinical perspective, LSCs are particularly concerning due to their resistance to standard cancer treatments, including chemotherapy, radiation, and targeted therapies, making them responsible for most cases of treatment failure and disease relapse. This multiple resistance is mainly due to their quiescent state, which hampers the effectiveness of therapies that rely on cell division (Tabe and Konopleva, 2014). In myeloid leukemias, the generation of LSCs can occur at various stages of hematopoiesis. However, in the specific case of CML, the defining features of the LSCs also depends on the developmental phase of the disease (Riether *et al.*, 2015).

CML progression and clinical evolution are typically categorized into three distinct phases: chronic, accelerated, and blast crisis phase (**Figure 7B**) (Büsche and Kreipe, 2011):

(1) **Chronic phase (CP):** The CP is the initial stage of CML and can last for several years, during which the disease remains stable. Patients in this phase are usually asymptomatic or present mild symptoms, such as an increased presence of myeloid granulocyte-like cells in peripheral blood (PB). BM also shows a high number of relatively mature myeloid cells. At this stage, the disease can be effectively managed with TKIs, which maintain the disease stable.
(2) **Accelerated phase (AP):** In the AP, the disease becomes more aggressive, characterized by a higher presence of undifferentiated blast cells in both PB and BM. Symptoms may become more severe, including fatigue, weight loss, fever, and splenomegaly. The disease may become harder to control due to a reduced response to TKIs, often due to the emergence of new leukemogenic mutations in the LSCs. If untreated properly, AP can progress into the blast crisis phase within several months.
(3) **Blast crisis phase (BP):** The BP represents the most aggressive form of CML and shares clinical features with the AML. During BP-CML, blast cells are typically found in both PB and BM. Symptoms can be severe and may include bleeding, infections, and organ enlargement. The disease becomes highly resistant to TKIs, and treatment options are limited. If not adequately managed, BP-CML can be fatal.

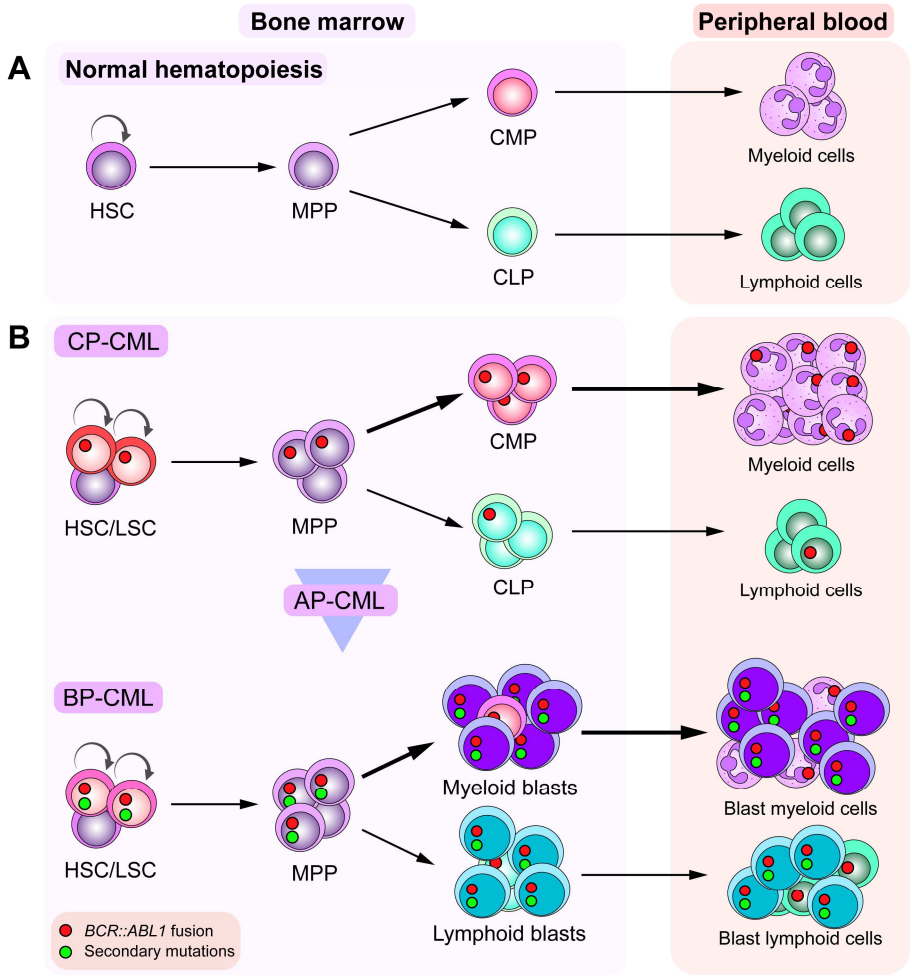

Figure 7. Triphasic progression of chronic myeloid leukemia (CML). (**A**) In normal hematopoiesis, hematopoietic stem cells (HSC) in the bone marrow (BM) maintain a stable pool of self-renewing cells while generating progenitors that progressively mature into differentiated blood lineages under tightly regulated control. (**B**) In CML, three well-defined clinical phases can be distinguished: chronic phase (CP), accelerated phase (AP), and blast crisis phase (BP). In CP, HSCs harboring the *BCR::ABL1* translocation (now termed leukemic stem cells (LSC)) acquire a proliferative advantage, leading to excessive production of myeloid cells and expansion of the granulocytic compartment in peripheral blood (PB). If left untreated, the disease progresses through AP to an acute leukemia-like BP. BP is characterized by the accumulation of secondary mutations beyond *BCR::ABL1*, conferring drug resistance, enhanced proliferation, and a block in differentiation, resulting in the massive accumulation of myeloid, lymphoid, or mixed-lineage blasts in the BM, PB, and extramedullary tissues. MPP: multipotent progenitor, CMP: common myeloid progenitor, CLP: common lymphoid progenitor.

In CP-CML, the presence of *BCR::ABL1* in both myeloid and lymphoid lineages suggests that LSCs originate from a minimally committed HSPC, likely a HSC or even a HPC with high self-renewal capacity (Martin *et al.*, 1980; Jonas *et al.*, 1992). Additionally, pre-

leukemic mutations are generally present in 15-20% of CP-CML patients, mostly due to CHIP, without a significant role in disease initiation (Schmidt *et al.*, 2014). However, in a reduced subset of cases, these mutations precede *BCR::ABL1* acquisition and may be linked with poorer outcomes (Kim *et al.*, 2017). Whereas pre-leukemic mutations seem to have a minor role in CP-CML development, they are probable significant risk factors for progression to BP-CML and AML. This supports the hypothesis that CP-CML LSCs arises primarily from a first single oncogenic hit (*BCR::ABL1*), while BP-CML LSCs and AML LSCs, which can also emerge from more committed and later-stage progenitors, require additional mutations frequently linked to CHIP (Vetrie *et al.*, 2020). In line with this, BP-CML LSCs and AML LSCs often display immunophenotypes of more lineage-restricted progenitors, such as lymphoid-primed MPPs or GMPs, indicating that leukemic transformation can also take place in more differentiated progenitors once they reacquire self-renewal capacity (Riether *et al.*, 2015). Interestingly, GMPs have been shown to acquire a stem cell-like self-renewal program during progression to BP-CML, driven by activation of the Wnt/β-catenin pathway, which positions them as candidate LSCs at this stage (Jamieson *et al.*, 2004). This idea is further supported by the fact that normal GMPs become leukemogenic when transformed with *BCR::ABL1 p210* (Minami *et al.*, 2008).

In summary, myeloid leukemias exhibit a shared developmental framework (**Figure 8**). While CP-CML follows a more linear, HSC-dependent model, both BP-CML and AML display a more plastic and heterogeneous LSC hierarchy. This indicates that AML and BP-CML share a common mechanism of leukemic evolution, where hierarchical flexibility facilitates committed progenitor cells to reacquire stem-like properties, driving disease progression and therapeutic resistance (Vetrie *et al.*, 2020).

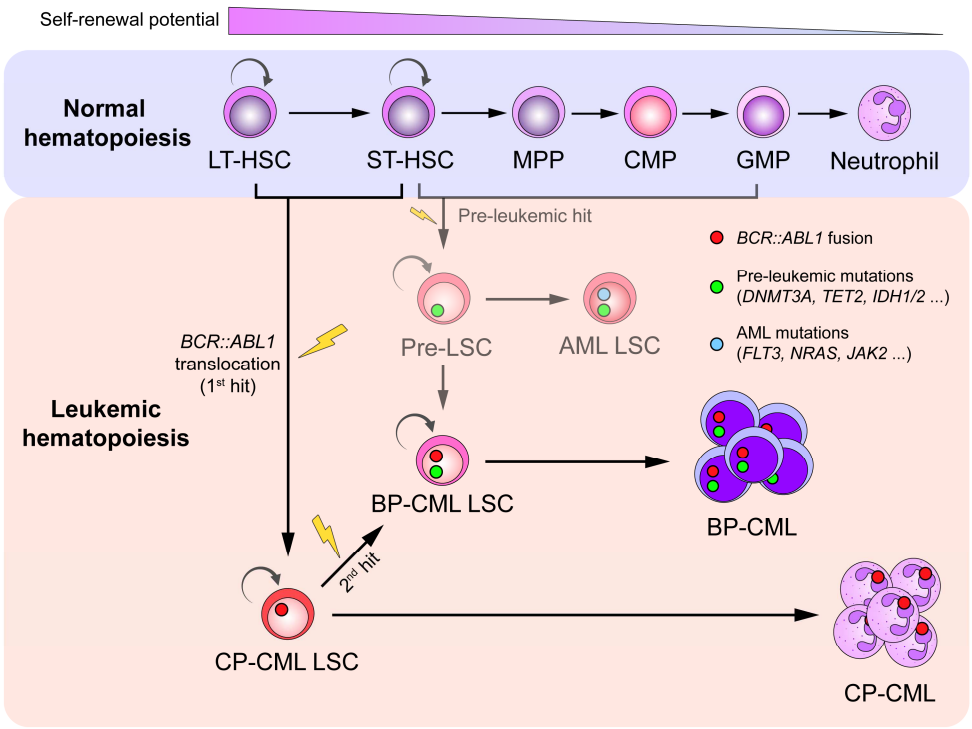

Figure 8. Leukemic hematopoiesis in chronic myeloid leukemia (CML). The origin and characteristics of CML leukemic stem cells (LSC) depend on the clinical phase of the disease. In chronic-phase (CP) CML, LSC derive from hematopoietic stem cells (HSC) that acquire the BCR::ABL1 leukemic hit (1st hit), driving the sustained expansion of myeloid cells characteristic of this phase. Progression to blast-phase (BP) CML occurs when CP-CML LSCs acquire secondary mutations (2nd hit), giving rise to BP-CML LSCs. Alternatively, BP-CML LSCs can originate from more committed progenitors that, through additional pre-leukemic mutations often associated with clonal hematopoiesis of indeterminate potential (CHIP), form pre-LSCs. These pre-LSCs may then either acquire *BCR::ABL1*, generating BP-CML LSCs, or accumulate acute myeloid leukemia (AML) typical mutations, leading to AML LSCs. LT/ST-HSC: long/short term hematopoietic stem cell, MPP: multipotent progenitor, CMP: common myeloid progenitor, GMP: granulocyte-monocyte progenitor.

1.4. Current and emerging treatments

The first documented treatment for leukemia dates back to the 1860s, when two leukemia patients were treated with arsenic (Lissauer, 1865). Since then, the treatment of CML has slowly evolved during 20th century, beginning with the use of spleen radiotherapy for symptomatic relief in the early years (Goldman, 2010), followed by the introduction of alkylating agents in the 1950s (Galton, 1953) and recombinant interferon-alpha (IFN-α) in the 1980s (Talpaz *et al.*, 1986). Conventional chemotherapeutics such as busulfan and hydroxyurea were also widely used to control disease progression, due to their ability to limit the myeloproliferative phenotype (Rushing *et al.*, 1982). In parallel, allogeneic hematopoietic stem cell transplantation (Allo-HSCT) from sibling donors also emerged in

the 1980s as the only potentially curative therapy for CML, although it was applicable to only a small proportion of patients (Goldman *et al.*, 1982).

The major milestone in CML therapy, however, came with the discovery and clinical introduction of TKIs, which specifically target the abnormal kinase activity of BCR::ABL1 oncogenic protein.

1.4.1. Tyrosine kinase inhibitor therapy

CML is the first disease in history to be successfully treated with TKIs (Cohen, 2002). In the 1990s, a research group at the pharmaceutical company Novartis developed a derivative of the 2-phenylaminopyrimidine compound, initially named CGP57148, which was shown to inhibit ABL1 activity both *in vitro* and *in vivo* (Buchdunger *et al.*, 1996). These findings were further supported by a subsequent study demonstrating that this compound effectively inhibited the growth of BCR::ABL1-positive cells (Druker *et al.*, 1996). In the early 2000s, a clinical trial evaluating CGP57148 (later renamed STI-571) in CML patients with chronic phase demonstrated that the drug was well tolerated and exhibited significant antileukemic activity, underscoring its remarkable clinical efficacy (Druker *et al.*, 2001). Shortly after, STI-571 received FDA approval for the treatment of CML patients in the chronic phase and was marketed under the brand name Gleevec® (in the US) or Glivec® (in Europe and other regions), being the generic name imatinib (Cohen, 2002).

Over the following years, an increasing number of TKIs as CML treatment have been developed in different drug generations, each improving on the previous ones in terms of potency, specificity, and ability to overcome resistance (**Table 1**).

Table 1. Tyrosine kinase inhibitors (TKIs) approved to treat chronic myeloid leukemia (CML). Color goes from red (resistant) to green (non-resistant) to indicate drug effectiveness over BCR::ABL1 mutations.

	Generic name	Mechanism of action	Clinical resistances	Molecular structure
1st generation	Imatinib	Blocking ATP-binding	G250E Y253H E255V V299L T315I F317L M351T F359V H396R	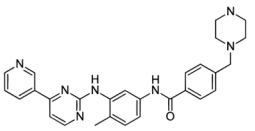
2nd generation	Nilotinib	Blocking ATP-binding	G250E Y253H E255V V299L T315I F317L M351T F359V H396R	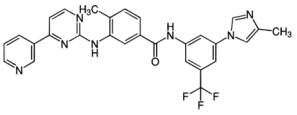
	Dasatinib	Blocking ATP-binding	G250E Y253H E255V V299L T315I F317L M351T F359V H396R	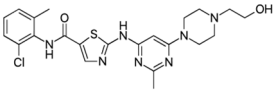
	Bosutinib	Blocking ATP-binding	G250E Y253H E255V V299L T315I F317L M351T F359V H396R	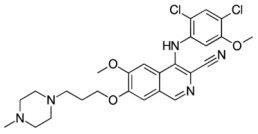
3rd generation	Ponatinib	Blocking ATP-binding	G250E Y253H E255V V299L T315I F317L M351T F359V H396R	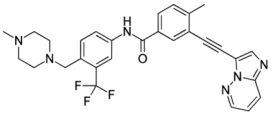
	Asciminib	Allosteric inhibition	G250E Y253H E255V V299L T315I F317L M351T F359V H396R	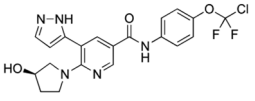

1. **First-generation TKIs** represent the first class of approved TKIs for CML, with imatinib being the only drug in this category and the first approved treatment for CML.
    - **Imatinib** functions as a competitive inhibitor of ATP binding to ABL1, thereby inactivating BCR::ABL1 kinase activity, and it is highly effective in CP-CML. However, resistance can appear, particularly due to point mutations in BCR::ABL1, making it relatively ineffective against several of these mutations (Melo and Chuah, 2007).
2. **Second-generation TKIs** were developed to address the increasing resistance and intolerance observed in some CML patients treated with imatinib. These TKIs display higher potency and enhanced activity against several imatinib-resistant BCR::ABL1 mutations, while maintaining the same mechanism of action, that is, targeting the ATP-binding site of BCR::ABL1.

- **Nilotinib** was developed by introducing structural modifications to the imatinib molecule to enhance its potency. It is significantly more potent than imatinib and is effective against some imatinib-resistant BCR::ABL1 mutations (Weisberg *et al.*, 2005).
- **Dasatinib** was identified in the search for a more potent and broader-spectrum inhibitor capable of overcoming BCR::ABL1 mutations. It is considerably more potent than imatinib, though less selective, as it also inhibits Src-family kinases (Han *et al.*, 2010). While effective against most BCR::ABL1 mutations, dasatinib is ineffective against the T315I mutation, which confers high-level resistance (Shah *et al.*, 2004).
- **Bosutinib** was initially designed as a Src inhibitor (Boschelli *et al.*, 2001), but it was later discovered to also exhibit inhibitory activity against BCR::ABL1, effectively preventing the growth of CML cell lines. Bosutinib is effective against several BCR::ABL1 mutations; however, similar to dasatinib, it is completely ineffective against T315I mutation (Puttini *et al.*, 2006).

3. **Third-generation TKIs** were developed to enhance potency and specifically target the pan-resistant T315I mutation, which was previously untreatable with available drugs. T315I substitution prevents critical hydrogen bonding with standard TKIs, blocking drug access and causing resistance (Kantarjian *et al.*, 2024).

- **Ponatinib** was developed to target the hydrophobic ATP pocket of mutant BCR::ABL1^{T315I}. It is highly effective against the T315I mutation and even capable of suppressing BCR::ABL1^{T315I} tumor growth in mice (O'Hare *et al.*, 2009).
- **Asciminib** is referred as a STAMP inhibitor, which stands for "specifically targeting the ABL1 myristoyl pocket", thereby being the first allosteric TKI approved for CML treatment. As a result, mutations that affect the ATP-binding site of ABL1, such as T315I, do not impact asciminib effectiveness (Réa *et al.*, 2021). The BCR::ABL1 translocation leads to the loss of the myristoylated N-terminal of ABL1, which normally occupies a site in the kinase domain and serves as an allosteric negative regulatory element. As a result, the myristoyl pocket remains empty. Asciminib targets this empty pocket to inhibit kinase activation in an allosteric manner, providing a novel approach to inactivate the oncogenic activity of BCR::ABL1 (Wylie *et al.*, 2017).

1.4.2. Monitoring treatment-responses

After starting treatment, CML patients undergo regular monitoring to evaluate their response to therapy. This assessment follows a sequential approach based on three main criteria: hematological, cytogenetic, and molecular responses (**Table 2**). Each response reflects a

progressively deeper reduction in leukemic burden, ranging from blood count normalization to the elimination of *BCR::ABL1* transcripts (Cortes *et al.*, 2011).

Table 2. Established criteria for monitorization of chronic myeloid leukemia (CML) patients during treatment. Response to therapy is assessed at three levels: hematologic, cytogenetic, and molecular. The complete achievement of each response indicates a decrease in the residual leukemic cell population. CHR: complete hematological response, WBC: white blood cell count, PCyR/CCyR: partial/complete cytogenetic response, Ph: Philadelphia chromosome, CBA: chromosome banding analysis, FISH: fluorescence in situ hybridization, MMR/DMR: major/deep molecular response.

Response to CML therapy	Stage		Criteria
Hematological response	CHR		WBC > 10×10^9/L (no immature granulocytes) Eosinophils > 5% Platelets > $450\cdot10^9$/L No splenomegaly
Cytogenetic response (CyR)	Minimal CyR		66%-95% Ph+ cells by CBA
	Minor CyR		36%-65% Ph+ cells by CBA
	PCyR		1%-35% Ph+ cells by CBA
	CCyR		No Ph+ cells by CBA, or <1% *BCR::ABL1* by FISH in 200 cells
Molecular response (MR)	MMR		<0.1% transcript level
	DMR	MR4	<0.01% (4-log reduction) transcript level
		MR4.5	<0.0032% (4.5-log reduction) transcript level
		MR5	<0.001% (5-log reduction) transcript level

1. **Hematological response:** PB is analyzed to monitor disease resolution. Complete hematological response (CHR) is defined by WBC count < 10×10^9/L, absence of immature granulocytes, basophils < 5%, platelets < 450×10^9/L, and no palpable splenomegaly, typically achieved within the first months of TKI therapy (Hochhaus *et al.*, 2017).
2. **Cytogenetic response (CyR):** The reduction or elimination of Ph+ metaphases in BM cells is assessed through the CyR, typically through chromosome banding analysis (CBA) or fluorescence *in situ* hybridization (FISH). CyR is categorized into different levels based on the percentage of cells with Ph+ metaphases detected: **minimal CyR**, **minor CyR**, **partial CyR** (**PCyR**) and **complete CyR** (**CCyR**) (A. Hochhaus *et al.*, 2017).
3. **Molecular response (MR):** *BCR::ABL1* mRNA levels are quantified using reverse transcription-quantitative polymerase chain reaction (RT-qPCR) relative to an internal

reference gene (e.g., *ABL1*, *GUSB*, *BCR)* and reported on the International Scale (IS), where 100% BCR::ABL1^{IS} represents the standard values for a pre-treatment CML patient. Patients are stratified into two MR categories (1) **major molecular response (MMR)** and (2) **deep molecular response (DMR):** further divided into **MR4**, **MR4.5** and **MR5** (Hochhaus *et al.*, 2017; White *et al.*, 2022).

Although CML is never considered fully "cured", achieving the deepest level of DMR means the disease becomes virtually undetectable. In fact, patients who reach and sustain DMR may be eligible for treatment-free remission (TFR), which is the closest concept to a functional cure (**Figure 9**) (Jabbour and Kantarjian, 2024).

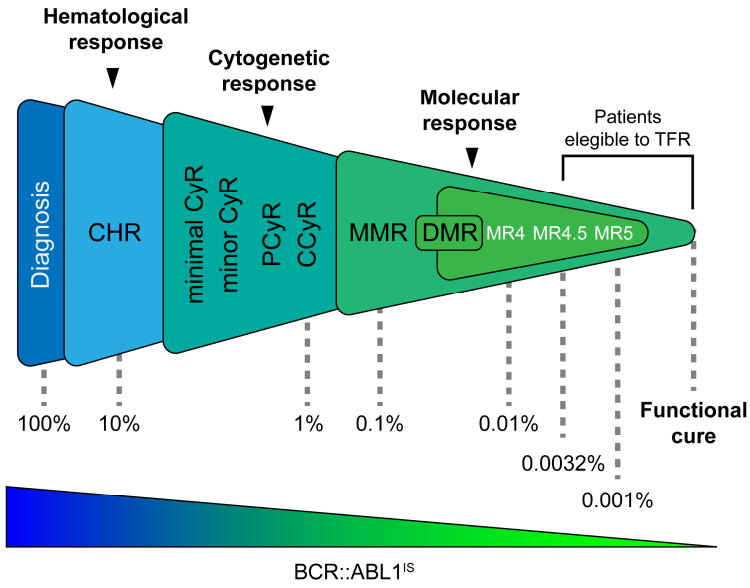

Figure 9. A proper therapeutic response in chronic myeloid leukemia (CML) can ultimately lead to a functional cure. Patients who achieve sustained deep molecular responses (DMR) may become eligible for treatment-free remission (TFR). In this state, tyrosine kinase inhibitors (TKIs) are discontinued, yet patients are able to maintain undetectable *BCR::ABL1* transcript levels for several years without ongoing therapy. Achieving and maintaining this condition represents a functional cure of CML. The estimated percentages of *BCR::ABL1* transcripts in each phase are shown, relative to the International Scale (IS) used in CML response monitoring guidelines. CHR: complete hematological response, PCyR/CCyR: partial/complete cytogenetic response, MMR: major molecular response.

Since the 2010s, studies on treatment discontinuation in CML patients with sustained DMR have demonstrated that TKI withdrawal is a viable option. The Stop Imatinib trial evaluated the risk of relapse in patients who had maintained DMR on imatinib for over two years before discontinuing treatment. The trial concluded that a subset of these patients could achieve TFR, as imatinib could be safely discontinued in those with hardly detectable

BCR::ABL1 levels (Mahon *et al.*, 2010). This finding raised the possibility that some CML patients could potentially be “cured” with TKIs.

1.4.3. HSC transplantation and emerging therapeutic strategies

Allogeneic hematopoietic stem cell transplantation (allo-HSCT), considered the definitive therapy for CML more than 20 years ago, has become a less common option with the advent of TKIs, which are now the first-line treatment for this disease. However, it remains essential for certain patients, particularly those who do not respond to TKIs or progress to a more aggressive disease phase (Radich, 2016). Each year, around 1-2% of CML patients develop resistance to many TKIs and thus require allo-HSCT as part of their treatment. For example, patients with the T315I mutation, which confers resistance to most TKIs, may require allo-HSCT if they fail to respond to ponatinib or asciminib. In fact, for patients who do not achieve CCyR even with continuous TKI treatment, allo-HSCT is one of the potential long-term survival options (Elmakaty *et al.*, 2024). Additionally, it remains a valuable approach for patients who have progressed to the AP or BP and need more intensive treatment, considering that TKIs are typically ineffective in these clinical phases (Saußele and Silver, 2015; Jabbour and Kantarjian, 2024).

Besides TKIs and, to a lesser extent allo-HSCT, which constitute the main treatment options for CML, emerging research has begun to reveal novel strategies aimed at treating or even curing this neoplasm by targeting the LSCs:

- **Combination therapies**: TKIs can be combined with drugs targeting key oncogenic pathways beyond BCR::ABL1, such as IFN-α (immune modulation), BCL-2 inhibitors (apoptosis induction), JAK2 inhibitors (blocking JAK/STAT signaling), PPAR-γ agonists (promoting LSC differentiation and TKI sensitization) (Mu *et al.*, 2021) or modulators of ROS production through inhibition of NADPH oxidases (Sánchez-Sánchez *et al.*, 2014) or xanthine oxidoreductases (Romo-González *et al.*, 2022), among others.
- **Immunotherapy:** Approaches like PD-1/CTLA-4 checkpoint inhibitors, CAR-T cells, and BCR::ABL1-targeted vaccines aim to eliminate LSCs and overcome resistance. IFN-α is also being repurposed to support TFR in TKI-treated patients (Yang *et al.*, 2020; Hsieh *et al.*, 2021).
- **Small-interfering RNAs (siRNA):** Targeting BCR::ABL1 mRNA could reduce fusion gene expression and bypass TKI resistance, although delivery and off-target immune effects remain challenges (Jyotsana *et al.*, 2019).
- **BCR::ABL1 degraders**: Proteolysis-targeting chimeras (PROTACs) have emerged as a promising strategy. These molecules recruit E3 ubiquitin ligases to

degrade BCR::ABL1, overcoming resistance caused by kinase mutations and representing a promising clinical strategy (Li and Song, 2020; Lim *et al.*, 2023).

- **Genome editing:** CRISPR-Cas9 can be designed to directly disrupt *BCR::ABL1* oncogene, correcting the genetic basis of CML (García-Tuñón *et al.*, 2017). Using this approach, preclinical studies in transgenic mice have shown that *ex vivo*-edited LSCs can restore normal hematopoiesis after transplantation (Vuelta *et al.*, 2021).

2. C3G: a guanine nucleotide exchange factor of Rap1

In humans, the protein C3G is encoded by the *RAPGEF1* gene, located on chromosome 9 at the q34.3 region (Takai *et al.*, 1994). C3G primarily functions as a GEF for specific small GTPases of the Ras superfamily, mainly Rap1 (Gotoh *et al.*, 1995), and to a lesser extent Rap2 (Ohba *et al.*, 2000b), R-Ras (Gotoh *et al.*, 1997), and TC-21 (Ohba *et al.*, 2000a). However, C3G can also act through Rap1-independent mechanisms, likely involving regions of the protein outside the GEF domain (Guerrero *et al.*, 1998, 2004).

C3G is ubiquitously expressed in both fetal and adult tissues (Tanaka *et al.*, 1994; Guerrero *et al.*, 1998). Importantly, its absence is lethal from embryonic day 7.5 in whole-body C3G-knockout (KO) mice, probably due to its critical role in cell adhesion and spreading of embryonic fibroblasts during early mouse embryogenesis (Ohba, 2001).

2.1. Structural domains

C3G was first identified as a guanine nucleotide-releasing protein (GNRP) that binds to the SH3 domain of Crk through a region containing a proline-rich sequence. It was initially named "Crk SH3-binding GNRP", which led to the abbreviation C3G (Tanaka *et al.*, 1994). The C3G sequence shares high similarity with Cdc25 and SOS proteins; however, it differs in substrate specificity, showing a strong preference for Rap1A and Rap1B, the two isoforms of Rap1 (Gotoh *et al.*, 1995).

In humans, at least three different isoforms of C3G have been described (**Figure 10A**) (Radha *et al.*, 2011), and additional shorter transcripts have also been detected (Guerrero *et al.*, 1998). Alternative splicing generates two 140-kDa isoforms (sometimes referred as to p140C3G), A and B, which differ at the N-terminus: isoform A contains three amino acids that are replaced by 21 amino acids in isoform B (Radha *et al.*, 2011). Interestingly, a third shorter isoform of 87 kDa, known as p87C3G, has been associated with CML since it has been detected in patients and CML cell lines. The main difference between the p140C3G and p87C3G isoforms is that the latter lacks the first 305 amino acids of the N-terminus (Gutiérrez-Berzal *et al.*, 2006).

In mice, two ubiquitously expressed isoforms of C3G have also been identified, resulting from the alternative splicing of a 114-base-pair exon located in the N-terminus (**Figure 10B**). Notably, mouse *Rapgef1* cDNA shares 88% nucleotide identity with its human counterpart, suggesting a high degree of evolutionary conservation (Zhai *et al.*, 2001).

The full-length C3G protein consists of three well-defined domains (**Figure 10**):

(1) The **N-terminal domain (NTD)** of C3G contains a E-cadherin-binding domain (EBD). E-cadherin, a key protein involved in epithelial cell-cell adhesion, can recruit C3G to contact sites and activate Rap1. The C3G–Rap1 signaling pathway is essential for the proper localization of E-cadherin at developing cell-cell junctions (Hogan *et al.*, 2004).

(2) The **central region** of C3G contains the SH3-binding domain, which includes five proline-rich motifs, designated P0 to P4 (Knudsen *et al.*, 1994). This domain mediates interactions with various proteins via their SH3 domains, including Crk (Tanaka *et al.*, 1994), Hck (Shivakrupa *et al.*, 2003), ABL1 (Radha *et al.*, 2007), and p130Cas (Kirsch *et al.*, 1998). Notably, the p87C3G isoform lacks the P0 and P1 motifs, altering its interaction profile and possibly conferring selectivity toward BCR::ABL1 (which preferentially binds to P2) over CrkL, which can engage multiple proline-rich regions (Gutiérrez-Berzal *et al.*, 2006). This central region also contains the autoinhibitory region (AIR), which, together with the NTD, plays a key role in regulating C3G activity (Carabias *et al.*, 2020).

(3) The catalytic domain is located at the **C-terminus** and can be further subdivided into two well-characterized regions: the Ras exchanger motif (REM) and the Cdc25 homology domain (Cdc25HD), which is named after its similarity to the catalytic domain of the Cdc25 protein, a GEF for Ras in yeast (Bos *et al.*, 2007).

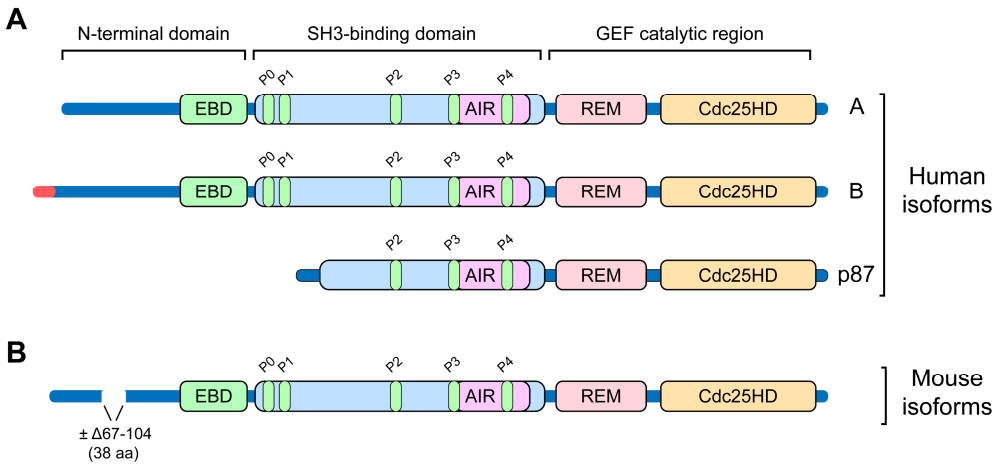

◄ Figure 10. Structural domains of C3G protein in the main human and mouse isoforms. (**A**) The human isoforms A and B differ in a short sequence within the N-terminal domain (NTD). The p87 isoform, which is expressed in CML samples and cell lines, lacks the NTD, as well as the P0 and P1 sites of the SH3-binding domain. (**B**) Two mouse isoforms, one with and one without 38 amino acids (aa) in the NTD, are expressed. EBD: E-cadherin-binding domain, P0-P4: polyproline motifs, AIR: autoinhibitory region, REM: Ras exchanger motif, Cdc25HD: Cdc25 homology domain.

2.2. Regulation and function

The transcriptional and translational regulation of the *RAPGEF1* gene remains poorly characterized, and currently, limited information is available. One known regulatory mechanism occurs at the post-transcriptional level through the above-mentioned alternative RNA splicing, which regulates isoform diversity and may allow adaptation to different cellular contexts (Zhai *et al.*, 2001). Moreover, different C3G isoforms show distinct expression patterns across tissues and developmental stages, with significant differences between embryonic and adult organs (Verma *et al.*, 2024).

C3G activation is regulated by phosphorylation at Y504, which can be mediated by various kinases, including Src (Ichiba *et al.*, 1999). In addition, C3G activity can also be stimulated by Crk proteins, which bind to its proline-rich motifs and modulate its function by relieving autoinhibition and promoting membrane localization (Rodríguez-Blázquez *et al.*, 2023). This autoinhibition under resting conditions is maintained by two distinct intramolecular mechanisms involving specific C3G domains. First, the AIR interacts with the catalytic Cdc25HD, thereby preventing GEF activity. This autoinhibitory interaction can be disrupted by CrkL binding, which relieves the inhibition and promotes activation. Second, the NTD interacts with the REM domain, a binding required for full GEF activity. Release of inhibition, through CrkL binding or tyrosine phosphorylation, enables C3G to become fully active (Carabias *et al.*, 2020).

When activated, C3G primarily functions as a GEF, activating small GTPases like Rap1 by facilitating the exchange of GDP for GTP. In simpler terms, small GTPases act as molecular switches, being "off" when bound to GDP and "on" when bound to GTP. GEFs promote the release of GDP from the inactive GTPase, allowing the now nucleotide-free GTPase to spontaneously bind GTP, which is far more abundant than GDP in the cytoplasm. On the other hand, the opposite reaction is mediated by GTPase-activating proteins (GAP), which deactivate small GTPases by promoting the hydrolysis of GTP to GDP (Bos *et al.*, 2007). The small GTPase Rap1 can be activated by various GEFs, including C3G, Epac, and CalDAG-GEFI; and deactivated by GAPs, such as SIPA1, RapGAP, and E6-TP1 (**Figure 11**) (Jaśkiewicz *et al.*, 2018).

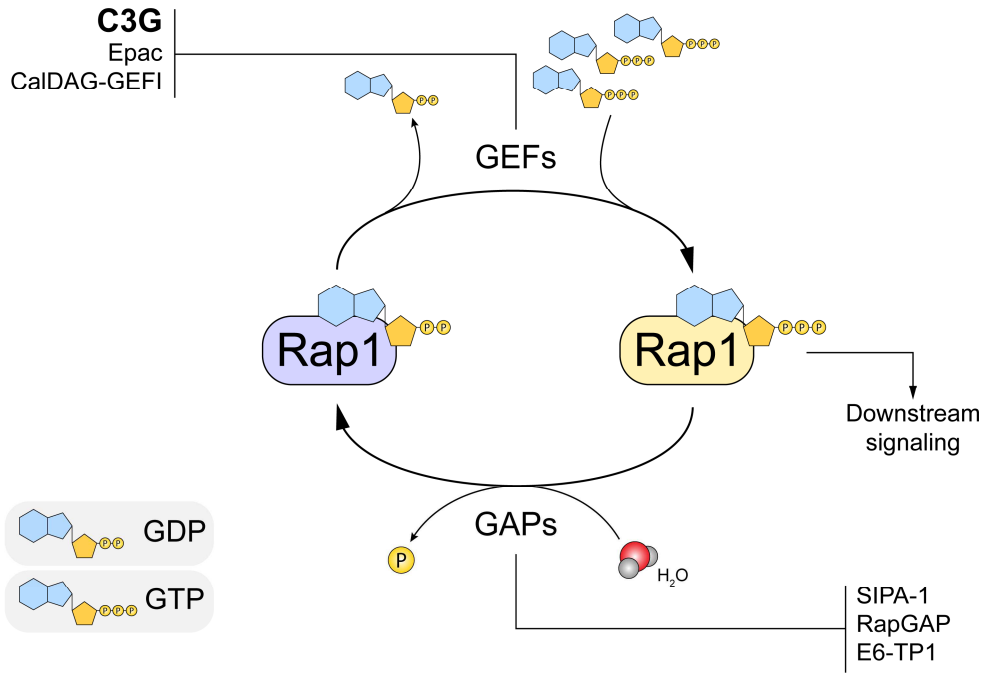

Figure 11. C3G functions primarily as a guanine nucleotide exchange factor (GEF) for the small GTPase Rap1. C3G, Epac, and CalDAG-GEFI promote the release of GDP from inactive Rap1-GDP. The higher cytoplasmic concentration of GTP allows its spontaneous binding to nucleotide-free Rap1, leading to Rap1 activation and the initiation of downstream signaling. Conversely, GTPase-activating proteins (GAPs) such as SIPA1, RapGAP, and E6-TP1 catalyze GTP hydrolysis to GDP, returning Rap1 to its inactive state.

Small GTPases, such as Rap1, are central regulators of signal transduction, integrating diverse stimuli to generate specific cellular responses that may act synergistically or antagonistically. In its active, GTP-bound state, Rap1 undergoes a conformational change that allows interaction with multiple downstream effectors (Stork and Dillon, 2005). Through these interactions, Rap1 promotes integrin-mediated adhesion (Lafuente *et al.*, 2004), is involved in cytoskeleton dynamics (Radha *et al.*, 2007), modulates ERK1/2 signaling by either activating it through B-Raf or inhibiting via Raf-1 (Peyssonnaux and Eychène, 2001), antagonizes p38-MAPK signaling (McDermott and O'Neill, 2002), and attenuates PI3K/AKT-dependent survival pathways (Singh *et al.*, 2021).

One of the most well-characterized roles of C3G is the regulation of integrin signaling, cell adhesion, and migration, primarily through Rap GTPases. In this context, Rap1 serves as a central intermediary of integrin-mediated adhesion via "inside-out" signaling, in which intracellular signaling pathways can induce conformational changes in integrins to high-affinity states. Additionally, Rap1 is also engaged by "outside-in" signals from integrin-ligand interactions, which can amplify and stabilize adhesion (Uemura and Griffin, 1999;

Stork and Dillon, 2005). As mentioned earlier, in C3G-deficient mouse fibroblasts, impaired Rap1 activation leads to defective adhesion, delayed spreading, and faster migration, which can be rescued by active Rap1 GEFs, highlighting their importance in this cellular process (Ohba, 2001).

C3G has also been associated with cytoskeleton remodeling through multiple mechanisms. It controls actin dynamics via the activation of Rap1, but also Rac1 and Cdc42 (Radha *et al.*, 2007; Fernández-Infante *et al.*, 2024), which are important pathways involved in cell migration, morphology, and immune synapse formation. The C3G–CrkL–Rap1 complex also plays an important role in *v-Abl*-transformed cells by regulating actin-dependent morphological changes, particularly filopodia formation. In this context, the regulation of actin dynamics occurs independently of its GEF activity but requires ABL1 catalytic activity and N-WASP, a key protein in filopodia formation (Lee *et al.*, 2008).

C3G regulates cellular proliferation and differentiation through both Rap1-dependent and Rap1-independent mechanisms (Radha *et al.*, 2011). For instance, when localized to the membrane, C3G activates Rap1 and Ras, leading to ERK1/2 pathway activation and mimicking Ras overactivity, thereby promoting proliferation (Ishimaru *et al.*, 1999). Conversely, C3G can impair cell survival via Rap1-independent pathways, such as directly inhibiting p38-MAPK (Gutiérrez-Uzquiza *et al.*, 2010) or activating PP2A phosphatases, which suppress ERK1/2 signaling and consequently reduce both survival and proliferation (Martín-Encabo *et al.*, 2007).

2.3. C3G in normal and dysregulated hematopoiesis

C3G is expressed across a wide range of tissues and carries out context-dependent functions, while retaining core activities common to many cell types, including those in the hematopoietic system. By activating small GTPases, C3G regulates key hematological processes such adhesion, migration, immune signaling, vesicle trafficking, differentiation, and apoptosis (Radha *et al.*, 2011).

In hematopoietic cell lines, the CrkL–C3G complex is recruited following phosphorylation of scaffolding proteins such as c-Cbl, p130Cas, or Gab1, leading to downstream activation of Rap1 (Stork and Dillon, 2005). While an enhanced CrkL–C3G signaling is associated with increased adhesion and migration (Arai *et al.*, 1999), this process can be disrupted in leukemic cells, which display a reduced CrkL–C3G association. These observations underscore the importance of tight regulation of this pathway to prevent leukemogenic transformation (de Jong *et al.*, 1998). Similarly, constitutive activation of C3G in hematopoietic cell lines also elevates integrin expression, such as LFA-1, further influencing adhesion dynamics (Carabias *et al.*, 2020).

Rap1 activation exerts distinct effects across hematopoietic cell subtypes. In MKs and myeloid precursors, Rap1 signals through B-Raf to activate ERK1/2, promoting differentiation. In contrast, in T cells, which lack B-Raf, and in B cells, Rap1 inhibits ERK1/2 signaling, thereby reducing proliferation (Stork and Dillon, 2005; Morán-Vaquero *et al.*, 2026). Interestingly, whole-body Rap1-null mice are viable, and under homeostatic conditions they show no major differences in hematopoietic populations in either BM or spleen. However, Rap1-deficient HSPCs are hypersensitive to DNA damage, displaying impaired BM reconstitution after myeloablative stress such as total-body irradiation or treatment with the chemotherapeutic agent 5-fluorouracil (5-FU) (Khattar *et al.*, 2019).

In T cells, C3G phosphorylation at Y504 requires WAVE2, an actin-remodeling protein from the WASP family, indicating that C3G activation is linked to actin dynamics during T cell signaling (Nolz *et al.*, 2008). This is consistent with the crucial role of the CrkL–C3G–Rap1 axis in T cells, which regulates integrin-mediated adhesion to the extracellular matrix and stromal cells, essential for proper immune cell function (Katagiri *et al.*, 2002). In B cells, Rap1 activation drives integrin inside-out signaling, which is critical for development and activation by promoting adhesion and actin-dependent spreading (McLeod *et al.*, 2004). Interestingly, constitutive activation of C3G in B-cell lymphoma lines decreases proliferation and enhances apoptosis, while also disrupting Rac2-dependent adhesion. This imbalance increases cell motility and invasiveness, leading to greater metastatic dissemination *in vivo* (Morán-Vaquero *et al.*, 2026).

C3G has been proposed as a central regulator of hematopoiesis, given that altering C3G activity changes the balance of HSPC fate by modulating the interactions with the BM niche via altered responsiveness to certain niche factors (Imai *et al.*, 2019) or through MK and adipocyte differentiation (**Figure 12**) (Ortiz-Rivero *et al.*, 2018; Herranz *et al.*, 2025).

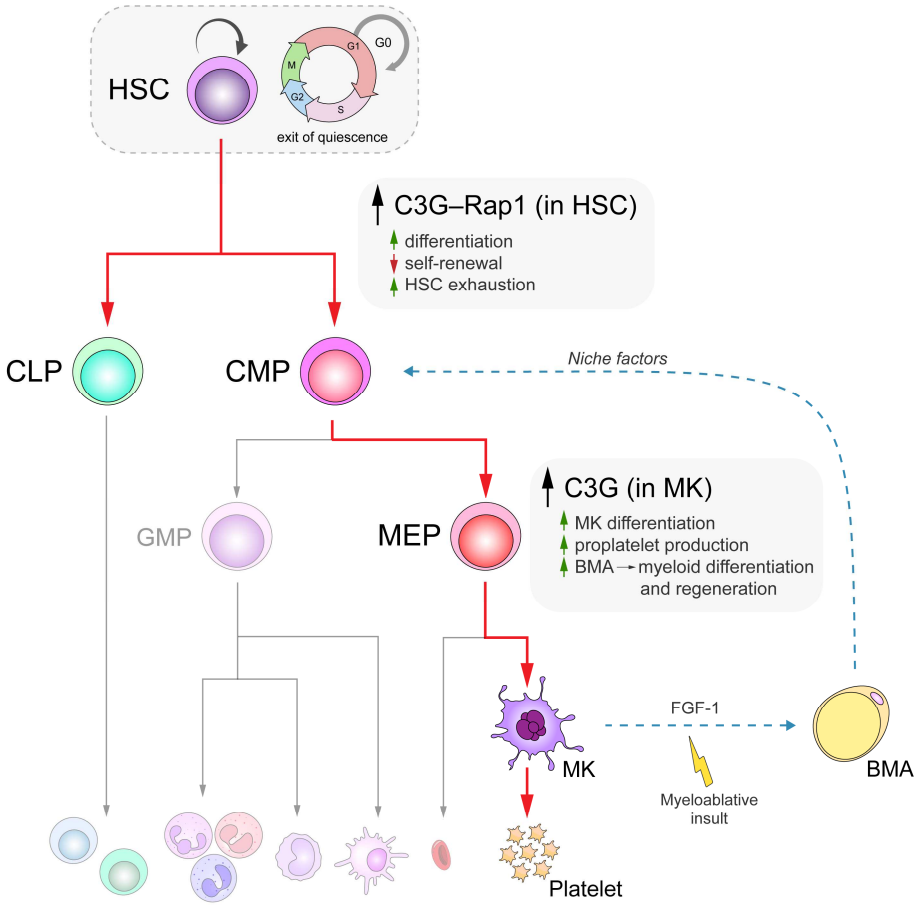

Figure 12. C3G regulates hematopoiesis at multiple levels. Sustained C3G–Rap1 signaling in hematopoietic stem cells (HSC) promotes exit from quiescence and favors differentiation, accompanied by a reduction in self-renewal potential that can lead to HSC exhaustion. In megakaryocytes (MK), C3G expression is associated with enhanced maturation and increased proplatelet formation. Moreover, following a myeloablative insult, C3G-overexpressing MKs engage in crosstalk with bone marrow adipocytes (BMA) through adipokines such as FGF-1, promoting adipocyte expansion within the bone marrow. In turn, these BMAs secrete niche factors that stimulate hematopoietic progenitor differentiation, contributing to myeloid regeneration. CMP: common myeloid progenitor, CLP: common lymphoid progenitor, GMP: granulocyte-monocyte progenitor, MEP: megakaryocyte-erythrocyte progenitor.

Basal activation status of Rap1 in HSPCs plays a crucial role in their maintenance within the BM niche. Sustained C3G activity, which leads to hyperactivation of Rap1, causes HSPCs to exhibit enhanced proliferation and differentiation in response to SCF and TPO, resulting in accelerated progenitor exhaustion, impaired long-term hematopoiesis, and defective BM reconstitution (Imai *et al.*, 2019). Consistent with this, mice deficient of one

of the main Rap1 GAPs, SIPA1, which also results in deregulated Rap1 activity, causes abnormal HSPC proliferation and a massive expansion of myeloid cells (Ishida *et al.*, 2003).

The role of C3G in hematopoietic differentiation has also been investigated in megakaryocytic lineages. Overexpression of C3G in MKs promotes their maturation, increasing the number of cells with high DNA content and upregulating differentiation markers. C3G-overexpressing MKs also display enhanced migration to the vascular niche and an increased capacity to form proplatelets (Ortiz-Rivero *et al.*, 2018). Following a myeloablative insult, C3G-overexpressing MKs influence hematopoietic reconstitution through interactions with bone marrow adipocytes (BMA), likely via adipokines such as FGF-1. Factors released by these adipocytes can enhance regeneration by favoring myeloid reconstitution, particularly in the MK and erythroid lineages (Herranz *et al.*, 2025).

2.3.1. C3G–Rap1 pathway in chronic myeloid leukemia

The central role of C3G in hematopoiesis suggests that it may contribute to the development of hematological malignancies characterized by disrupted hematopoietic homeostasis, such as leukemias. Consistent with this idea, dysregulation of Rap1 has been indirectly associated with hematological neoplasms (Stork and Dillon, 2005). On one hand, CalDAG-GEFI, another Rap1 GEF, has been identified as a proto-oncogene in BXH2 murine myeloid leukemia, where its aberrant activation supports the notion that Rap1 activation can drive oncogenesis in the myeloid lineage (Dupuy *et al.*, 2001). On the other hand, the Rap1 GAP *SIPA1* gene maps to 11q13, a chromosomal region frequently altered in cancer, suggesting that copy number or regulatory changes in *SIPA1* could also contribute to malignant transformation (Wada *et al.*, 1997). Indeed, the use of *SIPA1*-KO mice provided the first direct *in vivo* evidence for the oncogenic potential of Rap1 signaling dysregulation (Minato and Hattori, 2009).

Total-body SIPA1-deficient mice, although viable and normally developed, spontaneously develop myeloid disorders resembling human CML, including hematological abnormalities, splenomegaly, and leukemic blast infiltration in multiple organs (Ishida *et al.*, 2003). Moreover, transplantation of SIPA1-deficient BCR::ABL1^{+} HSPCs into immunodeficient mice led to faster disease progression with enhanced expansion of LSCs/HPCs, supporting a tumor-suppressive role for SIPA1 (Kometani *et al.*, 2006). Consistently, transplantation of HSPCs with hyperactivated Rap1, achieved through expression of a constitutively active farnesylated version of C3G combined with SIPA1 deficiency, resulted in the development of a T-ALL characterized by the expansion of abnormal CD4^{+}CD8^{+}CD3^{-}TCRβ^{-} thymocytes (Wang *et al.*, 2008).

In addition, SIPA1-deficient mice exhibit alterations in the BM niche, creating a dysregulated hematopoietic environment that favors the development of myeloproliferative

disorders, highlighting the importance of Rap1 signaling in both hematopoietic cells and BM microenvironment integrity (Xiao *et al.*, 2018). Interestingly, SIPA1 deficiency also triggers a host immune mechanism that eradicates transplanted BCR::ABL1^{+} HSPCs, revealing a protective role for SIPA1 in immune surveillance against leukemia and underscoring its multifaceted role in hematopoiesis (Xu *et al.*, 2018).

Beyond this, CrkL, an adaptor protein mentioned previously, is one of the most frequently tyrosine-phosphorylated proteins found in CML cells in patients (Nichols *et al.*, 1994; Oda *et al.*, 1994; ten Hoeve *et al.*, 1994). Its role in leukemia, however, has generally been attributed to its ability to recruit major protein complexes involved in leukemogenic signaling pathways, given that it lacks intrinsic enzymatic activity (Sattler and Salgia, 1998). Under normal conditions, C3G associates with CrkL, but this interaction is reduced in BCR::ABL1-expressing cells, likely because both proteins compete for CrkL binding (de Jong *et al.*, 1998). CrkL mediates the assembly of protein complexes containing C3G and BCR::ABL1, facilitating a hyperphosphorylated state within the complex. The resulting increase in phosphorylated C3G enhances downstream signaling through Rap1, suggesting a potential role for the BCR::ABL1–CrkL–C3G–Rap1 pathway in leukemogenesis (Cho *et al.*, 2005). Additionally, C3G has been shown to be phosphorylated by the Src family tyrosine kinase Hck (Shivakrupa *et al.*, 2003), which plays a positive role in BCR::ABL1-expressing cells by activating downstream targets that drive proliferation, survival, and cytoskeletal changes (Warmuth *et al.*, 1997).

As mentioned earlier, an 87-kDa isoform of C3G has been reported to be overexpressed in samples from CML patients as well as in the K562 CML cell line. This isoform, which lacks the NTD as well as the P0 and P1 polyproline motifs, is thought to preferentially bind BCR::ABL1 over Crk/CrkL, although this has not been experimentally confirmed. p87C3G is constitutively phosphorylated in CML cell lines in a BCR::ABL1-dependent manner, thereby activating downstream signaling and suggesting a direct contribution to leukemogenesis (Gutiérrez-Berzal *et al.*, 2006). C3G functionally interacts with p38-MAPK to modulate imatinib-induced apoptosis in K562 cell line. In this context, inhibition of the C3G–Rap1 pathway activates p38-MAPK, enhancing apoptosis, whereas overexpression of C3G promotes apoptosis via a Rap1-independent inhibition of the ERK and AKT pathways. These findings suggest that C3G can exert both pro-survival (**Figure 13A**) and pro-apoptotic (**Figure 13B**) effects depending on the cellular context and the specific signaling pathways engaged, effects that in this case are revealed by the apoptotic action of imatinib (Maia *et al.*, 2009).

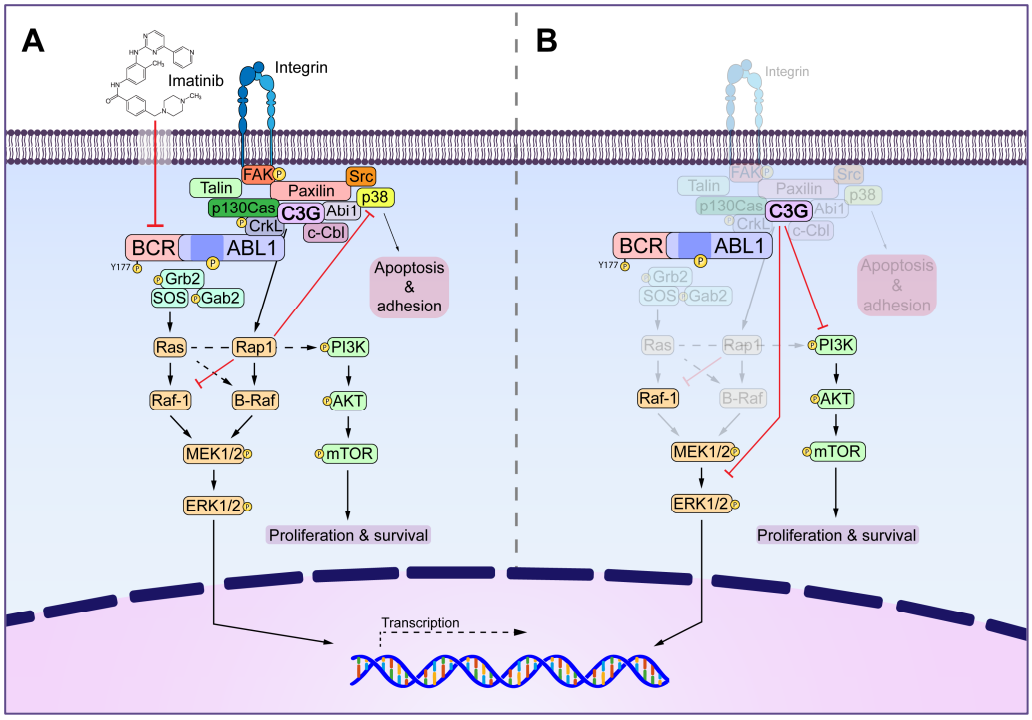

Figure 13. C3G modulates cellular dynamics in the CML cell line K562. C3G, particularly the p87 isoform, forms large multiprotein complexes with BCR::ABL1 and other adhesion-related proteins at focal adhesions in K562 cells, thereby promoting aberrant adhesion properties. In addition, C3G appears to play a dual role in these cells: (**A**) promoting cell proliferation and survival through Rap1-mediated activation of the ERK1/2 and PI3K/AKT pathways, while inhibiting pro-apoptotic signaling via suppression of p38-MAPK, and (**B**) repressing proliferation and survival through Rap1-independent inhibition of ERK1/2 and PI3K/AKT signaling.

Beyond its role in survival and apoptosis, C3G is also important for K562 cell adhesion. In these cells, BCR::ABL1 alters cytoskeletal function and impairs adhesion by interfering with focal adhesion (FA) proteins (Salgia *et al.*, 1996), thereby reducing their ability to adhere to specific stromal layers (Verfaillie *et al.*, 1992). C3G, and particularly its p87 isoform due to its higher abundance in these cells, interacts with BCR::ABL1 and becomes part of multiprotein complexes that include FA proteins such as CrkL, p130Cas, c-Cbl, and Abi1, among others (**Figure 13**). Interestingly, p38-MAPK also associates with these complexes, suggesting that p87C3G and p38-MAPK act within a common pathway regulating CML cell adhesiveness, in addition to their previously described roles. Among the C3G isoforms, p87C3G appears to dominate BCR::ABL1-FA interactions, promoting aberrant adhesion signaling, whereas full-length p140C3G likely exerts a more regulatory influence, helping to preserve balanced adhesion dynamics. Consistent with this, reduced p87C3G expression impairs CML cell adhesion to fibronectin, while increased C3G levels

lead to excessive or dysregulated FA assembly, ultimately resulting in abnormal adhesion (Maia *et al.*, 2013).

Apart from CML, alterations in C3G have also been linked, directly or indirectly, to other hematological disorders, including MPNs and lymphoid malignancies. MPNs are typically associated with mutations in three key genes: *JAK2*, *MPL*, and *CALR*. These genes encode proteins that act along the same signaling axis (TPO–MPL–JAK–STAT), whose aberrant activation results in cytokine-independent growth and excessive proliferation of hematopoietic progenitors, particularly those committed to the MK lineage (Soyfer and Fleischman, 2023).

Notably, the C3G–c-Cbl complex can be recruited to c-MPL upon TPO stimulation (Stork and Dillon, 2005), where it participates in receptor ubiquitination, internalization, and degradation (Hernández-Cano *et al.*, 2022), suggesting a potential role for C3G as a negative regulator of TPO signaling. Furthermore, in the HEL cell line (derived from a PV patient carrying the $JAK2^{V617F}$ mutation), C3G expression increases following stimulation with PMA, a compound used to promote MK differentiation (Ortiz-Rivero *et al.*, 2018), while C3G repression increases the levels of p-$JAK2^{V617F}$ (unpublished results from the group). Consistently, recent results indicate that C3G deficiency in HSPCs produces a phenotype resembling PV following 5-FU-induced myeloablation, potentially due to alterations in the TPO–c-Mpl signaling (Herranz Varea, 2024).

The prothrombotic state observed in MPNs appears to be partly driven by platelet-leukocyte aggregates (PLA), formed through interactions of platelets with neutrophils or monocytes via adhesion molecules (Oyarzún and Heller, 2019). Interestingly, overexpression of C3G in platelets enhances PLA formation, likely due to increased surface levels of adhesion molecules such as P-selectin and CD40L (Fernández Infante, 2023).

Regarding lymphoid malignancies, a few C3G alterations have been identified in patients. For example, C3G downregulation has been reported in CLL samples (Fernàndez *et al.*, 2008), while point mutations Y554H in follicular lymphoma (Green *et al.*, 2013) and M555K in diffuse large B-cell lymphoma (DLBCL) have also been described (Morin *et al.*, 2011). Importantly, these mutations disrupt C3G autoinhibitory mechanism, thereby causing aberrant constitutive activity (Carabias *et al.*, 2020).

Objectives

OBJECTIVES

Although chronic myeloid leukemia (CML) is genetically defined by the *BCR::ABL1* fusion oncogene, its biological behavior extends beyond this single alteration. Leukemic stem cells persist despite efficient BCR::ABL1 inhibition, relying on regulatory signaling networks that remain incompletely understood. How oncogenic signals are tuned in terms of intensity, timing, and feedback, and how these mechanisms govern hematopoietic stem and progenitor cells (HSPC) outcome, quiescence, and therapy resistance, are still open questions in CML biology.

Previous studies have shown that C3G regulates cell adhesion and proliferation in human CML cell lines and participates in BCR::ABL1 downstream signaling. *In vivo*, hematopoietic C3G has been implicated in differentiation, myeloid reconstitution, and modulation of HSPC fate under stress conditions.

Consequently, this study aims to further characterize the function of C3G in dysregulated hematopoiesis, as occurs in CML, and to clarify the mechanisms by which C3G modulates these processes. To achieve this, the following general objectives have been addressed:

1. To investigate the role of C3G in CML development using a p210-BCR::ABL1 transgenic mouse model with C3G ablation in the HSPC compartment.

2. To elucidate the cellular and molecular mechanisms by which C3G modulates BCR::ABL1-driven leukemic cell behavior.

3. To determine how C3G modulates cytokine-driven signaling pathways that contribute to the leukemic phenotype.

Objetivos

OBJETIVOS

Aunque la leucemia mieloide crónica (LMC) está definida genéticamente por el oncogén de fusión *BCR::ABL1*, su comportamiento biológico va más allá de esta única alteración. Las células madre leucémicas persisten a pesar de una inhibición eficaz de BCR::ABL1, apoyándose en redes de señalización reguladoras que todavía no se comprenden por completo. Cómo se ajustan las señales oncogénicas en términos de intensidad, temporalidad y retroalimentación, y cómo estos mecanismos regulan el destino, la quiescencia y la resistencia terapéutica de las células madre y progenitoras hematopoyéticas (HSPC), siguen siendo cuestiones abiertas en la biología de la LMC.

Estudios previos han demostrado que C3G regula la adhesión y la proliferación en líneas celulares humanas de LMC y participa en la señalización oncogénica de BCR::ABL1. *In vivo*, se ha demostrado la implicación de C3G en la diferenciación hematopoyética, la reconstitución mieloide y la modulación del destino de las HSPC bajo condiciones de estrés.

En consecuencia, este estudio tiene como objetivo caracterizar con mayor profundidad la función de C3G en la hematopoyesis desregulada, como ocurre en la LMC, y esclarecer los mecanismos mediante los cuales C3G modula estos procesos. Para ello, se han abordado los siguientes objetivos generales:

1. Investigar el papel de C3G en el desarrollo de la LMC utilizando un modelo murino transgénico p210-BCR::ABL1 con ablación de C3G en el compartimento de HSPC.

2. Elucidar los mecanismos celulares y moleculares mediante los cuales C3G modula el comportamiento de las células leucémicas impulsado por BCR::ABL1.

3. Determinar cómo C3G modula las vías de señalización inducidas por citocinas que contribuyen al fenotipo leucémico.

Methods

METHODS

1. Mouse models

Mice bearing the *Rapgef1* gene with intronic *loxP* sites flanking exons 17–21 (*Rapgef1*$^{flox/flox}$) (Shah *et al.*, 2016) were crossed with mice carrying a tamoxifen (TAM)-inducible Cre recombinase under the control of the hematopoietic Scl 3′ (HSC-*Scl*) promoter (HSC-*Scl*-CreER^{T}) (Göthert *et al.*, 2005). This cross generated hematopoietic progenitor-inducible C3G-KO mice (*Rapgef1*$^{flox/flox}$; HSC-*Scl*-CreER$^{T+/-}$) hereinafter referred to as C3G$^{HSC\text{-}Scl}$-KO, and its corresponding control littermates (*Rapgef1*$^{flox/flox}$; HSC-*Scl*-CreER$^{T-/-}$), referred to as C3G$^{HSC\text{-}Scl}$-wt. These mice were then crossed with *Tec*-p210 (hereinafter referred to as p210) transgenic animals, which express the *BCR::ABL1* p210 transgene under the control of the hematopoietic *Tec* promoter. p210 mice develop a myeloproliferative disease resembling human CML, characterized by marked granulocytic hyperplasia and thrombocytosis after a long latency period (Honda *et al.*, 1998). The resulting animals (*Rapgef1*$^{flox/flox}$; HSC-*Scl*-CreER$^{T+/-}$; *Tec*-p210$^{+/-}$) and their controls (*Rapgef1*$^{flox/flox}$; HSC-*Scl*-CreER$^{T-/-}$, *Tec*-p210$^{+/-}$) are hereinafter referred to as p210/C3G$^{HSC\text{-}Scl}$-KO and p210/C3G$^{HSC\text{-}Scl}$-wt, respectively. This triple-transgenic model enables the investigation of C3G deficiency in BCR::ABL1 p210-driven leukemogenesis. More details of the mice used are listed in **Table 3**.

Table 3. Mouse models used in this work. The table lists the common and officially standardized names of the genetically modified mice, their description, and the reference article in which they were first described.

Common name	Standardized name	Description	Reference
***Rapgef1*^{flox}**	C57BL/6N-Rapgef1tm(flox/flox)Wtsi/J	Floxed *Rapgef1* gene	Shah *et al*., 2016
HSC-*Scl*-CreER^{T}	C57BL/6-Tg(Tal1-cre/ERT)42-056Jrg/J	Transgenic expression of CreER^{T} under HSC-*Scl* promoter	Göthert *et al*., 2005
***Tec*-p210**	B6.Cg-Tg(Tec-p210 BCR/ABL1)1Homy	Transgenic expression of BCR::ABL1 p210 under *Tec* promoter	Honda *et al*., 1998

All mice were maintained on a 12-hour light/12-hour dark cycle with *ad libitum* access to food and water. In all experiments, age- and sex-matched controls were used. When possible, males and females were analyzed separately to identify sex-dependent effects.

2. Mouse genotyping

2.1. Murine genomic DNA isolation

At weaning, a small ear biopsy was clipped into 500 µL of lysis buffer (100 mM Tris-HCl pH=8.0; 5 mM EDTA pH=8.0; 200 mM NaCl; 0.2% SDS; and 0.25 mg/mL proteinase K (Roche, #3115887001)) and incubated overnight (o/n) at 55 °C in a water bath. The following day, samples were centrifuged at 12,000 × g for 10 minutes, and the supernatants were transferred to new tubes. DNA was precipitated by adding 900 µL of cold absolute ethanol and gently mixing. Tubes were centrifuged again at 12,000 × g for 10 minutes at 4 °C, and the resulting pellets were washed with 700 µL of cold 70% ethanol. After a final centrifugation step under the same conditions, tubes were left open to air-dry at room temperature (RT). DNA pellets were then resuspended in 200 µL of DNase-free water and stored at 4 °C for short-term or at −20 °C for long-term storage until use.

2.2. Amplification of DNA by polymerase chain reaction (PCR)

For genotyping, the genomic region containing the genetic alteration was amplified by polymerase chain reaction (PCR). The PCR mixture consisted of 1× reaction buffer, 0.2 mM of each dNTPs, 1.5 mM $MgCl_2$, 5% DMSO, 0.5 µM of each primer, and 0.05 U/µL Taq DNA polymerase (NZYTech, #MB35401). PCR conditions are listed in **Table 4**.

Table 4. PCR conditions used for mouse genotyping. The table lists the genetic features, the oligonucleotide sequences, and the cycling conditions for amplification. F: forward, R: reverse.

Genetic feature	Sequence (5'→ 3')	Cycle conditions
Rapgef1 **conditional alelle**	**Lox-F:** AGCCTGTTGGCAAGTTTGG **Lox-R:** CTGATGGAGAACCTAGCTGTGG	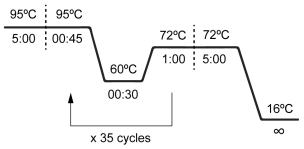
Rapgef1 **knockout alelle**	**Lox-F:** AGCCTGTTGGCAAGTTTGG **Int21-R:** GGACTGGAGCATCTTTCAG	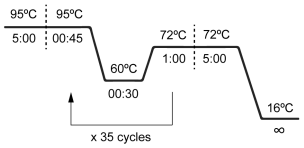
HSC-*Scl*-CreER^T transgene	**F:** TCGATGCAACGAGTGATGAG **R:** TTCGGCTATACGTAACAGGG	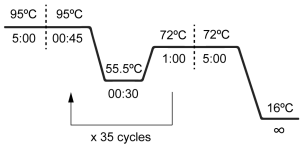
***Tec*-p210 transgene**	**F:** CCCTATGCTAGGCTCTGATG **R:** GCAACGTCTGCAGGTAGATC	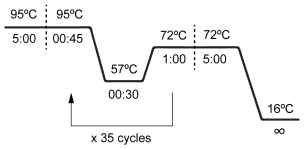

2.3. Agarose gel electrophoresis

PCR products were resolved by electrophoresis on 2% agarose gels containing 0.4 µg/mL ethidium bromide. For each sample, 10 µL of PCR products were mixed with 2 µL of 6× loading buffer (40% sucrose; 0.025% bromophenol blue) and loaded into the gel wells alongside the GeneRuler 1 kb DNA Ladder (Thermo Fisher Scientific, #SM0311) as a molecular weight marker. Electrophoresis was performed at a constant voltage of 120 V for 15-20 minutes. DNA bands were visualized using a Molecular Imager® Gel Doc™ XR+ System (Bio-Rad) under ultraviolet (UV) illumination.

3. Tamoxifen administration

The Cre-LoxP system enables targeted genetic manipulation in mouse models. In our model, exons 17 to 21 of the *Rapgef1* gene are flanked by LoxP sites (*Rapgef1*^{flox}), and the mice express a transgenic Cre recombinase, fused to the estrogen receptor (ER), in hematopoietic stem and progenitor cells (HSPCs). This fusion protein, CreER^{T}, remains inactive under basal conditions but is activated upon tamoxifen (TAM) administration, which induces its translocation to the nucleus (Schwenk *et al.*, 1998). This approach allows *Rapgef1* deletion to occur in a tissue-specific and temporally controlled manner.

Induction of the CreER^{T} recombinase was achieved by intraperitoneal (i.p.) injection of 5 mg of TAM (MedChemExpress, #HY-13757A) administered in three doses, spaced 24 hours apart (1.5, 1.5 and 2 mg, respectively). Each TAM dose was dissolved in 200 µL of corn oil (Sigma-Aldrich, #C8267) containing 10% DMSO. To control for potential off-target TAM effects, C3G$^{HSC\text{-}Scl}$-wt and p210/C3G$^{HSC\text{-}Scl}$-wt mice (lacking Cre expression) were also treated under the same conditions.

In most experiments, mice were TAM-injected at 1 month of age to induce early C3G deletion. In experiments examining the effect of C3G deletion on CML onset, corresponding to an average age of 6 months, TAM treatment was administered at 6 months of age (**Figure 14**).

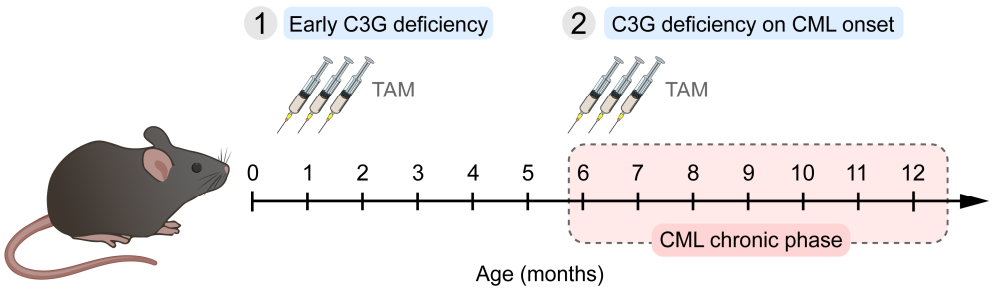

◄ Figure 14. Schematic representation of the experimental setup used to induce C3G deletion at different time points. Tamoxifen (TAM) was administered when mice were (1) one month old, to induce early C3G deficiency, or (2) six months old, to induce C3G deficiency at the onset of the chronic phase of chronic myeloid leukemia (CML).

4. 5-Fluorouracil treatment

To accelerate HSPCs turnover for the quantification of C3G expression levels, mild myeloablation was induced by 5-FU administration. 5-FU (Sigma-Aldrich, #F6627) was prepared in an aqueous solution containing 0.9% NaCl and 10% DMSO and dissolved by heating at 55 ºC with vigorous shaking for 15 minutes. Mice were injected i.p. with a sublethal dose of 150 mg/kg seven days after the first TAM injection.

5. Isolation of hematopoietic murine cells

5.1. From peripheral blood

Approximately 200 µL of peripheral blood (PB) were collected from mice by submandibular vein puncture into EDTA-coated tubes (Sarstedt, #41.1395.005). Erythrocytes were lysed by incubation in ACK buffer (0.155 NH_4Cl; 10 mM $KHCO_3$; 10 mM EDTA pH=7.4) for 15 minutes at 4 ºC, followed by two consecutive washes with 1× PBS (1% fetal bovine serum (FBS)), each with centrifugation for 5 minutes at 300 × g. The lysis step was repeated once more to ensure complete erythrocyte removal. After an additional wash with 1× PBS (1% FBS), cells were used for downstream applications.

5.2. From hematopoietic tissues

5.2.1. Bone marrow

Femurs and tibias were harvested from mice and washed in 1× PBS. The epiphyses were cut open, and the bones were placed in 0.5 mL tubes with a hole pierced at the bottom and nested into 1.5 mL tubes containing 100 µL of 1× PBS (1% FBS). BM was collected by centrifugation, allowing cells to pass through the holes into the 1.5 mL tubes. This centrifugation method has been described in detail in previous studies (Song *et al.*, 2024). Erythrocytes were lysed by incubation in ACK as described above. The resulting BM cells were resuspended in 1× PBS (1% FBS) and used for downstream applications.

5.2.2. Spleen

Spleens were harvested from mice and washed in 1× PBS (1% FBS). Each spleen was placed in a 50 mL tube fitted with a 70 µm cell strainer (PluriSelect, #43-50070-50) and mechanically dissociated. 1× PBS (1% FBS) was gently added to the strainer to facilitate passage of the cells into the tube, which was then centrifuged for 5 minutes at 300 × g.

Erythrocytes were lysed by incubation in ACK buffer as described above. The resulting spleen cells were resuspended in 1× PBS (1% FBS) and used for downstream applications.

5.2.3. Thymus

Thymuses were harvested from mice and washed in 1× PBS. Each thymus was placed in a 50 mL tube fitted with a 70 µm cell strainer and mechanically dissociated. 1× PBS (1% FBS) was gently added to the strainer to facilitate passage of the cells into the tube, which was then centrifuged for 5 minutes at 300 × g. A wash step with 1× PBS (1% FBS) was performed by centrifugation for 5 minutes at 300 × g. The resulting thymus cells were resuspended in 1× PBS (1% FBS) and used for downstream applications.

6. Flow cytometry analysis

Flow cytometry is a multiparametric technique that enables rapid, single-cell analysis based on light scattering and fluorescence detection (Manohar *et al.*, 2021). In this work, it was mainly used for immunophenotyping hematopoietic cells, allowing the identification and quantification of distinct populations according to lineage and differentiation marker expression. All flow cytometry analyses were performed using FlowJo v10.10.0 software.

6.1. Immunophenotyping of mature hematopoietic cells

Cell suspensions from PB or hematopoietic tissues were analyzed by flow cytometry using a BD Accuri™ C6+ flow cytometer (BD Biosciences) to determine the proportions of the different mature hematopoietic cell populations. Samples were stained with the appropriate antibody combinations listed in **Table 5**.

Table 5. Fluorescent conjugated antibodies used for immunophenotyping of mature hematopoietic cells. The table lists the target antigen, the conjugated fluorochrome, the cell type detected, the dilution used, and the reference (Supplier: BioLegend).

Target	Fluorochrome	Cell type	Dilution	Reference
B220 (CD45R)	FITC	B cell	1:100	103205
CD3	APC	T cell	1:100	100236
CD4	FITC	$CD4^+$ T cell	1:100	100509
CD8a	PE	$CD8^+$ T cell	1:100	100707
CD41 (GPIIb)	FITC	Platelet	1:200	133903
Gr1 (Ly6G/Ly6C)	FITC	Granulocyte	1:100	108405
Mac1 (CD11b)	PE		1:100	101207

6.1.1. Immunophenotyping of peripheral blood mononuclear cells

PB cells isolated as described in **Methods section 5.1** were resuspended in 50 µL of 1× PBS (1% FBS) containing the appropriate antibody cocktail for staining (**Table 5**) and incubated for 20 minutes at 4 ºC in the dark. Prior to acquisition in a BD Accuri™ C6+ flow cytometer, cells were centrifuged and resuspended in 100 µL of 1× PBS (1% FBS) containing 1 µg/mL

of propidium iodide (PI) to exclude dead cells. All centrifugation steps were performed at 300 × g for 5 minutes.

6.1.2. Determination of peripheral blood platelet levels

PB was obtained as described in **Methods section 5.1**. 15 µL of PB were washed with pre-warmed Tyrode's buffer (134 mM NaCl; 0.34 mM Na_2HPO_4; 2.9 mM KCl; 12 mM $NaHCO_3$; 5 mM glucose; 20 mM HEPES pH=7.4) containing 3% bovine serum albumin (BSA) and centrifuged for 5 minutes at 1,300 × g. The supernatant was discarded, and the pellet was resuspended in 800 µL of Tyrode's buffer with 3% BSA. 30 µL of this suspension were stained with FITC-CD41 (**Table 5**) for 20 minutes at RT in the dark. After a subsequent wash, the pellet was resuspended in 500 µL of Tyrode's buffer with 3% BSA, and 50 µL was analyzed on a BD Accuri™ C6+ flow cytometer. The number of $CD41^+$ platelets per microliter of blood was calculated accounting for the dilutions used throughout the procedure.

6.1.3. Immunophenotyping of infiltrated cells in hematopoietic tissues

Cell suspensions from BM (see **Methods section 5.2.1**), spleen (see **Methods section 5.2.2**), and thymus (see **Methods section 5.2.3**) were resuspended in 50 µL of 1× PBS (1% FBS) and stained with the corresponding antibodies listed in **Table 5** for 20 minutes at 4 ºC in the dark. Prior to acquisition in BD Accuri™ C6+ flow cytometer, cells were centrifuged at 300 × g for 5 minutes and resuspended in 100 µL of 1× PBS (1% FBS) containing 1 µg/mL of PI to exclude dead cells.

6.2. Immunophenotyping of bone marrow hematopoietic stem and progenitor cells

Cell suspensions from BM (see **Methods section 5.2.1**) were resuspended in 100 µL of 1× PBS (1% FBS) and stained with the antibody mix listed in **Table 6** for 25-30 minutes at 4 ºC in the dark. Afterward, cells were washed with 1× PBS (1% FBS) and centrifuged at 300 × g for 5 minutes and resuspended in 100 µL of 1× PBS (1% FBS). For analysis, one million events were acquired in a BD FACSAria III flow cytometer (BD Biosciences).

Table 6. Fluorescent conjugated antibodies used for immunophenotyping of bone marrow hematopoietic stem and progenitor cells (HSPC) subpopulations. The table lists the target antigen, the conjugated fluorochrome, the dilution used, and the supplier with reference.

Target	Fluorochrome	Dilution	Supplier	Reference
CD16/32 (FcγRIII/II)	PE/Cy7	1:133	BioLegend	101318
CD34	PerCP/Cy5.5	1:50	BioLegend	138608
c-Kit (CD117)	PE	1:333	BioLegend	105808
Flt-3/Flk-2 (CD135)	PE/CF594	1:50	BD Biosciences	562537
IL-7Rα (CD127)	BV™ 510	1:80	Biolegend	135033
Lineage (Lin) cocktail (CD3ε, Gr1, Mac1, B220, Ter-119)	FITC	1:133	BioLegend	133302
Sca1 (Ly6A/E)	APC	1:100	BioLegend	108112

Identification of HSPC subpopulations is more complex than the immunophenotyping of mature hematopoietic cells, whose marker profiles are generally more consistent across studies, likely because they are better characterized (Haas *et al.*, 2018). As discussed in **Introduction section 1.3.1**, multiple strategies have been used to identify HSPCs, depending on the specific markers selected for immunophenotyping. In this work, HSPC identification was performed following previous studies (Challen *et al.*, 2009; Cheng *et al.*, 2020), in which different subpopulations of stem and progenitor cells are defined using well-established surface markers (**Table 7**), allowing us to distinguish the main types of HSPCs for further analysis. The gating strategy used to identify the HSPC subpopulations is shown in **Figure 15**.

Table 7. Immunophenotype used for the characterization of hematopoietic stem and progenitor cell (HSPC) subpopulations. The table lists each HSPC subpopulation along with the markers used in this work to define its immunophenotype. Lin^-: lineage-negative population, LKS: Lin^- $c\text{-}Kit^+$ $Sca1^+$ cells, LT/ST-HSC: long-term/short-term hematopoietic stem cell, MPP: multipotent progenitor, CLP: common lymphoid progenitor, CMP: common myeloid progenitor, MEP: megakaryocyte-erythrocyte progenitor, GMP: granulocyte-monocyte progenitor.

HSPC subpopulation	Immunophenotype
Lin^-	Lin^-
LKS	Lin^- $c\text{-}Kit^+$ $Sca1^+$
LT-HSC	Lin^- $c\text{-}Kit^+$ $Sca1^+$ $CD34^-$ $Flt3^-$
ST-HSC	Lin^- $c\text{-}Kit^+$ $Sca1^+$ $CD34^+$ $Flt3^-$
MPP	Lin^- $c\text{-}Kit^+$ $Sca1^+$ $CD34^+$ $Flt3^+$
CLP	Lin^- $c\text{-}Kit^{low}$ $Sca1^{low}$ $Flt3^+$ IL-7Rα$^+$
CMP	Lin^- $c\text{-}Kit^+$ $Sca1^-$ $CD34^+$ CD16/32$^-$
MEP	Lin^- $c\text{-}Kit^+$ $Sca1^-$ $CD34^-$ CD16/32$^-$
GMP	Lin^- $c\text{-}Kit^+$ $Sca1^-$ $CD34^+$ CD16/32$^+$

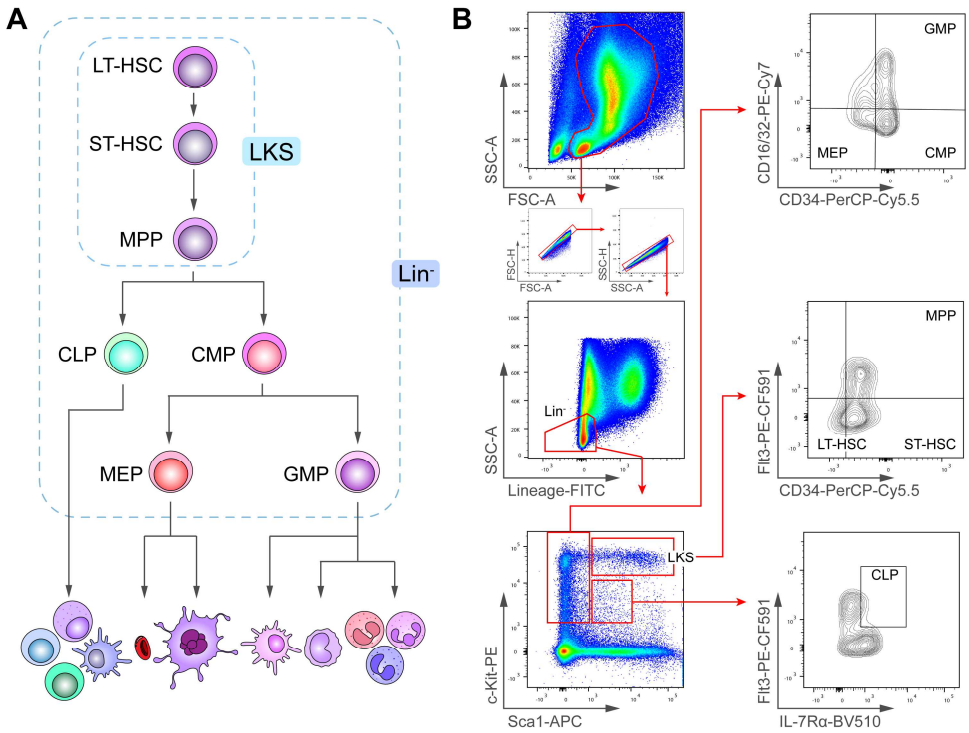

Figure 15. Identification of hematopoietic stem and progenitor cell (HSPC) subpopulations by flow cytometry. (**A**) Schematic representation of HSPC subpopulations within the hematopoietic hierarchy. Lineage-negative (Lin^-) cells correspond to bone marrow (BM) cells that lack mature lineage markers. Within this population, Lin^- c-Kit^+ $Sca1^+$ (LKS) cells represent the least-committed cells, including long- and short-term hematopoietic stem cells (LT/ST-HSC) and multipotent progenitors (MPP). Among the non-LKS Lin^- cells, the lymphoid branch is represented by common lymphoid progenitors (CLP), while the myeloid branch consists of common myeloid progenitors (CMP), which can further differentiate into megakaryocyte-erythrocyte progenitors (MEP) and granulocyte-monocyte progenitors (GMP). (**B**) Gating strategy used in the flow cytometry analysis. Gates were defined according to the immunophenotype of each HSPC subpopulation to determine the percentage of cells within the parent population.

7. Migration assay of bone marrow neutrophils

BM cells were isolated as described in **Methods section 5.2.1** and stained with FITC-Gr1 (1:100, BioLegend, #108405) and PE-Mac1 (1:100, BioLegend, #101207). A total of 1×10^6 stained BM cells were seeded in IMDM medium (Gibco, #12440053) on top of 5µm pore size Transwell® inserts (Corning, #3421). IMDM medium containing 0.1, 1.0, or 10.0 µM of the N-Formyl-Met-Leu-Phe (fMLP) peptide (Sigma-Aldrich, #F3506), used as a neutrophil chemoattractant, was added to the lower wells. As a positive control, 1×10^6 cells were seeded directly into IMDM without an insert. As a negative control, a well with an insert was used without fMLP in the lower compartment. After incubation for 1 hour at 37 °C, cells from the lower compartment were collected. BM neutrophils ($Gr1^+Mac1^+$) were

quantified using a BD Accuri™ C6+ flow cytometer, and results were expressed relative to the total number of neutrophils in the positive control of each genotype.

8. Imatinib treatment

Mice approximately 10 months old with established disease were treated with imatinib. The drug (MedChemExpress, #HY-15463) was dissolved in a solution of 90% PEG800 and 10% DMSO and administered orally at a dose of 100 mg/kg following a 5-days-on, 2-days-off regimen for 1 month, as used in other works (Tanaka *et al.*, 2020).

9. Cell lines

In this work different cell lines have been used (**Table 8**), whose main characteristics and culture conditions are described below.

Table 8. Cell lines used in this work. The table lists the name of each cell line, the organism of origin (including mouse strain when applicable), the cell type, and the corresponding Cellosaurus identifier.

Cell line	Organism	Cell type	Identifier
Ba/F3	Mouse (C3H)	Pro-B	CVCL_0161
Ba/F3-p210	Mouse (C3H)	Pro-B transformed with *BCR::ABL1 p210*	CVCL_UE63
32D	Mouse (C3H)	Myeloblast-like	CVCL_0118
WEHI-3	Mouse (BALB/c)	Myelomonocytic leukemia	CVCL_3622
HEK-293T	Human	Embryonic kidney	CVCL_0063

9.1. Ba/F3

Ba/F3 is an IL-3-dependent murine pro-B cell line (Palacios and Steinmetz, 1985). Although it was initially reported to be derived from the BALB/c mouse strain, SNP array analysis later identified a C3H strain background (Didion *et al.*, 2014). Transformation of these cells with the *BCR::ABL1 p210* oncogene confers IL-3 independence, providing a robust cellular model to study BCR::ABL1 function (Sánchez-García and Grütz, 1995). The resulting Ba/F3-p210 cells, also referred to as Boff-p210 (Gutiérrez-Berzal *et al.*, 2006), express the *BCR::ABL1 p210* gene under the control of a Tet-off system, allowing suppression of its expression in the presence of tetracycline or doxycycline. Ba/F3 were cultured in RPMI (Gibco, #11875093) supplemented with 10% FBS (Gibco, #A5256701), 10% WEHI-3 conditioned medium (CM) (see **Methods section 10**), 1% glutamine (Gibco, #25030-024), and 1% penicillin-streptomycin (Gibco, #15140-122). Ba/F3-p210 cells were cultured under the same conditions but without IL-3 supplementation.

9.2. 32D

32D is an IL-3-dependent, myeloid-committed murine hematopoietic progenitor cell line derived from long-term BM cultures of a C3H mouse infected with the Friend leukemia

virus (Heard *et al.*, 1986). These cells can respond to G-CSF, initiating a neutrophilic differentiation program (Nakajima and Ihle, 2001). 32D cells were cultured in RPMI supplemented with 10% FBS, 10% WEHI-3 CM, 1% glutamine, and 1% penicillin–streptomycin.

9.3. WEHI-3

WEHI-3 is a semi-adherent cell line originally established from a myelomonocytic leukemia found in a BALB/c mouse (Metcalf *et al.*, 1969). These cells secrete IL-3 into the culture medium (Lee *et al.*, 1982), which can be collected and used to support the growth of IL-3-dependent cell lines such as Ba/F3 and 32D (see **Methods section 10**). WEHI-3 cells were cultured in RPMI supplemented with 10% FBS, 1% glutamine, and 1% penicillin–streptomycin.

9.4. HEK-293T

HEK-293T are adherent cells derived from human embryonic kidney epithelial cells. They were generated by stably transfecting HEK-293 cells with a plasmid encoding the SV40 large T antigen, which enhances their capacity for high-efficiency transfection (DuBridge *et al.*, 1987). For this reason, HEK-293T cells were used in this work to produce lentiviral particles carrying our genes of interest, which were subsequently used for transducing target cells. These cells were cultured in DMEM (Gibco, #41965039) supplemented with 10% FBS, 1% glutamine, and 1% penicillin–streptomycin.

10. Production of IL-3-rich WEHI-3 conditioned medium (CM)

Ba/F3 and 32D cells require IL-3 for proliferation and survival in culture; in its absence, they undergo apoptosis. WEHI-3 cells were therefore used as a source of this cytokine to generate IL-3-rich CM for supplementation of Ba/F3 and 32D culture media.

IL-3-rich supernatants were collected from WEHI-3 cultures in exponential growth phase, avoiding overgrown cultures as indicated by acidification of the medium (yellow color). Briefly, WEHI-3 cells were seeded at 2×10^5 cells/mL and cultured for 48 hours. Culture supernatants were then harvested, centrifuged at 300 × g for 5 minutes to remove cellular debris, filtered through a 0.22 µm filter, aliquoted, and stored at −80 °C until use.

11. Lentiviral transduction of cell lines

11.1. Lentiviral production and titration

Lentiviruses are a subtype of retroviruses that have been adapted for gene delivery. Lentiviral vectors have a long history in cell biology for transduction, particularly because they can efficiently deliver genes into both dividing and non-dividing cells, which was a

limitation for earlier retroviral vectors (Wolff and Mikkelsen, 2022). In this work, a second-generation lentiviral packaging system was used, comprising three different plasmids:

- **Lentiviral transfer plasmid**, which carries the gene of interest. In this study, two different lentiviral transfer plasmids were used: pLenti-C-mEGFP-IRES-BSD (Origene #PS100071; **Figure 16A–B**) and pLVTHM-mEGFP (Addgene #12247; **Figure 16C–D**). The pLenti vector was employed for C3G overexpression and encodes the gene of interest fused to GFP, resulting in the expression of a C3G–GFP fusion protein. In addition, it contains a blasticidin-resistance cassette used for the selection of successfully transduced cells. By contrast, the pLVTHM vector was used to silence C3G expression, as it allows direct cloning and expression of short hairpin RNA (shRNA) sequences. This plasmid lacks an antibiotic-resistance cassette and has been used in previous studies of the group (Ortiz-Rivero *et al.*, 2018).
- **Packaging plasmid** (psPAX2; Addgene #12260; **Figure 16E**), which provides the genes encoding the retroviral core polyprotein (Gag), reverse transcriptase (Pol), and regulatory proteins (Rev and Tat).
- **Envelope plasmid** (VSV-G; Addgene #14888; **Figure 16F**), which is necessary for the formation of lentiviral particles, as it encodes the G glycoprotein (VSV-G).

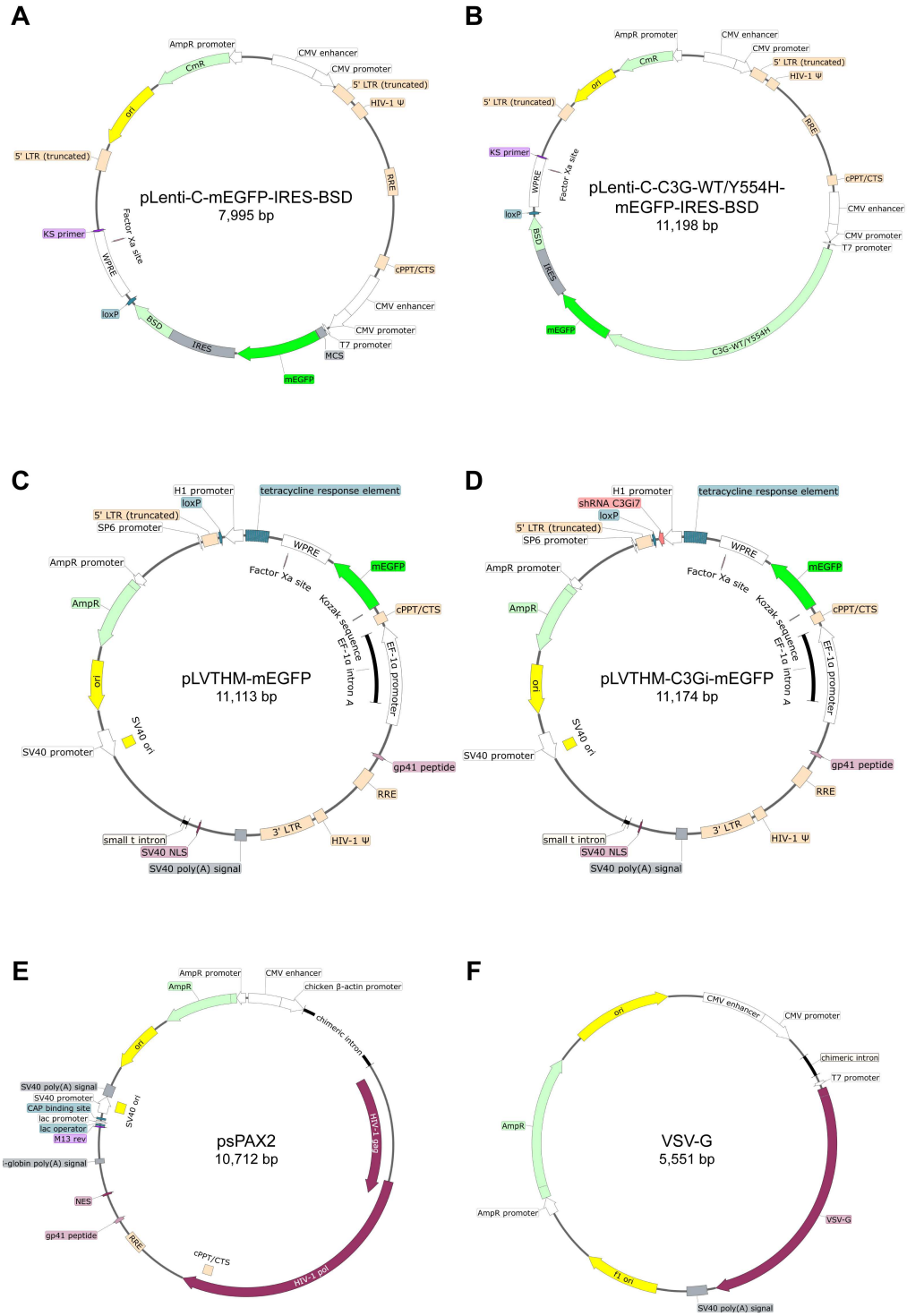
A
pLenti-C-mEGFP-IRES-BSD
7,995 bp
AmpR promoter
CmR
CMV enhancer
CMV promoter
5' LTR (truncated)
HIV-1 Ψ
ori
RRE
cPPT/CTS
CMV enhancer
CMV promoter
T7 promoter
MCS
mEGFP
IRES
BSD
loxP
WPRE
Factor Xa site
KS primer
B
pLenti-C-C3G-WT/Y554H-mEGFP-IRES-BSD
11,198 bp
C3G-WT/Y554H
C
pLVTHM-mEGFP
11,113 bp
H1 promoter
tetracycline response element
loxP
SP6 promoter
Kozak sequence
EF-1α intron A
EF-1α promoter
SV40 ori
SV40 promoter
gp41 peptide
3' LTR
small t intron
SV40 NLS
SV40 poly(A) signal
D
pLVTHM-C3Gi-mEGFP
11,174 bp
shRNA C3Gi7
E
psPAX2
10,712 bp
AmpR promoter
AmpR
chicken β-actin promoter
chimeric intron
SV40 poly(A) signal
CAP binding site
lac promoter
lac operator
M13 rev
β-globin poly(A) signal
NES
HIV-1 rev
HIV-1 pol
F
VSV-G
5,551 bp
f1 ori

◄ **Figure 16. Lentiviral plasmids used for viral production.** (**A-D**) Lentiviral transfer plasmids carrying our gene of interest. Overexpression of C3G was achieved using the pLenti-mEGFP plasmids: (**A**) empty, and (**B**) $C3G^{WT}$ / $C3G^{Y554H}$. Silencing of C3G expression was achieved using the pLVTHM-mEGFP plasmids: (**C**) empty, and (**D**) carrying the short hairpin RNA (shRNA) for C3G expression inhibition (C3Gi). (**E-F**) Lentiviral helper plasmids used for viral production. (**E**) psPAX2 was used as packaging plasmid and (**F**) VSV-G was used as envelope plasmid. Plasmid maps were generated using SnapGene v3.2.1 software.

Lentiviruses were produced in HEK-293T cells (see **Methods section 9.4**). Briefly, 6×10^6 cells were seeded in 100 mm tissue culture plates. The next day, the transfection mix (**Table 9**), previously incubated at RT for 25 minutes, was added to the plates. 24 hours after transfection, the medium was replaced with fresh medium and GFP expression was assessed by fluorescence microscopy using either an EVOS™ Imaging System (Thermo Fisher Scientific) or a Mateo Digital Microscope (Leica). Lentiviral supernatants were collected at 48 and 72 hours post-transfection. For concentration, the collected medium was transferred to a tube, and 1/3 volume of Lenti-X Concentrator (Clontech, #631231) was added, followed by incubation for at least 30 minutes at 4 °C. Supernatants collected on both days were then combined and centrifuged at 1,500 × g for 45 minutes at 4 °C. After centrifugation, the supernatant was removed, and the pellet was resuspended in 1/100 of the original volume using complete medium. The concentrated virus was divided into single-use aliquots and stored at –80 °C until use.

Table 9. Reagents used for the transfection mix in HEK-293T cells. Lentiviral transfer, packaging, and envelope plasmids were combined with polyethylenimine (PEI) (Polysciences, #24314) diluted in 150 mM NaCl.

Reagent	Amount
Lentiviral transfer plasmid (pLenti or pLVTHM)	9 µg
Packaging plasmid (psPAX2)	3 µg
Envelope plasmid (VSV-G)	5 µg
PEI	60 µL
NaCl (150 mM)	Up to 500 µL

Lentiviral aliquots were titrated to estimate the infectious units per milliliter (IFU/mL), a measure of the concentration of functional infectious viral particles capable of entering a target cell. For this, 8×10^4 HEK-293T cells per well were seeded into a 24-well plate and cultured for 24 hours. The next day, cells in triplicate wells were counted to estimate the number of cells per well, recording the average as **#cells plated**. The medium was then aspirated from the remaining wells, and fresh medium containing 8 µg/mL polybrene (Sigma-Aldrich, #107689) was added to each well. Different volumes of lentiviral aliquots were added to the wells, with one well maintained as a virus-free control. To facilitate viral transduction, spinoculation was performed by centrifuging the plates at 1,800 × g for 90 minutes at 32 °C. 24 hours after transduction, the medium was replaced with fresh medium. 72 hours post-transduction, cells were trypsinized and transferred into tubes

containing 1× PBS with 5 mM EDTA. The percentage of GFP^+ cells was analyzed by flow cytometry in a BD Accuri™ C6+ flow cytometer. Viral titer was calculated using only samples in which the percentage of GFP^+ cells ranged between 1–10%, using the following formula:

$$Infectious\ units\ per\ mL\ (IFU/mL) = \frac{\%\ GFP^+ \times \#cells\ plated \times 1000}{\mu l\ of\ viral\ suspension\ used}$$

11.2. Lentiviral transduction and selection

Lentiviral transduction of target cells was performed similarly in Ba/F3-p210 and 32D cells. The multiplicity of infection (MOI), which refers to the number of infectious units per target cell, was set to 1 for both cell lines. This MOI was sufficient to obtain 5–20% GFP^+ cells.

For transduction, 5×10^5 target cells per well were seeded into a 6-well plate in the corresponding medium containing 8 µg/mL polybrene, and the appropriate volume of viral concentrate was added. To enhance viral entry, spinoculation was performed by centrifuging the plates at 1,000 × g for 90 minutes at 32 °C. 24 hours later, the medium was replaced with fresh medium, and the cells were maintained in culture for expansion. In the case of the pLenti-transduced cells, 8 µg/mL of blasticidin (InvivoGen, #ant-bl) was added to the medium 48 hours post-transduction to enrich the GFP^+ population.

To isolate only the positively transduced cells, FACS was performed 72–96 hours post-transduction on a BD FACSAria III, selecting GFP^+ events within the live-cell gate. After sorting, blasticidin selection was maintained for at least 3 weeks in the pLenti-transduced cells to ensure stable maintenance.

12. Western blot analyses

12.1. Protein extraction

Cultured cells or isolated hematopoietic cells (see **Methods section 5**) were collected and lysed in 1× RIPA buffer (100 mM Tris-HCl pH=7.5; 100 mM NaCl; 1% Triton X-100; 1 mM EDTA; 0.1% sodium deoxycholate; 0.1% SDS; 1 mM Na_3VO_4; 25 mM NaF; 1 mM PMSF; 1× cOmplete™ protease inhibitor cocktail (Roche, #11697498001)) for at least 30 minutes on ice. To facilitate lysis, samples were briefly vortexed every 10 min. Next, samples were centrifuged for 10 min at 13,000 × g at 4 ºC, and supernatants were collected into new tubes. Protein lysates were then stored at –80 ºC until use.

12.2. Protein quantification

Protein concentrations were determined using the Bradford assay. Briefly, 1 µL of each lysate was mixed with 200 µl of Milli-Q water and 50 µl of Bradford reagent (0.25 mg/mL Coomasie Brilliant Blue G-250; 25% methanol; 42.5% H_3PO_4). After thorough mixing,

absorbance was measured at 595 nm using a TECAN Infinite M200 Pro microplate reader. Protein concentrations were calculated by interpolation from a standard curve generated with known concentrations of BSA.

12.3. Isolation of Rap1-GTP by pull-down assay

Active Rap1 (Rap1-GTP) was isolated by a pull-down assay based on the specific interaction between the GTP-bound form of the GTPase and its effector Ral-GDS. For this purpose, a plasmid encoding a fusion protein containing the Ras binding domain (RBD) of Ral-GDS fused to glutathione-S-transferase (GST) was used. The affinity of GST for Glutathione-Sepharose™ resin (ABT, #4B-GLU) allows selective isolation of Rap1-GTP. Briefly, cells were lysed in 1× RIPA for 30 minutes at 4 °C, and supernatants were collected after centrifugation for 10 min at 13,000 × g at 4 °C. A fraction of each sample was saved for total lysate analysis. The remaining lysate was incubated with purified GST-RalGDS-RBD (**Table 10**) and Glutathione-Sepharose™ resin, previously washed with 1× RIPA, for 1 hour at 4 °C with rotation. After incubation, resin was washed three times with 1× RIPA, and the bound fraction together with the saved lysates were used in the subsequent analysis.

Table 10. GST-fused protein used for pull-down assays. The table shows the construct used for Rap1-GTP purification and the plasmid, along with a brief description, target specificity, and source. GST: glutathione-S-transferase, RBD: Ras binding domain.

Construction	Plasmid	Description	Target	Source
GST-RalGDS-RBD	pGEX-4T3	Human RalGDS RBD (aa 701-852)	Active Rap1 (Rap1-GTP)	In-house generated. Details in Morán-Vaquero *et al*., 2026.

12.4. Polyacrylamide gel electrophoresis

Protein samples were prepared by mixing the appropriate volume of lysate with 4× Laemmli buffer (250 mM Tris-HCl pH=6.8; 40% glycerol, 8% SDS; 4% β-mercaptoethanol; 0.04% bromophenol blue) and heating for 5 minutes at 96 ºC. Samples were then loaded onto polyacrylamide-SDS gels, together with the molecular weight marker PageRuler™ Plus (Thermo Fischer Scientific, #26619). Gels containing 7.5-12% acrylamide were prepared depending on the molecular weight of the target protein. Electrophoresis was performed in running buffer (25 mM Tris-HCl pH=8.3; 200 mM glycine; 0.1% SDS) at a constant voltage of 70 V for 15 minutes, followed by 120 V for approximately 1 hour, until protein separation was complete.

12.5. Wet-transfer and membrane blocking

Gels were transferred onto 0.45 µm pore-size PVDF membranes (Merck, #IPVH00010) previously activated with methanol. Wet transfer was performed by submerging the gel–membrane cassettes in transfer buffer (25 mM Tris-HCl pH=8.3; 192 mM glycine; 20% methanol) and running at a constant current of 0.3 A for 2 hours at 4 °C using the Mini Trans-Blot® Cell system (Bio-Rad). Afterwards, membranes were blocked to reduce

nonspecific antibody binding by incubating them for 1 hour at RT in 5% non-fat dried milk prepared in TBS-T buffer (25 mM Tris-HCl pH=8.3; 50 mM NaCl; 2.5 mM KCl; 0.05% Tween-20 (Sigma-Aldrich, #P1379)).

12.6. Protein immunodetection and quantification

After blocking, membranes were rinsed with TBS-T and incubated with the corresponding primary antibody diluted in TBS-T containing 2% BSA (**Table 11, upper section**). Membranes were then washed three times, for 5 minutes each, to remove excess antibody and subsequently incubated with the appropriate secondary antibody diluted in TBS-T containing 2% of non-fat dried milk (**Table 11, lower section**). The secondary antibodies are fluorochrome-conjugated, allowing its detection in an Odyssey® M Imaging System (LICORbio).

Densitometric quantification of protein bands was performed using ImageJ analysis software. The signal intensity of each band was normalized to the total protein signal in the corresponding lane according to established methods (Westerberg *et al.*, 2025). In Western blot experiments analyzing the expression of a single protein (e.g., C3G), protein levels were normalized to an internal loading control, typically the housekeeping protein β-actin. When analyzing phosphorylated (p-) proteins, signals were normalized to the corresponding total protein levels (e.g., p-STAT5/total STAT5). In these cases, β-actin is shown as a qualitative loading control but was not used for quantification, as analysis was based exclusively on the phospho/total protein ratio.

Table 11. Antibodies used for Western blot. The table lists the antibody name, host species, dilution and incubation time, and supplier with reference. Primary antibodies shown in the upper section and secondary antibodies in the lower section. o/n: overnight, RT: room temperature, p-: phosphorylated.

Antibody	Host	Dilution	Incubation	Supplier	Reference
Primary antibodies					
ABL1	Mouse	1/1000	o/n 4 ºC	Santa Cruz Biotechnology	sc-23
p-ABL1	Mouse	1/1000	o/n 4 ºC	Santa Cruz Biotechnology	sc-293130
AKT1/2/3	Rabbit	1/1000	o/n 4 ºC	Santa Cruz Biotechnology	sc-8312
p-AKT1/2/3	Rabbit	1/1000	o/n 4 ºC	Cell Signaling Technology	9271
C3G (C-19)	Rabbit	1/1000	o/n 4 ºC	Santa Cruz Biotechnology	sc-869
C3G (G-4)	Mouse	1/1000	o/n 4 ºC	Santa Cruz Biotechnology	sc-17840
CrkL	Rabbit	1/1000	o/n 4 ºC	Santa Cruz Biotechnology	sc-319
p-CrkL	Rabbit	1/1000	o/n 4 ºC	Cell Signaling Technology	3181
ERK1/2	Rabbit	1/1000	o/n 4 ºC	Santa Cruz Biotechnology	sc-94
p-ERK1/2	Mouse	1/1000	o/n 4 ºC	Santa Cruz Biotechnology	sc-7383
GFP	Rabbit	1/1000	o/n 4 ºC	Santa Cruz Biotechnology	sc-8334
JAK2	Rabbit	1/1000	o/n 4 ºC	Cell Signaling Technology	3230
p-JAK2	Rabbit	1/1000	o/n 4 ºC	Cell Signaling Technology	3771

STAT3	Mouse	1/1000	o/n 4 ºC	Santa Cruz Biotechnology	sc-8019
p-STAT3	Rabbit	1/1000	o/n 4 ºC	Cell Signaling Technology	D3A7
STAT5	Mouse	1/1000	o/n 4 ºC	Santa Cruz Biotechnology	sc-74442
p-STAT5	Mouse	1/1000	o/n 4 ºC	Santa Cruz Biotechnology	sc-81524
	Mouse	1/3000	o/n 4 ºC	Invitrogen	MA5-47643
Rap1	Mouse	1/800	o/n 4 ºC	Santa Cruz Biotechnology	sc-398755
β-actin	Mouse	1/10000	1 h RT	Proteintech	66009-1-Ig
Secondary antibodies					
Anti-mouse IgG (H+L) DyLight™ 680	Goat	1/5000	1 h RT	Invitrogen	35518
Anti-mouse IgG (H+L) DyLight™ 800	Goat	1/5000	1 h RT	Invitrogen	35521
Anti-rabbit IgG (H+L) DyLight™ 680	Goat	1/10000	1 h RT	Invitrogen	35568
Anti-rabbit IgG (H+L) DyLight™ 800	Goat	1/10000	1 h RT	Invitrogen	10036

13. Cell culture analyses

13.1. Cell proliferation assay

Cell proliferation was assessed by counting live cells every 24 hours using the BD Accuri™ C6+ flow cytometer. For this, 1×10^5 cells per well were seeded in triplicate in 6-well plates, and samples were collected at 24-hour intervals for quantification. Only GFP-positive cells within the live-cell gate were counted. The cell counts at time 0 was used as a reference, and counts at subsequent time points were expressed relative to this initial value.

13.2. Evaluation of Ba/F3-p210 viability response to imatinib

For the analysis of Ba/F3-p210 cell viability in response to imatinib, 5×10^3 cells per well were seeded in 100 µL of culture medium in 96-well plates, with multiple replicates for each cell line. Imatinib was added at the desired concentrations. At 24, 48, and 72 hours after seeding, 10 µL of 5 mg/mL MTT reagent (Sigma-Aldrich, #M2128) was added to each well, except for the blank wells, and the plates were incubated at 37 °C for 2 hours. After incubation, the culture medium was removed, and the formazan crystals formed were solubilized in 100 µL of DMSO. Absorbance was then measured at 570 nm using a TECAN Infinite M200 Pro microplate reader. After subtraction of the blank, results were normalized to untreated cells at the corresponding time points.

13.3. Evaluation of imatinib-induced apoptosis in Ba/F3-p210

For apoptosis analysis of Ba/F3-p210 cells, imatinib concentrations close to the IC_{50} at 72 hours were selected for each generated line (pLenti lines: 0.6 µM; pLVTHM lines: 1.6 µM), and cells were treated for 72 hours. Apoptotic and/or dead cells were then assessed using the Apoptosis Detection Kit (ImmunoStep), following the manufacturer's instructions. Apoptotic responses were assessed using fluorochrome-labeled Annexin V, a protein that specifically binds phosphatidylserine, a lipid exposed on the outer leaflet of the plasma membrane during apoptosis (Vermes *et al.*, 1995). In combination with Annexin V, the DNA-intercalating dye 7-AAD was used to assess membrane integrity. 7-AAD cannot enter viable cells, but it penetrates cells with compromised membranes, binding DNA and rendering these cells fluorescent (Zembruski *et al.*, 2012). Cells positive for Annexin V but negative for 7-AAD (Annexin V^+ 7-AAD^-) were considered apoptotic.

13.4. Stimulation of 32D cells with G-CSF

To induce the neutrophilic differentiation program, 32D cells were stimulated with G-CSF, a cytokine that regulates the proliferation, differentiation, and survival of granulocyte precursors (Chakraborty and Tweardy, 1998).

Under basal conditions, 32D cells require IL-3 for survival, as it induces the expression of genes involved in cell survival and proliferation. Signal transduction triggered by both IL-3 and G-CSF is primarily mediated by the JAK/STAT pathway, although important differences exist between the two signaling programs. While both IL-3 and G-CSF receptors activate JAK2, the recruitment and activation of downstream STAT effectors differ in a cytokine receptor-dependent manner. In this context, IL-3 predominantly promotes STAT5 activation, driving the transcription of genes associated with proliferation and survival (Podolska *et al.*, 2024), whereas G-CSF preferentially signals through STAT3, inducing the expression of genes involved in granulocytic differentiation and maturation (Park *et al.*, 2022). These distinct signaling outputs underlie the ability of IL-3 to maintain 32D cells in a proliferative state, while G-CSF redirects them toward a neutrophil differentiation program (Zhang *et al.*, 2023). Although both IL-3 and G-CSF can activate the ERK1/2 and PI3K/AKT pathways, these pathways are predominantly engaged upon IL-3 stimulation to support cell survival and proliferation, whereas during G-CSF stimulation they play a more secondary role, mainly supporting cell survival throughout the neutrophil differentiation process (**Figure 17**) (Park *et al.*, 2022; Podolska *et al.*, 2024).

To analyze signaling pathway activation in 32D cells, cultures were stimulated with either IL-3 (as steady-state control) or G-CSF. Briefly, 32D cells were starved for 5 hours in IL-3-free RPMI medium supplemented with 0.5% FBS, 1% glutamine, and 1% penicillin-streptomycin. Subsequently, 3×10^6 cells were either treated with 10% IL-3 for 30 minutes

(control) or stimulated with 50 ng/mL of murine G-CSF (Thermo Fischer Scientific, #250-05) for 0, 5, 15, or 30 minutes. Cells were then placed on ice and rapidly lysed for protein analysis, as described in **Methods section 12.1**. Activation of STAT3, STAT5, ERK1/2 and AKT1/2/3 under the different experimental conditions was evaluated by Western blot.

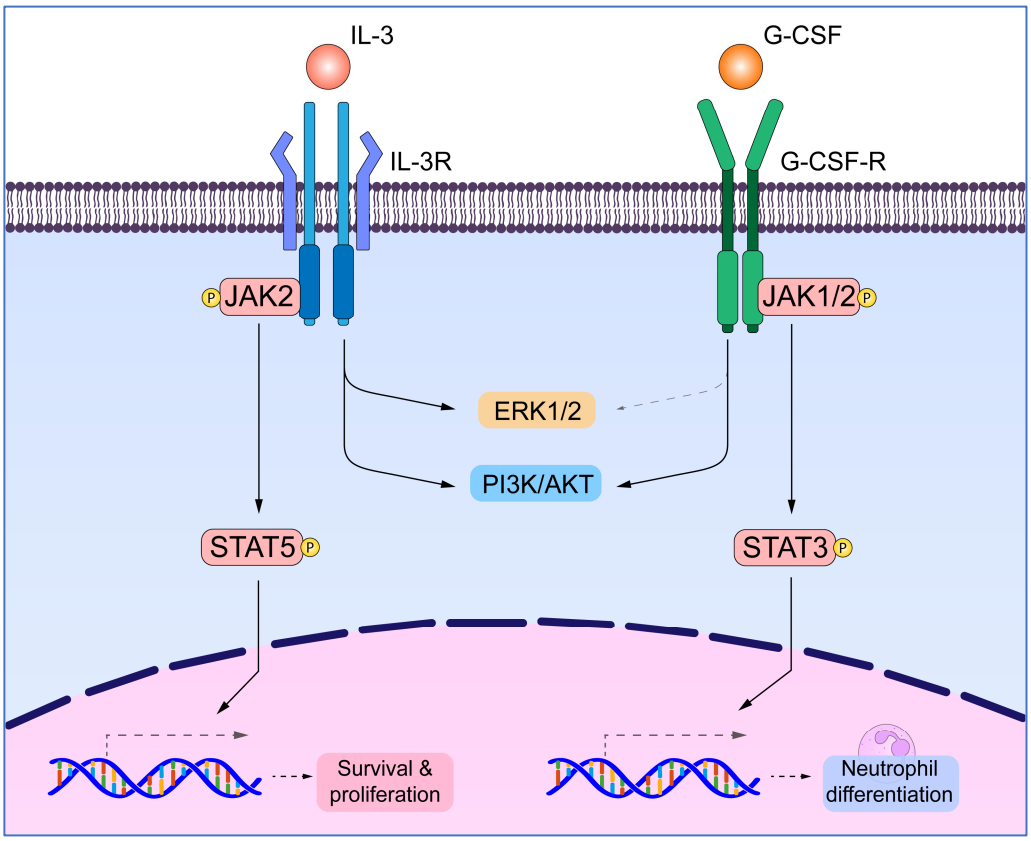

Figure 17. Schematic representation of the main signaling pathways activated by interleukin-3 (IL-3) and granulocyte colony-stimulating factor (G-CSF) in 32D cells. Stimulation of 32D cells with IL-3 maintains their proliferative state and supports cell growth. Upon binding to the IL-3 receptor (IL-3R), JAK2 is activated and subsequently phosphorylates STAT5, leading to the transcription of target genes involved in cell survival and proliferation. In parallel, IL-3 activates the ERK1/2 and PI3K/AKT pathways, further reinforcing the pro-survival and pro-proliferative phenotype. In contrast, G-CSF stimulation promotes a neutrophilic differentiation program in 32D cells. Binding of G-CSF to its receptor (G-CSF-R) activates JAK1 and JAK2, which preferentially signals through STAT3 rather than STAT5, inducing the expression of genes associated with neutrophil differentiation. G-CSF also activates the ERK1/2 and PI3K/AKT pathways, although to a lesser extent than IL-3, thereby supporting granulocytic maturation.

14. Statistical analysis

Unless otherwise specified, all results are presented as the mean ± standard error of the mean (SEM) from at least three independent biological replicates. Data normality was assessed

using the Shapiro-Wilk test. Comparisons between two groups were performed using two-tailed unpaired t-tests. Comparisons among three or more conditions involving two factors (e.g., genotype and time point) were performed using two-way ANOVA, followed by the appropriate post hoc test for multiple comparisons. Kaplan-Meier survival curves were analyzed using the log-rank test. In all cases, a p value ≤ 0.05 was considered statistically significant. All statistical analyses were performed using GraphPad Prism version 8.0.1.

15. Ethical considerations

All animal procedures were conducted in accordance with European guidelines (EU Directive 2010/63/EU) and the 3Rs principles (Replacement, Reduction, and Refinement) to ensure the ethical and humane use of laboratory animals. Measures were taken to minimize animal suffering, following established recommendations (Langford *et al.*, 2010). All experimental protocols were approved by the Committee on the Ethics of Animal Experimentation of the University of Salamanca (project no. 1097) and by the Council of Agriculture, Livestock and Rural Development of the Regional Government of Castilla y León, Spain.

Results

RESULTS

1. Effect of C3G deficiency in the development of chronic myeloid leukemia

1.1. Generation of a BCR::ABL1 p210 transgenic mouse model with C3G deletion on HSPCs

Despite studies in cellular models indicating a contribution of C3G to CML (Gutiérrez-Berzal *et al.*, 2006; Maia *et al.*, 2009, 2013), a comprehensive analysis of C3G role in disease development requires an *in vivo* model that closely mimics the human disease and allows modulation of C3G status. To this end, we generated and used a triple-genotype mouse model that (1) expresses the p210 isoform of *BCR::ABL1* transgene in HSPCs, (2) carries a TAM-inducible CreER^{T} recombinase in the same hematopoietic compartment, and (3) contains the *Rapgef1* gene floxed, enabling its excision upon TAM-induced Cre recombination. Therefore, four different mice groups were used in the following experiments: C3G$^{HSC\text{-}Scl}$-KO and C3G$^{HSC\text{-}Scl}$-wt as controls, without p210 expression; and p210/C3G$^{HSC\text{-}Scl}$-KO and p210/C3G$^{HSC\text{-}Scl}$-wt as CML mice, with p210 expression. More details of the mouse strains used are detailed in **Methods section 1**.

The floxed *Rapgef1* allele is inactivated upon Cre-mediated recombination through excision of exons 17–21 (**Figure 18A**), generating a knockout (KO) allele that encodes a defective C3G protein, resulting in impaired C3G activity, as previously described in other mouse models (Shah *et al.*, 2016; Gutiérrez-Herrero *et al.*, 2020; Hernández-Cano *et al.*, 2022; Fernández-Infante *et al.*, 2024; Herranz *et al.*, 2025). Seven days after TAM administration, *Rapgef1* deletion was detectable by PCR in genomic DNA from BM cells. In contrast, TAM administration in mice lacking CreER^{T} did not produce the *Rapgef1-KO* allele. The presence or absence of the p210 transgene did not interfere with this process (**Figure 18B**).

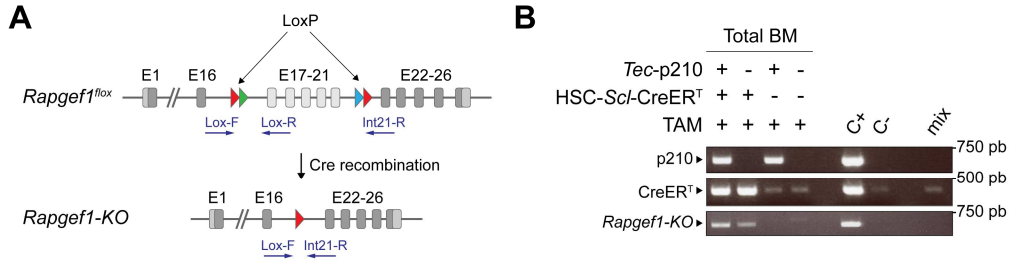

Figure 18. Deletion of *Rapgef1* gene in tamoxifen (TAM)-treated mice. (**A**) Schematic representation of the induction of the *Rapgef1-knockout* (KO) allele. Exons 17–21 of the *Rapgef1* gene are flanked by loxP sites (floxed) and are excised upon Cre-mediated recombination. The resulting KO allele can be detected by PCR using the specific primers Lox-F and Int21-R. (**B**) Agarose gel electrophoresis of PCR products amplified from DNA extracted from bone marrow (BM) cells. The *Rapgef1-KO* allele is detected in HSC-*Scl*-CreER^{T} mice seven days after TAM administration, confirming successful deletion of the *Rapgef1* gene.

To assess the loss of C3G protein levels, we first tried to isolate protein from low-committed HSPCs. Several attempts were made to detect C3G protein expression in FACS-purified LKS cells by WB. However, C3G could not be detected in these populations, likely due to its low expression in poorly committed hematopoietic progenitors. Consequently, we turned to evaluate reduction in C3G levels in more mature hematopoietic cells, where its expression is higher and, hence, detection can be easier. For this purpose, mature splenocytes were used, as they ultimately originate from HSCs in the BM (Hey *et al.*, 2017). To accelerate the turnover of these cells and better assess C3G reduction, a mild myeloablation was induced by treating C3G$^{HSC\text{-}Scl}$-wt and C3G$^{HSC\text{-}Scl}$-KO mice with 150 mg/kg 5-FU seven days after TAM administration. Seven days after the myeloablative treatment, spleens were harvested and splenocyte protein lysates were collected.

A moderate reduction in C3G levels was detected in splenocyte lysates (**Figure 19A, B**), confirming efficient inactivation of the floxed *Rapgef1* allele and persistence of reduced C3G expression in mature cells. The incomplete decrease in C3G levels is consistent with a mosaic Cre activation, indicating that *Rapgef1* excision occurred in only a subset of HSPCs. Similar patterns of partial recombination have been reported in other TAM-inducible models (Guo *et al.*, 2002; Ilchuk *et al.*, 2022), which likely explains the residual C3G expression observed here.

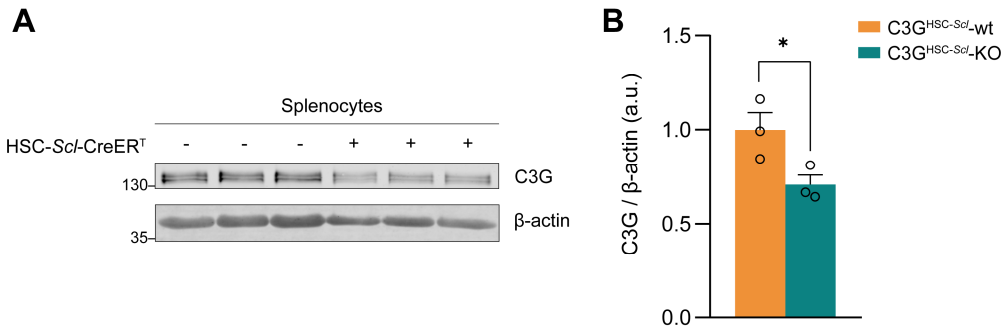

Figure 19. Reduction of C3G protein levels in mature hematopoietic cells. (**A**) Western blot analysis of C3G protein in splenocyte lysates from tamoxifen-injected and 5-fluorouracil-treated mice. β-actin levels were used as loading control. The molecular weights of the protein marker ladder are indicated in kDa. (**B**) Bar plots indicate the mean ± SEM of the densitometric quantification of C3G levels normalized to β-actin. Statistical analysis was performed using an unpaired two-tailed t-test. *p ≤ 0.05. Sample sizes: C3G$^{HSC\text{-}Scl}$-wt, n=3; C3G$^{HSC\text{-}Scl}$-KO, n=3. a.u., arbitrary units.

1.2. C3G deficiency attenuates neutrophil expansion in peripheral blood

Transgenic p210 mice develop a CP-CML-like myeloproliferative disease after a long latency period of approximately 6-8 months. This condition is characterized by a gradual expansion of mature neutrophils in PB, accompanied by thrombocytosis, splenomegaly, and

myeloid hyperplasia in hematopoietic tissues. Ultimately, p210 mice succumb to complications of the myeloproliferative disease often within 2-3 months after the disease onset (Honda *et al.*, 1998).

To explore the role of C3G in disease development, we first analyzed possible alterations in disease kinetics by analyzing the myeloproliferative phenotype in C3G-deficient p210 mice. One-month-old animals were treated with TAM to induce *Rapgef1* deletion during the early stages, before the disease was established. Both p210 and non-p210 control mice were monitored for one year. PB samples were subsequently collected monthly and analyzed by flow cytometry to determine the levels of mature neutrophils ($Gr1^+Mac1^+$), platelets ($CD41^+$), T cells ($CD3^+$), and B cells ($B220^+$).

In p210 mice, C3G deficiency did not induce immediate changes in PB, since both p210/$C3G^{HSC\text{-}Scl}$-wt and p210/$C3G^{HSC\text{-}Scl}$-KO mice showed normal levels of all hematopoietic populations during the first months following TAM treatment (**Figure 20**). However, after CML onset, which occurs between 6 and 9 months of age, differences became apparent, particularly within the myeloid compartment. At months 9 and 10, corresponding to full CML development and advanced disease stages, p210/$C3G^{HSC\text{-}Scl}$-KO mice displayed significantly reduced PB neutrophil levels compared with p210/$C3G^{HSC\text{-}Scl}$-wt mice (**Figure 20A**).

During advanced stages, p210 mice typically develop thrombocytosis (Honda *et al.*, 1998). However, platelet counts were not significantly affected by C3G deficiency at any disease stage (**Figure 20B**), despite C3G involvement in platelet production (Ortiz-Rivero *et al.*, 2018; Herranz *et al.*, 2025). The myeloid expansion in p210 mice was accompanied by a reduction in lymphocytes, mainly T cells; in p210/$C3G^{HSC\text{-}Scl}$-KO mice, T-cell levels tended to be slightly higher than in p210/$C3G^{HSC\text{-}Scl}$-wt animals, although the differences did not reach statistical significance (**Figure 20C**). These modest T-cell changes likely reflect the altered neutrophil population, as lower myeloid cell levels are often associated with higher lymphocyte numbers to maintain hematopoietic balance (Ueda *et al.*, 2005). The B-cell compartment remained largely unaffected and showed no differences related to either C3G status or p210 expression (**Figure 20D**).

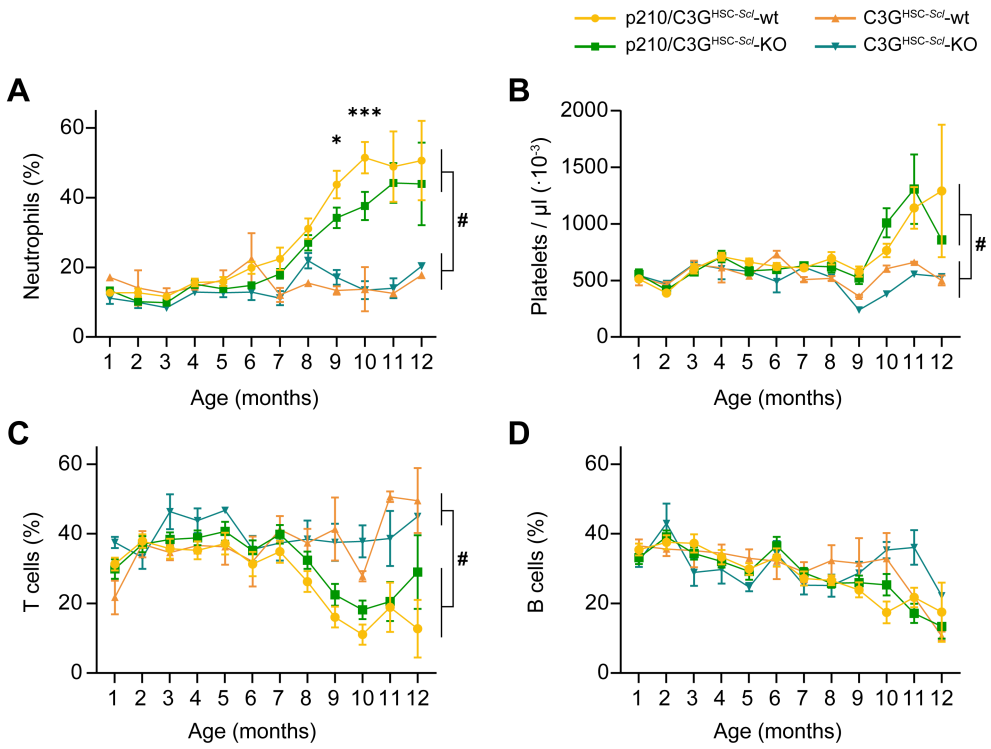

Figure 20. p210 mice deficient in C3G display lower neutrophil levels in peripheral blood (PB) after chronic myeloid leukemia (CML) onset. XY plots show the mean value ± SEM of the percentage of total PB leukocytes corresponding to (**A**) neutrophils ($Gr1^+Mac1^+$), (**B**) platelets ($CD41^+$), (**C**) T cells ($CD3^+$), and (**D**) B cells ($B220^+$) over a 1-year monitoring period in both p210 and non-p210 groups. The PB sample collected at month 1 was obtained prior to tamoxifen administration. Statistical analysis was performed using two-way ANOVA followed by a multiple-comparison test. * p210/C3G$^{HSC\text{-}Scl}$-wt vs p210/C3G$^{HSC\text{-}Scl}$-KO, # p210 group vs non-p210 group; three symbols indicate $p \leq 0.001$, one symbol indicates $p \leq 0.05$. Sample sizes: p210/C3G$^{HSC\text{-}Scl}$-wt, n=15; p210/C3G$^{HSC\text{-}Scl}$-KO, n=19; C3G$^{HSC\text{-}Scl}$-wt, n=4; C3G$^{HSC\text{-}Scl}$-KO, n=7.

At the latest monitoring time points, when the disease is fully established, data variability increased in both p210/C3G$^{HSC\text{-}Scl}$-wt and p210/C3G$^{HSC\text{-}Scl}$-KO cohorts. This reflects the progressive mortality of p210 mice from around 10 months of age due to CML, which reduces sample size at later stages and inflates data dispersion. Beyond month 12, data are not shown because only a small number of mice remain alive, and these survivors tend to be the healthier individuals. This survivorship bias underlies the decision to limit the analysis to the first 12 months of age.

In this experiment, non-p210 mice were used as controls to assess baseline hematopoietic kinetics in the absence of BCR::ABL1. Across the 12-month follow-up, PB populations remained largely stable, with no major fluctuations. Deletion of C3G in non-p210 mice did not produce significant changes in PB neutrophils, lymphocytes, or platelets over the

analyzed period (**Figure 20A–D**), consistent with previous studies in our group using this model (Herranz Varea, 2024). These results indicate that the alterations observed in the p210/C3G$^{HSC\text{-}Scl}$-KO cohort likely depend on the BCR::ABL1 background and are not caused by C3G loss alone.

1.3. CML onset is delayed in p210/C3G$^{HSC\text{-}Scl}$-KO mice

Notably, the reduced PB neutrophil levels after CML onset in p210/C3G$^{HSC\text{-}Scl}$-KO mice suggest a delay in disease initiation. The p210 mice lacking C3G still develop the myeloproliferative disease, characterized by a gradual increase in PB neutrophil counts. However, compared with the typical disease course observed in p210/C3G$^{HSC\text{-}Scl}$-wt, p210/C3G$^{HSC\text{-}Scl}$-KO mice exhibit an attenuated myeloproliferative phenotype.

To compare disease onset among p210 mice, chronic-phase CML was diagnosed applying the following criterion: a proportion of ≥ 40% neutrophils (Gr1^{+}Mac1^{+}) in PB over two consecutive months. Based on this criterion, mice were classified as either healthy or CML-positive to generate a leukemia-free survival curve.

Both p210/C3G$^{HSC\text{-}Scl}$-wt and p210/C3G$^{HSC\text{-}Scl}$-KO mice developed CML, indicating that C3G at the HSPC level is dispensable for neoplasia development. However, and consistent with the alterations in the PB neutrophil levels, C3G-deficient mice exhibited a delayed onset of the myeloproliferative disease, with an average delay of approximately one month (**Figure 21A**). Notably, when comparing post-onset survival, defined as the period from disease onset to death, no significant differences were observed (**Figure 21B**), indicating that C3G deficiency does not affect disease duration.

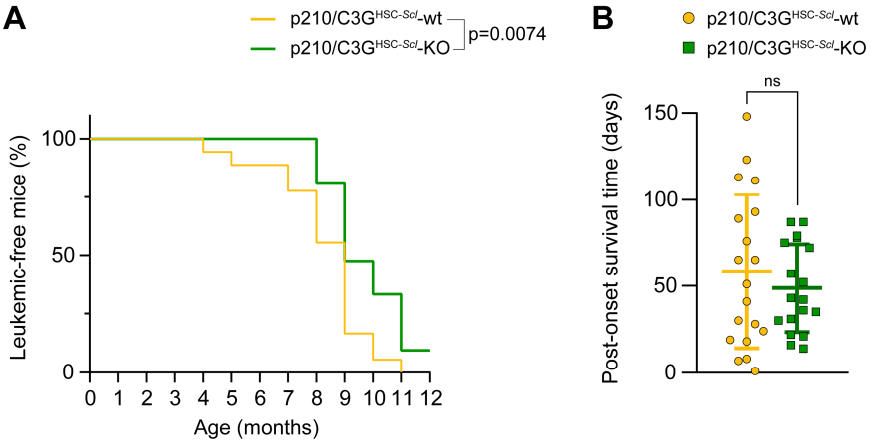

◄ Figure 21. C3G-deficient p210 mice take longer to develop chronic myeloid leukemia (CML), while post-onset survival remains unchanged. (**A**) Kaplan-Meyer plot represents the leukemia-free survival during 1 year of monitoring, shown as the percentage of disease-free mice according to the established criterion. Statistical analysis was performed using the log-rank test. (**B**) Comparison of p210 survival time from disease onset, indicating overall disease duration. Statistical analysis was performed using an unpaired t-test. ns: non-significant. Sample sizes: p210/C3G$^{HSC\text{-}Scl}$-wt, n=19; p210/C3G$^{HSC\text{-}Scl}$-KO, n=18.

The data indicate that the absence of hematopoietic C3G may act as a brake on the development of the myeloproliferative disease in CML-predisposed mice, attenuating disease severity and delaying its onset. Since the overall disease duration is unaffected, C3G appears to act primarily during the initial stages of CML. The fact that nearly all mice eventually develop the disease, though at different times, further supports this idea, indicating that C3G role is restricted to a temporal window near disease establishment rather than during later progression.

1.4. Overall survival is improved in C3G-deficient females

The delayed CML onset observed in p210/C3G$^{HSC\text{-}Scl}$-KO mice together with unchanged post-onset survival, suggests that C3G deficiency may provide partial protection by postponing disease development. However, a delayed onset does not necessarily translate into improved overall survival. Indeed, in the p210 model death typically results from the progressive myeloproliferative disorder rather than a single acute event, with mice ultimately succumbing to disease-related complications during the CP-CML-like stage (Honda *et al.*, 1998). By contrast, human CML patients can progress from the CP-CML to AP-CML or BP-CML stages, often driven by additional mutations that confer more aggressive leukemic behavior (Ochi *et al.*, 2018). p210 mice generally do not acquire these secondary mutations and therefore do not progress to BP-CML, highlighting a key limitation of this model for studying late-stage disease progression. Nonetheless, assessing survival in these mice provides a useful measure of the severity and kinetics of myeloproliferative disease development, even if it does not directly reflect CML-related death.

To evaluate this, overall survival was monitored in p210 mice, which typically succumb to the disease at an average age of around one year. Mice were sacrificed upon exhibiting at least two signs of distress, which include weight loss, labored breathing, hunched posture, or reduced mobility, as described in established guidelines (Langford *et al.*, 2010). The presence of these signs is indicative of advanced CML progression.

Comparison of the overall survival between p210/C3G$^{HSC\text{-}Scl}$-wt and p210/C3G$^{HSC\text{-}Scl}$-KO mice revealed no significant differences (**Figure 22A**). Interestingly, when the data were stratified by sex, survival differences became evident only in females. Thus, female p210/C3G$^{HSC\text{-}Scl}$-KO mice survived significantly longer than female p210/C3G$^{HSC\text{-}Scl}$-wt

mice with an approximate survival advantage of two months (**Figure 22B**). In contrast, no significant differences were observed among male p210 mice (**Figure 22C**).

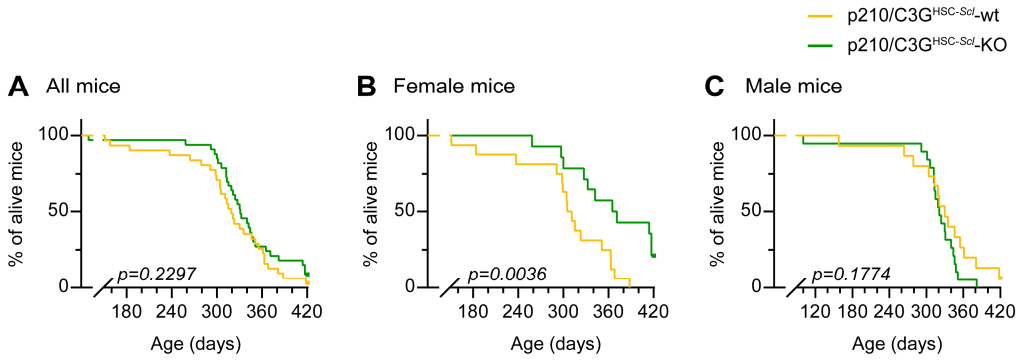

Figure 22. Female C3G-deficient p210 mice show increased survival. Kaplan-Meyer plots represent the overall survival of the analyzed mice. (**A**) Overall survival of all monitored p210 mice over the 14-month duration of the experiment. (**B**) Overall survival of female p210 mice, showing the notable increase in survival of C3G-deficient mice. (**C**) Overall survival of male p210 mice, showing no differences between groups. Statistical analysis was performed using the log-rank test. Sample sizes: p210/C3G$^{HSC\text{-}Scl}$-wt, n=30; p210/C3G$^{HSC\text{-}Scl}$-KO, n=34.

The presence of these notable sex-biased differences prompted a reanalysis of the previous monitoring and leukemic survival data, separating the data by sex. Consistently, more pronounced differences were observed when focusing exclusively on female p210 mice, both in neutrophil levels in PB and, consequently, in CML onset (see **Figure 50**; **Annexes**). Interestingly, this behavior has been reported previously in other C3G conditional knockout models, with more evident differences found also in females (Herranz *et al.*, 2025). Sex-specific effects in the normal development of the myeloproliferative disease were ruled out, as overall survival of female and male p210/C3G$^{HSC\text{-}Scl}$-wt mice remained comparable (see **Figure 51**; **Annexes**).

1.5. Leukemic infiltration is attenuated in C3G knockout p210 mice

The development of the myeloproliferative disease in p210 is typically accompanied of leukemic cell infiltration into various hematopoietic organs (Honda *et al.*, 1998). Extensive myeloid infiltration in extramedullary tissues, particularly the spleen, is a hallmark of full-blown CML and leads to splenomegaly in affected mice (Schemionek *et al.*, 2010). For this reason, analysis of tissue leukemic infiltration in C3G-deficient mice is of particular interest, as these mice experience an attenuated CML course.

At the terminal endpoint, when leukemic p210 mice were sacrificed due to advanced disease, BM, spleen, thymus, and liver were collected for analysis. This included evaluation of typical leukemic hallmarks to assess disease severity, including leukemic infiltration in medullary and extramedullary tissues, as well as hepatosplenomegaly, defined as increased

spleen and liver size and weight. Cell suspensions from hematopoietic organs were analyzed by flow cytometry to determine the proportion of infiltrating mature neutrophils. Since these organs normally contain mature hematopoietic cells, healthy non-p210 mice (~ 6-8 months old) were used as controls. Additionally, both spleen and liver were analyzed macroscopically and weighed to assess disease severity.

In the BM, p210 mice exhibited altered proportions of mature hematopoietic cells compared with non-p210 controls (**Figure 23A–C**), reflecting disrupted hematopoietic balance and early signs of BM failure in advanced CML. Specifically, neutrophil levels were elevated in p210 mice, indicative of pronounced myeloproliferation. However, p210/C3G$^{HSC\text{-}Scl}$-KO mice showed reduced neutrophil levels compared to p210/C3G$^{HSC\text{-}Scl}$-wt (**Figure 23A**), approaching the physiological proportions observed in non-p210 mice. This suggests that the absence of C3G may restore the hematopoietic balance disrupted by CML. T-cell proportions were similar across all groups, with no significant differences between p210 and non-p210 mice groups or between p210/C3G$^{HSC\text{-}Scl}$-wt and p210/C3G$^{HSC\text{-}Scl}$-KO mice (**Figure 23B**). Mature B-cell proportions, which were markedly reduced in p210 mice, were partially restored in p210/C3G$^{HSC\text{-}Scl}$-KO mice (**Figure 23A–C**), again resembling non-p210 controls and supporting a more normalized BM composition.

In the spleen, p210 mice showed marked alterations compared with non-p210 controls (**Figure 23D–F**), including pronounced neutrophil infiltration (**Figure 23D**) and reduced B-cell levels (**Figure 23F**), while T-cell proportions remained unchanged (**Figure 23E**). Comparison of p210/C3G$^{HSC\text{-}Scl}$-KO and p210/C3G$^{HSC\text{-}Scl}$-wt mice revealed no significant differences in neutrophil infiltration in spleen (**Figure 23D**), and the T-cell compartment remained largely unaffected by C3G deletion (**Figure 23E**). Interestingly, p210/C3G$^{HSC\text{-}Scl}$-KO mice exhibited increased mature B-cell levels (**Figure 23F**), partially restoring spleen composition toward physiological proportions, similar to the effect observed in the BM.

Finally, p210 mice exhibited aberrant hematopoietic composition in the thymus (**Figure 23G–I**). The thymus is a primary lymphoid organ that controls proper T-cell maturation, a process essential for adaptive immunity, and under physiological conditions it is mainly composed of developing T cells, particularly $CD4^+CD8^+$ double-positive thymocytes (Thapa and Farber, 2019). In leukemic p210 mice, however, the thymic composition was disrupted, showing abnormal hematological proportions. A mild neutrophil infiltration was detected (**Figure 23G**), despite the fact that the thymus normally lacks myeloid cells. In addition, T-cell populations were altered, with an abnormal expansion of $CD3^+CD4^-CD8^-$ cells (**Figure 23H**), likely reflecting collateral effects of BCR::ABL1 expression in this model, as previously reported (Honda *et al.*, 1998). B cells were also unexpectedly detected in the thymus of p210 mice (**Figure 23I**), further supporting the presence of hematopoietic imbalance in this tissue. Interestingly, differences were detected between p210/C3G$^{HSC\text{-}Scl}$-

wt and p210/C3G$^{HSC\text{-}Scl}$-KO mice. Myeloid infiltration was reduced in p210/C3G$^{HSC\text{-}Scl}$-KO animals compared with its p210 control (**Figure 23G**), whereas both T and B lymphoid compartments were not significantly affected (**Figure 23H–I**). This decrease in the abnormal presence of neutrophils in the thymus of p210/C3G$^{HSC\text{-}Scl}$-KO mice is consistent with previous observations and suggests a partial restoration toward a more physiological hematopoietic balance in this extramedullary organ.

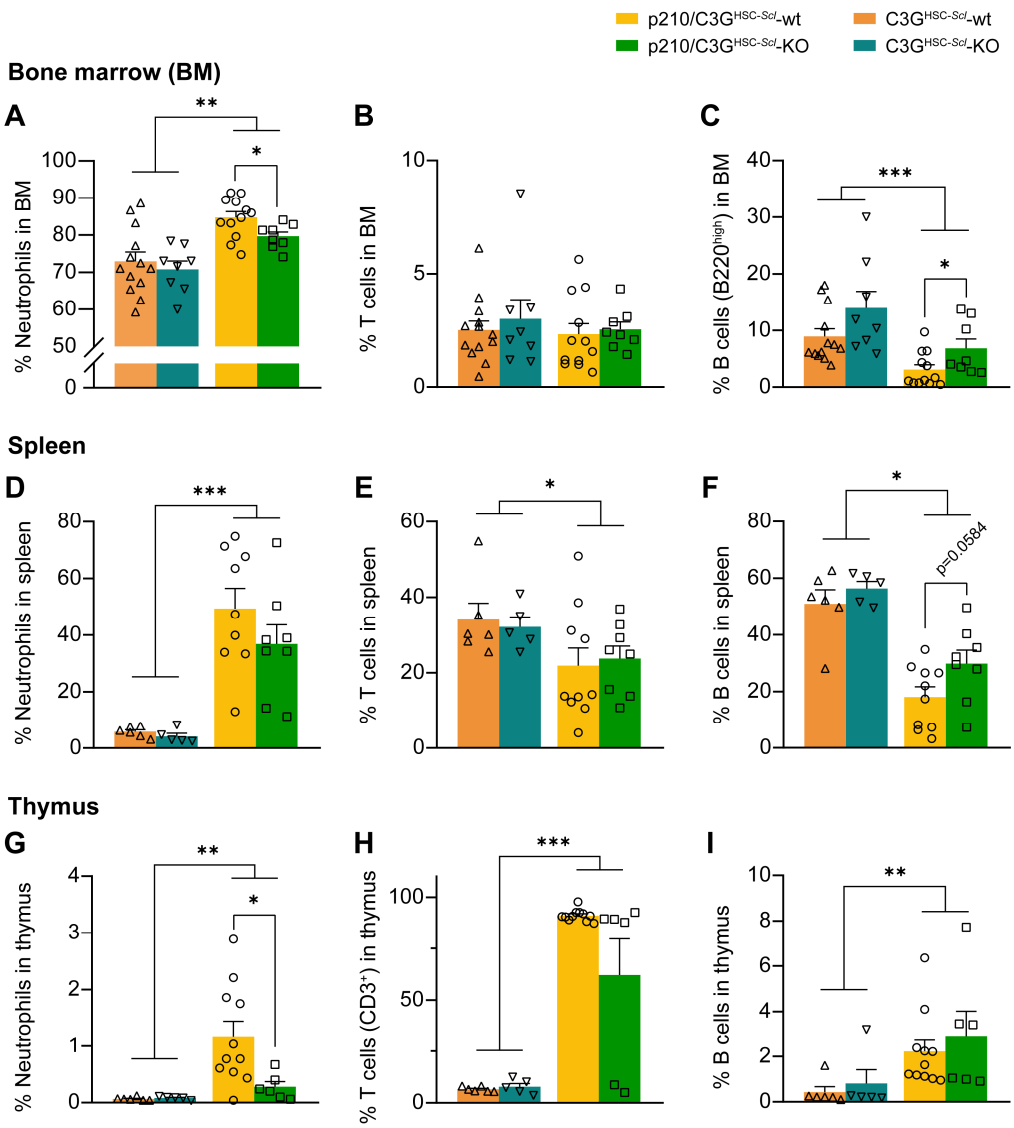

◄ Figure 23. Leukemic infiltration in hematopoietic tissues is reduced in C3G-deficient p210 mice at the endpoint disease. Bar plots indicate the mean ± SEM of the percentage of the corresponding hematopoietic cells of the non-p210 and p210 mice. Non-p210 mice aged 6–8 months were used as controls. (**A-C**) Analysis of the presence of hematopoietic cells in bone marrow (BM), including (**A**) neutrophils, (**B**) T cells, and (**C**) mature B220^{high} B cells. (**D-F**) Analysis of the presence of hematopoietic cells in spleen, including (**D**) neutrophils, (**E**) T cells, and (**F**) B cells. (**G-I**) Analysis of the presence of hematopoietic cells in thymus, including (**G**) neutrophils, (**H**) CD3^{+} T cells, and (**I**) B cells. Statistical analysis was performed using an unpaired t-test. *p ≤ 0.05, **p ≤ 0.01, ***p ≤ 0.001. Sample sizes: p210/C3G$^{HSC\text{-}Scl}$-wt, n=10-12; p210/C3G$^{HSC\text{-}Scl}$-KO, n=6-8; C3G$^{HSC\text{-}Scl}$-wt, n=6; C3G$^{HSC\text{-}Scl}$-KO, n=5.

In addition to leukemic infiltration, hepatosplenomegaly provides an independent readout of disease severity at the CML endpoint. Therefore, spleen and liver weights were measured to assess organ enlargement, using healthy non-p210 mice (~ 6-8 months old) as controls. Organ weights were normalized to total body weight to account for age and sex differences in control and leukemic mice to minimize bias. As expected, p210 mice exhibited clear hepatosplenomegaly, with significantly increased relative spleen and liver weights compared with non-p210 controls (**Figure 24A, B**). However, comparison between p210/C3G$^{HSC\text{-}Scl}$-wt and p210/C3G$^{HSC\text{-}Scl}$-KO mice revealed only a mild, non-significant trend toward reduced spleen weight (**Figure 24A**) and no appreciable differences in liver weight (**Figure 24B**), indicating that C3G deficiency does not markedly alter organ enlargement at terminal disease stages.

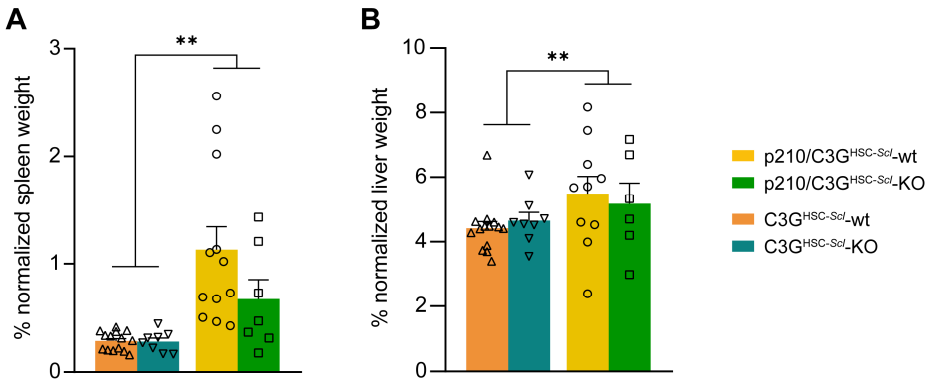

Figure 24. p210 mice show increased spleen and liver weight, with no effect of C3G deficiency. Bar plots indicate the mean ± SEM of the percentage of the (**A**) spleen and (**B**) liver weight normalized to total body weight of the non-p210 and p210 mice. Non-p210 mice aged 6–8 months were used as controls. Statistical analysis was performed using an unpaired t-test. **p ≤ 0.01. Sample sizes: p210/C3G$^{HSC\text{-}Scl}$-wt, n=12; p210/C3G$^{HSC\text{-}Scl}$-KO, n=7; C3G$^{HSC\text{-}Scl}$-wt, n=14; C3G$^{HSC\text{-}Scl}$-KO, n=8.

Overall, terminal-stage p210 mice displayed the expected features of advanced CML, including myeloid expansion, disruption of hematopoietic balance, leukemic infiltration of multiple organs, and marked hepatosplenomegaly. Although C3G deficiency did not block disease development, it consistently attenuated the severity of the phenotype. C3G

deficiency partially normalized hematopoietic cell composition across organs, reducing neutrophils and restoring B cells, but had minimal impact on organ enlargement at endpoint. These findings indicate that hematopoietic C3G modulates the intensity and tissue imbalance of the p210-driven myeloproliferative disease without fully determining terminal disease outcome.

1.6. p210 mice show no response to 1-month imatinib treatment

The attenuated CML observed in p210/C3G$^{HSC\text{-}Scl}$-KO mice prompted us to further investigate the characteristics of this altered disease kinetics. One aspect of particular interest was the efficacy of imatinib, the first-line TKI used in CML therapy, which exerts its therapeutic effect by inhibiting BCR::ABL1 kinase activity (Puttini *et al.*, 2006), as described in **Introduction section 1.4.1**. Therefore, it would be of interest to explore whether combining a TKI, which effectively targets CML, with C3G deficiency, which appears to attenuate the myeloproliferative phenotype, could be a useful strategy to improve disease control.

To this end, TAM-treated p210 mice with approximately 10 months of age, coinciding with fully established disease, were selected for the treatment regimen. At this stage, these mice exhibit elevated neutrophil levels in PB, reflecting the full course of the chronic phase of CML in patients, which corresponds to the typical clinical window for initiating TKI therapy (Kong *et al.*, 2020). Imatinib was administered orally at a dose of 100 mg/kg by oral gavage using a 5-days-on/2-days-off regimen for one month, and PB was analyzed weekly to monitor hematological changes.

Imatinib treatment of leukemic p210 mice failed to halt or slow disease progression under our experimental conditions. Weekly analysis of PB populations revealed that neutrophil counts continued to rise during and after treatment (**Figure 25A**), while other populations, such as T cells (**Figure 25B**) and B cells (**Figure 25C**), remained largely unchanged between genotypes. These results indicate that imatinib administration in this p210 mouse model was ineffective, as the mice still developed the typical signs of myeloproliferative disease.

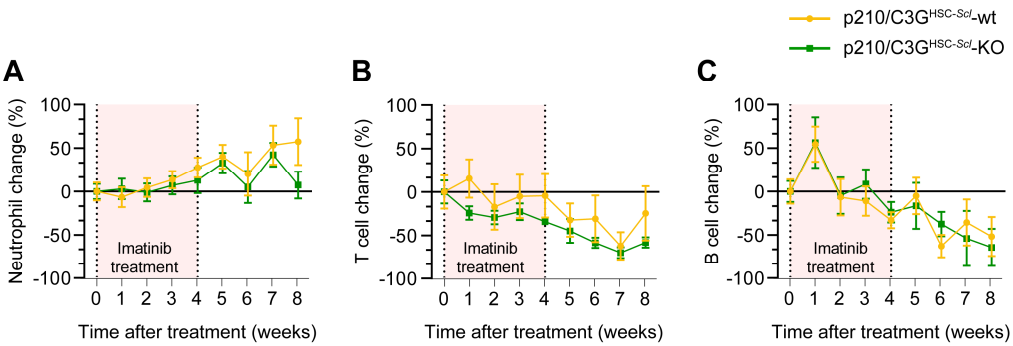

Figure 25. Imatinib treatment did not ameliorate the myeloproliferative disease course in p210 mice. The 1-month imatinib treatment window is indicated in the plots. Only mice older than 10 months were included in the study. XY plots show the mean value ± SEM of the change in the percentage of total peripheral blood leukocytes corresponding to (**A**) neutrophils ($Gr1^+Mac1^+$), (**B**) T cells ($CD3^+$), and (**C**) B cells ($B220^+$) over the two-month monitoring period. Sample sizes: p210/C3G$^{HSC\text{-}Scl}$-wt, n = 9; p210/C3G$^{HSC\text{-}Scl}$-KO, n = 9.

No differences in overall CML survival were detected between p210/C3G$^{HSC\text{-}Scl}$-wt and p210/C3G$^{HSC\text{-}Scl}$-KO mice (**Figure 26**). Moreover, comparison of survival between imatinib-treated and untreated p210 mice revealed no significant differences (see **Figure 52**; **Annexes**), suggesting that imatinib treatment was ineffective in our experimental conditions in this mouse model.

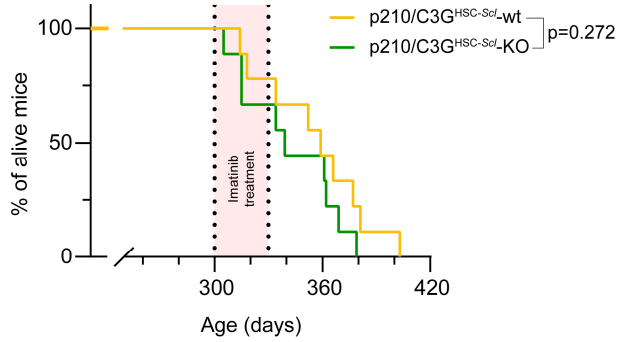

Figure 26. Overall survival of p210/C3G$^{HSC\text{-}Scl}$-wt and p210/C3G$^{HSC\text{-}Scl}$-KO mice did not show differences upon treatment with imatinib. The 1-month imatinib treatment window is indicated in the plots. Only mice older than 10 months were included in the study. Kaplan-Meyer plot represents the overall survival of treated p210 mice from 10 to 14 months. Statistical analysis was performed using the log-rank test. Sample sizes: p210/C3G$^{HSC\text{-}Scl}$-wt, n = 9; p210/C3G$^{HSC\text{-}Scl}$-KO, n = 9.

The lack of attenuation of CML progression in p210 mice following imatinib treatment was unexpected, given the extensive evidence in the literature supporting the *in vivo* efficacy of TKIs targeting BCR::ABL1 (Deininger *et al.*, 2005; Baran and Saydam, 2012). However, the negative outcome of this set of experiments prevents drawing conclusions about the

impact of TKI treatment in a C3G-deficient CML context, regardless of the underlying cause, such as limited model sensitivity, suboptimal pharmacokinetics, or insufficient treatment duration.

1.7. Late deletion of C3G moderately reduces disease severity

The experiments conducted so far indicate that deleting C3G in HSCs before CML is established (corresponding to 1 month of age in p210 mice) leads to a delayed disease onset accompanied by milder symptoms. These results suggest that C3G plays an important role during the early phases of leukemogenesis, likely by modulating myeloid cell expansion and helping maintain hematopoietic balance. Based on these observations, we aimed to determine whether deleting C3G at a later stage, once the disease is already established, would produce a similar effect. This approach would better mimic a potential clinical scenario in which C3G inhibition is initiated after CML diagnosis, providing insight into whether targeting C3G could still influence disease progression or reduce leukemic burden in an established pathological context.

To investigate the effect of C3G deletion at disease onset, p210 mice were treated with TAM at approximately 6 months of age, which corresponds to the average onset of the myeloproliferative disease. Following TAM administration, PB was collected monthly to monitor leukemic progression through hematological parameters, and mice were observed for signs of distress indicative of advanced disease.

No immediate changes in PB populations were observed after TAM treatment (**Figure 27A-C**). Additionally, compared with C3G deletion performed at an earlier stage, the effects of late deletion were more moderate. PB neutrophil monitoring revealed slight reductions at specific time points, most notably at month 9 (month 3 post-TAM) (**Figure 27A**), while other time points showed no major changes. T-cell levels remained largely unchanged between both genotypes (**Figure 27B**). Interestingly, B-cell levels were increased in p210/C3G$^{\text{HSC-}Scl}$-KO mice at month 9 (**Figure 27C**), coinciding with the transient decrease in neutrophils and likely reflecting a partial restoration of hematopoietic balance in the PB.

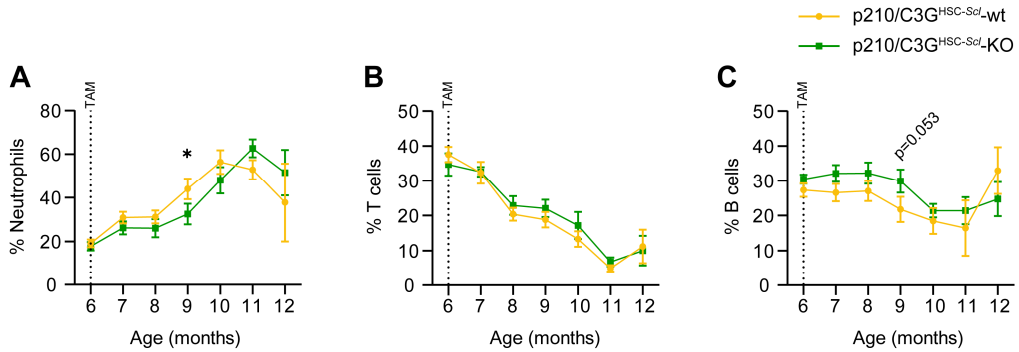

Figure 27. C3G deletion at 6 months of age, corresponding to disease onset in p210 mice, modestly attenuates the myeloproliferative phenotype. XY plots show the mean value ± SEM of the percentage of total peripheral blood leukocytes corresponding to (**A**) neutrophils ($Gr1^+Mac1^+$), (**B**) T cells ($CD3^+$), and (**C**) B cells ($B220^+$) from 6 months onwards monitoring period in both p210 and non-p210 groups. The peripheral blood sample collected at month 6 was obtained prior to tamoxifen administration. Statistical analysis was performed using two-way ANOVA followed by a multiple-comparison test. * $p \leq 0.05$. Sample sizes: p210/C3G$^{HSC\text{-}Scl}$-wt, n = 15; p210/C3G$^{HSC\text{-}Scl}$-KO, n = 16. TAM: tamoxifen.

These results suggest that C3G deletion at CML onset produces only modest and transient effects on PB composition, in contrast to the more pronounced impact observed when C3G is deleted earlier. While late deletion can partially restore hematopoietic balance, its influence on leukemic progression appears limited, suggesting that C3G role is more critical during the initial phases of CML development.

We also compared disease onset between p210/C3G$^{HSC\text{-}Scl}$-wt and p210/C3G$^{HSC\text{-}Scl}$-KO mice, in which C3G deletion was induced at month 6, using the criteria described in **Results section 1.3**. Analysis of the leukemia-free survival curve revealed no statistically significant differences between groups, although p210/C3G$^{HSC\text{-}Scl}$-KO mice showed a trend toward delayed disease onset (**Figure 28A**). Consistent with previous results, post-onset survival was unchanged in p210/C3G$^{HSC\text{-}Scl}$-KO mice compared with p210/C3G$^{HSC\text{-}Scl}$-wt mice (**Figure 28B**), indicating that disease duration was not affected by C3G deletion at this later stage.

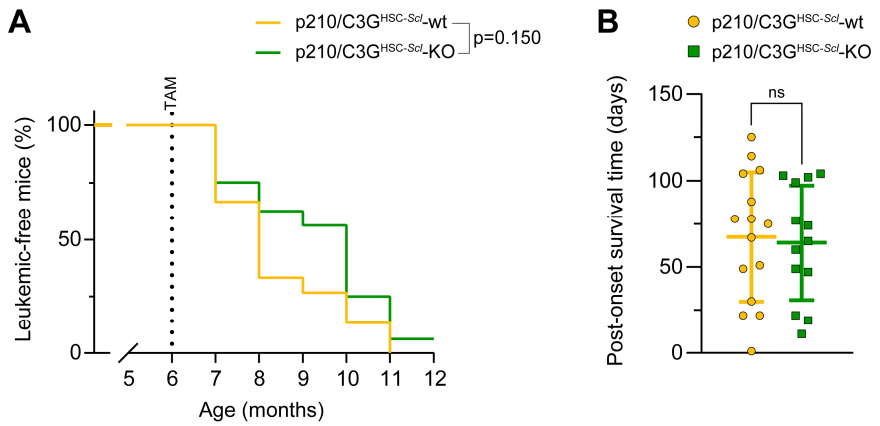

Figure 28. Late C3G deletion in p210 mice displays a moderate trend toward increased leukemia-free survival, while post-onset survival remains unchanged. (**A**) Kaplan-Meyer plot represents the leukemia-free survival of all monitored p210 mice from 6 to 12 months, based on the established diagnostic criteria. Statistical analysis was performed using the log-rank test. (**B**) Comparison of p210 survival time from disease onset, indicating overall disease duration. Statistical analysis was performed using an unpaired t-test. ns: non-significant. Sample sizes: p210/C3G$^{HSC\text{-}Scl}$-wt, n = 15; p210/C3G$^{HSC\text{-}Scl}$-KO, n = 13. TAM: tamoxifen.

Overall survival in p210 mice with late C3G deletion also remained unchanged (**Figure 29A**), although some trends were apparent. Because early C3G deletion had previously shown a clear survival benefit in females, the data were analyzed separately by sex. Interestingly, as in the previous experiments (**Figure 22**), female p210/C3G$^{HSC\text{-}Scl}$-KO mice displayed a notable, although still non-significant, trend toward extended survival (**Figure 29B**) compared with male p210 mice (**Figure 29C**), suggesting a potential sex-specific influence of C3G deletion on disease progression.

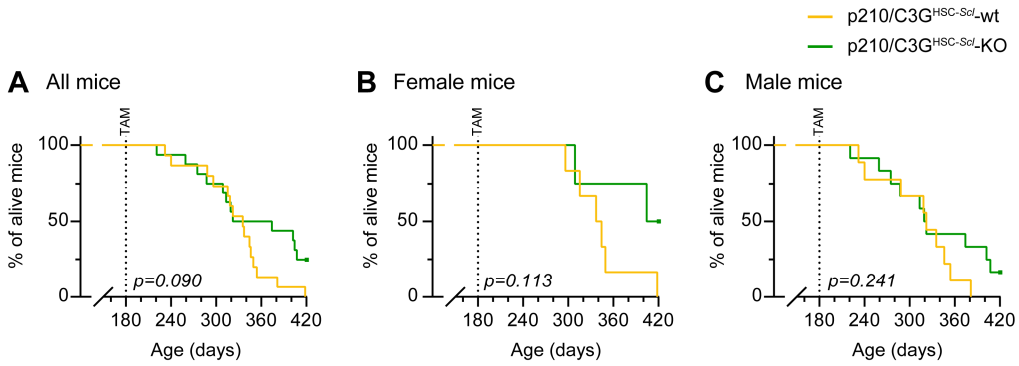

Figure 29. Late C3G deletion in p210 mice shows a slight trend toward increased overall chronic myeloid leukemia (CML) survival, being more evident in female mice. Kaplan-Meyer plots represent the overall survival of analyzed mice from month 6 to month 14. (**A**) Overall survival of all monitored p210 mice from 6 to 14 months. (**B**) Overall survival of female p210 mice. (**C**) Overall survival of male p210 mice. Statistical analysis was performed using the log-rank test. Sample sizes: p210/C3G$^{HSC\text{-}Scl}$-wt, n = 15; p210/C3G$^{HSC\text{-}Scl}$-KO, n = 16.

In summary, deletion of C3G at the time of CML establishment produced a phenotype similar, though less pronounced, than that observed when C3G was deleted prior to disease onset. Mice with C3G deletion at disease initiation showed modest reduction in neutrophil levels and partial restoration of B-cell proportions in peripheral blood. These effects were smaller and less durable than those observed with early deletion, indicating that the impact of C3G loss on disease progression depends on the timing of deletion.

1.8. Deficiency of C3G alters bone marrow hematopoiesis at CML onset

So far, the results suggest that C3G deficiency may act as a brake on CML development, as its absence in initial stages of leukemogenesis is associated with delayed disease onset and milder symptoms at the terminal endpoint. To understand what was behind these observations, we focused on studying the status of hematopoiesis in the BM, where the disease is first established.

In CML, BCR::ABL1 pushes HSPCs into a highly proliferative and partially dedifferentiated state, promoting myeloid lineage and consequently reshaping all the hematopoietic framework (Quintás-Cardama and Cortes, 2009). HSPC composition shows major alterations in CML relative to healthy hematopoiesis, with modest expansions in certain progenitor populations, reflecting early disruption of hematopoiesis (Harada *et al.*, 2021). These changes become more pronounced and heterogeneous as CP-CML progresses to BP-CML, highlighting the dynamic remodeling of the hematopoietic hierarchy during disease evolution (Kinstrie *et al.*, 2016).

Our p210 transgenic mice, however, only develop CP-CML without progressing to the acute leukemic phase, at least in the absence of genetic events that drive progression to blast-phase CML, such as p53 loss, as previously described (Honda *et al.*, 1998). Consequently, this model limits our analysis to the early stages of the disease, allowing us to focus on alterations in HSPCs proportions and dynamics during the initiation and establishment of CP-CML, but excluding the study of mechanisms involved in disease acceleration or transformation to BP-CML.

To address whether C3G may influence HSPC composition in our mouse models, we analyzed the levels of lineage-committed and less-committed HSPCs (**Figure 30A**) at the mean time of CML onset, specifically in six-month-old p210 mice, using age-matched non-p210 mice as controls. For this purpose, BM cell suspensions were isolated from mice that had been treated with TAM during the first month of life and analyzed by flow cytometry. This approach allowed the simultaneous quantification of immature and lineage-restricted progenitor populations within the same samples, providing a comprehensive overview of HSPC composition during early leukemogenesis. The fluorochrome panel with the markers

used for the identification of the different HSPC subpopulations are detailed in **Methods section 6.2**.

Notably, when comparing HSPC subpopulation proportions on CML onset between p210/C3G$^{HSC\text{-}Scl}$-wt and p210/C3G$^{HSC\text{-}Scl}$-KO, several differences emerged (**Figure 30B**). Firstly, lineage negative (Lin$^-$) cells, representing the immature BM compartment, was expanded in p210/C3G$^{HSC\text{-}Scl}$-KO mice, suggesting an accumulation of hematopoietic progenitors in this tissue. Within this Lin$^-$ pool, which encompasses all the HSPC subpopulations, additional alterations were detected. LKS (Lin$^-$ c-Kit$^+$ Sca1$^+$), the cells that comprise the least-committed progenitors and include the true HSC fraction, were reduced in p210/C3G$^{HSC\text{-}Scl}$-KO mice, pointing to a weakened stem-cell reservoir. However, the composition of the LKS compartment itself remained largely stable, as LT-HSC, ST-HSC, and MPP proportions were comparable between both p210 genotypes.

At the early lymphoid-myeloid bifurcation, CLPs were increased while CMPs were reduced, indicating a putative shift toward the lymphoid branch. Within the myeloid lineage, several changes suggested that C3G deficiency alters myeloid differentiation dynamics, which is of particular interest in the context of a myeloid neoplasm. In addition to the reduction in CMPs, which may reflect diminished production of early myeloid progenitors, p210/C3G$^{HSC\text{-}Scl}$-KO mice displayed increased GMPs and reduced MEPs (**Figure 30B**). The accumulation of GMPs in the BM may be indicative of a defect in granulopoiesis, with differentiation arrested at an intermediate stage and preventing full maturation into circulating neutrophils, consistent with the phenotype observed in the PB of p210/C3G$^{HSC\text{-}Scl}$-KO mice. Conversely, reduced MEPs could indicate a bias away from the erythroid/megakaryocytic program, a shift that might coexist with GMP expansion when granulopoiesis is impaired downstream.

As controls, BM from C3G$^{HSC\text{-}Scl}$-wt and C3G$^{HSC\text{-}Scl}$-KO mice was analyzed at the same time point to determine whether the differences observed were driven by BCR::ABL1 rather than by C3G loss alone. Interestingly, the non-p210 mice showed much more moderate alterations (**Figure 30C**). No differences were detected in the Lin$^-$ compartment or in the overall LKS proportions. Notably, however, the proportion of MPPs within the LKS gate was increased in C3G$^{HSC\text{-}Scl}$-KO mice, suggesting subtle changes in early progenitor dynamics. Among more committed progenitors, a trend toward increased CLPs was observed in C3G$^{HSC\text{-}Scl}$-KO mice, pointing to a mild bias toward the lymphoid lineage in the absence of C3G. In contrast, CMP, GMP, and MEP populations were unchanged, indicating that the pronounced alterations previously observed within the myeloid HSPC compartment are specific to the BCR::ABL1 background and are not a general consequence of C3G deficiency alone.

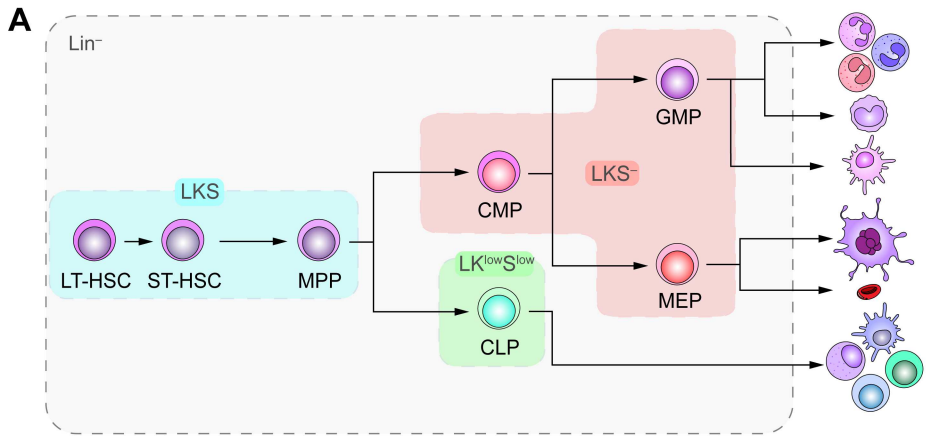
A
Lin⁻
LKS
LT-HSC
ST-HSC
MPP
CMP
GMP
LKS⁻
LK^lowS^low
CLP
MEP

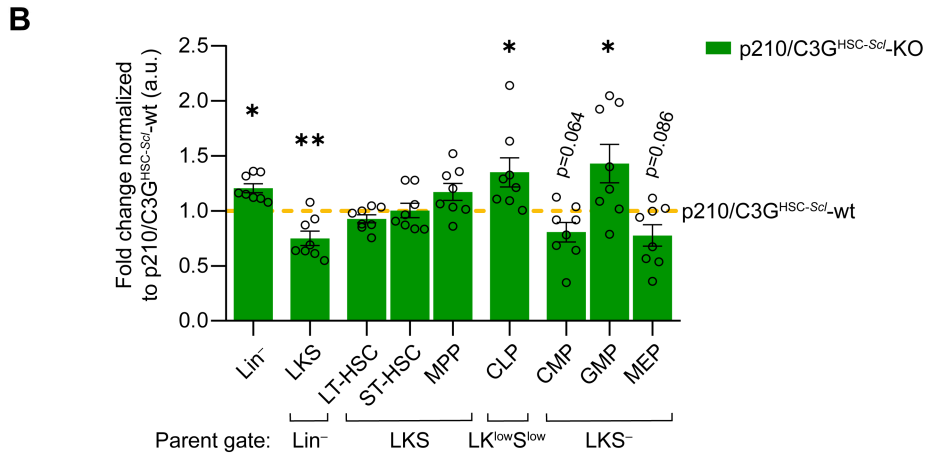
B
p210/C3G^HSC-Scl-KO
p210/C3G^HSC-Scl-wt
Fold change normalized to p210/C3G^HSC-Scl-wt (a.u.)
2.5
2.0
1.5
1.0
0.5
0.0
*
**
*
*
p=0.064
p=0.086
Lin⁻
LKS
LT-HSC
ST-HSC
MPP
CLP
CMP
GMP
MEP
Parent gate:
Lin⁻
LKS
LK^lowS^low
LKS⁻

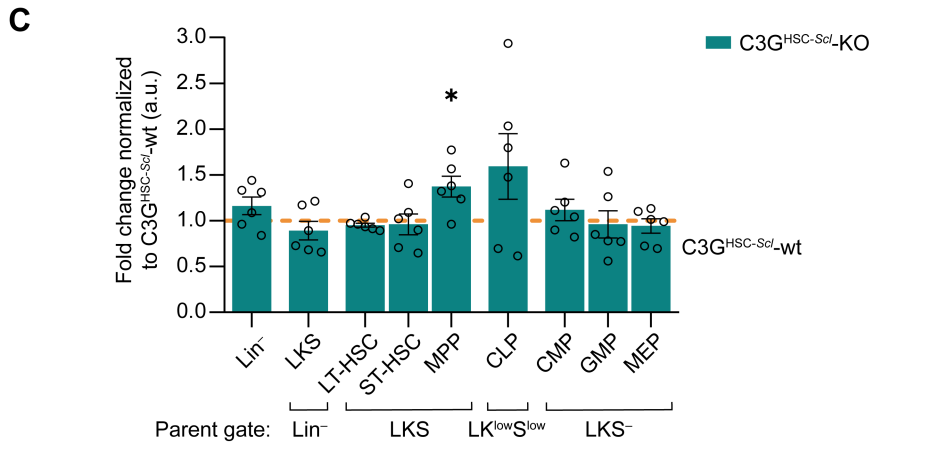
C
C3G^HSC-Scl-KO
C3G^HSC-Scl-wt
Fold change normalized to C3G^HSC-Scl-wt (a.u.)
3.0
2.5
2.0
1.5
1.0
0.5
0.0
*
Lin⁻
LKS
LT-HSC
ST-HSC
MPP
CLP
CMP
GMP
MEP
Parent gate:
Lin⁻
LKS
LK^lowS^low
LKS⁻

◄ Figure 30. C3G deficiency in p210 mice alters hematopoietic stem and progenitor cell (HSPC) proportions in the bone marrow (BM) at disease onset. (**A**) Schematic representation of HSPC subpopulations within the hematopoietic hierarchy. Lineage-negative (Lin^-) cells lack mature lineage markers. Within this population, $Lin^-c\text{-}Kit^+Sca1^+$ (LKS) cells represent the least-committed compartment, including long- and short-term hematopoietic stem cells (LT/ST-HSC) and multipotent progenitors (MPP). Also within the Lin^- fraction, the lymphoid branch comprises common lymphoid progenitors (CLP), gated as $Lin^-c\text{-}Kit^{low}Sca1^{low}$ ($LK^{low}S^{low}$), whereas the myeloid branch includes common myeloid progenitors (CMP), which further differentiate into megakaryocyte-erythroid progenitors (MEP) and granulocyte-monocyte progenitors (GMP); these populations were gated within the $Lin^-c\text{-}Kit^+Sca1^-$ fraction (LKS^-). (**B**) Bar plots show the mean ± SEM of the percentage of each p210/C3G$^{HSC\text{-}Scl}$-KO HSPC subpopulation within the parental gate, normalized to p210/C3G$^{HSC\text{-}Scl}$-wt values (see **Figure 53**; **Annexes**). (**C**) Bar plots show the mean ± SEM of the percentage of each C3G$^{HSC\text{-}Scl}$-KO HSPC subpopulation within the parental gate, normalized to C3G$^{HSC\text{-}Scl}$-wt values (see **Figure 53**; **Annexes**). Parental gating markers are indicated below. Only 6-month-old mice were analyzed. Statistical analysis was performed using an unpaired t-test. *$p \leq 0.05$, **$p \leq 0.01$. Sample sizes: p210/C3G$^{HSC\text{-}Scl}$-wt, n = 7; p210/C3G$^{HSC\text{-}Scl}$-KO, n = 8, C3G$^{HSC\text{-}Scl}$-wt, n = 6; C3G$^{HSC\text{-}Scl}$-KO, n = 6. a.u., arbitrary units.

Collectively, these results suggest that the deletion of C3G in HSCs reshapes the hematopoietic landscape under conditions of hematopoietic stress, such as a myeloproliferative disease. The previous observation that p210/C3G$^{HSC\text{-}Scl}$-KO mice display lower neutrophil levels in PB during advanced disease stages, together with these findings, indicates a possible defect in myeloid maturation in the BM or in the release of mature cells into circulation. In summary, whereas BCR::ABL1 drives massive neutrophil differentiation and their subsequent release into the blood, C3G deficiency appears to slow down this process.

1.9. p210/C3G$^{HSC\text{-}Scl}$-KO bone marrow neutrophils display impaired migration properties

The possible impaired neutrophil maturation observed in the p210/C3G$^{HSC\text{-}Scl}$-KO mice at CML onset raised the question of their functionality. Neutrophil migration in response to a chemotactic stimulus is one of the main responses carried out by these cells, critical in inflammatory responses. In CML, neutrophil migration is typically altered, often displaying abnormal speed, directionality, or responsiveness to chemoattractants (Radhika *et al.*, 2000).

To address this, we performed a Transwell assay (**Figure 31A**) to assess the ability of BM neutrophils to migrate in response to fMLP, a small bacterial peptide recognized by innate immune cells as a danger signal, acting thereby as a potent chemoattractant. For this experiment, BM from six-month-old p210 mice that had been TAM-treated during the first month of life was isolated and stained with neutrophil markers for identification by flow cytometry. BM suspensions were then seeded into the upper chamber of Transwell inserts, with different concentrations of fMLP placed in the lower chamber. After 1 hour of incubation, BM neutrophils that migrated from the upper to the lower chamber were quantified by flow cytometry and normalized to a control condition.

Results obtained showed that crescent concentrations of fMLP promoted a higher migration of BM neutrophils to the lower chamber, as expected. Interestingly, BM neutrophils from p210/C3G$^{HSC\text{-}Scl}$-KO mice displayed defective migration at higher concentrations of fMLP (**Figure 31B**), suggesting an impaired mobilization capacity.

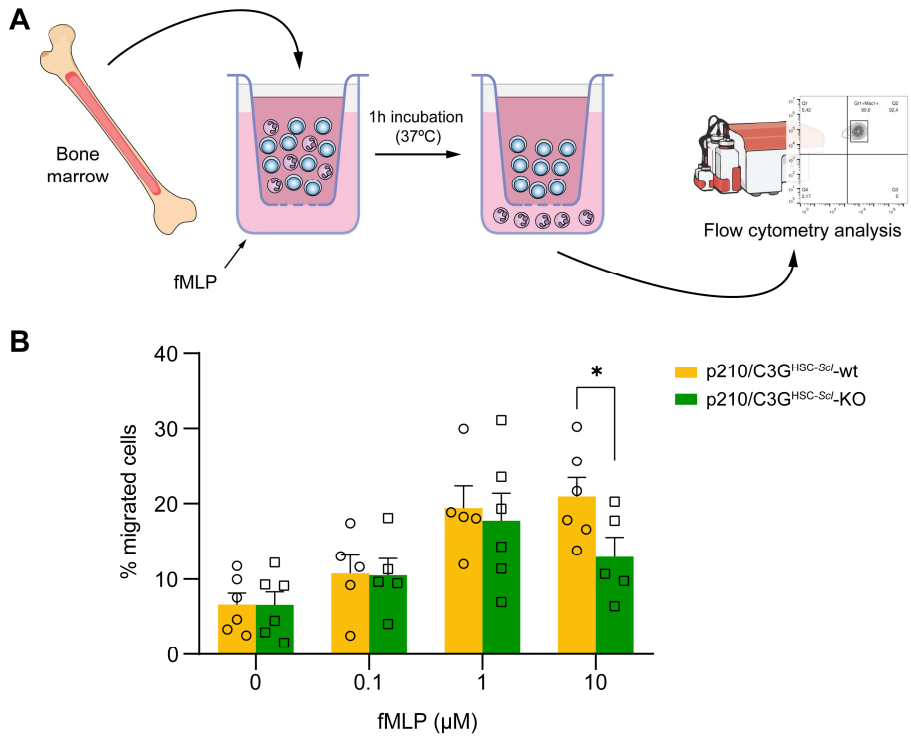

Figure 31. C3G deficiency in p210 mice impairs bone marrow (BM) neutrophil migration at disease onset. (**A**) Schematic of the Transwell assay. Briefly, Gr1^{+}Mac1^{+}-marked BM cells were seeded in the top chamber and allowed to migrate toward the bottom chamber containing fMLP, a potent neutrophil chemoattractant. Migrated Gr1^{+}Mac1^{+} cells were then quantified by flow cytometry. (**B**) Bar plots show the mean ± SEM of the percentage of migrated Gr1^{+}Mac1^{+} cells relative to the total Gr1^{+}Mac1^{+} BM population. Statistical analysis was performed using two-way ANOVA followed by multiple-comparison tests. *p ≤ 0.05. Sample sizes: p210/C3G$^{HSC\text{-}Scl}$-wt, n = 5-6; p210/C3G$^{HSC\text{-}Scl}$-KO, n = 5-6, depending on the condition.

Defective migration in response to chemotactic stimulus in p210/C3G$^{HSC\text{-}Scl}$-KO neutrophils, may reflect an underlying impairment in their maturation process. This finding, together with the altered levels of myeloid-committed HSPCs, raised the possibility that C3G is required for proper neutropoiesis, and that its absence hampers neutrophil production, thereby attenuating the myeloproliferative phenotype characteristic of CP-CML.

2. Analysis of the role of C3G in a cellular model of CML

2.1. C3G expression is reduced in Ba/F3 cells expressing BCR::ABL p210

To further investigate the role of C3G in CML and to gain insight into the underlying cellular and molecular mechanisms, the results obtained from the transgenic mouse model were complemented with experiments performed in a cellular CML model. This approach allows the performance of experiments that would be difficult to carry out *in vivo*, while also reducing the number of animals required for the study. For this purpose, the Ba/F3 cell line was selected.

Ba/F3 is a hematopoietic cell line derived from mouse BM progenitor cells of C3H mice (Didion *et al.*, 2014) and corresponds to an early-stage B-lymphoid precursor, specifically at the pro-B stage (Palacios and Steinmetz, 1985). Owing to its poorly committed hematopoietic cellular background, Ba/F3 represents a suitable model for this study, as CML LSCs are thought to arise from weakly-committed hematopoietic progenitor cells, as discussed in **Introduction section 1.3.2**.

First, we asked whether exogenous expression of the *BCR::ABL1 p210* oncogene alters C3G expression under basal conditions. C3G expression levels were assessed by comparing parental Ba/F3 cells with Ba/F3 cells transformed with *BCR::ABL1 p210* (hereinafter referred as Ba/F3-p210, also known as Boff-p210). Interestingly, expression of BCR::ABL1 p210 was associated with reduced full-length C3G protein levels (**Figure 32A, B**). This observation suggests that BCR::ABL1 regulates C3G levels and, consequently, C3G activity, pointing to a functional relationship between these two proteins and a potential role for C3G in leukemogenic signaling. A BCR::ABL1–C3G crosstalk has been previously described in human CML cell lines (Gutiérrez-Berzal *et al.*, 2006; Maia *et al.*, 2009, 2013), but has not yet been explored in murine hematopoietic cell lines engineered to express exogenous BCR::ABL1 p210.

As described in the **Introduction section 2.3.1**, hematopoietic cells also express the shorter p87C3G isoform; however, under our experimental conditions it was not clearly detectable (see **Figure 54**; **Annexes**).

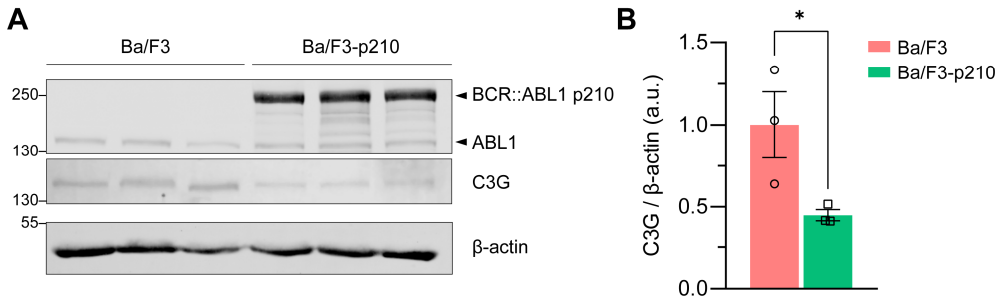

Figure 32. Transformation of Ba/F3 cells with *BCR::ABL1 p210* downregulates C3G expression. (**A**) Analysis of three independent protein lysates of Ba/F3 and Ba/F3-p210 cells showing BCR::ABL1 p210 and ABL1, alongside full-length C3G. β-actin levels were used as loading control. The molecular weights of the protein marker ladder are indicated in kDa. (**B**) Bar plots show the mean ± SEM of the densitometric quantification of C3G expression of all replicates normalized to β-actin, with values expressed relative to Ba/F3 control cells. Statistical analysis was performed using an unpaired t-test. *$p \leq 0.05$. a.u., arbitrary units.

This inverse correlation between BCR::ABL1 and C3G expression prompted us to further explore the role of C3G in Ba/F3-p210 cells. Specifically, we asked whether the leukemic properties of Ba/F3-p210 cells could be altered by exogenous modulation of C3G levels, in a manner comparable to the transgenic p210 mouse model in which C3G is inactivated.

2.2. Generation of Ba/F3-p210 cell lines with C3G overexpression and knockdown

Continuing along this line, Ba/F3-p210 cell lines with either C3G overexpression or knockdown were generated. By experimentally modulating C3G levels, this approach aims to clarify how C3G influences signaling and cellular behavior in BCR::ABL1-expressing cells. Ideally, protein function is assessed using knockout lines with complete loss of expression; however, previous attempts to generate C3G-knockout Ba/F3-p210 cells were unsuccessful, possibly due to the critical role of C3G in B-cell progenitor growth (Morán-Vaquero *et al.*, 2026). Therefore, in this work an alternative strategy was adopted to modify C3G expression levels using viral transduction, method that is much more efficient in cell lines.

For overexpression, cells were transduced with lentiviruses expressing either wild-type (WT) C3G or a constitutively active form carrying the Y554H mutation (Carabias *et al.*, 2020), to assess whether C3G activation, rather than mere overexpression, influences leukemic behavior. For gene knockdown, a construct encoding a shRNA targeting *Rapgef1* mRNA (C3Gi) was used to reduce C3G expression (Ortiz-Rivero *et al.*, 2018). Generated Ba/F3-p210 cell lines were named according to the lentiviral transfer plasmid used (pLenti or pLVTHM), the specific construct carried, and the reporter protein (GFP in all lines).

Seventy-two to ninety-six hours after lentiviral transduction of parental Ba/F3-p210 cells, GFP^+ cells were isolated by FACS and subsequently expanded in culture for experiments. pLenti lines were additionally cultured with 8 µg/mL blasticidin to enhance the selection of positive cells. Successful isolation of GFP^+ cells was confirmed by fluorescence microscopy and by flow cytometric analysis of the FACS-purified populations (**Figure 33**).

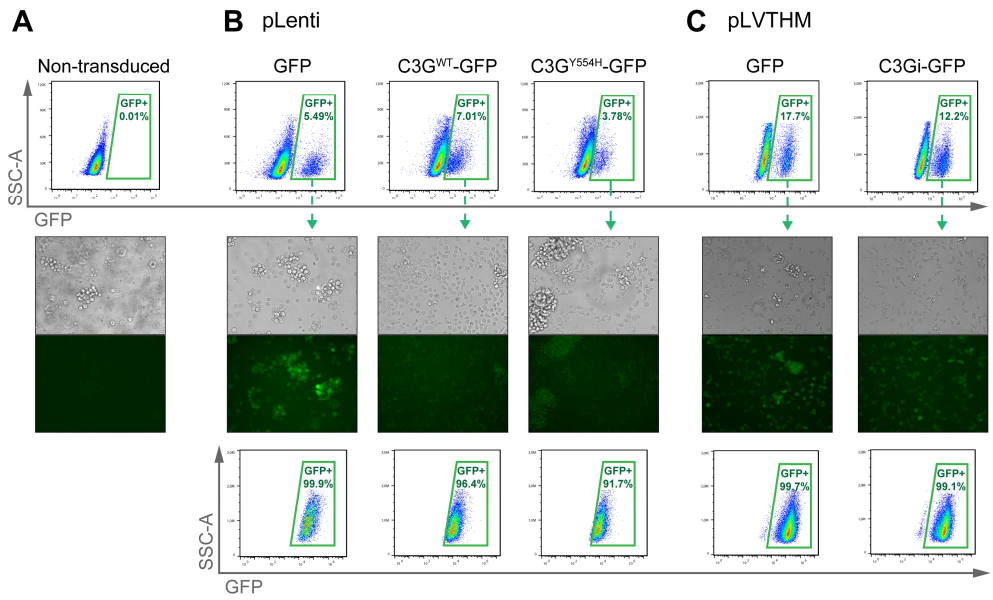

Figure 33. Generation of stable Ba/F3-p210 cell lines with C3G overexpression or knockdown via lentiviral transduction. (**A**) Non-transduced Ba/F3-p210 cells, showing no GFP signal by flow cytometry or fluorescence microscopy. (**B**) Ba/F3-p210 cells transduced with pLenti constructs: empty (GFP) or C3G overexpression ($C3G^{WT}$ and $C3G^{Y554H}$). Positively transduced cells were isolated by FACS and expanded in 8 µg/mL blasticidin. GFP expression was confirmed by both flow cytometry and fluorescence microscopy. (**C**) Ba/F3-p210 cells transduced with pLVTHM constructs: empty (GFP) or C3G knockdown (C3Gi). Positively transduced cells were isolated by FACS. GFP expression was confirmed by both flow cytometry and fluorescence microscopy.

C3G expression under steady-state conditions was assessed in the newly generated lines (**Figure 34**). Ba/F3-p210 cell lines overexpressing C3G exhibited, in addition to endogenous C3G, high levels of the C3G-GFP fusion protein, both for the WT and the Y554H mutant forms. In addition, the C3G-knockdown Ba/F3-p210 line showed a moderate reduction in C3G protein levels, confirming effective repression by the C3Gi shRNA. GFP expression was also verified, detecting both free GFP (in pLenti-empty and pLVTHM lines) and the C3G-GFP fusion protein in the overexpressing lines.

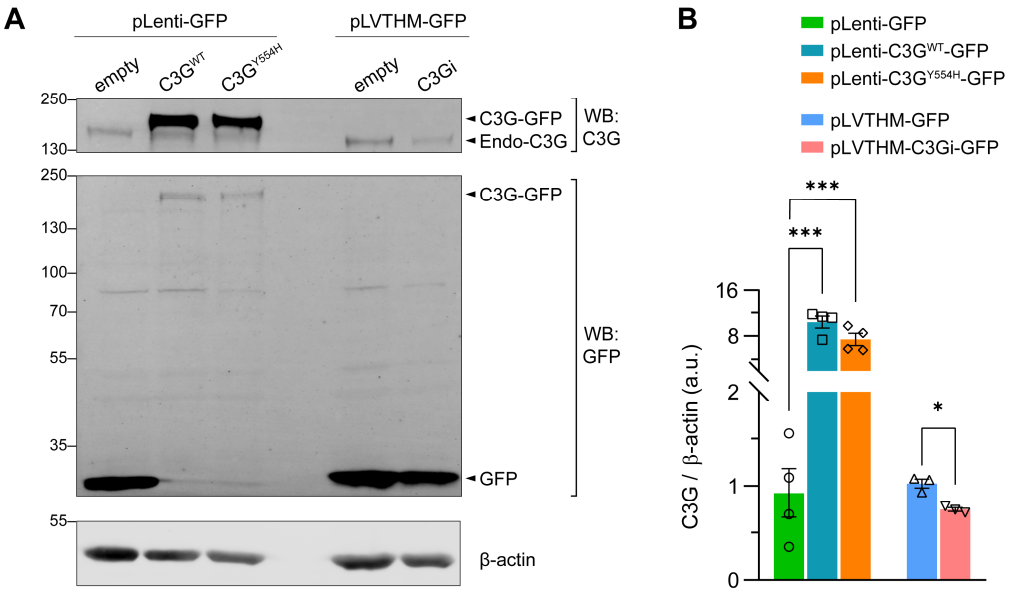

Figure 34. Assessment of C3G expression levels in the generated Ba/F3-p210 cells. (**A**) Representative experiment showing C3G expression. Immunoblotting with anti-C3G detected endogenous C3G (endo-C3G) and the C3G-GFP fusion in pLenti-C3G^{WT}-GFP and pLenti-C3G^{Y554H}-GFP overexpression lines, as well as a reduction in C3G expression in pLVTHM-C3Gi-GFP cells. Anti-GFP detected GFP alone or the C3G-GFP fusion, depending on the cell line. β-actin levels were used as loading control. The molecular weights of the protein marker ladder are indicated in kDa. (**B**) Bar plots show the mean ± SEM of the densitometric quantification of C3G expression normalized to β-actin for pLenti and pLVTHM lines, with values expressed relative to empty vector controls. At least three independent experiments were done. Statistical analysis was performed using an unpaired t-test. *p ≤ 0.05, ***p ≤ 0.001. a.u., arbitrary units, WB: Western blot.

C3G, as a Rap1 GEF, can activate the small GTPase Rap1 (Ichiba *et al.*, 1999). Therefore, alterations in C3G expression are likely to affect Rap1 activation. Assessing changes in Rap1 activation is particularly relevant in this context, given the established link between Rap1 and myeloproliferative diseases (Ishida *et al.*, 2003; Minato and Hattori, 2009), as described in **Introduction section 2.3.1**.

Rap1 activation was assessed in the different Ba/F3-p210 cell lines by pull-down assay (**Figure 35**). This approach allows quantification of Rap1-GTP, which can be normalized to total Rap1 to determine activation status. C3G-overexpressing lines displayed a marked increase in Rap1 activation, with the Y554H mutant showing slightly higher levels than the WT protein, consistent with observations in other cell lines (Carabias *et al.*, 2020). In contrast, the C3G-knockdown line exhibited only a modest reduction in Rap1 activation, suggesting that additional Rap1 GEFs may remain active and maintain Rap1-GTP levels (Stork and Dillon, 2005).

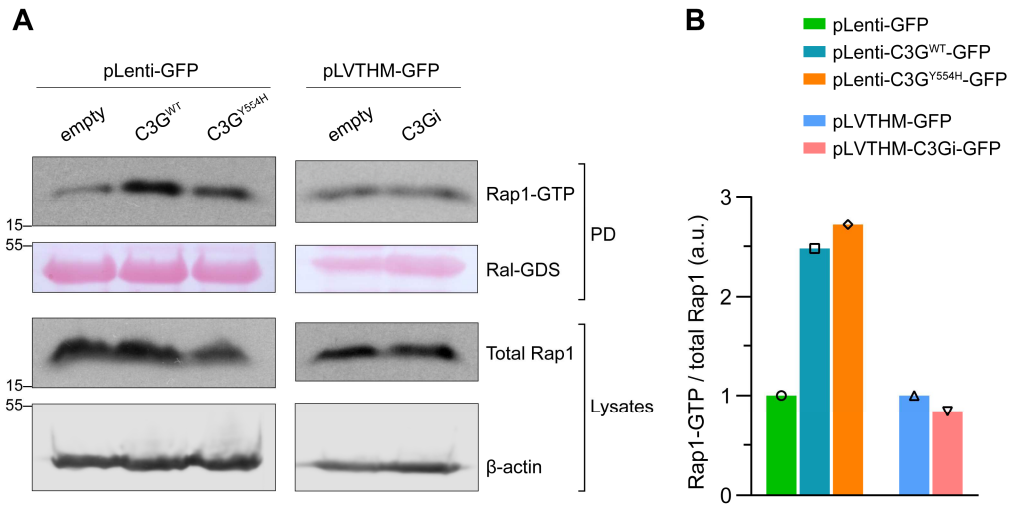

Figure 35. Assessment of Rap1 activation in the generated Ba/F3-p210 cells. (**A**) Rap1-GTP levels were determined by pull-down (PD) assay using GST-RalGDS-RBD as bait (shown). Total Rap1 levels were analyzed from protein lysates of the same samples. β-actin and Ral-GDS are shown as qualitative loading controls. The molecular weights of the protein marker ladder are indicated in kDa. (**B**) Bar plots show the values of the densitometric quantification of the Rap1-GTP/total Rap1 ratio for pLenti and pLVTHM lines, with values expressed relative to empty vector controls. a.u., arbitrary units.

Overall, these results indicate that the Ba/F3-p210 cell lines generated exhibit the expected alterations in C3G expression and Rap1 activation and are therefore suitable experimental models for examining the effect of C3G levels in a CML cellular context.

2.3. C3G status does not affect cell proliferation levels

Cell proliferation was first evaluated in the new generated lines. C3G can influence key pathways that regulate proliferation, such as the ERK1/2 pathway through the C3G–Rap1–B-Raf signaling axis (Ishimaru *et al.*, 1999). Moreover, the presence of BCR::ABL1 upstream in this pathway may further modify this process.

Proliferation was monitored over a 4-day period at 24-hour intervals by flow-cytometry-based cell counting. However, no significant differences in cell proliferation ratios were detected between Ba/F3-p210 cells overexpressing C3G (**Figure 36A**) or carrying C3G-knockdown (**Figure 36B**) and their respective controls at any time point.

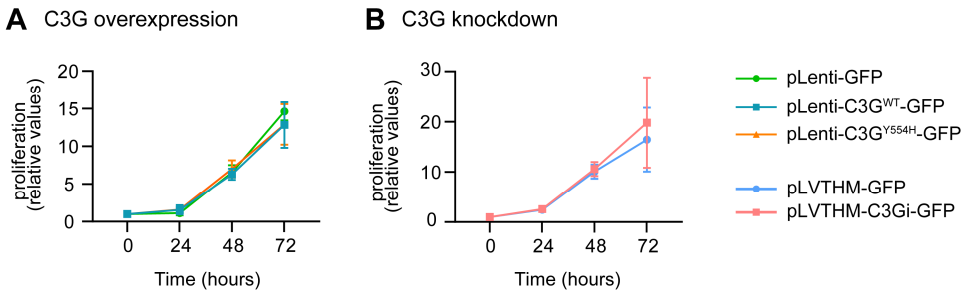

Figure 36. Altered C3G expression does not affect proliferation of Ba/F3-p210 cells. XY plots show the mean ± SEM of the cell counts at 24, 48 and 72 hours, normalized to hour 0, in the (**A**) pLenti and (**B**) pLVTHM lines. Three independent experiments were performed. a.u., arbitrary units.

These results indicate that C3G does not contribute to the proliferative pathways triggered by BCR::ABL1 in Ba/F3-p210 cells. Consequently, any phenotypic differences observed in these C3G-modified cells in subsequent assays are unlikely to originate from intrinsic alterations in cell growth.

2.4. Altered C3G expression levels modulate response to imatinib

As C3G did not alter basal proliferation, we examined whether stress stimuli uncovers C3G-dependent effects by inhibiting BCR::ABL1 with imatinib. Moreover, the apparent lack of response to imatinib observed in p210 mice under our experimental conditions prompted us to evaluate the effects of this drug in our C3G-modified Ba/F3-p210 cell models, in order to assess whether C3G expression levels could modulate imatinib response, as previously reported in other systems (Maia *et al.*, 2009). For this purpose, we assessed both cell viability and apoptotic responses to imatinib in the Ba/F3-p210 cell lines generated.

2.4.1. Effects of imatinib on Ba/F3-p210 cell viability

Viability of Ba/F3-p210 cells upon imatinib treatment was assessed by an MTT assay. Cells were exposed to imatinib at concentrations ranging from 0 to 2.0 µM, and viability was measured at 24, 48, and 72 hours post-treatment. This approach allowed us to estimate an approximate half-maximal inhibitory concentration (IC_{50}), defined as the drug concentration that reduced cell viability to 50%, which was subsequently used as the dose for apoptosis assays.

2.4.1.1. C3G overexpression reduces cell viability upon imatinib exposure

Notably, both Ba/F3-p210 lines overexpressing C3G^{WT} or C3G^{Y554H} generally exhibited increased sensitivity to imatinib compared to the control line (**Figure 37**). The effects varied with drug concentration, ranging from near insensitivity of Ba/F3-p210 cells at low concentrations (**Figure 37A**) to markedly reduced viability at higher concentrations (**Figure 37D–F**). At intermediate concentrations, differences between lines became apparent, most

clearly at 0.6 µM (**Figure 37B**) and less pronounced at 1.0 µM (**Figure 37C**) and 1.3 µM (**Figure 37D**). C3G^{Y554H}-overexpressing cells showed only slightly higher, non-significant, sensitivity than C3G^{WT}-overexpressing cells, suggesting that additional catalytic dysregulation of C3G moderately influence the survival of C3G-overexpressing CML cells upon imatinib treatment.

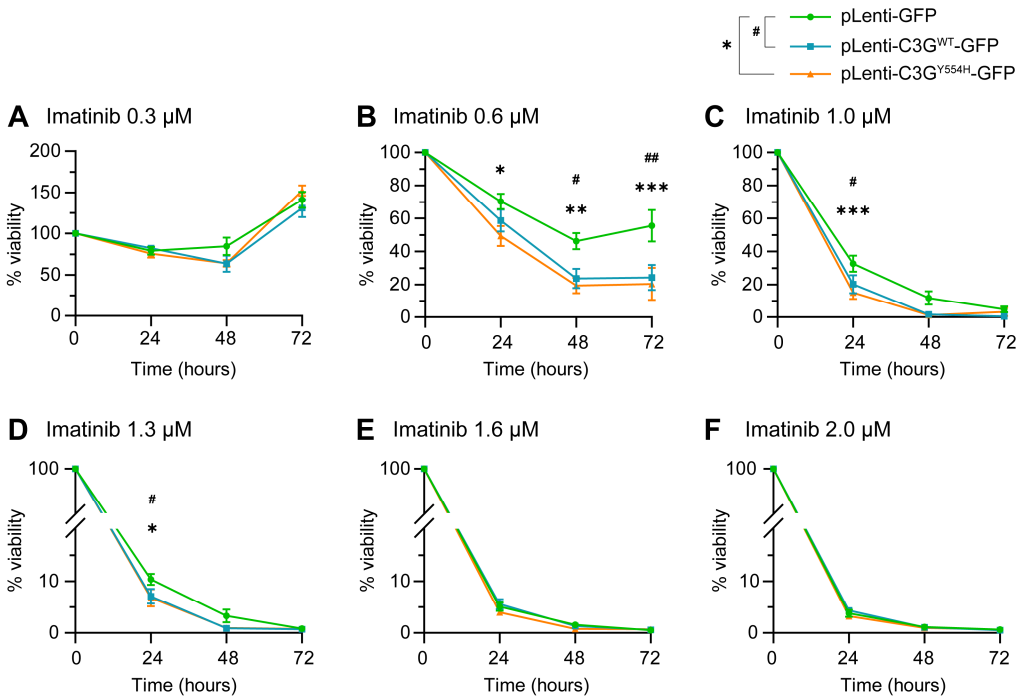

Figure 37. C3G overexpression reduces viability of Ba/F3-p210 cells upon imatinib treatment. XY plots show the mean ± SEM of the cell viability, expressed as a percentage relative to an untreated sample. Viability was measured by MTT assay at 24, 48, and 72 hours after treatment with imatinib at (**A**) 0.3 µM, (**B**) 0.6 µM, (**C**) 1.0 µM, (**D**) 1.3 µM, (**E**) 1.6 µM, and (**F**) 2.0 µM. Three independent experiments were performed. Statistical analysis was performed using two-way ANOVA followed by a multiple-comparison test. * pLenti-GFP vs pLenti-C3G^{Y554H}-GFP, # pLenti-GFP vs pLenti-C3G^{WT}-GFP; three symbols indicate $p \leq 0.001$, two symbols indicate $p \leq 0.01$, one symbol indicates $p \leq 0.05$.

2.4.1.2. C3G knockdown leads to decreased cell viability in response to imatinib

Interestingly, a similar effect was observed in the C3G-knockdown line. Ba/F3-p210 cells expressing the C3Gi shRNA showed an overall increased sensitivity to imatinib compared with the empty control cell line (**Figure 38**). As in the pLenti lines, the response was dose-dependent, ranging from minimal effects at low imatinib concentrations (**Figure 38A–C**) to more pronounced reductions in viability at higher doses (**Figure 38D–F**). Divergence in response between the cell lines became apparent at higher imatinib doses (**Figure 38D–F**).

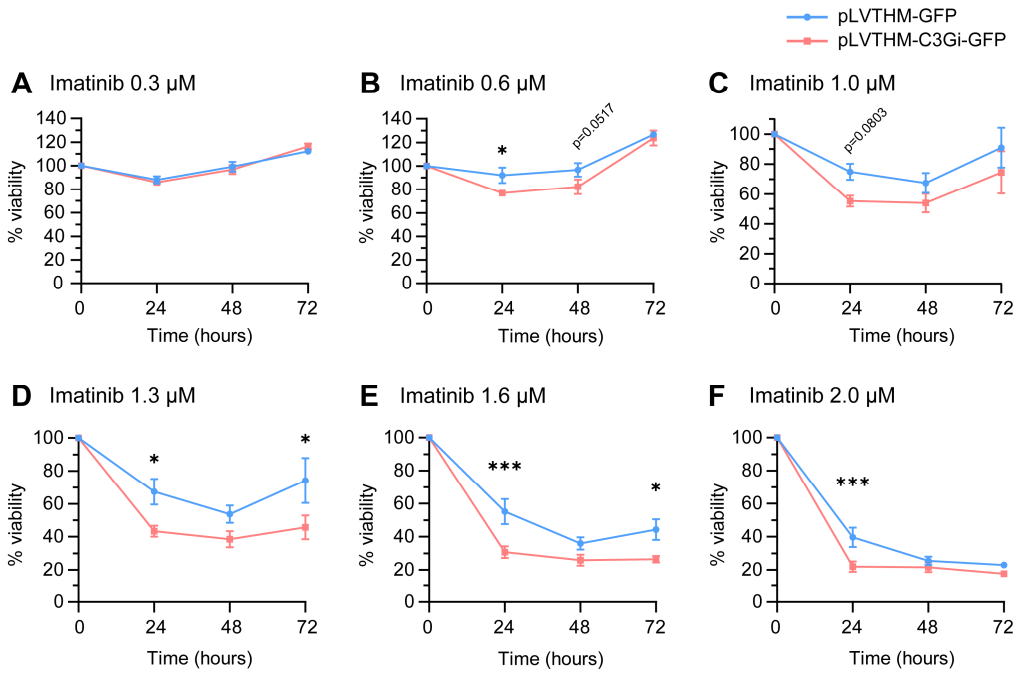

Figure 38. C3G knockdown reduces viability of Ba/F3-p210 cells upon imatinib treatment. XY plots show the mean ± SEM of the cell viability, expressed as a percentage relative to an untreated sample. Viability was measured by MTT assay at 24, 48, and 72 hours after treatment with imatinib at (**A**) 0.3 µM, (**B**) 0.6 µM, (**C**) 1.0 µM, (**D**) 1.3 µM, (**E**) 1.6 µM, and (**F**) 2.0 µM. Three independent experiments were performed. Statistical analysis was performed using two-way ANOVA followed by a multiple-comparison test. *$p \leq 0.05$, ***$p \leq 0.001$.

Notably, the pLenti-GFP cell lines displayed higher sensitivity to imatinib than the pLVTHM-GFP cell lines. This difference suggests that the lentiviral backbone itself may influence cellular physiology and modulate drug responsiveness, potentially through vector-specific effects on gene expression, metabolic state, or stress-response pathways, as reported in other studies (Ranjbar *et al.*, 2016). This observation highlights the importance of considering vector-related effects when comparing drug responses across independently generated cell lines.

Interestingly, in both experiments using pLenti- and pLVTHM-transduced Ba/F3-p210 cells, low concentrations of imatinib resulted in apparent cell viabilities exceeding 100% relative to untreated controls (**Figure 37A** and **Figure 38A–B**). This seemingly paradoxical effect is consistent with a hormetic response, in which low doses of a cytotoxic agent may stimulate proliferation or metabolic activity before having inhibitory effects at higher concentrations (Bao *et al.*, 2015). Since the MTT assay estimates cell viability based on metabolic activity, cells exposed to low drug doses that are metabolically more active may

appear to have “higher viability” than untreated cells, a phenomenon also reported in previous studies (Zhang *et al.*, 2015).

In summary, these experiments indicate a non-linear relationship between C3G expression levels and TKI resistance in BCR::ABL1-expressing cells. Both upregulation and downregulation of C3G enhanced sensitivity to imatinib, suggesting that C3G abundance must be tightly regulated to sustain pro-survival signaling and preserve drug tolerance in leukemic cells, as suggested in previous studies (Maia *et al.*, 2009).

2.4.2. Effects of C3G on imatinib-induced apoptosis in Ba/F3-p210 cells

To confirm that imatinib exerts a stronger effect on Ba/F3-p210 lines with either C3G overexpression or knockdown, we evaluated the apoptotic response to the drug. Imatinib induces apoptosis in CML cells primarily by inhibiting BCR::ABL1, thereby suppressing pro-survival signaling. Specifically, inhibition of BCR::ABL1 activity shuts down key pathways, including PI3K/AKT, JAK/STAT (particularly STAT5), and Ras-ERK1/2, ultimately triggering mitochondrial, caspase-dependent cell death (Belloc *et al.*, 2007).

Cells were treated with imatinib for 72 hours at concentrations close to the 72-hour IC_{50} determined by the MTT assay (pLenti: 0.6 µM; pLVTHM: 1.6 µM), providing optimal conditions for apoptosis assessment. Apoptosis was evaluated by flow cytometry through detection of phosphatidylserine exposure on the outer layer of the plasma membrane, an early hallmark of apoptotic cells. Apoptotic cells were therefore defined as Annexin V^+/7-AAD^- events, representing cells with intact plasma membranes that expose phosphatidylserine.

2.4.2.1. C3G overexpression enhances imatinib-induced apoptosis

Consistent with the viability assay results, apoptosis was increased following 72 hours of imatinib treatment in both Ba/F3-p210 cells lines overexpressing $C3G^{WT}$ and $C3G^{Y554H}$, compared to empty vector control (**Figure 39**). $C3G^{Y554H}$ induced a slightly higher apoptotic response than $C3G^{WT}$, mirroring the viability results and suggesting that differences in C3G catalytic activity modestly contribute to TKI-induced apoptosis.

No appreciable differences in apoptotic responses were observed under steady-state conditions, with the proportion of apoptotic cells comparable between C3G-overexpressing and control cell lines.

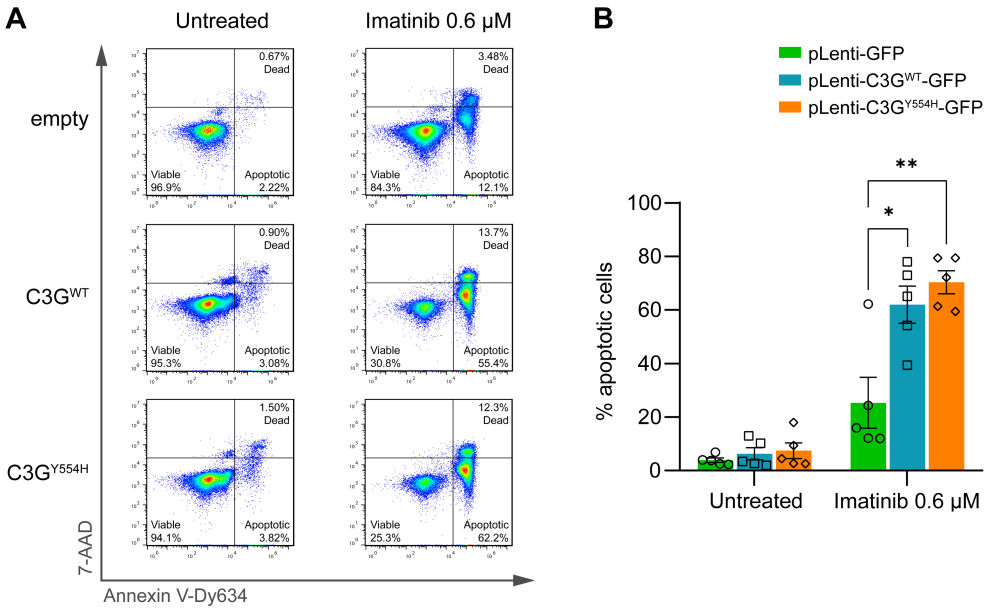

Figure 39. C3G overexpression enhances the apoptotic response of Ba/F3-p210 cells to imatinib. (**A**) Representative flow cytometry plots showing apoptotic cell levels in pLenti cell lines under control and imatinib-treated conditions. (**B**) Bar plots show the mean ± SEM of the percentage of apoptotic cells (Annexin V^+ 7-AAD^-) measured by flow cytometry 72 hours after drug addition. At least three independent experiments were performed. Statistical analysis was performed using an unpaired t-test. *$p \leq 0.05$, **$p \leq 0.01$.

2.4.2.2. C3G knockdown increases apoptosis in response to imatinib

Consistent with the previous assays, a slight but significant increase in apoptotic cells was observed in the C3G-knockdown cell line after 72 hours of imatinib treatment (**Figure 40**). Under basal conditions, no differences in the proportion of apoptotic cells were detected, similar to the pattern observed in C3G-overexpressing cells.

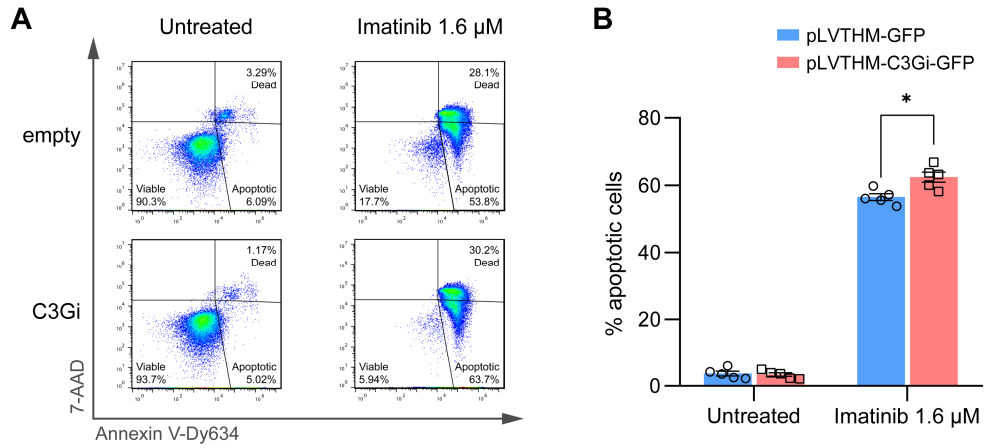

◄ Figure 40. C3G knockdown enhances the apoptotic response of Ba/F3-p210 cells to imatinib. (**A**) Representative flow cytometry plots showing apoptotic cell levels in pLVTHM cell lines under control and imatinib-treated conditions. (**B**) Bar plots show the mean ± SEM of the percentage of apoptotic cells (Annexin V^+ 7-AAD^-) measured by flow cytometry 72 hours after drug addition. At least three independent experiments were performed. Statistical analysis was performed using an unpaired t-test. *$p \leq 0.05$, **$p \leq 0.01$.

These results confirm the enhanced responsiveness to imatinib of CML cells with altered C3G expression, as reflected by both reduced viability and increased apoptotic responses. This dual phenomenon, also observed in other C3G-modified leukemic cell lines (Maia *et al.*, 2009, 2013), suggests that dysregulated C3G expression compromises CML cell survival under stress, prompting further investigation into the molecular mechanisms underlying this increased TKI sensitivity.

2.5. Altered C3G expression modulates major leukemogenic signaling pathways

C3G participates as a modulatory factor in multiple signaling pathways downstream of BCR::ABL1, as described in **Introduction section 2.3.1**. In K562 cells, for instance, C3G can exert dual roles in proliferation signaling: it can activate ERK1/2 via Rap1, but it can also inhibit both ERK1/2 and PI3K/AKT pathways through Rap1-independent mechanisms (Maia *et al.*, 2009). This signaling complexity in BCR::ABL1-expressing cells prompted us to examine how C3G modulation affects steady-state oncogenic signaling in Ba/F3-p210 cells.

2.5.1. Changes in C3G expression tend to attenuate BCR::ABL1 activation

BCR::ABL1 is a constitutively active tyrosine kinase that drives oncogenic signaling by phosphorylating multiple downstream substrates, reshaping all cellular signaling network. Accordingly, evaluating its activation status is crucial for assessing the intensity of leukemogenic signaling. The phosphorylation state of the ABL1 kinase domain serves as a functional readout of BCR::ABL1 activity; in particular, phosphorylation at Y412 reflects kinase activation. Mechanistically, the coiled-coil domain of the BCR moiety of BCR::ABL1 promote its dimerization, allowing its transactivation through phosphorylation of the ABL1 kinase domain (**Figure 41A**) (Hantschel, 2012).

Interestingly, analysis of BCR::ABL1 phosphorylation in Ba/F3-p210 cells with altered C3G expression revealed notable trends. Although some differences did not reach statistical significance, both C3G overexpression and knockdown showed a tendency toward reduced p-BCR::ABL1 levels (**Figure 41B, C**), suggesting that deviations from physiological C3G expression may compromise oncogenic signaling. In parallel, p-ABL1 levels were also markedly decreased under both conditions (**Figure 41B, D**), likely reflecting that BCR::ABL1 and endogenous ABL1 share common regulatory mechanisms and respond similarly to perturbations in the signaling network.

Interestingly, overexpression of C3G^{Y554H} led to a moderate lower reduction in both p-BCR::ABL1 and p-ABL1 level ratio compared to overexpression of C3G^{WT}, suggesting that the Y554H form sustains phosphorylation, possibly through altered signaling or positive feedback.

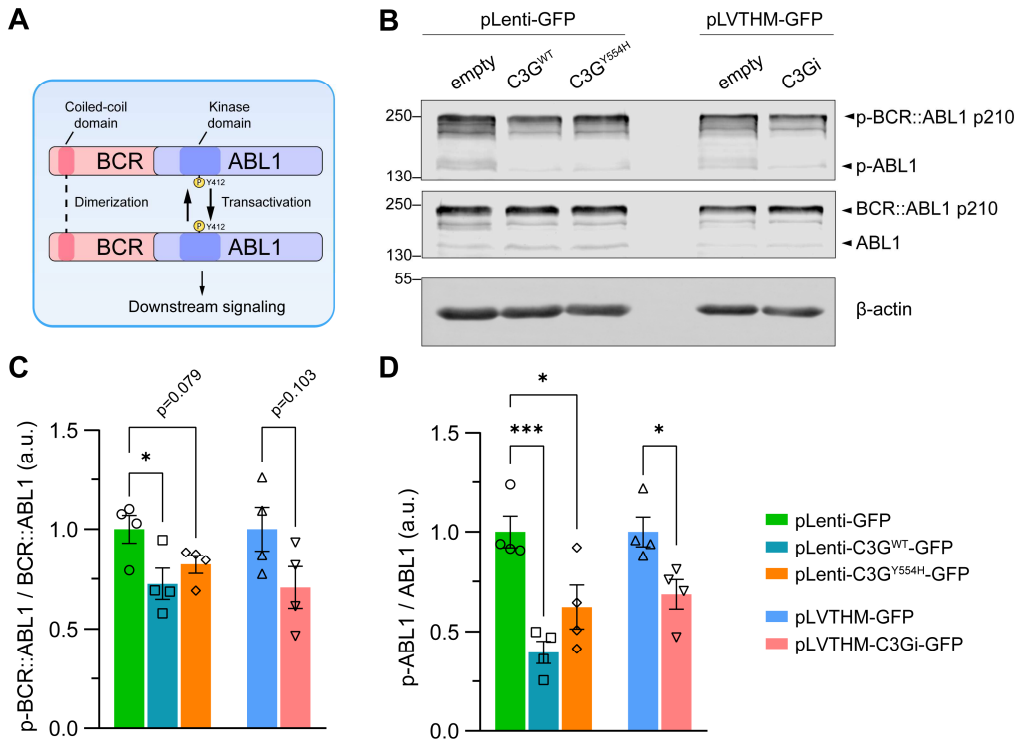

Figure 41. Alterations in C3G expression reduce the activation of BCR::ABL1 and ABL1. (**A**) Schematic representation of BCR::ABL1 activation. Through the coiled-coil domain of the BCR moiety, BCR::ABL1 dimerizes, enabling transactivation via phosphorylation of Y412 in the ABL1 kinase domain, thereby promoting downstream signaling. (**B**) Representative experiment showing the phosphorylation status of BCR::ABL1 and ABL1 under steady-state conditions. Immunoblotting with anti-ABL1 and anti-p-ABL1 antibodies detected both ABL1 (~130 kDa) and the BCR::ABL1 fusion protein (~250 kDa). β-actin is shown as a qualitative loading control. The molecular weights of the protein marker ladder are indicated in kDa. (**C–D**) Bar plots show the mean ± SEM of the densitometric quantification of the (**C**) p-BCR::ABL1/BCR::ABL1 ratio and (**D**) p-ABL1/ABL1 ratio in the different Ba/F3-p210 lines, with values expressed relative to empty vector controls. At least three independent experiments were performed. Statistical analysis was performed using an unpaired t-test. *p ≤ 0.05, ***p ≤ 0.001. a.u., arbitrary units.

Beyond BCR::ABL1 itself, analysis of its downstream substrates provides additional insight. As described in **Introduction section 2.3.1**, CrkL is a major BCR::ABL1 substrate (**Figure 42A**), and p-CrkL levels are widely used as a readout of BCR::ABL1 kinase activity. Upon phosphorylation, CrkL links tyrosine kinases such as BCR::ABL1 to downstream signaling pathways, thereby transmitting signals that regulate proliferation, survival, and

cytoskeletal dynamics (Oda *et al.*, 1994). In addition, CrkL is the main C3G adaptor protein in hematopoietic cells (Smit *et al.*, 1996), further supporting a BCR::ABL1–C3G relationship.

However, analysis of p-CrkL in the generated cell lines revealed no significant differences between conditions, with levels largely comparable in both C3G-overexpressing and C3G-knockdown Ba/F3-p210 cell lines (**Figure 42B, C**). This suggests that, although BCR::ABL1 signaling may be partially attenuated upon C3G modulation, residual kinase activity is sufficient to sustain CrkL phosphorylation.

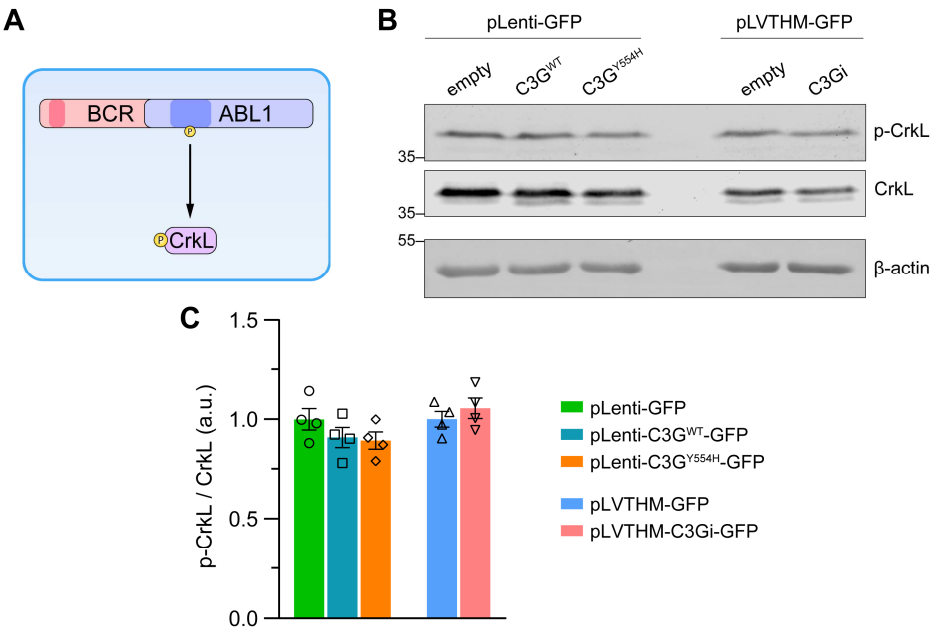

Figure 42. Phosphorylation of CrkL is not affected by altered C3G expression. (**A**) Schematic representation of CrkL activation via direct phosphorylation by BCR::ABL1. (**B**) Representative experiment showing the phosphorylation status of CrkL under steady-state conditions. β-actin is shown as a qualitative loading control. The molecular weights of the protein marker ladder are indicated in kDa. (**C**) Bar plots show the mean ± SEM of the densitometric quantification of the p-CrkL/CrkL ratio in the different Ba/F3-p210 lines, with values expressed relative to empty vector controls. At least three independent experiments were performed. Statistical analysis was performed using an unpaired t-test. a.u., arbitrary units.

2.5.2. ERK1/2 and PI3K/AKT pathways remain largely unaffected by C3G expression modulation

The ERK1/2 pathway acts as a major downstream effector of BCR::ABL1-driven signaling. Although it is not the most critical pathway in CML pathogenesis, BCR::ABL1 chronically activates this signaling axis, thereby promoting sustained proliferative signaling (**Figure 43A**). In a similar manner, the PI3K/AKT pathway plays a supportive role in BCR::ABL1-

mediated transformation by maintaining leukemic cell survival and metabolic activity, which are required to sustain high proliferative rates (**Figure 43A**) (McCubrey *et al.*, 2008).

Analysis of the activation status of the effector protein in these pathways in the generated Ba/F3-p210 cell lines revealed no significant differences upon modulation of C3G expression (**Figure 43B–D**). Notably, a slight tendency toward reduced ERK1/2 phosphorylation (**Figure 43B, C**) and increased AKT1/2/3 phosphorylation (**Figure 43B, D**) was observed in the C3G-knockdown cell line, potentially reflecting a feedback mechanism aimed at maintaining signaling homeostasis. Consistent with the proliferation assays presented in **Results section 2.3**, the lack of major alterations in ERK1/2 and PI3K/AKT signaling may explain the absence of detectable changes in cell proliferation, as these pathways are key regulators of this process (Jasek-Gajda *et al.*, 2020).

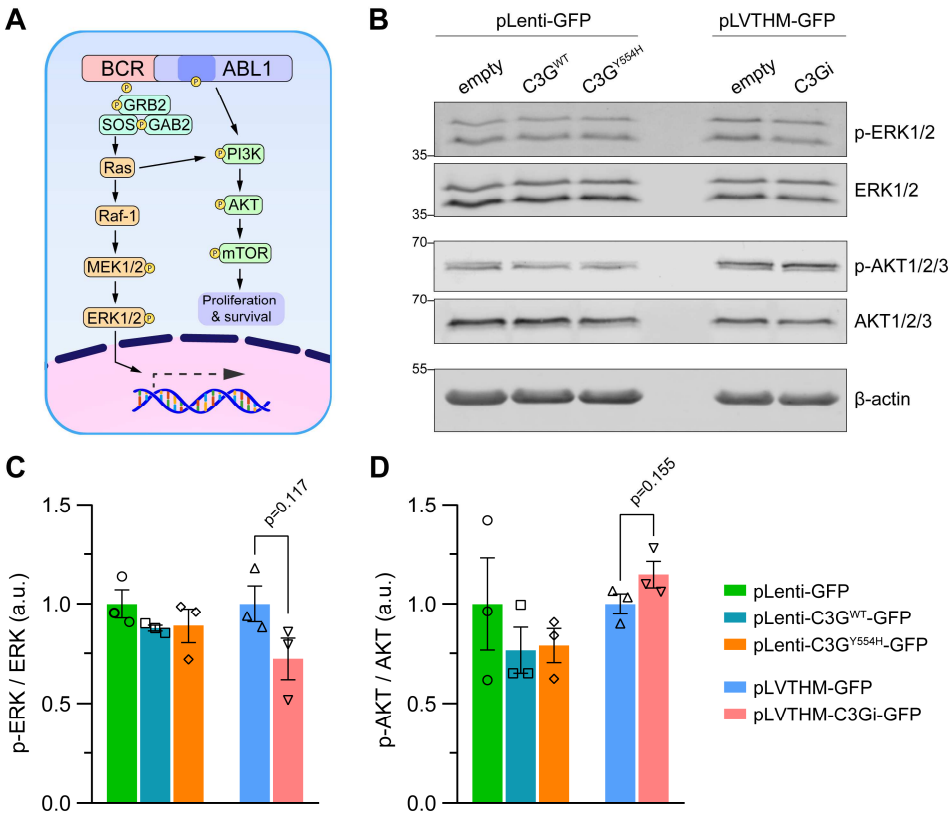

◄ Figure 43. Alterations in C3G expression have minimal impact on the activation of ERK1/2 and PI3K/AKT pathway. (**A**) Schematic representation of BCR::ABL1-mediated activation of the Ras-ERK1/2 and PI3K/AKT pathways. BCR::ABL1 constitutively activates the Ras pathway, ultimately leading to persistent ERK1/2 activation and promoting cell proliferation. Similarly, BCR::ABL1 activates PI3K, maintaining AKT and mTOR activity and promoting cell survival and metabolic activity. (**B**) Representative experiment showing the phosphorylation status of ERK1/2 and AKT1/2/3 under steady-state conditions. β-actin is shown as a qualitative loading control. The molecular weights of the protein marker ladder are indicated in kDa. (**C–D**) Bar plots show the mean ± SEM of the densitometric quantification of the (**C**) p-ERK1/2 / ERK1/2 ratio and (**D**) p-AKT1/2/3 / AKT1/2/3 ratio in the different Ba/F3-p210 lines, with values expressed relative to empty vector controls. At least three independent experiments were performed. Statistical analysis was performed using an unpaired t-test. a.u., arbitrary units.

2.5.3. Modulation of C3G expression markedly disrupts JAK/STAT signaling

In CML, the JAK/STAT pathway is considered a central leukemogenic signaling axis. Under physiological conditions, different JAK/STAT signaling pathways are activated upon cytokine binding to its receptor, which triggers intracellular signal transduction through receptor-associated JAK kinases (Hu *et al.*, 2021). In CML, however, BCR::ABL1 constitutively activates JAK kinases independently of cytokine stimulation, particularly JAK2, resulting in persistent phosphorylation and activation of STAT proteins, most notably STAT5 (**Figure 44A**). Once activated, STAT5 promotes a transcriptional program that defines the LSC phenotype, including not only constitutive proliferative and pro-survival signaling, but also the marked resistance to apoptosis that is typical of BCR::ABL1-expressing cells (Valent, 2014).

Analysis of the JAK/STAT pathway in our C3G-altered Ba/F3-p210 cell lines revealed notable differences between them (**Figure 44B–E**). Phosphorylation levels of JAK2 were significantly reduced in both C3G-overexpressing and C3G-silenced cells (**Figure 44B, C**), with no differences between $C3G^{WT}$ and $C3G^{Y554H}$ lines. Consistently, phosphorylation of both STAT3 (**Figure 44B, D**) and STAT5 (**Figure 44B, E**) was also decreased compared to the corresponding controls. In line with previous results, reduced BCR::ABL1 activity may contribute to the partial decrease in downstream targets such as JAK2, leading to weaker STAT activation. Functionally, these data indicate that modulation of C3G levels could perturb the BCR::ABL1–JAK/STAT signaling axis.

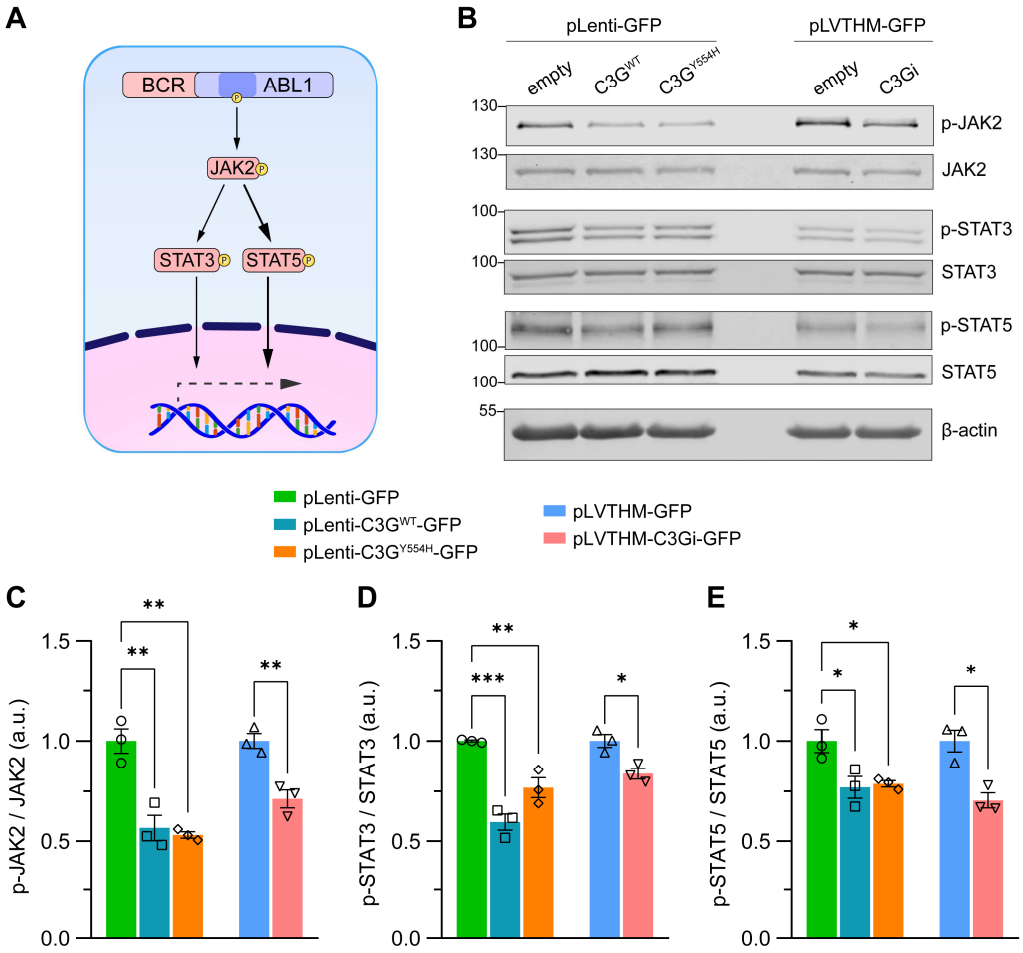

Figure 44. Alterations in C3G expression disrupt the JAK/STAT signaling pathway in Ba/F3-p210 cells. (**A**) Schematic representation of BCR::ABL1-mediated activation of the JAK/STAT pathway. BCR::ABL1 constitutively activates JAK2, leading to persistent STAT activation, particularly STAT5, which regulates the expression of genes essential for maintaining the leukemic phenotype. (**B**) Representative experiment showing the phosphorylation status of JAK2, STAT3, and STAT5 under steady-state conditions. β-actin is shown as a qualitative loading control. The molecular weights of the protein marker ladder are indicated in kDa. (**C–E**) Bar plots show the mean ± SEM of the densitometric quantification of the (**C**) p-JAK2/JAK2 ratio, (**D**) p-STAT3/STAT3 ratio, and (**E**) p-STAT5/STAT5 ratio in the different Ba/F3-p210 cells line, with values expressed relative to empty vector controls. Three independent experiments were performed. Statistical analysis was performed using an unpaired t-test. *p ≤ 0.05, **p ≤ 0.01, ***p ≤ 0.001. a.u., arbitrary units.

Interestingly, these findings align with the increased sensitivity of the C3G-altered cell lines to imatinib, as high STAT activation is known to mediate resistance of CML cells to TKIs (Warsch *et al.*, 2011), providing a plausible explanation for the phenotype observed in **Results section 2.4**.

The concordant reduction of p-JAK2, p-STAT3, and p-STAT5 levels indicates that modulation of C3G affects signaling upstream in the JAK/STAT pathway, likely at the level of JAK2 itself. Both C3G overexpression and knockdown appear to impair JAK2 activation in BCR::ABL1-expressing cells, suggesting that precise C3G levels are required to maintain optimal pathway activity. This bidirectional effect may reflect a non-linear relationship, similar to the TKI-mediated effects on cell survival, in which either excessive or insufficient C3G disrupts the formation or stability of signaling complexes necessary for efficient JAK2 phosphorylation and downstream STAT activation.

3. Study of C3G role in regulating neutrophil differentiation *in vitro*

3.1. Generation of 32D cell lines with overexpression and knockdown of C3G

Results obtained in the CML mouse model, which displayed impaired granulopoiesis, together with the disrupted JAK/STAT signaling observed in CML cell models, prompted further investigation into the potential role of C3G in hematopoietic differentiation.

JAK/STAT signaling is a central regulator of hematopoietic differentiation, transducing cytokine-mediated signals that control proliferation, survival, and lineage specification. In particular, this pathway is essential for proper neutrophil maturation, with STATs orchestrating the differentiation of myeloid progenitors (Coffer *et al.*, 2000; Zhang *et al.*, 2010). Disruptions of JAK/STAT signaling impair these processes, leading to defective hematopoietic cell output (Fasouli and Katsantoni, 2021), as evidenced by conditional *Jak1*-deficient mice, which exhibit impaired progenitor potential (Kleppe *et al.*, 2017). The modulation of this signaling pathway by C3G, as observed in our CML cell models, together with the altered distribution of myeloid progenitors in C3G-deficient mice, indicates that C3G might contribute to the regulation of myeloid maturation and differentiation.

To explore this possibility in more detail, an *in vitro* neutrophil differentiation model was used, employing for that purpose the 32D cell line. 32D is a murine IL-3-dependent myeloblast-like cell line that can be stimulated with granulocyte colony-stimulating factor (G-CSF), a cytokine that triggers the initiation of a neutrophilic differentiation program (Nakajima and Ihle, 2001). Based on the results obtained throughout this work, we hypothesize that C3G plays a functional role in this process, such that alterations in C3G expression in either direction may compromise the proper execution of the myeloid differentiation program through modulation of JAK/STAT signaling.

To evaluate the contribution of C3G to this process, 32D cell lines with modified C3G expression were generated using the same strategy applied to Ba/F3-p210 cells. As no notable differences were observed between $C3G^{WT}$ and $C3G^{Y554H}$ overexpression lines in

Ba/F3-p210 cells, only the C3G^{WT} overexpression line was generated in 32D cells, together with the C3G knockdown line.

C3G-modified stable 32D cell lines were generated by lentiviral transduction, followed by isolation of GFP^{+} cells by FACS and subsequent expansion of the cultures (**Figure 45**). The pLenti-GFP 32D cell lines were cultured in the presence of 8 µg/mL blasticidin for at least 3 weeks to ensure stable selection. As with Ba/F3-p210, generated 32D cell lines were named according to the lentiviral transfer plasmid used (pLenti or pLVTHM), the specific construct carried, and the reporter protein (GFP in all lines).

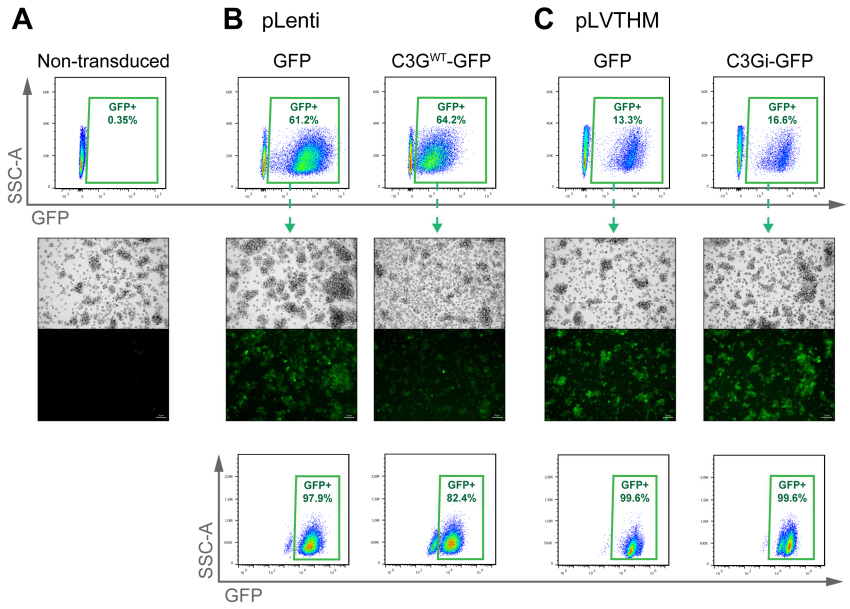

Figure 45. Generation of stable 32D cell lines with C3G overexpression or knockdown via lentiviral transduction. (**A**) Non-transduced 32D cells, showing no GFP signal by flow cytometry or fluorescence microscopy. (**B**) 32D cells transduced with pLenti constructs: empty (GFP) or C3G overexpression (C3G^{WT}). Positively transduced cells were expanded in 8 µg/mL blasticidin and isolated by FACS. GFP expression was confirmed by both flow cytometry and fluorescence microscopy. (**C**) 32D cells transduced with pLVTHM constructs: empty (GFP) or C3G silencing (C3Gi). Positively transduced cells were isolated by FACS. GFP expression was confirmed by both flow cytometry and fluorescence microscopy.

Basal C3G expression was assessed to confirm altered protein levels in the obtained 32D cell lines. The C3G^{WT}-overexpressing 32D cell line exhibited high levels of the C3G-GFP fusion protein in addition to the endogenous C3G. In addition, the C3Gi shRNA-expressing 32D cell line showed a marked reduction in C3G protein levels compared with its empty vector control (**Figure 46**).

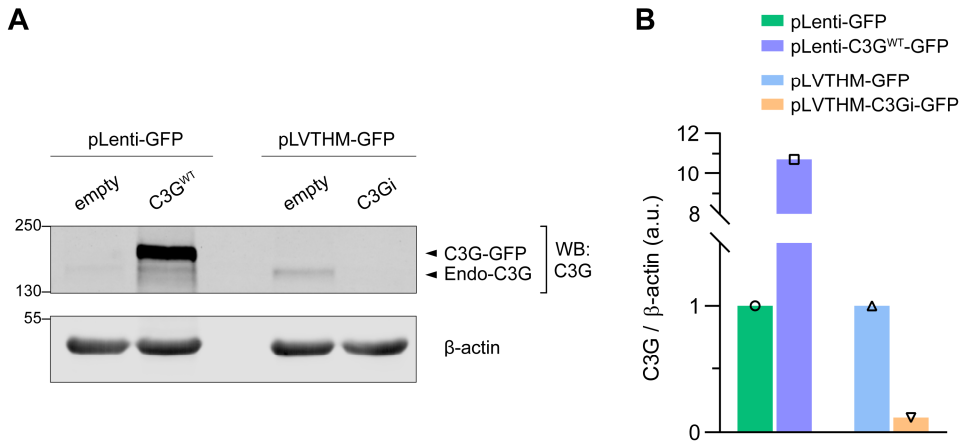

Figure 46. Assessment of C3G expression levels in the generated 32D cell lines. (**A**) Experiment showing C3G expression. Immunoblotting with anti-C3G antibody detected endogenous C3G (endo-C3G) and the C3G-GFP fusion in pLenti-C3G^{WT}-GFP overexpressing cell line, as well as a decline in C3G expression in pLVTHM-C3Gi-GFP cells. β-actin levels were used as loading control. The molecular weights of the protein marker ladder are indicated in kDa. (**B**) Bar plots show the values of the densitometric quantification of C3G expression normalized to β-actin for pLenti and pLVTHM lines, with values expressed relative to empty vector controls. a.u., arbitrary units, WB: Western blot.

In general, 32D cells express low levels of C3G, with endogenous C3G being barely detectable even when high amounts of protein were loaded (70 µg per lane in **Figure 46A**). Nevertheless, the generated 32D cell lines displayed the expected modulation of C3G expression and are therefore suitable for studying the impact of altered C3G levels in this myeloid differentiation model.

3.2. C3G modulates G-CSF-induced signaling in 32D cells

Myeloid cells arise in the BM from hematopoietic progenitors upon stimulation by cytokines such as the aforementioned G-CSF, as well as granulocyte-macrophage colony stimulating factor (GM-CSF) and macrophage colony-stimulating factor (M-CSF), each signaling through distinct pathways (Ushach and Zlotnik, 2016). G-CSF engages JAK1 or JAK2 proteins to promote neutrophil maturation via STAT3, directing progenitors toward the neutrophilic lineage. In contrast, GM-CSF preferentially activates JAK2 and STAT5, which antagonizes STAT3 by promoting monocyte development and limiting neutrophil production, primarily through induction of suppressors of cytokine signaling (SOCS), that inhibits the JAK/STAT3 pathway. This antagonistic interplay between STAT3 and STAT5 is a key determinant of myeloid lineage commitment (Zhang *et al.*, 2023). M-CSF, by contrast, signals largely through JAK/STAT-independent mechanisms, relying instead on ERK1/2 and PI3K/AKT pathways to regulate proliferation, survival, and functional maturation of monocytes/macrophages (Rolph and Das, 2020). In G-CSF and GM-CSF signaling, ERK1/2 and PI3K/AKT exert complementary functions, supporting progenitor proliferation,

survival, and metabolic competence (Souza *et al.*, 2013). Together, these pathways orchestrate the balanced differentiation and expansion of myeloid lineages under homeostatic conditions.

G-CSF drives neutropoiesis by activating its receptor, G-CSF-R (CD114), which triggers a signaling cascade primarily mediated by the JAK/STAT pathway (**Figure 17** in **Methods section 13.4**). Within this network, individual STAT proteins play distinct roles, being specifically STAT3 critical for G-CSF-induced neutrophilic differentiation, supporting both proliferation and survival of specific myeloid progenitors (Park *et al.*, 2022).

In Ba/F3-p210 cells, alterations in C3G expression level in any direction disrupted JAK/STAT activation, suggesting that precise regulation of C3G levels is critical for proper signaling. Consequently, altered C3G levels may impair G-CSF-induced signal transduction, delaying the initiation of the differentiation program in myeloid-committed hematopoietic progenitors. Based on the previous results, we hypothesized that C3G may modulate neutrophil differentiation by regulating signaling downstream of G-CSF-R.

To test this hypothesis, the generated 32D cell lines were stimulated with IL-3 (as a control for steady-state conditions) or G-CSF, and the activation status of key downstream effectors in the JAK/STAT, ERK1/2, and PI3K/AKT pathways was analyzed.

3.2.1. C3G overexpression maintains STAT3 while reducing ERK activation upon G-CSF stimulation

Serum- and IL-3-starved C3G-overexpressing and control 32D cells were stimulated with 10% IL-3 for 30 min or 50 ng/mL G-CSF for 5, 15 and 30 min, a common time window to observe robust STAT3 activation upon this stimulus (Zhang *et al.*, 2023). This high cytokine concentration was used to strongly activate the JAK/STAT3 and associated signaling pathways responsible for initiating neutrophilic differentiation (**Figure 47A**), allowing us to detect potential differences between the two conditions.

G-CSF stimulation induced a rapid increase in STAT3 phosphorylation, detectable 5 minutes after cytokine addition, which gradually declined over time (**Figure 47B, C**). This confirms intact receptor-mediated signaling and proper responsiveness of 32D cells to G-CSF. However, the magnitude of STAT3 activation at all incubation times in the C3G-overexpressing cells was comparable to that observed in control cells, indicating that elevated levels of C3G does not alter STAT3 pathway output in a neutrophil-differentiating context. As expected, STAT3 was not activated upon IL-3 stimulation given that IL-3-induced signaling is mainly mediated by the JAK/STAT5 axis (Podolska *et al.*, 2024) (**Figure 47B, C**).

Indeed, STAT5 was robustly activated upon IL-3 stimulation. In contrast, G-CSF induced only modest STAT5 activation, consistent with the notion that G-CSF signaling is primarily driven through JAK/STAT3 (Park *et al.*, 2022). C3G overexpression caused a marked reduction in STAT5 activation following IL-3 stimulation, revealing a negative effect of C3G on STAT5 activation (**Figure 47B, D**). Notably, C3G overexpression preferentially attenuated STAT5 rather than STAT3 activation, as STAT3 levels remained largely unchanged after G-CSF stimulation (**Figure 47B, C**). In line with observations in Ba/F3-p210 cells, increased C3G expression correlated with reduced STAT signaling, here predominantly affecting STAT5. This differential inhibitory pattern suggests that C3G does not directly target STAT proteins but rather modulates the upstream signaling environment that governs STAT activation, likely at the level of JAK kinase-cytokine receptor complexes.

ERK was strongly activated upon IL-3 stimulation in 32D cells, consistent with the proliferative role of this cytokine (Heard *et al.*, 1986). Overexpression of C3G attenuated ERK phosphorylation in response to IL-3, and a similar reduction was observed upon G-CSF stimulation, despite the more moderate ERK activation induced by this cytokine (**Figure 47B, E**). Under IL-3, this effect occurred alongside decreased STAT5 activation (**Figure 47B, D**), indicating that C3G-mediated modulation of receptor-associated signaling complexes can simultaneously inhibit both the JAK/STAT5 and ERK1/2 pathways. The reduction of ERK phosphorylation under both IL-3 and G-CSF suggests that elevated C3G levels targets a shared downstream pathway rather than cytokine-specific signaling.

Regarding the AKT pathway, IL-3 induced a moderate activation, whereas G-CSF triggered a stronger response, peaking later than STAT3 and ERK at approximately 15 minutes. However, no significant differences in AKT activation were detected upon C3G overexpression, either under steady-state conditions, in the IL-3 control, or following G-CSF stimulation (**Figure 47B, F**).

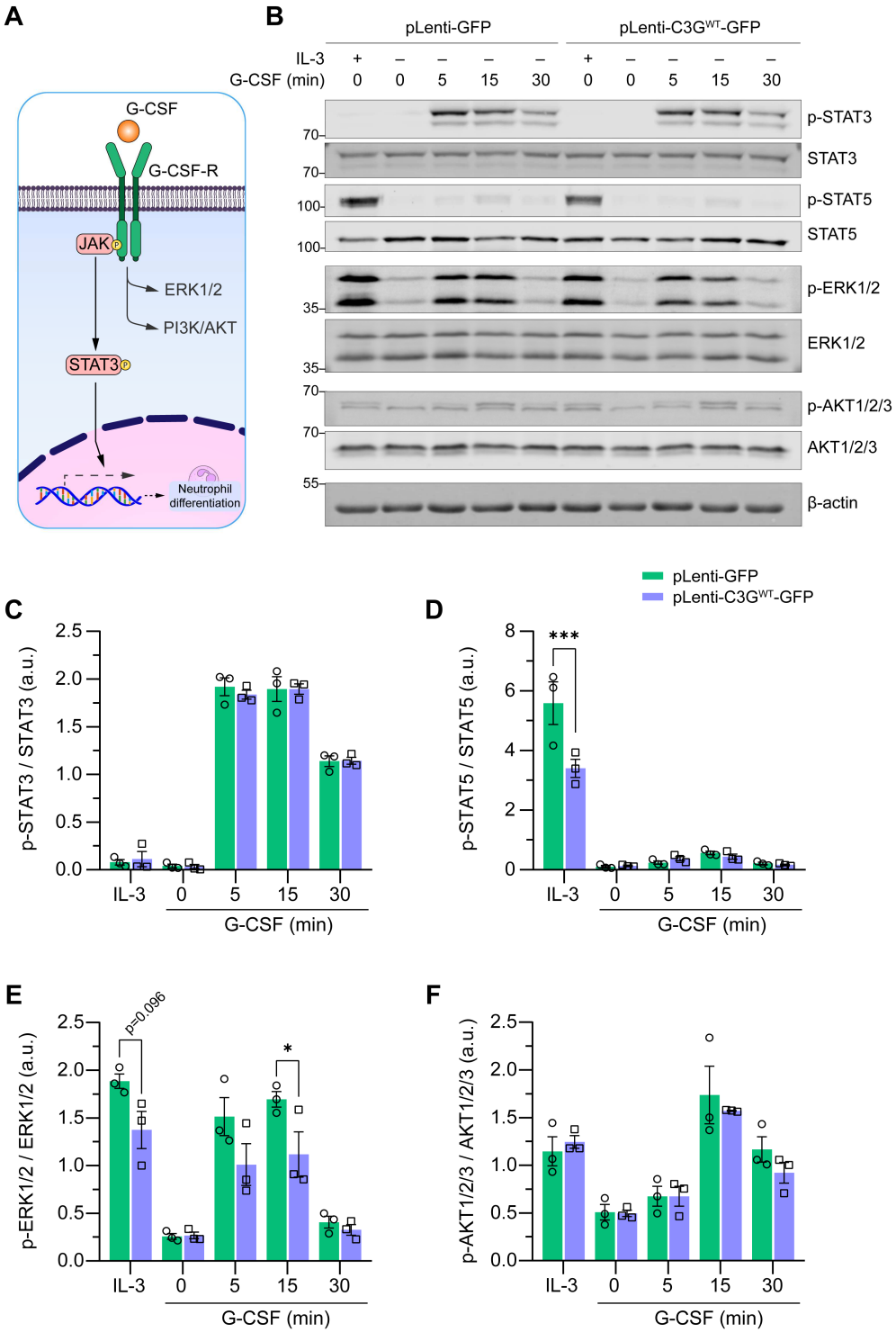
A
G-CSF
G-CSF-R
JAK
ERK1/2
PI3K/AKT
STAT3
Neutrophil differentiation
B
pLenti-GFP
pLenti-C3G^WT-GFP
IL-3
G-CSF (min)
p-STAT3
STAT3
p-STAT5
STAT5
p-ERK1/2
ERK1/2
p-AKT1/2/3
AKT1/2/3
β-actin
C
p-STAT3 / STAT3 (a.u.)
D
p-STAT5 / STAT5 (a.u.)
***
E
p-ERK1/2 / ERK1/2 (a.u.)
p=0.096
*
F
p-AKT1/2/3 / AKT1/2/3 (a.u.)

◄ Figure 47. C3G overexpression reduces ERK activation but does not affect STAT3 activation in 32D cells upon G-CSF stimulation. (**A**) Schematic representation of G-CSF-R downstream signaling. Upon binding G-CSF, the receptor activates JAK, leading to STAT3 activation, the main mediator of the neutrophil differentiation program. STAT3 then translocates into the nucleus and regulates the expression of genes driving neutrophil differentiation. ERK1/2 and PI3K/AKT pathways are also activated upon G-CSF binding, supporting cell proliferation and survival during neutrophil maturation. (**B**) Representative experiment showing the phosphorylation status of STAT3, STAT5, ERK1/2, and AKT1/2/3. Starved 32D cells were incubated with IL-3 as a control for 30 min, or with G-CSF (50 ng/mL) for 0, 5, 15, and 30 min. β-actin is shown as a qualitative loading control. The molecular weights of the protein marker ladder are indicated in kDa. (**C–F**) Bar plots show the mean ± SEM of the densitometric quantification of the (**C**) p-STAT3/STAT3 ratio, (**D**) p-STAT5/STAT5 ratio, (**E**) p-ERK1/2/3 / ERK1/2/3 ratio, and (**F**) p-AKT 1/2/3 / AKT 1/2/3 ratio in the 32D pLenti lines, with values expressed relative to empty vector control. Three independent experiments were performed. Statistical analysis was performed using two-way ANOVA followed by a multiple-comparison test. *$p \leq 0.05$, ***$p \leq 0.001$. a.u., arbitrary units.

In summary, overexpression of C3G in a neutrophil-differentiating cellular context does not appear to counteract this process, as it does not alter STAT3 activation, in contrast to what was observed in Ba/F3-p210 cells. However, high levels of C3G were associated with attenuated ERK and STAT5 signaling under basal IL-3 conditions and/or upon G-CSF stimulation, suggesting that in an active cellular state, C3G inhibits these pro-survival pathways. This effect does not appear to be specific to the cytokine used and, therefore, is likely independent of the neutrophil differentiation process.

3.2.2. C3G knockdown reduces STAT3 and ERK activation upon G-CSF stimulation

As in the previous experimental setting, serum- and IL-3-starved C3G-knockdown and control 32D cells were stimulated with 10% IL-3 or 50 ng/mL G-CSF for the same time points to robustly activate the JAK/STAT3 signaling pathway (**Figure 48A**).

In C3G knockdown 32D cells, G-CSF stimulation strongly induced STAT3 activation, with timing similar to that observed in the C3G-overexpressing cell line. However, STAT3 phosphorylation was significantly attenuated in C3G-deficient cells, as reflected by a reduced p-STAT3/STAT3 ratio at both 5 and 15 minutes of stimulation compared to empty vector control (**Figure 48B, C**). This reduction suggests that low C3G levels impair proper cytokine signal transduction, potentially hindering STAT3 nuclear translocation and the initiation of the neutrophilic differentiation program. Consistently, IL-3 stimulation did not activate STAT3 in knockdown cells (**Figure 48B, C**), as observed previously in overexpression lines (**Figure 47B, C**).

In line with previous observations, IL-3 robustly induced STAT5 activation in C3G knockdown and control cells (**Figure 48B, D**). However, in contrast to the C3G-overexpressing 32D cell lines, IL-3-driven STAT5 activation in knockdown cells remained largely unchanged. As observed, G-CSF did not activate STAT5, and no additional

differences were detected in C3G-deficient cells (**Figure 48B, D**). Together with the previous results, these findings suggest that alterations in C3G expression modulate both JAK/STAT3 and JAK/STAT5 signaling in a complex, context-dependent manner, likely through effects on receptor-associated signaling complexes rather than through direct inhibition of individual pathways.

Both IL-3 and G-CSF stimulation induced ERK activation in C3G knockdown and control cells. Interestingly, ERK phosphorylation was reduced under both IL-3 and G-CSF stimulation in C3G knockdown cells (**Figure 48B, E**), mirroring the attenuation observed in C3G-overexpressing cells (**Figure 47B, E**). This pattern suggests that ERK activation in this cell type is regulated in a non-linear manner, as both increased and decreased C3G levels dampen the ERK1/2 pathway upon cytokine stimulation. A similar non-linear regulation was also observed in Ba/F3-p210 cells across other signaling contexts throughout this work.

AKT phosphorylation was induced by IL-3 and slightly more strongly by G-CSF, as observed previously. While no major changes were detected in the C3G knockdown 32D cell lines, there was a general trend toward higher AKT activation (**Figure 48B, F**). Although not statistically significant, this trend is opposite to the effect observed on ERK signaling (**Figure 48B, F**), with reduced p-ERK levels upon IL-3/G-CSF stimulation coinciding with higher p-AKT. This may reflect a feedback mechanism aimed at maintaining signaling homeostasis.

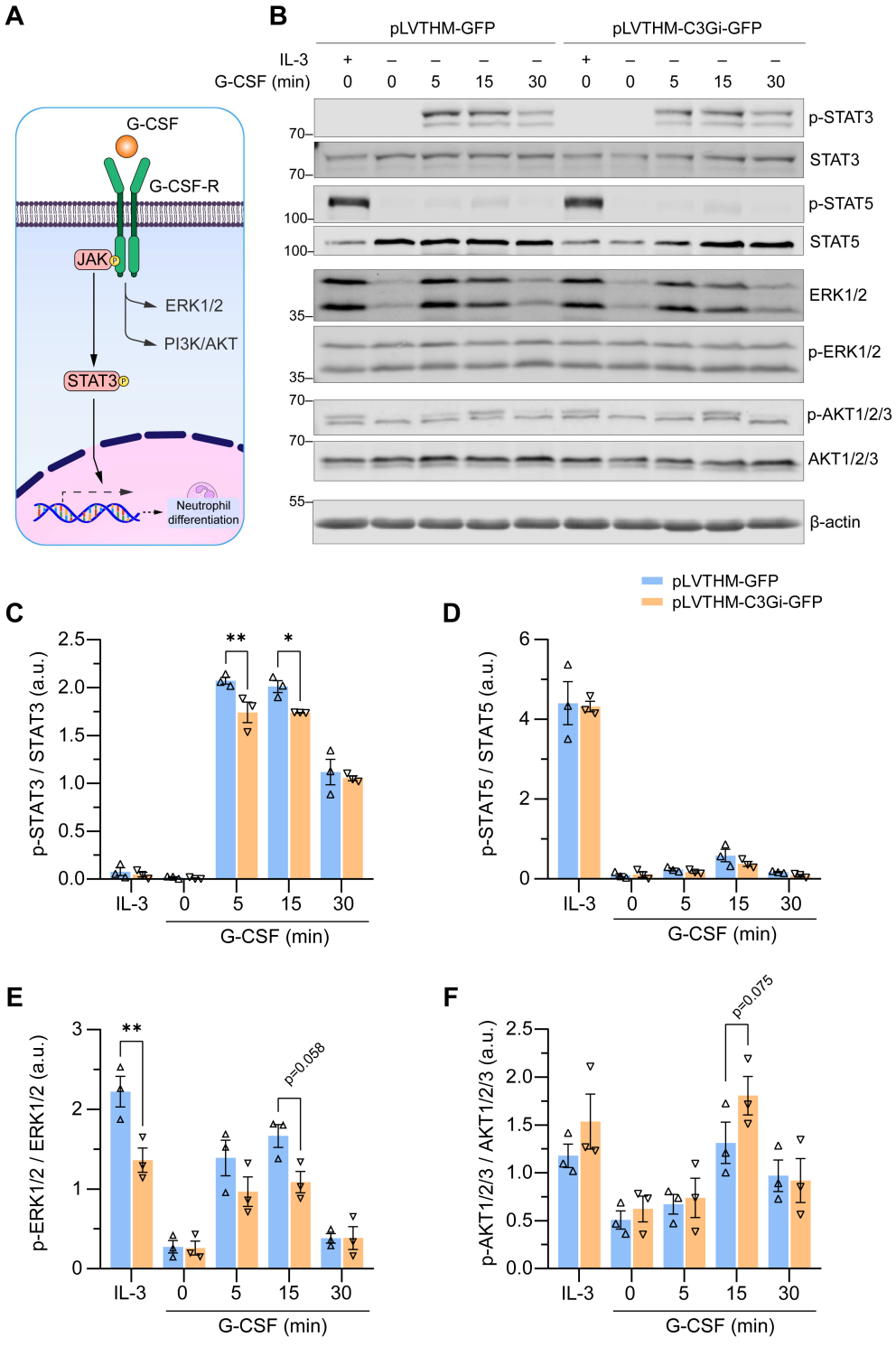
A
G-CSF
G-CSF-R
JAK
ERK1/2
PI3K/AKT
STAT3
Neutrophil differentiation
B
pLVTHM-GFP
pLVTHM-C3Gi-GFP
IL-3
G-CSF (min)
p-STAT3
STAT3
p-STAT5
STAT5
ERK1/2
p-ERK1/2
p-AKT1/2/3
AKT1/2/3
β-actin
C
p-STAT3 / STAT3 (a.u.)
D
p-STAT5 / STAT5 (a.u.)
E
p-ERK1/2 / ERK1/2 (a.u.)
p=0.058
F
p-AKT1/2/3 / AKT1/2/3 (a.u.)
p=0.075

◄ Figure 48. C3G knockdown reduces STAT3 and ERK activation in 32D cells upon G-CSF stimulation. (**A**) Schematic representation of G-CSF-R downstream signaling. Upon binding G-CSF, the receptor activates JAK, leading to STAT3 activation, the main mediator of the neutrophil differentiation program. STAT3 then translocates into the nucleus and regulates the expression of genes driving neutrophil differentiation. ERK1/2 and PI3K/AKT pathways are also activated upon G-CSF binding, supporting cell proliferation and survival during neutrophil maturation. (**B**) Representative experiment showing the phosphorylation status of STAT3, STAT5, ERK1/2, and AKT1/2/3. Starved 32D cells were incubated with IL-3 as a control for 30 min, or with G-CSF (50 ng/mL) for 0, 5, 15, and 30 min. β-actin is shown as a qualitative loading control. The molecular weights of the protein marker ladder are indicated in kDa. (**C–F**) Bar plots show the mean ± SEM of the densitometric quantification of the (**C**) p-STAT3/STAT3 ratio, (**D**) p-STAT5/STAT5 ratio, (**E**) p-ERK1/2/3 / ERK1/2/3 ratio, and (**F**) p-AKT 1/2/3 / AKT 1/2/3 ratio in the 32D pLVTHM cell lines, with values expressed relative to empty vector control. Three independent experiments were performed. Statistical analysis was performed using two-way ANOVA followed by a multiple-comparison test. *$p \leq 0.05$, **$p \leq 0.01$. a.u., arbitrary units.

Overall, upon G-CSF stimulation, low C3G levels appear to inhibit STAT3 activation, the key signaling mediator required for neutrophil differentiation. Extrapolating these findings to an *in vivo* context, C3G deficiency would likely act as an attenuating factor, impairing the proper differentiation of G-CSF-stimulated myeloid-committed HSPCs into neutrophils, provided that cellular processes occur within a physiological context. Interestingly, altering C3G expression in either direction paradoxically produces a similar outcome, here manifested as attenuation of the ERK1/2 pathway. Although this effect does not appear to be cytokine-specific, results from both C3G-overexpressing and C3G-knockdown cells suggest a common mechanism where proper downstream signaling, particularly ERK1/2, depends on tightly regulated C3G levels in this cell type.

Discussion

DISCUSSION

CML is often described as a genetically simple disease, defined by a specific chromosomal translocation that gives rise to the *BCR::ABL1* oncogene, which drives the initiation of leukemic transformation. However, the behavior of leukemic cells reflects a considerably more complex reality that cannot be explained exclusively by this single oncogenic event. Although BCR::ABL1 is essential for leukemic transformation, it is insufficient to account for the wide range of cellular behaviors observed in CML, many of which remain incompletely understood (Perrotti *et al.*, 2017; Rinke *et al.*, 2020).

A particularly important and unresolved area of CML research concerns LSCs, specifically their pronounced resistance to TKIs via mechanisms that remain only partially elucidated (Houshmand *et al.*, 2019). While bulk leukemic cells remain largely dependent on BCR::ABL1-driven oncogenic signaling, LSCs appear to be less reliant on this pathway. Instead, their survival is more closely associated with alternative signaling cascades modulated downstream of BCR::ABL1. Consequently, one promising path in CML research focuses on eradicating LSCs by targeting components of these survival pathways, either individually or in combination with TKIs, representing a potential strategy to overcome their intrinsic therapeutic resistance (Sinclair *et al.*, 2013).

Another unresolved aspect of CML biology relates to the regulation of oncogenic signaling rather than its mere activation. The presence of BCR::ABL1 alone does not fully explain the LSC phenotype, as it remains unclear how signaling intensity, timing, and feedback mechanisms are regulated to induce leukemic transformation and maintain leukemic fitness (Titz *et al.*, 2010). In addition, metabolic adaptation, interactions with the BM microenvironment, and the maintenance of cellular quiescence as a protective state of LSCs are further aspects of CML biology that remain incompletely understood (Shah and Bhatia, 2018; Naka, 2021), representing open and active fields of research in this neoplasm.

Throughout this work, we have focused on gaining knowledge about the role of C3G in CML biology, aiming to address some aspects of the disease discussed above that remain not fully elucidated. Overall, our data indicate that, although C3G is not an essential driver of CML, it can modulate disease progression likely by influencing BCR::ABL1 downstream signaling and shaping the fate of HSPCs. These findings support the concept that CML progression is determined not only by BCR::ABL1, but also by modulatory proteins that fine-tune signaling intensity and stem cell behavior, as exemplified by C3G, thereby highlighting novel potential targets for therapeutic intervention.

1. C3G deficiency in HSCs reduces myeloproliferative disease in a CML mouse model

The specific role of C3G in CML development *in vivo* has not been previously addressed. However, the involvement of C3G-related proteins in CML progression has been investigated. For instance, deregulation of Rap1 signaling has been associated with a CML-like phenotype, as observed in mice deficient in the Rap1 GAP SIPA1, which develop features consistent with myeloproliferative disease (Ishida *et al.*, 2003), suggesting a leukemogenic role for Rap1. In addition, other GEFs have been implicated in CML progression. Notably, SOS1, a GEF for Ras, has been shown to be required for the development of characteristic CML hallmarks. In CML-predisposed mouse models, SOS1 deficiency suppresses typical disease manifestations, indicating a critical role for Ras activation in CML pathogenesis (Gómez *et al.*, 2022). Together, these observations suggest that deregulated activity of small GTPases, such as Rap1 and Ras, contributes to the establishment and progression of leukemic features in CML. In this context, C3G, as a key regulator of Rap1 activity, emerges as a compelling candidate for modulating CML progression.

CML development during the chronic phase is primarily marked by a massive expansion of the myeloid compartment, the hallmark feature of what is clinically recognized as a myeloproliferative disease. At the cellular level, BCR::ABL1 acts as the main driver of this process, pushing hematopoietic cells (particularly those of the myeloid lineage) toward uncontrolled proliferation. Despite its relentless activity, the signaling cascades downstream of BCR::ABL1 are not entirely dysregulated; they can be fine-tuned, at least in part, by intermediary proteins (Amarante-Mendes *et al.*, 2022). It is at this regulatory point that C3G appears to play a role, as evidenced by results from our CML mouse model lacking C3G in myeloid-committed BCR::ABL1-expressing HSPCs.

C3G-deficient CML-predisposed mice still develop the myeloproliferative disease, indicating that hematopoietic C3G is not strictly required for leukemia initiation. Nevertheless, the disease in these mice exhibits several notable differences compared to a typical CML course:

(1) Circulating myeloid cell levels remain unaltered during the first months of life in C3G-deficient p210 mice. However, after CML onset, p210/C3G$^{HSC\text{-}Scl}$-KO mice exhibit reduced levels of circulating neutrophils, accompanied by a non-significant increase in lymphoid cells, specifically T cells. This phenotype suggests a partial impairment in myeloproliferative disease progression. Thus, although C3G deficiency has little impact under basal conditions, these differences become evident under hematopoietic stress.

(2) The reduced levels of myeloid cells in PB correlate with delayed disease onset, implying that BCR::ABL1 expression alone is insufficient to drive rapid disease development in the absence of C3G. However, once the disease is established, C3G deficiency does not alter CML progression, as mice reach disease endpoints in the same timeframe as controls. These results suggest that C3G plays a role during disease initiation rather than in disease progression.

(3) Overall survival in CML is unchanged but is increased in female C3G-KO p210 mice. Throughout this study, differences were more pronounced in females (see **Figure 51**; **Annexes**), suggesting the presence of sex-biased effects on C3G activity. A recent study reported a comparable phenotype: female mice overexpressing C3G in MK/platelets show increased survival after 5-FU-induced myeloablation, whereas those with C3G deletion in MK/platelets exhibit reduced survival (Herranz *et al.*, 2025). Interestingly, in CML patients, the epidemiological male:female ratio is approximately 1.7:1. However, the underlying causes of this difference are not fully understood and may involve genetic, hormonal, and environmental factors, among others (Radivoyevitch *et al.*, 2014).

(4) At the time of death, p210/C3G$^{\text{HSC-}Scl}$-KO mice display milder CML-related symptoms, as reflected by reduced myeloid hematopoietic infiltration in affected tissues such as the BM and thymus. Interestingly, this reduction in myeloid cells was accompanied by an increase in lymphoid populations, specifically B cells in the BM and spleen, reflecting a more physiological, and thus healthier, phenotype. However, some typical CML hallmarks, such as myeloid spleen infiltration and hepatosplenomegaly, remained unchanged, indicating that C3G-deficient mice still develop the characteristic consequences of CML. Overall, these results suggest that C3G deficiency attenuates the endpoint CML phenotype but does not completely abrogate the full leukemic disease.

Collectively, these features support the idea that C3G functions as a modulatory factor rather than as a critical driver of leukemogenesis. While BCR::ABL1 initiates the oncogenic program in hematopoietic stem cells, the absence of C3G appears to modify the progression and phenotypic characteristics of the disease in myeloid-committed progenitors.

In addition, our data indicate that the impact of C3G deletion on CML development is dependent on the timing of gene inactivation. When C3G was deleted early, that is, when mice were one month old, the myeloproliferative disease exhibited reduced circulating myeloid cell counts, prolonged disease-free survival, and attenuated leukemic tissue infiltration. In contrast, late deletion of C3G at six months of age, corresponding to the stage at which the disease is beginning to establish, resulted in only a moderate attenuation of the myeloproliferative phenotype. This suggests that C3G is not equally required throughout all

phases of CML progression, making its role more critical during the earliest phases of leukemogenesis. Timing of C3G loss seems to be a key determinant of its impact on disease progression: early deletion can more effectively delay leukemic onset and reduce disease severity, whereas deletion at the point of disease establishment can only partially modulate the phenotype. These findings highlight the importance of C3G in shaping the trajectory of CML development and suggest that therapeutic strategies targeting C3G might be most effective if applied before or during the initial stages of leukemogenesis rather than after the disease is fully established.

A comparable time-dependent requirement has been described for C/EBPα in AML. This transcription factor is essential for the initiation of AML driven by *MLL* (Mixed-Lineage Leukemia) fusion genes, due to its functions at the onset of leukemic transformation, but is dispensable for disease maintenance (Roe and Vakoc, 2014). In a similar manner, early in leukemogenesis, C3G might play a role in the establishment and expansion of pre-leukemic cells, potentially by facilitating the remodeling of signaling networks, interactions with the hematopoietic niche, and the amplification of myeloid progenitor populations. These hypothesis are further supported on the recently described role of C3G in hematopoiesis (Herranz Varea, 2024). By contrast, once the disease is established, the leukemic system may become less dependent on C3G, such that C3G deletion perturbs disease maintenance only modestly.

Regarding the imatinib response in our mouse models, unfortunately, both p210/C3G$^{\text{HSC-}Scl}$-wt and p210/C3G$^{\text{HSC-}Scl}$-KO mice did not respond to the treatment under our experimental conditions. Supporting this result, the sensitivity of BCR::ABL1 transgenic mouse models to imatinib has been debated in the literature, with some models showing responsiveness (Sánchez-Sánchez *et al.*, 2014; Schubert *et al.*, 2017; García-Navas *et al.*, 2025) while others do not (Pérez-Caro *et al.*, 2009), reflecting the heterogeneity of leukemic context and properties across different transgenic models and experimental setups. In our study, several factors could explain the lack of effect observed: (1) suboptimal drug pharmacokinetics, in terms of timing and/or dose (2) BCR::ABL1 expression being restricted to certain hematopoietic progenitors, limiting the impact on the leukemic source, with chronic expression potentially reducing imatinib sensitivity, and (3) the disease being driven by partially transformed progenitors that are less dependent on BCR::ABL1 signaling. Whatever the underlying cause, no conclusions can be drawn from this part of the work.

2. C3G loss alters bone marrow myelopoiesis in BCR::ABL1-expressing mice

Hematopoietic C3G deficiency in CML mouse models delay the progression of the myeloproliferative disease, but understanding the underlying mechanisms is crucial to

explain the observed phenotype. To address this, the next phase of the work focused on studying the BM, the primary site and source of leukemogenesis.

In CP-CML, the BCR::ABL1 translocation confers a clonal advantage, leading to the expansion of a neoplastic HSC clone (later termed LSC) in the BM, which drives myeloproliferation. These LSCs predominantly give rise to myeloid cells, reflecting a lineage bias induced by BCR::ABL1 signaling. In contrast to normal hematopoiesis, where HSCs maintain a dynamic balance among lineages, CP-CML LSCs exhibit a restricted differentiation pattern with excessive myeloid output (Brown, 2022). It is therefore plausible that C3G exerts its function at this stage, corresponding to HSC fate decisions, given its known physiological roles in HSC differentiation and lineage choice at multiple levels of the hematopoietic hierarchy (Imai *et al.*, 2019; Herranz *et al.*, 2025). Under 5-FU-induced myeloablative stress, C3G$^{HSC\text{-}Scl}$-KO mice display alterations in HSC/HSPC fate, as described recently (Herranz Varea, 2024). Likewise, during strong myeloproliferative stress, such as the presence of BCR::ABL1 in HSPCs, C3G influence on HSC fate may also be perturbed.

Consistent with this hypothesis, analysis of HSPC subpopulations in the BM of p210/C3G$^{HSC\text{-}Scl}$-KO mice at CML onset revealed notable differences. Compared to controls, p210/C3G$^{HSC\text{-}Scl}$-KO mice displayed higher levels of immature BM cells (Lin$^-$ cells), suggesting an accumulation of hematopoietic progenitors, due to reduced numbers of fully matured hematopoietic cells in this tissue. Conversely, these mice exhibited reduced levels of LKS cells, which represent the main HSC pool, possibly indicating a weakened stem cell reservoir.

At the first lineage fate decision (corresponding to the bifurcation between myeloid and lymphoid lineages) p210/C3G$^{HSC\text{-}Scl}$-KO mice showed increased levels of CLPs at the expense of CMPs, indicating a lymphoid bias at this stage. Interestingly, a similar phenotype was observed in 5-FU-treated mice with C3G-KO in MKs, which displayed elevated CLP levels seven days after treatment (Herranz *et al.*, 2025). More strikingly, significant differences were observed among myeloid-committed HSPCs, which differentiate downstream of CMPs. While MEPs were reduced, GMPs were increased. This pattern, together with the elevated Lin$^-$ population, suggests an accumulation of granulocyte-committed HSPCs at an intermediate stage, reflecting impaired granulopoiesis. This interpretation is further supported by the observation that p210/C3G$^{HSC\text{-}Scl}$-KO mice display lower neutrophil levels in PB at later stages of CML, potentially due to incomplete maturation and retention of these cells within the BM.

Interestingly, compared to healthy individuals, CML patients also display alterations in myeloid progenitors in the BM, typically with increased levels of MEPs and decreased

levels of GMPs, among other differences in progenitor populations (Harada *et al.*, 2021). In contrast, the pattern of HSPC alterations in our p210/C3G$^{HSC\text{-}Scl}$-KO mice (characterized by increased GMPs and reduced MEPs) may reflect a partial return toward physiological progenitor proportions under myeloproliferative stress. In this sense, C3G deficiency could act by partially "normalizing" progenitor distribution relative to the leukemic skew, counteracting the BCR::ABL1-driven bias observed in a normal CML course.

The impaired maturation of the granulocytic compartment in p210/C3G$^{HSC\text{-}Scl}$-KO mice is reflected in defective functional behavior. Neutrophils are key effectors of the innate immune response, rapidly sensing pathogens, migrating to sites of infection, and initiating early antimicrobial defense before adaptive immunity is engaged. The ability to detect chemotactic cues and migrate efficiently is therefore a hallmark of full granulocytic maturation (Leliefeld *et al.*, 2016). Consistent with this, p210/C3G$^{HSC\text{-}Scl}$-KO neutrophils display defective chemotactic migration, supporting the notion that they fail to acquire a fully mature functional phenotype. An interesting contrast is provided by p210 transgenic mice lacking Cas-L, a focal adhesion adaptor protein required for proper hematopoietic cell adhesion. In this model, Cas-L deletion renders granulocytes hypermigratory and less adhesive, promoting extramedullary infiltration and accelerating disease progression (Seo *et al.*, 2011), precisely the opposite phenotype to that observed in the C3G-deficient p210 model. According to that, the behavior of our C3G-deficient p210 model appears contradictory, given the essential role of C3G in cell adhesion, where C3G and Cas-L, or its homolog p130Cas, are components of the focal adhesion complexes (Radha *et al.*, 2011; Shagisultanova *et al.*, 2015), highlighting the complex role of C3G in CML biology.

Overall, p210/C3G$^{HSC\text{-}Scl}$-KO mice show that normal levels of C3G are important for proper BCR::ABL1-driven myeloid expansion. Its absence destabilizes the stem/progenitor compartment, modulates CMP/GMP expansion, and impairs neutrophil migration, leading to lower granulocytosis and delayed CML progression. This indicates that C3G is not "intrinsically myeloid," but facilitates BCR::ABL1 in imposing its pathological differentiation bias.

3. Changes in C3G levels affect leukemogenic pathways in CML cell lines

Our results so far suggest that deletion of C3G in HSPCs expressing BCR::ABL1 attenuates the myeloproliferative phenotype, possibly through perturbations in the differentiation of hematopoietic progenitors that ultimately alter HSC fate. It is therefore plausible that C3G interferes with CML development by modulating key leukemogenic pathways in a BCR::ABL1 context, attenuating the main features of the LSC phenotype.

To gain deeper insight into the molecular mechanisms underlying these effects, we used the Ba/F3-p210 CML cell line, in which we altered C3G expression to examine the consequences of both overexpression and depletion in a BCR::ABL1-driven setting. The generation of these C3G-altered models revealed notable changes in leukemic cell behavior, helping explain the phenotype observed in the C3G-deficient CML mouse model.

Firstly, transformation of Ba/F3 cells with the *BCR::ABL1 p210* oncogene led to a decrease in full-length C3G levels (p140C3G), although the p87C3G isoform, described in other CML cells (Gutiérrez-Berzal *et al.*, 2006), was not detectable under our experimental conditions. As discussed in **Introduction section 2.3.1**, in K562 cells p140C3G exerts a regulatory influence, helping to maintain balanced adhesion dynamics, whereas p87C3G disrupts BCR::ABL1-focal adhesion interactions, promoting aberrant adhesion signaling (Maia *et al.*, 2013). This could explain the observed reduction in full-length C3G levels, as p140C3G may act to counterbalance full leukemic cell behavior. Consistently, an inverse relationship has been reported: repression of BCR::ABL1 in Ba/F3-p210 cells leads to upregulation of p140C3G (Gutiérrez-Berzal *et al.*, 2006). In agreement with this, preliminary interrogation of CML patient databases indicates that *RAPGEF1* expression is downregulated in BM leukemic cells (see **Figure 55**; **Annexes**).

In our Ba/F3-p210 cell lines generated, alterations in C3G expression did not modulate the proliferation rate of Ba/F3-p210 cells. Indeed, the impact of C3G on cell proliferation has been reported to be highly context-dependent in other cellular systems. For instance, C3G-null mouse embryonic stem cells (mESCs) display reduced proliferation (Vishnu *et al.*, 2021), and hyperactivation of C3G in *Drosophila* results in an hyperproliferative phenotype (Ishimaru *et al.*, 1999). In various tumorigenic contexts, C3G repression has been associated with decreased proliferation and tumor growth (Priego *et al.*, 2016; Sequera *et al.*, 2020; Manzano *et al.*, 2021), whereas a constitutively active form of C3G in the B-cell lymphoma line A20 reduces proliferation rates (Morán-Vaquero *et al.*, 2026). Together, these observations highlight the strong cell type-specificity and functional heterogeneity of C3G in the regulation of cell proliferation.

Interestingly, the sensitivity of Ba/F3-p210 cells to imatinib increased when C3G levels were altered in either direction; i.e., both overexpression and depletion of C3G in BCR::ABL1-expressing cells reduced cell viability and enhanced apoptotic responses upon imatinib treatment. Although this scenario may seem paradoxical, a similar dual role of C3G has been observed in K562 cells, where both overexpression and silencing sensitize cells to imatinib via a BCR::ABL1–C3G signaling axis (Maia *et al.*, 2009), as described in **Introduction section 2.3.1**. These observations confirm that C3G levels must be tightly regulated in leukemic cells to maintain their homeostasis, likely because perturbations in C3G disrupt BCR::ABL1-induced apoptotic resistance, favoring TKI actions.

In summary, C3G likely helps maintaining a balanced survival-signaling state, and deviations in either direction create a more fragile cellular condition. Particularly in Ba/F3-p210 cells, this fragility may become apparent when BCR::ABL1 is inhibited by imatinib.

Oncogenic BCR::ABL1 downstream signaling was partially altered in C3G-modified Ba/F3-p210 cells under steady-state conditions. In LSCs, BCR::ABL1 functions as a central signaling hub by directly or indirectly activating multiple pathways that control proliferation, differentiation, migration, adhesion and apoptosis. Rather than operating through a linear cascade, BCR::ABL1 signaling is organized as a modular, phosphorylation-dependent network, providing a mechanistic framework for how diverse signals are integrated to drive leukemic transformation. In simpler terms, BCR::ABL1 supplies the catalytic activity, whereas associated proteins determine how this activity is interpreted by the cell (Titz *et al.*, 2010). Our results suggest that C3G may act as one of these modulatory adaptor proteins within the BCR::ABL1 signaling network. However, the lymphoid origin of Ba/F3 cells may influence downstream signaling, representing an important limitation of this model. This issue has been highlighted in studies comparing the p210 and p190 BCR::ABL1 isoforms (Reckel *et al.*, 2017; Adnan-Awad *et al.*, 2021), which are typically associated with myeloid and lymphoid contexts, respectively.

First, the status of BCR::ABL1 kinase activity, reflecting the state of the oncogenic kinase (Hantschel, 2012), appeared attenuated when C3G expression was altered. Specifically, both overexpression and silencing of C3G led to a reduction in phosphorylation of Y412 within the kinase domain of the ABL1 moiety, suggesting that non-physiological C3G levels prevent BCR::ABL1 from reaching full kinase activity. However, when we examined the phosphorylation of CrkL, a major downstream substrate of BCR::ABL1, no significant differences were detected. One possible explanation for this apparently contradictory result is that, although BCR::ABL1 signaling is partially attenuated upon C3G modulation, the remaining kinase activity is still sufficient to sustain CrkL phosphorylation. Alternatively, CrkL phosphorylation could be influenced by other kinases, such as Src family members, as suggested by previous studies (Erdreich-Epstein *et al.*, 1999).

Next key downstream signaling pathways involved in leukemogenesis were analyzed by assessing the activation status of the main effector proteins of the ERK1/2, PI3K/AKT and JAK/STAT signaling axes, under steady-state conditions:

(1) The ERK1/2 pathway is critical in solid tumors and often serves as the main oncogenic driver, frequently harboring activating mutations (Fei and Guo, 2025). While BCR::ABL1 can engage the ERK1/2 pathway, which contribute to proliferation and survival, it is not the principal driver of CML (Amarante-Mendes *et al.*, 2022). In our models, altering C3G expression in leukemic cells did not lead to notable changes in

ERK1/2 activation, except for a slight reduction in p-ERK1/2 levels under C3G silencing conditions. This maintenance of activation levels aligns with the absence of differences in cell proliferation rates, consistent with the central role of ERK1/2 signaling in this process (Meloche and Pouysségur, 2007). Interestingly, similar to the context-dependent effects of C3G on cell proliferation, ERK1/2 regulation by C3G also appears to be highly cell-dependent. In the literature, C3G has been reported to both inhibit this pathway (Guerrero *et al.*, 2004; Priego *et al.*, 2016; Morán-Vaquero *et al.*, 2026) and to contribute to its activation (Wang *et al.*, 2006; Maia *et al.*, 2009; Vishnu *et al.*, 2021), likely reflecting cell-specific differences in the B-Raf/Raf-1 ratio (Vossler *et al.*, 1997).

(2) A similar scenario occurs with the PI3K/AKT pathway: it can be activated by BCR::ABL1, but it is not critical for the LSC program and instead plays a more collaborative role in shaping its phenotype. In CML, this pathway can promote proliferation, survival, and enhance metabolism to support leukemic growth and increase resistance to TKIs (Wiese *et al.*, 2023). As observed with ERK1/2 activation, in our CML cell model, alterations in C3G expression did not significantly change p-AKT1/2/3 levels, although there was a slight tendency toward an increase in C3G-silenced cells. Interestingly, this trend is opposite to that seen for ERK1/2 activation in these cells, suggesting the presence of feedback mechanisms between the two pathways, a well-documented phenomenon (Carracedo *et al.*, 2008; Turke *et al.*, 2012). As with ERK1/2, alterations in AKT1/2/3 activation by C3G are highly context-dependent: in some cases is induced (Kumar *et al.*, 2015) or inhibited (Voss *et al.*, 2006; Priego *et al.*, 2016), reflecting the cell type-specific regulation of this pathway.

(3) The JAK/STAT pathway is considered a critical signaling axis that defines the LSC phenotype. As mentioned, BCR::ABL1 constitutively activates JAK2, which in turn phosphorylates STAT proteins, primarily STAT5, promoting typical LSC characteristics, including survival, proliferation, and, importantly, resistance to TKIs (Schafranek *et al.*, 2015). Notably, our Ba/F3-p210 cells displayed significant alterations in this pathway, revealing a non-linear regulation of JAK/STAT activation by C3G. Alterations in C3G expression levels in either direction disrupt the pathway, as evidenced by the concomitant reduction in p-JAK2, p-STAT3, and p-STAT5 levels under steady-state conditions. The fact that both overexpression and silencing of C3G produce similar effects may seem paradoxical, but it aligns with our previous results regarding imatinib sensitivity, since high levels of STAT activation are strongly associated with TKI resistance (Warsch *et al.*, 2011). This non-linear regulation reflects C3G role as an adaptor protein and central node within multiprotein signaling complexes, meaning its activity may be more context-dependent rather than a simple

on-off switch. Its effects on JAK/STAT signaling likely depend on factors such as protein abundance and interacting partners, with both overexpression and depletion capable of disrupting signal propagation. This suggests that C3G shapes JAK/STAT signaling through complex interactions, rather than simply turning it on or off.

The classical inhibitors of JAK/STAT signaling are the SOCS family of proteins. SOCS act as negative-feedback regulators of this pathway, capable of directly or indirectly inhibiting JAK kinases, thereby preventing excessive activation of hematopoietic cells and maintaining controlled JAK/STAT signaling (Liau *et al.*, 2018). Interestingly, non-physiological levels of C3G in a BCR::ABL1 context also appear to inhibit the JAK/STAT pathway at the level of JAK2, the same target of SOCS proteins. This raises the possibility that C3G may exert its effects, at least in part, by modulating SOCS activity, a mechanism that calls for further investigation to elucidate the details of JAK/STAT–C3G crosstalk.

Regulation of JAK/STAT by C3G has not been extensively studied. However, the limited evidence available also points toward cell-type-specific effects: for example, C3G-null mESCs show increased p-STAT3 levels (Vishnu *et al.*, 2021) and in the PV-derived HEL cell line, C3G repression increases p-JAK2^{V617F} levels (unpublished data from our group). It is also important to note that in our study, JAK/STAT is examined in a BCR::ABL1-driven cellular model, where the pathway is constitutively activated and essential for leukemic survival and proliferation, which may amplify cell-type-specific differences.

In summary, non-physiological levels of C3G in a BCR::ABL1 cellular context lead to deregulation of key leukemogenic pathways, like JAK/STAT signaling. Extrapolating these findings to our C3G-deficient CML mouse model, it is plausible that loss of C3G attenuates this pathway in HSPCs, thereby weakening leukemic development, consistent with the established importance of JAK/STAT signaling in CML (Mojtahedi *et al.*, 2021). Disruption of this pathway may also account for the defects observed in neutrophilic maturation in the BM of p210/C3G$^{HSC\text{-}Scl}$-KO mice, as evidenced by imbalances in myeloid-committed progenitor populations and impaired neutrophil maturation. This interpretation is consistent with the pivotal role of JAK/STAT signaling, particularly STAT3, in regulating normal myeloid differentiation (Zhang *et al.*, 2010).

Physiologically, JAK/STAT is a central mediator of cytokine receptor signaling in hematopoietic cells and plays a crucial role in transmitting differentiation cues, among other processes (Hu *et al.*, 2021). This leads to the hypothesis that alterations in C3G expression in a BCR::ABL1 setting may impair the proper differentiation program of hematopoietic progenitors through disruption of JAK/STAT signaling. Such a defect could underlie the

blockade in myeloid maturation observed in our C3G-deficient mouse model and contribute to the attenuated myeloproliferative phenotype.

4. C3G is required for proper initiation of cytokine-induced neutrophilic differentiation

Taking these last results into account, the next logical step was to investigate whether alterations in C3G expression are linked to disruptions in the differentiation program of potentially myeloid-committed cells. For this purpose, we performed experiments in the murine myeloblast-like 32D cell line, in which a neutrophil differentiation program can be induced by stimulation with G-CSF, a granulocyte colony-stimulating cytokine. To directly assess the impact of C3G, we generated 32D cell lines with C3G overexpression or knockdown, following the same experimental strategy used for the Ba/F3-p210 model.

As described in **Methods section 13.4**, G-CSF induces neutrophil differentiation in 32D cells primarily via the JAK/STAT pathway, where specifically STAT3 is the key mediator of this process (Zhang *et al.*, 2023). Remarkably, modulation of C3G expression levels in G-CSF-stimulated 32D cells significantly altered the activation of several signaling pathways downstream of G-CSF-R:

(1) STAT3 activation was reduced in C3G knockdown cells upon G-CSF treatment, implying an impairment of the JAK/STAT3 signaling axis, the main transducer of G-CSF stimulation. Consequently, weakened STAT3 activation in this context could compromise proper initiation of the neutrophilic differentiation program and could be associated with the reduced neutrophil counts observed *in vivo* in the p210 mouse model.
(2) STAT5 was not activated by G-CSF. Interestingly, C3G-overexpressing cells displayed lower STAT5 activation in response to IL-3, highlighting a differential C3G-mediated inhibitory pattern within the JAK/STAT signaling network.
(3) ERK1/2 and AKT1/2/3 were induced by both G-CSF and IL-3. Notably, ERK1/2 activation was attenuated in both C3G-overexpressing and knockdown cells, a process that appeared largely independent of the cytokine used for stimulation and likely unrelated to neutrophilic differentiation.

The reduced activation of STAT3, even under high concentrations of G-CSF, suggests that low C3G levels compromise the initiation of the neutrophilic differentiation program in 32D cells. In contrast, elevated C3G did not inhibit G-CSF-induced STAT3 but selectively reduced IL-3-driven STAT5 activation. These findings highlight a preferential, context-dependent inhibition of JAK/STAT3 and JAK/STAT5 signaling by either excessive or insufficient C3G, indicating that the modulation of this pathway by C3G is more complex

in cytokine-stimulated cells. This behavior contrasts with observations in Ba/F3-p210 cells, where both high and low C3G levels produced a simpler outcome, characterized by general JAK/STAT inhibition.

Notably, these results were consistent with our previous hypothesis that C3G modulates JAK/STAT signaling not only under steady-state conditions but also in response to myeloid differentiation cues, thereby affecting proper myeloid maturation. Extrapolating to the C3G-deficient p210 mouse model, it is plausible that alterations in JAK/STAT signaling in HSPCs caused by C3G deletion impair neutrophil maturation, resulting in an attenuated myeloproliferative phenotype.

The reduced response of C3G knockdown 32D cells to G-CSF prompted us to investigate whether neutrophil differentiation was also functionally impaired by assessing the expression of canonical mature neutrophil markers, such as Gr1 and Mac1. Several attempts were made, but 32D cells failed to undergo proper differentiation. G-CSF induced only very low percentages of $Gr1^{+}Mac1^{+}$ cells over several days (data not shown), and most cells eventually died, likely due to the absence of IL-3, which is required for their survival and proliferation. One possible explanation for these observations is the existence of different 32D cell subclones, such as 32Dcl3 (Guchhait *et al.*, 2003), 32D.C10 (Dong *et al.*, 1995), 32D G, or 32D GM (Shimada *et al.*, 1993). These subclones may exhibit differential expression of G-CSF-R, resulting in variable responsiveness to G-CSF stimulation. Since the exact origin of our 32D cell line is unknown, it is plausible that the subclone we used displays only a low response to G-CSF, sufficient to detect signaling differences but insufficient to induce full neutrophil differentiation without compromising cell survival. Interestingly, engineered 32D lines expressing the human *CSF3R* gene, which encodes the G-CSF receptor, respond strongly to G-CSF and undergo proper neutrophil differentiation, making them suitable for the functional differentiation assays we aim to perform (Zjablovskaja *et al.*, 2018).

5. C3G inhibition as a potential strategy for JAK/STAT modulation in clinics

Taken together, the results obtained in this work support a preliminary model explaining the role of C3G in CML (**Figure 49**). Our data indicate that C3G functions as a key modulatory factor in leukemogenesis, fine-tuning BCR::ABL1-driven signaling rather than acting as a simple on/off switch.

In CML with physiological C3G levels, BCR::ABL1 activity in HSCs drives hyperproliferation and differentiation into mature granulocytes, primarily neutrophils, resulting in the characteristic myeloid expansion in circulation (**Figure 49A**). However, in

the absence of C3G, HSCs display an altered fate, deviating from the BCR::ABL1-driven myeloid bias toward decreased myeloid output. C3G deficiency under these conditions leads to impaired hematopoietic maturation and the accumulation of intermediate granulocytic progenitors in the BM. As a result, fewer mature granulocytes are released into circulation, attenuating the myeloproliferative phenotype (**Figure 49B**). At the cellular level, neutrophil-committed progenitors with reduced levels of C3G expression may be less responsive to differentiation signals. Both excessive and insufficient C3G destabilize JAK/STAT3 signaling, a critical pathway for proper neutrophil differentiation upon G-CSF stimulation, leading to defective maturation of these progenitors (**Figure 49C**).

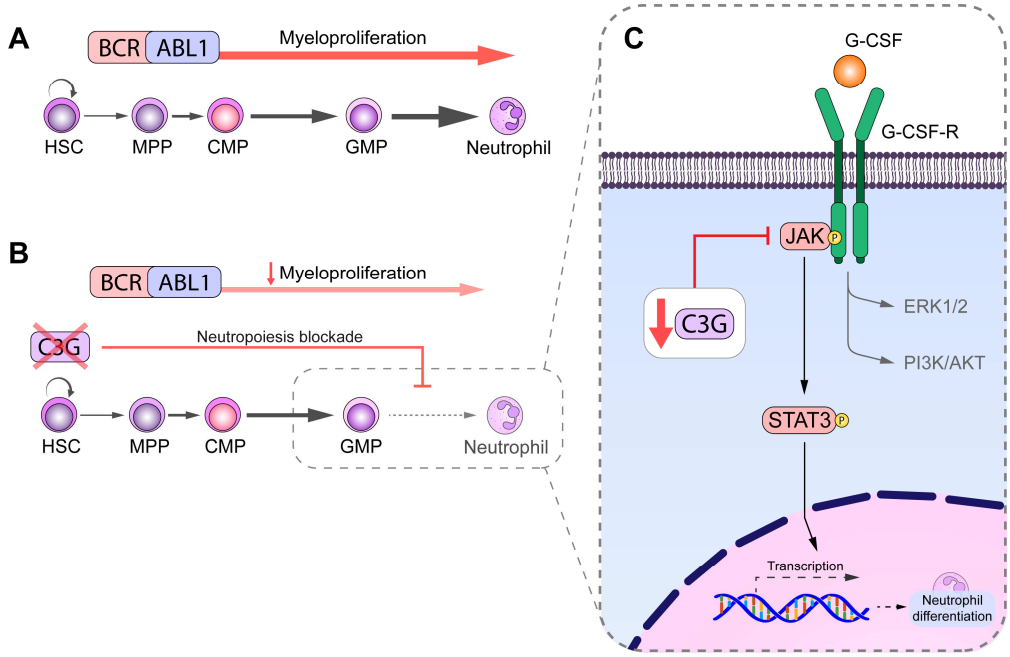

Figure 49. Proposed model of C3G function in myeloproliferative diseases like chronic myeloid leukemia (CML). (**A**) Constitutive BCR::ABL1 signaling pushes hematopoietic stem cells (HSC) toward excessive proliferation, resulting in massive myeloid lineage expansion. This overproduction of neutrophils underlies the characteristic myeloproliferative phenotype of chronic-phase CML. (**B**) Loss of C3G in these HSCs attenuates this myeloproliferative state, resulting in reduced myeloid expansion due to impaired neutrophil differentiation and maturation, with accumulation of myeloid progenitors in the bone marrow. (**C**) Neutrophil-committed progenitors with altered C3G expression may display an impaired response to granulocyte colony-stimulating factor (G-CSF), due to defective JAK/STAT3 pathway activation, resulting in reduced expression of genes required for neutrophil differentiation. MPP: multipotent progenitor, CMP: common myeloid progenitor, GMP: granulocyte-monocyte progenitor, G-CSF-R: G-CSF receptor.

Although the extensive neutrophil differentiation observed in CML is mainly driven by BCR::ABL1 rather than by aberrant G-CSF signaling, the impaired neutrophil commitment observed in a non-BCR::ABL1 physiological model such as 32D cells helps to explain why

C3G behaves as a brake in a myeloproliferative context, such as the chronic phase of CML. Thus, C3G contributes to physiological neutrophil differentiation, and when oncogenic pressure is imposed by BCR::ABL1, loss of this support limits how far the myeloproliferative program can progress.

In summary, C3G, through its role in modulating the myeloproliferative phenotype in CML, emerges as a promising druggable target. Attenuating C3G activity in chronic-phase CML patients could potentially slow disease progression and help prevent transition to advanced phases, in a manner analogous to how busulfan and hydroxyurea were historically used to control the myeloproliferative stage of CML (Rushing *et al.*, 1982). While C3G inhibition may not fully prevent the acquisition of mutations in LSCs that drive progression to the blastic phase, it could extend the chronic phase by limiting excessive leukocyte production and alleviating key CML-associated symptoms.

Nevertheless, the most promising potential application of C3G inhibition lies in combination therapies with TKIs, as a putative C3G inhibitor could sensitize LSCs to TKI treatment. This sensitization is thought to occur through modulation of the JAK/STAT pathway, which plays a key role in resistance to TKI-induced apoptosis (Warsch *et al.*, 2011). Indeed, combination therapies using a BCR::ABL1-targeting TKI together with a JAK/STAT pathway inhibitor have been widely studied, with ruxolitinib being the most extensively investigated in CML (Gallipoli *et al.*, 2014; Sweet *et al.*, 2018). Although STAT5 is the main mediator of TKI resistance in LSCs, directly targeting STAT5 is challenging because it is not a kinase and lacks enzymatic domains suitable for conventional inhibitor design (Orlova *et al.*, 2019). Therefore, JAK2 inhibition represents an alternative approach to interfere with STAT5 function, and ruxolitinib is a good candidate due to its selective inhibition of JAK1 and JAK2. Initially approved for the treatment of PV, MF, and graft-versus-host disease (Mesa *et al.*, 2012), ruxolitinib specific JAK1/2 inhibition makes it an attractive candidate for use in CML patients in combination with standard TKIs, where it has been shown to target LSCs effectively (Gallipoli *et al.*, 2014). Furthermore, clinical trials are already evaluating this strategy (Sweet *et al.*, 2018). In this context, a putative C3G inhibitor emerges as a promising JAK/STAT-modulating agent that could be used in a similar combinatorial approach, sensitizing LSCs to TKIs and addressing one of the main challenges in CML treatment.

Conclusions

CONCLUSIONS

1. Hematopoietic C3G deficiency one month after birth attenuates the development of BCR::ABL1 p210-induced myeloproliferative disease, likely by reducing circulating neutrophil levels and thereby increasing survival, particularly in females. Leukemic infiltration in hematopoietic tissues is also reduced in C3G-knockout p210 mice, partially restoring a more physiological hematopoietic balance.

2. At CML onset, occurring after 6 months of age, HSPC subpopulations in the BM are altered in C3G-deficient mice, with notable changes in myeloid-committed progenitors, suggesting disrupted myelopoiesis.

3. Migration of BM neutrophils in response to chemotactic stimuli is impaired in p210 C3G-knockout mice, reflecting defective cell functionality.

4. Under the experimental conditions in this work, p210 mice show little to no response to imatinib treatment.

5. C3G deletion at CML onset produces a modest delay in disease progression, supporting a time-dependent role of C3G in leukemogenesis.

6. BCR::ABL1 p210-transformed Ba/F3 cells show reduced full-length C3G expression levels, suggesting functional crosstalk between BCR::ABL1 and C3G in these leukemic cells.

7. Alterations in C3G expression levels do not alter basal Ba/F3-p210 proliferation but increases sensitivity to imatinib, reducing viability and enhancing apoptosis. This is accompanied by decreased BCR::ABL1 activity and weakened JAK/STAT signaling, without affecting CrkL, ERK, or AKT activation.

8. Reduced C3G expression in 32D cells, but not C3G overexpression, leads to decreased G-CSF-induced STAT3 activation, compromising the initiation of the neutrophilic differentiation program.

Conclusiones

CONCLUSIONES

1. La deficiencia hematopoyética de C3G un mes después del nacimiento atenúa el desarrollo de la enfermedad mieloproliferativa inducida por BCR::ABL1 p210, probablemente al reducir los niveles de neutrófilos circulantes y, con ello, aumentar la supervivencia, especialmente en hembras. La infiltración leucémica en tejidos hematopoyéticos también se reduce en los ratones p210 con deleción de C3G, restaurando parcialmente un equilibrio hematopoyético más fisiológico.

2. En el inicio de la LMC, que ocurre a los 6 meses de edad, las subpoblaciones de HSPC en la médula ósea se alteran en ratones deficientes en C3G, con cambios notables en progenitores mieloides, lo que sugiere una mielopoyesis alterada.

3. La migración de neutrófilos de médula ósea en respuesta a estímulos quimiotácticos está comprometida en ratones p210 con deficiencia de C3G, lo que refleja una funcionalidad celular defectuosa.

4. Bajo las condiciones experimentales de este trabajo, los ratones p210 muestran escasa o nula respuesta al tratamiento con imatinib.

5. La deleción de C3G en el inicio de la LMC produce un retraso moderado en la progresión de la enfermedad, apoyando un papel dependiente del tiempo de C3G en la leucemogénesis.

6. Las células Ba/F3 transformadas con BCR::ABL1 p210 muestran niveles reducidos de C3G de longitud completa, lo que sugiere una interacción funcional entre BCR::ABL1 y C3G en estas células leucémicas.

7. Las alteraciones en los niveles de expresión de C3G no modifican la proliferación basal de Ba/F3-p210, pero aumentan la sensibilidad a imatinib, reduciendo la viabilidad y potenciando la apoptosis. Esto se acompaña de una disminución de la actividad de BCR::ABL1 y de una señalización JAK/STAT debilitada, sin afectar la activación de CrkL, ERK ni AKT.

8. La reducción de C3G en células 32D, pero no su sobreexpresión, conduce a una menor activación de STAT3 inducida por G-CSF, comprometiendo el inicio del programa de diferenciación neutrofílica.

Bibliography

BIBLIOGRAPHY

Abelson HT, Rabstein LS. Lymphosarcoma: virus-induced thymic-independent disease in mice. *Cancer Res* 30(8):2213–2222, 1970.

Adnan-Awad S, Kim D, Hohtari H, Javarappa KK, Brandstoetter T, Mayer I, Potdar S, Heckman CA, Kytölä S, Porkka K, Doma E, Sexl V, Kankainen M, Mustjoki S. Characterization of p190-Bcr-Abl chronic myeloid leukemia reveals specific signaling pathways and therapeutic targets. *Leukemia* 35(7):1964–1975, 2021.

Adolfsson J, Månsson R, Buza-Vidas N, Hultquist A, Liuba K, Jensen CT, Bryder D, Yang L, Borge O-J, Thoren LAM, Anderson K, Sitnicka E, Sasaki Y, Sigvardsson M, Jacobsen SEW. Identification of Flt3+ lympho-myeloid stem cells lacking erythro-megakaryocytic potential a revised road map for adult blood lineage commitment. *Cell* 121(2):295–306, 2005.

Akashi K, Traver D, Miyamoto T, Weissman IL. A clonogenic common myeloid progenitor that gives rise to all myeloid lineages. *Nature* 404(6774):193–197, 2000.

Amarante-Mendes GP, Rana A, Datoguia TS, Hamerschlak N, Brumatti G. BCR-ABL1 Tyrosine Kinase Complex Signaling Transduction: Challenges to Overcome Resistance in Chronic Myeloid Leukemia. *Pharmaceutics* 14(1):215, 2022.

Arai A, Nosaka Y, Kohsaka H, Miyasaka N, Miura O. CrkL Activates Integrin-Mediated Hematopoietic Cell Adhesion Through the Guanine Nucleotide Exchange Factor C3G. *Blood* 93(11):3713–3722, 1999.

Arber DA, Orazi A, Hasserjian RP, Borowitz MJ, Calvo KR, Kvasnicka H-M, Wang SA, Bagg A, Barbui T, Branford S, Bueso-Ramos CE, Cortes JE, Dal Cin P, DiNardo CD, Dombret H, Duncavage EJ, Ebert BL, Estey EH, Facchetti F, Foucar K, et al. International Consensus Classification of Myeloid Neoplasms and Acute Leukemias: integrating morphologic, clinical, and genomic data. *Blood* 140(11):1200–1228, 2022.

Baccarani M, Castagnetti F, Gugliotta G, Rosti G, Soverini S, Albeer A, Pfirrmann M, International BCR-ABL Study Group. The proportion of different BCR-ABL1 transcript types in chronic myeloid leukemia. An international overview. *Leukemia* 33(5):1173–1183, 2019.

Bao J, Huang B, Zou L, Chen S, Zhang C, Zhang Y, Chen M, Wan J-B, Su H, Wang Y, He C. Hormetic Effect of Berberine Attenuates the Anticancer Activity of Chemotherapeutic Agents. *PLoS One* 10(9):e0139298, 2015.

Baran Y, Saydam G. Cumulative clinical experience from a decade of use: imatinib as first-line treatment of chronic myeloid leukemia. *J Blood Med* 3:139–150, 2012.

Belloc F, Moreau-Gaudry F, Uhalde M, Cazalis L, Jeanneteau M, Lacombe F, Praloran V, Mahon F-X. Imatinib and nilotinib induce apoptosis of chronic myeloid leukemia cells through a Bim-dependant pathway modulated by cytokines. *Cancer Biol Ther* 6(6):912–919, 2007.

Bennett JH. *Case of Hypertrophy of the Spleen and Liver, which Death Took Place from Suppuration of the Blood*. Stark and Company, 1845.

Bertacchini J, Heidari N, Mediani L, Capitani S, Shahjahani M, Ahmadzadeh A, Saki N. Targeting PI3K/AKT/mTOR network for treatment of leukemia. *Cell Mol Life Sci* 72(12):2337–2347, 2015.

Bonnet D, Dick JE. Human acute myeloid leukemia is organized as a hierarchy that originates from a primitive hematopoietic cell. *Nat Med* 3(7):730–737, 1997.

Bos JL, Rehmann H, Wittinghofer A. GEFs and GAPs: Critical Elements in the Control of Small G Proteins. *Cell* 129(5):865–877, 2007.

Boschelli DH, Ye F, Wang YD, Dutia M, Johnson SL, Wu B, Miller K, Powell DW, Yaczko D, Young M, Tischler M, Arndt K, Discafani C, Etienne C, Gibbons J, Grod J, Lucas J, Weber JM, Boschelli F. Optimization of 4-Phenylamino-3-quinolinecarbonitriles as Potent Inhibitors of Src Kinase Activity. *J Med Chem* 44(23):3965–3977, 2001.

Brehme M, Hantschel O, Colinge J, Kaupe I, Planyavsky M, Köcher T, Mechtler K, Bennett KL, Superti-Furga G. Charting the molecular network of the drug target Bcr-Abl. *Proc Natl Acad Sci U S A* 106(18):7414–7419, 2009.

Brown G. Hematopoietic and Chronic Myeloid Leukemia Stem Cells: Multi-Stability versus Lineage Restriction. *Int J Mol Sci* 23(21):13570, 2022.

Brumatti G, Weinlich R, Chehab CF, Yon M, Amarante-Mendes GP. Comparison of the anti-apoptotic effects of Bcr-Abl, Bcl-2 and Bcl-x(L) following diverse apoptogenic stimuli. *FEBS Lett* 541(1–3):57–63, 2003.

Buchdunger E, Zimmermann J, Mett H, Meyer T, Müller M, Druker BJ, Lydon NB. Inhibition of the Abl Protein-Tyrosine Kinase in Vitro and in Vivo by a 2-Phenylaminopyrimidine Derivative. *Cancer Res* 56(1):100–104, 1996.

Büsche G, Kreipe H. Chronic myelogenous leukemia. *In*: *Blood and Bone Marrow Pathology (Second Edition)*. Porwit A , McCullough J , Erber WN (eds.). pp.361–370. Churchill Livingstone, Edinburgh, 2011.

Carabias A, Gómez-Hernández M, de Cima S, Rodríguez-Blázquez A, Morán-Vaquero A, González-Sáenz P, Guerrero C, de Pereda JM. Mechanisms of autoregulation of C3G, activator of the GTPase Rap1, and its catalytic deregulation in lymphomas. *Sci Signal* 13(647):eabb7075, 2020.

Carracedo A, Ma L, Teruya-Feldstein J, Rojo F, Salmena L, Alimonti A, Egia A, Sasaki AT, Thomas G, Kozma SC, Papa A, Nardella C, Cantley LC, Baselga J, Pandolfi PP. Inhibition of mTORC1 leads to MAPK pathway activation through a PI3K-dependent feedback loop in human cancer. *J Clin Invest* 118(9):3065–3074, 2008.

Chai SK, Nichols GL, Rothman P. Constitutive activation of JAKs and STATs in BCR-Abl-expressing cell lines and peripheral blood cells derived from leukemic patients. *J Immunol* 159(10):4720–4728, 1997.

Chakraborty A, Tweardy DJ. Stat3 and G-CSF-induced myeloid differentiation. *Leuk Lymphoma* 30(5–6):433–442, 1998.

Challen GA, Boles N, Lin KK, Goodell MA. Mouse hematopoietic stem cell identification and analysis. *Cytometry Pt A* 75A(1):14–24, 2009.

Chen Y-J, Liou Y-J, Chang C-M, Li H-Y, Chen C-Y, Twu N-F, Yen M-S, Chang Y-L, Peng C-H, Chiou S-H, Chen C-P, Chao K-C. Reprogramming human endometrial fibroblast into induced pluripotent stem cells. *Taiwan J Obstet Gynecol* 51(1):35–42, 2012.

Cheng H, Zheng Z, Cheng T. New paradigms on hematopoietic stem cell differentiation. *Protein Cell* 11(1):34–44, 2020.

Cho YJ, Hemmeryckx B, Groffen J, Heisterkamp N. Interaction of Bcr/Abl with C3G, an exchange factor for the small GTPase Rap1, through the adapter protein Crkl. *Biochem Biophys Res Commun* 333(4):1276–1283, 2005.

Chu S, Li L, Singh H, Bhatia R. BCR-tyrosine 177 plays an essential role in Ras and Akt activation and in human hematopoietic progenitor transformation in chronic myelogenous leukemia. *Cancer Res* 67(14):7045–7053, 2007.

Coffer PJ, Koenderman L, de Groot RP. The role of STATs in myeloid differentiation and leukemia. *Oncogene* 19(21):2511–2522, 2000.

Cohen P. Protein kinases — the major drug targets of the twenty-first century? *Nat Rev Drug Discov* 1(4):309–315, 2002.

Coltro G, Loscocco GG, Vannucchi AM. Classical Philadelphia-negative myeloproliferative neoplasms (MPNs): A continuum of different disease entities. *Int Rev Cell Mol Biol* 365:1–69, 2021.

Coluccia AML, Vacca A, Duñach M, Mologni L, Redaelli S, Bustos VH, Benati D, Pinna LA, Gambacorti-Passerini C. Bcr-Abl stabilizes beta-catenin in chronic myeloid leukemia through its tyrosine phosphorylation. *EMBO J* 26(5):1456–1466, 2007.

Cortes J, Quintás-Cardama A, Kantarjian HM. Monitoring Molecular Response in Chronic Myeloid Leukemia. *Cancer* 117(6):1113–1122, 2011.

Cortez D, Kadlec L, Pendergast AM. Structural and signaling requirements for BCR-ABL-mediated transformation and inhibition of apoptosis. *Mol Cell Biol* 15(10):5531–5541, 1995.

Czabotar PE, Lessene G, Strasser A, Adams JM. Control of apoptosis by the BCL-2 protein family: implications for physiology and therapy. *Nat Rev Mol Cell Biol* 15(1):49–63, 2014.

CzEch Leukemia Study Group - for Life (CELL). Atlas of Haematological Cytology. .

Daley GQ, Van Etten RA, Baltimore D. Induction of chronic myelogenous leukemia in mice by the P210bcr/abl gene of the Philadelphia chromosome. *Science* 247(4944):824–830, 1990.

Deininger M, Buchdunger E, Druker BJ. The development of imatinib as a therapeutic agent for chronic myeloid leukemia. *Blood* 105(7):2640–2653, 2005.

Deininger MW, Goldman JM, Melo JV. The molecular biology of chronic myeloid leukemia. *Blood* 96(10):3343–3356, 2000.

Didion JP, Buus RJ, Naghashfar Z, Threadgill DW, Morse HC, de Villena FP-M. SNP array profiling of mouse cell lines identifies their strains of origin and reveals cross-contamination and widespread aneuploidy. *BMC Genomics* 15(1):847, 2014.

Diekmann D, Brill S, Garrett MD, Totty N, Hsuan J, Monfries C, Hall C, Lim L, Hall A. Bcr encodes a GTPase-activating protein for p21rac. *Nature* 351(6325):400–402, 1991.

Dong F, Brynes RK, Tidow N, Welte K, Löwenberg B, Touw IP. Mutations in the gene for the granulocyte colony-stimulating-factor receptor in patients with acute myeloid leukemia preceded by severe congenital neutropenia. *N Engl J Med* 333(8):487–493, 1995.

Druker BJ, Talpaz M, Resta DJ, Peng B, Buchdunger E, Ford JM, Lydon NB, Kantarjian H, Capdeville R, Ohno-Jones S, Sawyers CL. Efficacy and Safety of a Specific Inhibitor of the BCR-ABL Tyrosine Kinase in Chronic Myeloid Leukemia. *N Engl J Med* 344(14):1031–1037, 2001.

Druker BJ, Tamura S, Buchdunger E, Ohno S, Segal GM, Fanning S, Zimmermann J, Lydon NB. Effects of a selective inhibitor of the Abl tyrosine kinase on the growth of Bcr-Abl positive cells. *Nat Med* 2(5):561–566, 1996.

DuBridge RB, Tang P, Hsia HC, Leong PM, Miller JH, Calos MP. Analysis of mutation in human cells by using an Epstein-Barr virus shuttle system. *Mol Cell Biol* 7(1):379–387, 1987.

Dupuy AJ, Morgan K, von Lintig FC, Shen H, Acar H, Hasz DE, Jenkins NA, Copeland NG, Boss GR, Largaespada DA. Activation of the Rap1 Guanine Nucleotide Exchange Gene,*CalDAG-GEF I*, in BXH-2 Murine Myeloid Leukemia. *J Biol Chem* 276(15):11804–11811, 2001.

Elefanty AG, Hariharan IK, Cory S. bcr-abl, the hallmark of chronic myeloid leukaemia in man, induces multiple haemopoietic neoplasms in mice. *EMBO J* 9(4):1069–1078, 1990.

Elmakaty I, Saglio G, Al-Khabori M, Elsayed A, Elsayed B, Elmarasi M, Elsabagh AA, Alshurafa A, Ali E, Yassin M. The Contemporary Role of Hematopoietic Stem Cell Transplantation in the Management of Chronic Myeloid Leukemia: Is It the Same in All Settings? *Cancers (Basel)* 16(4):754, 2024.

Erdreich-Epstein A, Liu M, Kant AM, Izadi KD, Nolta JA, Durden DL. Cbl functions downstream of Src kinases in FCγRI signaling in primary human macrophages. *J Leukoc Biol* 65(4):523–534, 1999.

Faderl S, Talpaz M, Estrov Z, O'Brien S, Kurzrock R, Kantarjian HM. The Biology of Chronic Myeloid Leukemia. *N Engl J Med* 341(3):164–172, 1999.

Fasouli ES, Katsantoni E. JAK-STAT in Early Hematopoiesis and Leukemia. *Front Cell Dev Biol* 9:669363, 2021.

Fei J, Guo Y. MAPK/ERK Signaling in Tumorigenesis: mechanisms of growth, invasion, and angiogenesis. *EXCLI J* 24:854–879, 2025.

Feller SM, Knudsen B, Hanafusa H. c-Abl kinase regulates the protein binding activity of c-Crk. *EMBO J* 13(10):2341–2351, 1994.

Fernández Infante C. Role of platelet C3G in vesicle trafficking and spreading. Involvement in hemostasis and platelet-mediated inflammation. :1, 2023.

Fernàndez V, Jares P, Salaverria I, Giné E, Beà S, Aymerich M, Colomer D, Villamor N, Bosch F, Montserrat E, Campo E. Gene expression profile and genomic changes in disease progression of early-stage chronic lymphocytic leukemia. *Haematologica* 93(1):132–136, 2008.

Fernández-Infante C, Hernández-Cano L, Herranz Ó, Berrocal P, Sicilia-Navarro C, González-Porras JR, Bastida JM, Porras A, Guerrero C. Platelet C3G: a key player in vesicle exocytosis, spreading and clot retraction. *Cell Mol Life Sci* 81(1):84, 2024.

Fetisov TI, Lesovaya EA, Yakubovskaya MG, Kirsanov KI, Belitsky GA. Alterations in WNT Signaling in Leukemias. *Biochemistry (Mosc)* 83(12):1448–1458, 2018.

Fialkow PJ, Jacobson RJ, Papayannopoulou T. Chronic myelocytic leukemia: clonal origin in a stem cell common to the granulocyte, erythrocyte, platelet and monocyte/macrophage. *Am J Med* 63(1):125–130, 1977.

Gallipoli P, Cook A, Rhodes S, Hopcroft L, Wheadon H, Whetton AD, Jørgensen HG, Bhatia R, Holyoake TL. JAK2/STAT5 inhibition by nilotinib with ruxolitinib contributes to the elimination of CML CD34+ cells in vitro and in vivo. *Blood* 124(9):1492–1501, 2014.

Galton DA. Myleran in chronic myeloid leukaemia; results of treatment. *Lancet* 264(6753):208–213, 1953.

Gao S, Zhang Y, Liu F. Revisiting the lineage contribution of hematopoietic stem and progenitor cells. *Development* 150(14):dev201609, 2023.

García-Navas R, Gómez C, Zamora-Valdivieso B, Calvo-Jimenez S, Calzada N, Fernandez-Medarde A, Sierra M, Sánchez-Guijo F, Schenk RL, Hofmann MH, Kostyrko K, Santos E. Targeting SOS1 synergistically enhances efficacy of BCR/ABL tyrosine kinase inhibitors and overcomes resistance in chronic myeloid leukemia. *bioRxiv*:2025.09.29.679122, 2025.

García-Tuñón I, Hernández-Sánchez M, Ordoñez JL, Alonso-Pérez V, Álamo-Quijada M, Benito R, Guerrero C, Hernández-Rivas JM, Sánchez-Martín M. The CRISPR/Cas9 system efficiently reverts the tumorigenic ability of *BCR/ABL in vitro* and in a xenograft model of chronic myeloid leukemia. *Oncotarget* 8(16):26027–26040, 2017.

Genovese G, Kähler AK, Handsaker RE, Lindberg J, Rose SA, Bakhoum SF, Chambert K, Mick E, Neale BM, Fromer M, Purcell SM, Svantesson O, Landén M, Höglund M, Lehmann S, Gabriel SB, Moran JL, Lander ES, Sullivan PF, Sklar P, et al. Clonal hematopoiesis and blood-cancer risk inferred from blood DNA sequence. *N Engl J Med* 371(26):2477–2487, 2014.

Giladi A, Paul F, Herzog Y, Lubling Y, Weiner A, Yofe I, Jaitin D, Cabezas-Wallscheid N, Dress R, Ginhoux F, Trumpp A, Tanay A, Amit I. Single-cell characterization of haematopoietic progenitors and their trajectories in homeostasis and perturbed haematopoiesis. *Nat Cell Biol* 20(7):836–846, 2018.

Gíslason MH, Demircan GS, Prachar M, Furtwängler B, Schwaller J, Schoof EM, Porse BT, Rapin N, Bagger FO. BloodSpot 3.0: a database of gene and protein expression data in normal and malignant haematopoiesis. *Nucleic Acids Res* 52(D1):D1138–D1142, 2024.

Goldman JM. Chronic Myeloid Leukemia: A Historical Perspective. *Semin Hematol* 47(4):302–311, 2010.

Goldman JM, Baughan AS, McCarthy DM, Worsley AM, Hows JM, Gordon-Smith EC, Catovsky D, Batchelor JR, Goolden AW, Galton DA. Marrow transplantation for patients in the chronic phase of chronic granulocytic leukaemia. *Lancet* 2(8299):623–625, 1982.

Gómez C, Garcia-Navas R, Baltanás FC, Fuentes-Mateos R, Fernández-Medarde A, Calzada N, Santos E. Critical Requirement of SOS1 for Development of BCR/ABL-Driven Chronic Myelogenous Leukemia. *Cancers (Basel)* 14(16):3893, 2022.

Görgens A, Radtke S, Möllmann M, Cross M, Dürig J, Horn PA, Giebel B. Revision of the human hematopoietic tree: granulocyte subtypes derive from distinct hematopoietic lineages. *Cell Rep* 3(5):1539–1552, 2013.

Göthert JR, Gustin SE, Hall MA, Green AR, Göttgens B, Izon DJ, Begley CG. In vivo fate-tracing studies using the Scl stem cell enhancer: embryonic hematopoietic stem cells significantly contribute to adult hematopoiesis. *Blood* 105(7):2724–2732, 2005.

Gotoh T, Hattori ,Seisuke, Nakamura ,Shun, Kitayama ,Hitoshi, Noda ,Makoto, Takai ,Yoshimi, Kaibuchi ,Kozo, Matsui ,Hideki, Hatase ,Osamu, Takahashi ,Hidehiro, Kurata ,Takeshi, and Matsuda M. Identification of Rap1 as a Target for the Crk SH3 Domain-Binding Guanine Nucleotide-Releasing Factor C3G. *Mol Cell Biol* 15(12):6746–6753, 1995.

Gotoh T, Niino Y, Tokuda M, Hatase O, Nakamura S, Matsuda M, Hattori S. Activation of R-Ras by Ras-Guanine Nucleotide-releasing Factor. *J Biol Chem* 272(30):18602–18607, 1997.

Green MR, Gentles AJ, Nair RV, Irish JM, Kihira S, Liu CL, Kela I, Hopmans ES, Myklebust JH, Ji H, Plevritis SK, Levy R, Alizadeh AA. Hierarchy in somatic mutations arising during genomic evolution and progression of follicular lymphoma. *Blood* 121(9):1604–1611, 2013.

Groffen J, Stephenson JR, Heisterkamp N, de Klein A, Bartram CR, Grosveld G. Philadelphia chromosomal breakpoints are clustered within a limited region, bcr, on chromosome 22. *Cell* 36(1):93–99, 1984.

Guchhait P, Tosi MF, Smith CW, Chakaraborty A. The murine myeloid cell line 32Dcl3 as a model system for studying neutrophil functions. *J Immunol Methods* 283(1–2):195–204, 2003.

Guerrero C, Fernandez-Medarde A, Rojas J, Font De Mora J, Esteban L, Santos E. Transformation suppressor activity of C3G is independent of its CDC25-homology domain. *Oncogene* 16(5):613–624, 1998.

Guerrero C, Martín-Encabo S, Fernández-Medarde A, Santos E. C3G-mediated suppression of oncogene-induced focus formation in fibroblasts involves inhibition of ERK activation, cyclin A expression and alterations of anchorage-independent growth. *Oncogene* 23(28):4885–4893, 2004.

Guo C, Yang W, Lobe CG. A Cre recombinase transgene with mosaic, widespread tamoxifen-inducible action. *Genesis* 32(1):8–18, 2002.

Gutiérrez-Berzal J, Castellano E, Martín-Encabo S, Gutiérrez-Cianca N, Hernández JM, Santos E, Guerrero C. Characterization of p87C3G, a novel, truncated C3G isoform that is overexpressed in chronic myeloid leukemia and interacts with Bcr-Abl. *Exp Cell Res* 312(6):938–948, 2006.

Gutiérrez-Herrero S, Fernández-Infante C, Hernández-Cano L, Ortiz-Rivero S, Guijas C, Martín-Granado V, González-Porras JR, Balsinde J, Porras A, Guerrero C. C3G contributes to platelet activation and aggregation by regulating major signaling pathways. *Sig Transduct Target Ther* 5(1):29, 2020.

Gutiérrez-Uzquiza A, Arechederra M, Molina I, Baños R, Maia V, Benito M, Guerrero C, Porras A. C3G down-regulates p38 MAPK activity in response to stress by Rap-1 independent mechanisms: involvement in cell death. *Cell Signal* 22(3):533–542, 2010.

Haas S, Trumpp A, Milsom MD. Causes and Consequences of Hematopoietic Stem Cell Heterogeneity. *Cell Stem Cell* 22(5):627–638, 2018.

Han L, Schuringa JJ, Mulder A, Vellenga E. Dasatinib impairs long-term expansion of leukemic progenitors in a subset of acute myeloid leukemia cases. *Ann Hematol* 89(9):861–871, 2010.

Hantschel O. Structure, regulation, signaling, and targeting of abl kinases in cancer. *Genes Cancer* 3(5–6):436–446, 2012.

Hantschel O, Nagar B, Guettler S, Kretzschmar J, Dorey K, Kuriyan J, Superti-Furga G. A myristoyl/phosphotyrosine switch regulates c-Abl. *Cell* 112(6):845–857, 2003.

Harada I, Sasaki H, Murakami K, Nishiyama A, Nakabayashi J, Ichino M, Miyazaki T, Kumagai K, Matsumoto K, Hagihara M, Kawase W, Tachibana T, Tanaka M, Saito T, Kanamori H, Fujita H, Fujisawa S, Nakajima H, Tamura T. Compromised anti-tumor–immune features of myeloid cell components in chronic myeloid leukemia patients. *Sci Rep* 11(1):18046, 2021.

Hazlehurst LA, Bewry NN, Nair RR, Pinilla-Ibarz J. Signaling Networks Associated with BCR–ABL–Dependent Transformation. *Cancer Control* 16(2):100–107, 2009.

Heard JM, Sola B, Martial MA, Fichelson S, Gisselbrecht S. Long-term culture of bone marrow-derived preleukemic cells from F-MuLV-infected mice. *Blood* 68(1):193–199, 1986.

Hehlmann R, Lauseker M, Saußele S, Pfirrmann M, Krause S, Kolb HJ, Neubauer A, Hossfeld DK, Nerl C, Gratwohl A, Baerlocher GM, Heim D, Brümmendorf TH, Fabarius A, Haferlach C, Schlegelberger B, Müller MC, Jeromin S, Proetel U, Kohlbrenner K, et al. Assessment of imatinib as first-line treatment of chronic myeloid leukemia: 10-year survival results of the randomized CML study IV and impact of non-CML determinants. *Leukemia* 31(11):2398–2406, 2017.

Heisterkamp N, Jenster G, ten Hoeve J, Zovich D, Pattengale PK, Groffen J. Acute leukaemia in bcr/abl transgenic mice. *Nature* 344(6263):251–253, 1990.

Heisterkamp N, Stephenson JR, Groffen J, Hansen PF, de Klein A, Bartram CR, Grosveld G. Localization of the c-ab1 oncogene adjacent to a translocation break point in chronic myelocytic leukaemia. *Nature* 306(5940):239–242, 1983.

Hernández-Cano L, Fernández-Infante C, Herranz Ó, Berrocal P, Lozano FS, Sánchez-Martín MA, Porras A, Guerrero C. New functions of C3G in platelet biology: Contribution to ischemia-induced angiogenesis, tumor metastasis and TPO clearance. *Front Cell Dev Biol* 10:1026287, 2022.

Herranz Ó, Berrocal P, Sicilia-Navarro C, Fernández-Infante C, Hernández-Cano L, Porras A, Guerrero C. C3G promotes bone marrow adipocyte expansion and hematopoietic regeneration after myeloablation by enhancing megakaryocyte niche function. *J Hematol Oncol* 18(1):38, 2025.

Herranz Varea Ó. Impact of C3G on hematopoiesis after myeloablation: effects on hematopoietic precursors and megakaryocyte niche function. 2024.

Hey Y-Y, Quah B, O'Neill HC. Antigen presenting capacity of murine splenic myeloid cells. *BMC Immunol* 18(1):4, 2017.

Hochhaus Andreas, Larson RA, Guilhot F, Radich JP, Branford S, Hughes TP, Baccarani M, Deininger MW, Cervantes F, Fujihara S, Ortmann C-E, Menssen HD, Kantarjian H, O'Brien SG, Druker BJ. Long-Term Outcomes of Imatinib Treatment for Chronic Myeloid Leukemia. *N Engl J Med* 376(10):917–927, 2017.

Hochhaus A., Saussele S, Rosti G, Mahon F-X, Janssen JJWM, Hjorth-Hansen H, Richter J, Buske C. Chronic myeloid leukaemia: ESMO Clinical Practice Guidelines for diagnosis, treatment and follow-up. *Ann Oncol* 28:iv41–iv51, 2017.

ten Hoeve J, Arlinghaus RB, Guo JQ, Heisterkamp N, Groffen J. Tyrosine phosphorylation of CRKL in Philadelphia+ leukemia. *Blood* 84(6):1731–1736, 1994.

Hogan C, Serpente N, Cogram P, Hosking CR, Bialucha CU, Feller SM, Braga VMM, Birchmeier W, Fujita Y. Rap1 regulates the formation of E-cadherin-based cell-cell contacts. *Mol Cell Biol* 24(15):6690–6700, 2004.

Honda H, Oda H, Suzuki T, Takahashi T, Witte ON, Ozawa K, Ishikawa T, Yazaki Y, Hirai H. Development of acute lymphoblastic leukemia and myeloproliferative disorder in transgenic mice expressing p210bcr/abl: a novel transgenic model for human Ph1-positive leukemias. *Blood* 91(6):2067–2075, 1998.

Houshmand M, Simonetti G, Circosta P, Gaidano V, Cignetti A, Martinelli G, Saglio G, Gale RP. Chronic myeloid leukemia stem cells. *Leukemia* 33(7):1543–1556, 2019.

Hsieh Y-C, Kirschner K, Copland M. Improving outcomes in chronic myeloid leukemia through harnessing the immunological landscape. *Leukemia* 35(5):1229–1242, 2021.

Hu X, Li J, Fu M, Zhao X, Wang W. The JAK/STAT signaling pathway: from bench to clinic. *Sig Transduct Target Ther* 6(1):402, 2021.

Huang X, Cortes J, Kantarjian H. Estimations of the increasing prevalence and plateau prevalence of chronic myeloid leukemia in the era of tyrosine kinase inhibitor therapy. *Cancer* 118(12):3123–3127, 2012.

Ichiba T, Hashimoto Y, Nakaya M, Kuraishi Y, Tanaka S, Kurata T, Mochizuki N, Matsuda M. Activation of C3G guanine nucleotide exchange factor for Rap1 by phosphorylation of tyrosine 504. *J Biol Chem* 274(20):14376–14381, 1999.

Ilchuk LA, Stavskaya NI, Varlamova EA, Khamidullina AI, Tatarskiy VV, Mogila VA, Kolbutova KB, Bogdan SA, Sheremetov AM, Baulin AN, Filatova IA, Silaeva YY, Filatov MA, Bruter AV. Limitations of Tamoxifen Application for In Vivo Genome Editing Using Cre/ERT2 System. *Int J Mol Sci* 23(22):14077, 2022.

Imai T, Tanaka H, Hamazaki Y, Minato N. Rap1 signal modulators control the maintenance of hematopoietic progenitors in bone marrow and adult long-term hematopoiesis. *Cancer Sci* 110(4):1317–1330, 2019.

Ishida D, Kometani K, Yang H, Kakugawa K, Masuda K, Iwai K, Suzuki M, Itohara S, Nakahata T, Hiai H, Kawamoto H, Hattori M, Minato N. Myeloproliferative stem cell disorders by deregulated Rap1 activation in SPA-1-deficient mice. *Cancer Cell* 4(1):55–65, 2003.

Ishimaru S, Williams R, Clark E, Hanafusa H, Gaul U. Activation of the Drosophila C3G leads to cell fate changes and overproliferation during development, mediated by the RAS-MAPK pathway and RAP1. *EMBO J* 18(1):145–155, 1999.

Izzo B, Gottardi EM, Errichiello S, Daraio F, Baratè C, Galimberti S. Monitoring Chronic Myeloid Leukemia: How Molecular Tools May Drive Therapeutic Approaches. *Front Oncol* 9 2019.

Jabbour E, Kantarjian H. Chronic myeloid leukemia: 2025 update on diagnosis, therapy, and monitoring. *Am J Hematol* 99(11):2191–2212, 2024.

Jamieson CHM, Ailles LE, Dylla SJ, Muijtjens M, Jones C, Zehnder JL, Gotlib J, Li K, Manz MG, Keating A, Sawyers CL, Weissman IL. Granulocyte-macrophage progenitors as candidate leukemic stem cells in blast-crisis CML. *N Engl J Med* 351(7):657–667, 2004.

Jasek-Gajda E, Jurkowska H, Jasińska M, Lis GJ, Jasek-Gajda E, Jurkowska H, Jasińska M, Lis GJ. Targeting the MAPK/ERK and PI3K/AKT Signaling Pathways Affects NRF2, Trx and GSH Antioxidant Systems in Leukemia Cells. *Antioxidants* 9(7) 2020.

Jaśkiewicz A, Pająk B, Orzechowski A. The Many Faces of Rap1 GTPase. *Int J Mol Sci* 19(10):2848, 2018.

Jonas D, Lübbert M, Kawasaki ES, Henke M, Bross KJ, Mertelsmann R, Herrmann F. Clonal analysis of bcr-abl rearrangement in T lymphocytes from patients with chronic myelogenous leukemia. *Blood* 79(4):1017–1023, 1992.

de Jong R, van Wijk A, Heisterkamp N, Groffen J. C3G is tyrosine-phosphorylated after integrin-mediated cell adhesion in normal but not in Bcr/Abl expressing cells. *Oncogene* 17(21):2805–2810, 1998.

Jyotsana N, Sharma A, Chaturvedi A, Budida R, Scherr M, Kuchenbauer F, Lindner R, Noyan F, Sühs K-W, Stangel M, Grote-Koska D, Brand K, Vornlocher H-P, Eder M, Thol F, Ganser A, Humphries RK, Ramsay E, Cullis P, Heuser M. Lipid nanoparticle-mediated siRNA delivery for safe targeting of human CML in vivo. *Ann Hematol* 98(8):1905–1918, 2019.

Kantarjian HM, Chifotides HT, Haddad FG, Short NJ, Loghavi S, Jabbour E. Ponatinib-review of historical development, current status, and future research. *Am J Hematol* 99(8):1576–1585, 2024.

Karamitros D, Stoilova B, Aboukhalil Z, Hamey F, Reinisch A, Samitsch M, Quek L, Otto G, Repapi E, Doondeea J, Usukhbayar B, Calvo J, Taylor S, Goardon N, Six E, Pflumio F, Porcher C, Majeti R, Göttgens B, Vyas P. Single-cell analysis reveals the continuum of human lympho-myeloid progenitor cells. *Nat Immunol* 19(1):85–97, 2018.

Katagiri K, Hattori M, Minato N, Kinashi T. Rap1 functions as a key regulator of T-cell and antigen-presenting cell interactions and modulates T-cell responses. *Mol Cell Biol* 22(4):1001–1015, 2002.

Kelliher MA, McLaughlin J, Witte ON, Rosenberg N. Induction of a chronic myelogenous leukemia-like syndrome in mice with v-abl and BCR/ABL. *Proc Natl Acad Sci U S A* 87(17):6649–6653, 1990.

Khattar E, Maung KZY, Chew CL, Ghosh A, Mok MMH, Lee P, Zhang J, Chor WHJ, Cildir G, Wang CQ, Mohd-Ismail NK, Chin DWL, Lee SC, Yang H, Shin Y-J, Nam D-H, Chen L, Kumar AP, Deng LW, Ikawa M, et al. Rap1 regulates hematopoietic stem cell survival and affects oncogenesis and response to chemotherapy. *Nat Commun* 10(1):5349, 2019.

Kim T, Tyndel MS, Kim HJ, Ahn J-S, Choi SH, Park HJ, Kim Y-K, Kim SY, Lipton JH, Zhang Z, Kim DDH. Spectrum of somatic mutation dynamics in chronic myeloid leukemia following tyrosine kinase inhibitor therapy. *Blood* 129(1):38–47, 2017.

Kinstrie R, Karamitros D, Goardon N, Morrison H, Hamblin M, Robinson L, Clark RE, Copland M, Vyas P. Heterogeneous leukemia stem cells in myeloid blast phase chronic myeloid leukemia. *Blood Adv* 1(3):160–169, 2016.

Kirsch KH, Georgescu M-M, Hanafusa H. Direct Binding of p130Cas to the Guanine Nucleotide Exchange Factor C3G. *J Biol Chem* 273(40):25673–25679, 1998.

Kleppe M, Spitzer MH, Li S, Hill CE, Dong L, Papalexi E, De Groote S, Bowman RL, Keller M, Koppikar P, Rapaport FT, Teruya-Feldstein J, Gandara J, Mason CE, Nolan GP, Levine RL. Jak1 Integrates Cytokine Sensing to Regulate Hematopoietic Stem Cell Function and Stress Hematopoiesis. *Cell Stem Cell* 21(4):489-501.e7, 2017.

Knudsen BS, Feller SM, Hanafusa H. Four proline-rich sequences of the guanine-nucleotide exchange factor C3G bind with unique specificity to the first Src homology 3 domain of Crk. *J Biol Chem* 269(52):32781–32787, 1994.

Kometani K, Aoki M, Kawamata S, Shinozuka Y, Era T, Taniwaki M, Hattori M, Minato N. Role of SPA-1 in Phenotypes of Chronic Myelogenous Leukemia Induced by BCR-ABL–Expressing Hematopoietic Progenitors in a Mouse Model. *Cancer Res* 66(20):9967–9976, 2006.

Kondo M, Weissman IL, Akashi K. Identification of clonogenic common lymphoid progenitors in mouse bone marrow. *Cell* 91(5):661–672, 1997.

Kong JH, Winton EF, Heffner LT, Gaddh M, Hill B, Neely J, Hatcher A, Joseph M, Arellano M, El-Rassi F, Kim A, Khoury JH, Kota VK. Outcomes of Chronic Phase Chronic Myeloid Leukemia after Treatment with Multiple Tyrosine Kinase Inhibitors. *J Clin Med* 9(5) 2020.

Koolivand Z, Bahreini F, Rayzan E, Rezaei N. Inducing apoptosis in acute myeloid leukemia; mechanisms and limitations. *Heliyon* 11(1):e41355, 2025.

Koretzky GA. The legacy of the Philadelphia chromosome. *J Clin Invest* 117(8):2030, 2007.

Kurzrock R, Gutterman JU, Talpaz M. The molecular genetics of Philadelphia chromosome-positive leukemias. *N Engl J Med* 319(15):990–998, 1988.

Lafuente EM, van Puijenbroek AAFL, Krause M, Carman CV, Freeman GJ, Berezovskaya A, Constantine E, Springer TA, Gertler FB, Boussiotis VA. RIAM, an Ena/VASP and Profilin Ligand, Interacts with Rap1-GTP and Mediates Rap1-Induced Adhesion. *Dev Cell* 7(4):585–595, 2004.

Langford DJ, Bailey AL, Chanda ML, Clarke SE, Drummond TE, Echols S, Glick S, Ingrao J, Klassen-Ross T, LaCroix-Fralish ML, Matsumiya L, Sorge RE, Sotocinal SG, Tabaka JM, Wong D, van den Maagdenberg AMJM, Ferrari MD, Craig KD, Mogil JS. Coding of facial expressions of pain in the laboratory mouse. *Nat Methods* 7(6):447–449, 2010.

Laurenti E, Göttgens B. From haematopoietic stem cells to complex differentiation landscapes. *Nature* 553(7689):418–426, 2018.

Lee H, Gaughan JP, Tsygankov AY. c-Cbl facilitates cytoskeletal effects in v-Abl transformed fibroblast through Rac1- and Rap1-mediated signaling. *Int J Biochem Cell Biol* 40(9):1930–1943, 2008.

Lee JC, Hapel AJ, Ihle JN. Constitutive production of a unique lymphokine (IL 3) by the WEHI-3 cell line. *J Immunol* 128(6):2393–2398, 1982.

Leliefeld PHC, Wessels CM, Leenen LPH, Koenderman L, Pillay J. The role of neutrophils in immune dysfunction during severe inflammation. *Crit Care* 20(1):73, 2016.

Lew VL, Tiffert T. On the Mechanism of Human Red Blood Cell Longevity: Roles of Calcium, the Sodium Pump, PIEZO1, and Gardos Channels. *Front Physiol* 8:977, 2017.

Li X, Song Y. Proteolysis-targeting chimera (PROTAC) for targeted protein degradation and cancer therapy. *J Hematol Oncol* 13(1):50, 2020.

Liau NPD, Laktyushin A, Lucet IS, Murphy JM, Yao S, Whitlock E, Callaghan K, Nicola NA, Kershaw NJ, Babon JJ. The molecular basis of JAK/STAT inhibition by SOCS1. *Nat Commun* 9(1):1558, 2018.

Liggett LA, Sankaran VG. Unraveling Hematopoiesis through the Lens of Genomics. *Cell* 182(6):1384–1400, 2020.

Lim YS, Jeong N-R, Yoo S-M, KIM HW, Lee SH, Kim D-W. A Novel BCR-ABL1 Degrader, Ubx-362, Can Overcome Resistance By BCR-ABL1 Kinase Domain Mutations in Chronic Myeloid Leukemia. *Blood* 142(Supplement 1):5012, 2023.

Lissauer H. Zwei fälle von leucaemie. *Berl Klin Wochenschr* 2:403–404, 1865.

Lozzio CB, Lozzio BB. Human Chronic Myelogenous Leukemia Cell-Line With Positive Philadelphia Chromosome. *Blood* 45(3):321–334, 1975.

Ma G, Lu D, Wu Y, Liu J, Arlinghaus RB. Bcr phosphorylated on tyrosine 177 binds Grb2. *Oncogene* 14(19):2367–2372, 1997.

Macaulay IC, Svensson V, Labalette C, Ferreira L, Hamey F, Voet T, Teichmann SA, Cvejic A. Single-Cell RNA-Sequencing Reveals a Continuous Spectrum of Differentiation in Hematopoietic Cells. *Cell Rep* 14(4):966–977, 2016.

Mahon F-X, Réa D, Guilhot J, Guilhot F, Huguet F, Nicolini F, Legros L, Charbonnier A, Guerci A, Varet B, Etienne G, Reiffers J, Rousselot P, Intergroupe Français des Leucémies Myéloïdes Chroniques. Discontinuation of imatinib in patients with chronic myeloid leukaemia who have maintained complete molecular remission for at least 2 years: the prospective, multicentre Stop Imatinib (STIM) trial. *Lancet Oncol* 11(11):1029–1035, 2010.

Maia V, Ortiz-Rivero S, Sanz M, Gutierrez-Berzal J, Álvarez-Fernández I, Gutierrez-Herrero S, De Pereda JM, Porras A, Guerrero C. C3G forms complexes with Bcr-Abl and p38α MAPK at the focal adhesions in chronic myeloid leukemia cells: implication in the regulation of leukemic cell adhesion. *Cell Commun Signal* 11(1):9, 2013.

Maia V, Sanz M, Gutierrez-Berzal J, De Luis A, Gutierrez-Uzquiza A, Porras A, Guerrero C. C3G silencing enhances STI-571-induced apoptosis in CML cells through p38 MAPK activation, but it antagonizes STI-571 inhibitory effect on survival. *Cell Signal* 21(7):1229–1235, 2009.

Mandanas RA, Leibowitz DS, Gharehbaghi K, Tauchi T, Burgess GS, Miyazawa K, Jayaram HN, Boswell HS. Role of p21 RAS in p210 bcr-abl transformation of murine myeloid cells. *Blood* 82(6):1838–1847, 1993.

Manohar SM, Shah P, Nair A. Flow cytometry: principles, applications and recent advances. *Bioanalysis* 13(3):181–198, 2021.

Manzano S, Gutierrez-Uzquiza A, Bragado P, Sequera C, Herranz Ó, Rodrigo-Faus M, Jauregui P, Morgner S, Rubio I, Guerrero C, Porras A. C3G downregulation induces the acquisition of a mesenchymal phenotype that enhances aggressiveness of glioblastoma cells. *Cell Death Dis* 12(4):348, 2021.

Marin Oyarzún CP, Heller PG. Platelets as Mediators of Thromboinflammation in Chronic Myeloproliferative Neoplasms. *Front Immunol* 10:1373, 2019.

Marnell CS, Bick A, Natarajan P. Clonal Hematopoiesis of Indeterminate Potential (CHIP): Linking Somatic Mutations, Hematopoiesis, Chronic Inflammation and Cardiovascular Disease. *J Mol Cell Cardiol* 161:98–105, 2021.

Martin PJ, Najfeld V, Hansen JA, Penfold GK, Jacobson RJ, Fialkow PJ. Involvement of the B-lymphoid system in chronic myelogenous leukaemia. *Nature* 287(5777):49–50, 1980.

Martín-Encabo S, Santos E, Guerrero C. C3G mediated suppression of malignant transformation involves activation of PP2A phosphatases at the subcortical actin cytoskeleton. *Exp Cell Res* 313(18):3881–3891, 2007.

McCubrey JA, Steelman LS, Abrams SL, Bertrand FE, Ludwig DE, Bäsecke J, Libra M, Stivala F, Milella M, Tafuri A, Lunghi P, Bonati A, Martelli AM. Targeting survival cascades induced by activation of Ras/Raf/MEK/ERK, PI3K/PTEN/Akt/mTOR and Jak/STAT pathways for effective leukemia therapy. *Leukemia* 22(4):708–722, 2008.

McDermott EP, O'Neill LAJ. Ras Participates in the Activation of p38 MAPK by Interleukin-1 by Associating with IRAK, IRAK2, TRAF6, and TAK-1. *J Biol Chem* 277(10):7808–7815, 2002.

McLeod SJ, Shum AJ, Lee RL, Takei F, Gold MR. The Rap GTPases regulate integrin-mediated adhesion, cell spreading, actin polymerization, and Pyk2 tyrosine phosphorylation in B lymphocytes. *J Biol Chem* 279(13):12009–12019, 2004.

Melo JV. The Diversity of BCR-ABL Fusion Proteins and Their Relationship to Leukemia Phenotype. *Blood* 88(7):2375–2384, 1996.

Melo JV, Chuah C. Resistance to imatinib mesylate in chronic myeloid leukaemia. *Cancer Lett* 249(2):121–132, 2007.

Meloche S, Pouysségur J. The ERK1/2 mitogen-activated protein kinase pathway as a master regulator of the G1- to S-phase transition. *Oncogene* 26(22):3227–3239, 2007.

Mesa RA, Yasothan U, Kirkpatrick P. Ruxolitinib. *Nat Rev Drug Discov* 11(2):103–104, 2012.

Metcalf D, Moore MAS, Warner NL. Colony Formation In Vitro by Myelomonocytic Leukemic Cells23. *J Natl Cancer Inst* 43(4):983–1001, 1969.

Minami Y, Stuart SA, Ikawa T, Jiang Y, Banno A, Hunton IC, Young DJ, Naoe T, Murre C, Jamieson CHM, Wang JYJ. BCR-ABL-transformed GMP as myeloid leukemic stem cells. *Proc Natl Acad Sci U S A* 105(46):17967–17972, 2008.

Minato N, Hattori M. Spa-1 (Sipa1) and Rap signaling in leukemia and cancer metastasis. *Cancer Sci* 100(1):17–23, 2009.

Mojtahedi H, Yazdanpanah N, Rezaei N. Chronic myeloid leukemia stem cells: targeting therapeutic implications. *Stem Cell Res Ther* 12(1):603, 2021.

Morán-Vaquero A, Herranz Ó, Dávila-Hidalgo A, Rodríguez-Blázquez A, Fernández-Infante C, García-Tuñón I, Vuelta E, van der Meer F, Margadant C, Guerrero C, de Pereda JM. C3G deregulation uncovers a dual role in B-cell lymphoma: tumor suppression and enhanced metastasis via Rap1 and Rac2 signaling. *Cell Commun Signal* 24(11):23, 2026.

Morin RD, Mendez-Lago M, Mungall AJ, Goya R, Mungall KL, Corbett RD, Johnson NA, Severson TM, Chiu R, Field M, Jackman S, Krzywinski M, Scott DW, Trinh DL, Tamura-Wells J, Li S, Firme MR, Rogic S, Griffith M, Chan S, et al. Frequent mutation of histone-modifying genes in non-Hodgkin lymphoma. *Nature* 476(7360):298–303, 2011.

Morrison SJ, Wandycz AM, Hemmati HD, Wright DE, Weissman IL. Identification of a lineage of multipotent hematopoietic progenitors. *Development* 124(10):1929–1939, 1997.

Mu H, Zhu X, Jia H, Zhou L, Liu H. Combination Therapies in Chronic Myeloid Leukemia for Potential Treatment-Free Remission: Focus on Leukemia Stem Cells and Immune Modulation. *Front Oncol* 11:643382, 2021.

Naka K. New routes to eradicating chronic myelogenous leukemia stem cells by targeting metabolism. *Int J Hematol* 113(5):648–655, 2021.

Nakajima H, Ihle JN. Granulocyte colony-stimulating factor regulates myeloid differentiation through CCAAT/enhancer-binding protein ε. *Blood* 98(4):897–905, 2001.

National Cancer Institute. What Is Cancer? - NCI. 2007.

Neshat MS, Raitano AB, Wang HG, Reed JC, Sawyers CL. The survival function of the Bcr-Abl oncogene is mediated by Bad-dependent and -independent pathways: roles for phosphatidylinositol 3-kinase and Raf. *Mol Cell Biol* 20(4):1179–1186, 2000.

Nichols GL, Raines MA, Vera JC, Lacomis L, Tempst P, Golde DW. Identification of CRKL as the constitutively phosphorylated 39-kD tyrosine phosphoprotein in chronic myelogenous leukemia cells. *Blood* 84(9):2912–2918, 1994.

Nolz JC, Nacusi LP, Segovis CM, Medeiros RB, Mitchell JS, Shimizu Y, Billadeau DD. The WAVE2 complex regulates T cell receptor signaling to integrins via Abl- and CrkL-C3G-mediated activation of Rap1. *J Cell Biol* 182(6):1231–1244, 2008.

Nowell PC, Hungerford DA. A minute chromosome in human chronic granulocytic leukemia. *Science* 132:1497, 1960.

Ochi Y, Yoshida K, Huang Y-J, Kuo M-C, Shiozawa Y, Nannya Y, Shiraishi Y, Okada A, Chiba K, Tanaka H, Miyano S, Takaori-Kondo A, Shih L-Y, Ogawa S. Molecular Profiling of Blastic Transformation in Chronic Myeloid Leukemia. *Blood* 132(Supplement 1):1725, 2018.

Oda T, Heaney C, Hagopian JR, Okuda K, Griffin JD, Druker BJ. Crkl is the major tyrosine-phosphorylated protein in neutrophils from patients with chronic myelogenous leukemia. *J Biol Chem* 269(37):22925–22928, 1994.

O'Hare T, Shakespeare WC, Zhu X, Eide CA, Rivera VM, Wang F, Adrian LT, Zhou T, Huang W-S, Xu Q, Metcalf CA, Tyner JW, Loriaux MM, Corbin AS, Wardwell S, Ning Y, Keats JA, Wang Y, Sundaramoorthi R, Thomas M, et al. AP24534, a Pan-BCR-ABL Inhibitor for Chronic Myeloid Leukemia, Potently Inhibits the T315I Mutant and Overcomes Mutation-Based Resistance. *Cancer Cell* 16(5):401–412, 2009.

Ohba Y. Requirement for C3G-dependent Rap1 activation for cell adhesion and embryogenesis. *EMBO J* 20(13):3333–3341, 2001.

Ohba Y, Mochizuki N, Yamashita S, Chan AM, Schrader JW, Hattori S, Nagashima K, Matsuda M. Regulatory Proteins of R-Ras, TC21/R-Ras2, and M-Ras/R-Ras3. *J Biol Chem* 275(26):20020–20026, 2000a.

Ohba Y, Mochizuki ,Naoki, Matsuo ,Keiko, Yamashita ,Shigeko, Nakaya ,Mie, Hashimoto ,Yuko, Hamaguchi ,Michinari, Kurata ,Takeshi, Nagashima ,Kazuo, and Matsuda M. Rap2 as a Slowly Responding Molecular Switch in the Rap1 Signaling Cascade. *Mol Cell Biol* 20(16):6074–6083, 2000b.

Orkin SH. Diversification of haematopoietic stem cells to specific lineages. *Nat Rev Genet* 1(1):57–64, 2000.

Orlova A, Wagner C, de Araujo ED, Bajusz D, Neubauer HA, Herling M, Gunning PT, Keserű GM, Moriggl R. Direct Targeting Options for STAT3 and STAT5 in Cancer. *Cancers (Basel)* 11(12):1930, 2019.

Ortiz-Rivero S, Baquero C, Hernández-Cano L, Roldán-Etcheverry JJ, Gutiérrez-Herrero S, Fernández-Infante C, Martín-Granado V, Anguita E, De Pereda JM, Porras A, Guerrero C. C3G, through its GEF activity, induces megakaryocytic differentiation and proplatelet formation. *Cell Commun Signal* 16(1):101, 2018.

Palacios R, Steinmetz M. IL3-dependent mouse clones that express B-220 surface antigen, contain ig genes in germ-line configuration, and generate B lymphocytes in vivo. *Cell* 41(3):727–734, 1985.

Pane F, Intrieri M, Quintarelli C, Izzo B, Muccioli GC, Salvatore F. BCR/ABL genes and leukemic phenotype: from molecular mechanisms to clinical correlations. *Oncogene* 21(56):8652–8667, 2002.

Park SD, Saunders AS, Reidy MA, Bender DE, Clifton S, Morris KT. A review of granulocyte colony-stimulating factor receptor signaling and regulation with implications for cancer. *Front Oncol* 12 2022.

Pellicano F, Scott MT, Helgason GV, Hopcroft LEM, Allan EK, Aspinall-O'Dea M, Copland M, Pierce A, Huntly BJP, Whetton AD, Holyoake TL. The antiproliferative activity of kinase inhibitors in chronic myeloid leukemia cells is mediated by FOXO transcription factors. *Stem Cells* 32(9):2324–2337, 2014.

Pendergast AM, Quilliam LA, Cripe LD, Bassing CH, Dai Z, Li N, Batzer A, Rabun KM, Der CJ, Schlessinger J. BCR-ABL-induced oncogenesis is mediated by direct interaction with the SH2 domain of the GRB-2 adaptor protein. *Cell* 75(1):175–185, 1993.

Pérez-Caro M, Cobaleda C, González-Herrero I, Vicente-Dueñas C, Bermejo-Rodríguez C, Sánchez-Beato M, Orfao A, Pintado B, Flores T, Sánchez-Martín M, Jiménez R, Piris MA, Sánchez-García I. Cancer induction by restriction of oncogene expression to the stem cell compartment. *EMBO J* 28(1):8–20, 2009.

Perrotti D, Silvestri G, Stramucci L, Yu J, Trotta R. Cellular and Molecular Networks in Chronic Myeloid Leukemia: The Leukemic Stem, Progenitor and Stromal Cell Interplay. *Curr Drug Targets* 18(4):377–388, 2017.

Peyssonnaux C, Eychène A. The Raf/MEK/ERK pathway: new concepts of activation. *Biology of the Cell* 93(1–2):53–62, 2001.

Podolska MJ, Grützmann R, Pilarsky C, Bénard A. IL-3: key orchestrator of inflammation. *Front Immunol* 15 2024.

Priego N, Arechederra M, Sequera C, Bragado P, Vázquez-Carballo A, Gutiérrez-Uzquiza Á, Martín-Granado V, Ventura JJ, Kazanietz MG, Guerrero C, Porras A. C3G knock-down enhances migration and invasion by increasing Rap1-mediated p38α activation, while it impairs tumor growth through p38α-independent mechanisms. *Oncotarget* 7(29):45060–45078, 2016.

Puttini M, Coluccia AML, Boschelli F, Cleris L, Marchesi E, Donella-Deana A, Ahmed S, Redaelli S, Piazza R, Magistroni V, Andreoni F, Scapozza L, Formelli F, Gambacorti-Passerini C. In vitro and in vivo activity of SKI-606, a novel Src-Abl inhibitor, against imatinib-resistant Bcr-Abl+ neoplastic cells. *Cancer Res* 66(23):11314–11322, 2006.

Quintás-Cardama A, Cortes J. Molecular biology of bcr-abl1–positive chronic myeloid leukemia. *Blood* 113(8):1619–1630, 2009.

Radha V, Mitra A, Dayma K, Sasikumar K. Signalling to actin: role of C3G, a multitasking guanine-nucleotide-exchange factor. *Bioscience Reports* 31(4):231–244, 2011.

Radha V, Rajanna A, Mitra A, Rangaraj N, Swarup G. C3G is required for c-Abl-induced filopodia and its overexpression promotes filopodia formation. *Exp Cell Res* 313(11):2476–2492, 2007.

Radhika V, Naik N r., Advani S h., Bhisey A n. Actin polymerization in response to different chemoattractants is reduced in granulocytes from chronic myeloid leukemia patients. *Cytometry* 42(6):379–386, 2000.

Radich J. When to Consider Allogeneic Transplantation in CML. *Clin Lymphoma Myeloma Leuk* 16:S93–S95, 2016.

Radivoyevitch T, Jankovic GM, Tiu RV, Saunthararajah Y, Jackson RC, Hlatky LR, Gale RP, Sachs RK. Sex differences in the incidence of chronic myeloid leukemia. *Radiat Environ Biophys* 53(1):55–63, 2014.

Ranjbar B, Krogh LB, Laursen MB, Primo MN, Marques SC, Dybkær K, Mikkelsen JG. Anti-Apoptotic Effects of Lentiviral Vector Transduction Promote Increased Rituximab Tolerance in Cancerous B-Cells. *PLoS One* 11(4):e0153069, 2016.

Rao TP, Kühl M. An Updated Overview on Wnt Signaling Pathways. *Circ Res* 106(12):1798–1806, 2010.

Réa D, Mauro MJ, Boquimpani C, Minami Y, Lomaia E, Voloshin S, Turkina A, Kim D-W, Apperley JF, Abdo A, Fogliatto LM, Kim DDH, le Coutre P, Saussele S, Annunziata M, Hughes TP, Chaudhri N, Sasaki K, Chee L, García-Gutiérrez V, et al. A phase 3, open-label, randomized study of asciminib, a STAMP inhibitor, vs bosutinib in CML after 2 or more prior TKIs. *Blood* 138(21):2031–2041, 2021.

Reckel Sina, Gehin C, Tardivon D, Georgeon S, Kükenshöner T, Löhr F, Koide A, Buchner L, Panjkovich A, Reynaud A, Pinho S, Gerig B, Svergun D, Pojer F, Güntert P, Dötsch V, Koide S, Gavin A-C, Hantschel O. Structural and functional dissection of the DH and PH domains of oncogenic Bcr-Abl tyrosine kinase. *Nat Commun* 8:2101, 2017.

Reckel S, Hamelin R, Georgeon S, Armand F, Jolliet Q, Chiappe D, Moniatte M, Hantschel O. Differential signaling networks of Bcr–Abl p210 and p190 kinases in leukemia cells defined by functional proteomics. *Leukemia* 31(7):1502–1512, 2017.

Ren R. Mechanisms of BCR–ABL in the pathogenesis of chronic myelogenous leukaemia. *Nat Rev Cancer* 5(3):172–183, 2005.

Reuther GW, Fu H, Cripe LD, Collier RJ, Pendergast AM. Association of the protein kinases c-Bcr and Bcr-Abl with proteins of the 14-3-3 family. *Science* 266(5182):129–133, 1994.

Riether C, Schürch CM, Ochsenbein AF. Regulation of hematopoietic and leukemic stem cells by the immune system. *Cell Death Differ* 22(2):187–198, 2015.

Rinke J, Hochhaus A, Ernst T. CML - Not only BCR-ABL1 matters. *Best Pract Res Clin Haematol* 33(3):101194, 2020.

Rodríguez-Blázquez A, Carabias A, Morán-Vaquero A, De Cima S, Luque-Ortega JR, Alfonso C, Schuck P, Manso JA, Macedo-Ribeiro S, Guerrero C, De Pereda JM. Crk proteins activate the Rap1 guanine nucleotide exchange factor C3G by segregated adaptor-dependent and -independent mechanisms. *Cell Commun Signal* 21(1):30, 2023.

Roe J-S, Vakoc CR. C/EBPα: critical at the origin of leukemic transformation. *J Exp Med* 211(1):1–4, 2014.

Rolph D, Das H. Transcriptional Regulation of Osteoclastogenesis: The Emerging Role of KLF2. *Front Immunol* 11 2020.

Romo-González M, Ijurko C, Hernández-Hernández Á. Reactive Oxygen Species and Metabolism in Leukemia: A Dangerous Liaison. *Front Immunol* 13:889875, 2022.

Rossi L, Challen GA, Sirin O, Lin KK-Y, Goodell MA. Hematopoietic Stem Cell Characterization and Isolation. *Methods Mol Biol* 750:47–59, 2011.

Rowley JD. Letter: A new consistent chromosomal abnormality in chronic myelogenous leukaemia identified by quinacrine fluorescence and Giemsa staining. *Nature* 243(5405):290–293, 1973.

Rushing D, Goldman A, Gibbs G, Howe R, Kennedy BJ. Hydroxyurea versus busulfan in the treatment of chronic myelogenous leukemia. *Am J Clin Oncol* 5(3):307, 1982.

Salgia R, Pisick E, Sattler M, Li J-L, Uemura N, Wong W-K, Burky SA, Hirai H, Chen LB, Griffin JD. p130CAS Forms a Signaling Complex with the Adapter Protein CRKL in Hematopoietic Cells Transformed by the *BCR/ABL* Oncogene. *J Biol Chem* 271(41):25198–25203, 1996.

Sánchez-García I, Grütz G. Tumorigenic activity of the BCR-ABL oncogenes is mediated by BCL2. *Proc Natl Acad Sci U S A* 92(12):5287–5291, 1995.

Sánchez-Sánchez B, Gutiérrez-Herrero S, López-Ruano G, Prieto-Bermejo R, Romo-González M, Llanillo M, Pandiella A, Guerrero C, Miguel JFS, Sánchez-Guijo F, Del Cañizo C, Hernández-Hernández A. NADPH oxidases as therapeutic targets in chronic myelogenous leukemia. *Clin Cancer Res* 20(15):4014–4025, 2014.

Sasaki K, Haddad FG, Short NJ, Jain N, Issa G, Jabbour E, Kantarjian H. Outcome of Philadelphia chromosome-positive chronic myeloid leukemia in the United States since the introduction of imatinib therapy-The Surveillance, Epidemiology, and End Results database, 2000-2019. *Cancer* 129(23):3805–3814, 2023.

Sasi Kumar K, Ramadhas A, Nayak SC, Kaniyappan S, Dayma K, Radha V. C3G (RapGEF1), a regulator of actin dynamics promotes survival and myogenic differentiation of mouse mesenchymal cells. *Biochim Biophys Acta* 1853(10 Pt A):2629–2639, 2015.

Sattler M, Mohi MG, Pride YB, Quinnan LR, Malouf NA, Podar K, Gesbert F, Iwasaki H, Li S, Van Etten RA, Gu H, Griffin JD, Neel BG. Critical role for Gab2 in transformation by BCR/ABL. *Cancer Cell* 1(5):479–492, 2002.

Sattler M, Salgia R. Role of the adapter protein CRKL in signal transduction of normal hematopoietic and BCR/ABL-transformed cells. *Leukemia* 12(5):637–644, 1998.

Saußele S, Silver RT. Management of chronic myeloid leukemia in blast crisis. *Ann Hematol* 94(2):159–165, 2015.

Sawyers CL, Callahan W, Witte ON. Dominant negative MYC blocks transformation by ABL oncogenes. *Cell* 70(6):901–910, 1992.

Schafranek L, Nievergall E, Powell JA, Hiwase DK, Leclercq T, Hughes TP, White DL. Sustained inhibition of STAT5, but not JAK2, is essential for TKI-induced cell death in chronic myeloid leukemia. *Leukemia* 29(1):76–85, 2015.

Schemionek M, Elling C, Steidl U, Bäumer N, Hamilton A, Spieker T, Göthert JR, Stehling M, Wagers A, Huettner CS, Tenen DG, Tickenbrock L, Berdel WE, Serve H, Holyoake TL, Müller-Tidow C, Koschmieder S. BCR-ABL enhances differentiation of long-term repopulating hematopoietic stem cells. *Blood* 115(16):3185–3195, 2010.

Schmidt M, Rinke J, Schäfer V, Schnittger S, Kohlmann A, Obstfelder E, Kunert C, Ziermann J, Winkelmann N, Eigendorff E, Haferlach T, Haferlach C, Hochhaus A, Ernst T. Molecular-defined clonal evolution in patients with chronic myeloid leukemia independent of the BCR-ABL status. *Leukemia* 28(12):2292–2299, 2014.

Schubert C, Chatain N, Braunschweig T, Schemionek M, Feldberg K, Hoffmann M, Dufva O, Mustjoki S, Brümmendorf TH, Koschmieder S. The SCLtTAxBCR-ABL transgenic mouse model closely reflects the

differential effects of dasatinib on normal and malignant hematopoiesis in chronic phase-CML patients. *Oncotarget* 8(21):34736–34749, 2017.

Schwenk F, Kühn R, Rajewsky K, Angrand P-O, Stewart AF. Temporally and spatially regulated somatic mutagenesis in mice. *Nucleic Acids Res* 26(6):1427–1432, 1998.

Seo S, Nakamoto T, Takeshita M, Lu J, Sato T, Suzuki T, Kamikubo Y, Ichikawa M, Noda M, Ogawa S, Honda H, Oda H, Kurokawa M. Crk-associated substrate lymphocyte type regulates myeloid cell motility and suppresses the progression of leukemia induced by p210Bcr/Abl. *Cancer Sci* 102(12):2109–2117, 2011.

Sequera C, Bragado P, Manzano S, Arechederra M, Richelme S, Gutiérrez-Uzquiza A, Sánchez A, Maina F, Guerrero C, Porras A. C3G Is Upregulated in Hepatocarcinoma, Contributing to Tumor Growth and Progression and to HGF/MET Pathway Activation. *Cancers (Basel)* 12(8):2282, 2020.

Shagisultanova E, Gaponova AV, Gabbasov R, Nicolas E, Golemis EA. Preclinical and clinical studies of the NEDD9 scaffold protein in cancer and other diseases. *Gene* 567(1):1–11, 2015.

Shah B, Lutter D, Bochenek ML, Kato K, Tsytsyura Y, Glyvuk N, Sakakibara A, Klingauf J, Adams RH, Püschel AW. C3G/Rapgef1 Is Required in Multipolar Neurons for the Transition to a Bipolar Morphology during Cortical Development. *PLoS ONE* 11(4):e0154174, 2016.

Shah M, Bhatia R. Preservation of Quiescent Chronic Myelogenous Leukemia Stem Cells by the Bone Marrow Microenvironment. *Adv Exp Med Biol* 1100:97–110, 2018.

Shah NP, Tran C, Lee FY, Chen P, Norris D, Sawyers CL. Overriding imatinib resistance with a novel ABL kinase inhibitor. *Science* 305(5682):399–401, 2004.

Shimada Y, Migliaccio G, Ralph H, Migliaccio AR. Erythropoietin-specific cell cycle progression in erythroid subclones of the interleukin-3-dependent cell line 32D. *Blood* 81(4):935–941, 1993.

Shivakrupa R, Radha V, Sudhakar C, Swarup G. Physical and functional interaction between Hck tyrosine kinase and guanine nucleotide exchange factor C3G results in apoptosis, which is independent of C3G catalytic domain. *J Biol Chem* 278(52):52188–52194, 2003.

Shtivelman E, Lifshitz B, Gale RP, Canaani E. Fused transcript of abl and bcr genes in chronic myelogenous leukaemia. *Nature* 315(6020):550–554, 1985.

Sinclair A, Latif AL, Holyoake TL. Targeting survival pathways in chronic myeloid leukaemia stem cells. *Br J Pharmacol* 169(8):1693–1707, 2013.

Singh B, Kosuru R, Lakshmikanthan S, Sorci-Thomas MG, Zhang DX, Sparapani R, Vasquez-Vivar J, Chrzanowska M. Endothelial Rap1 (Ras-Association Proximate 1) Restricts Inflammatory Signaling to Protect From the Progression of Atherosclerosis. *Arterioscler Thromb Vasc Biol* 41(2):638–650, 2021.

Smit L, van der Horst G, Borst J. Sos, Vav, and C3G participate in B cell receptor-induced signaling pathways and differentially associate with Shc-Grb2, Crk, and Crk-L adaptors. *J Biol Chem* 271(15):8564–8569, 1996.

Song R, Bafit M, Tullett KM, Tan PS, Lahoud MH, O'Keeffe M, Purcell AW, Braun A. A Simple and Rapid Protocol for the Isolation of Murine Bone Marrow Suitable for the Differentiation of Dendritic Cells. *Methods Protoc* 7(2):20, 2024.

Souza LR, Silva E, Calloway E, Cabrera C, McLemore ML. G-CSF activation of AKT is not sufficient to prolong neutrophil survival. *J Leukoc Biol* 93(6):883–893, 2013.

Soyfer EM, Fleischman AG. Myeloproliferative neoplasms – blurring the lines between cancer and chronic inflammatory disorder. *Front Oncol* 13:1208089, 2023.

Spangrude GJ, Heimfeld S, Weissman IL. Purification and characterization of mouse hematopoietic stem cells. *Science* 241(4861):58–62, 1988.

Steensma DP, Bejar R, Jaiswal S, Lindsley RC, Sekeres MA, Hasserjian RP, Ebert BL. Clonal hematopoiesis of indeterminate potential and its distinction from myelodysplastic syndromes. *Blood* 126(1):9–16, 2015.

Stork PJS, Dillon TJ. Multiple roles of Rap1 in hematopoietic cells: complementary versus antagonistic functions. *Blood* 106(9):2952–2961, 2005.

Sweet K, Hazlehurst L, Sahakian E, Powers J, Nodzon L, Kayali F, Hyland K, Nelson A, Pinilla-Ibarz J. A phase I clinical trial of ruxolitinib in combination with nilotinib in chronic myeloid leukemia patients with molecular evidence of disease. *Leuk Res* 74:89–96, 2018.

Swerdlow SH, Campo E, Pileri SA, Harris NL, Stein H, Siebert R, Advani R, Ghielmini M, Salles GA, Zelenetz AD, Jaffe ES. The 2016 revision of the World Health Organization classification of lymphoid neoplasms. *Blood* 127(20):2375–2390, 2016.

Tabe Y, Konopleva M. Advances in understanding the leukaemia microenvironment. *Br J Haematol* 164(6):767–778, 2014.

Takai S, Tanaka M, Sugimura H, Yamada K, Naito Y, Kino I, Matsuda M. Mapping of the human C3G gene coding a guanine nucleotide releasing protein for Ras family to 9q34.3 by fluorescence in situ hybridization. *Hum Genet* 94(5):549–550, 1994.

Talpaz M, Kantarjian HM, McCredie K, Trujillo JM, Keating MJ, Gutterman JU. Hematologic remission and cytogenetic improvement induced by recombinant human interferon alpha A in chronic myelogenous leukemia. *N Engl J Med* 314(17):1065–1069, 1986.

Tanaka S, Morishita T, Hashimoto Y, Hattori S, Nakamura S, Shibuya M, Matuoka K, Takenawa T, Kurata T, Nagashima K. C3G, a guanine nucleotide-releasing protein expressed ubiquitously, binds to the Src homology 3 domains of CRK and GRB2/ASH proteins. *Proc Natl Acad Sci U S A* 91(8):3443–3447, 1994.

Tanaka Y, Fukushima T, Mikami K, Adachi K, Fukuyama T, Goyama S, Kitamura T. Efficacy of tyrosine kinase inhibitors on a mouse chronic myeloid leukemia model and chronic myeloid leukemia stem cells. *Exp Hematol* 90:46-51.e2, 2020.

Thapa P, Farber DL. The Role of the Thymus in the Immune Response. *Thorac Surg Clin* 29(2):123–131, 2019.

Till JE, McCulloch EA. A direct measurement of the radiation sensitivity of normal mouse bone marrow cells. *Radiat Res* 178(2):AV3-7, 1961.

Titz B, Low T, Komisopoulou E, Chen SS, Rubbi L, Graeber TG. The proximal signaling network of the BCR-ABL1 oncogene shows a modular organization. *Oncogene* 29(44):5895–5910, 2010.

Turke AB, Song Y, Costa C, Cook R, Arteaga CL, Asara JM, Engelman JA. MEK inhibition leads to PI3K/AKT activation by relieving a negative feedback on ERBB receptors. *Cancer Res* 72(13):3228–3237, 2012.

Tybulewicz VL, Crawford CE, Jackson PK, Bronson RT, Mulligan RC. Neonatal lethality and lymphopenia in mice with a homozygous disruption of the c-abl proto-oncogene. *Cell* 65(7):1153–1163, 1991.

Ueda Y, Kondo M, Kelsoe G. Inflammation and the reciprocal production of granulocytes and lymphocytes in bone marrow. *J Exp Med* 201(11):1771–1780, 2005.

Uemura N, Griffin JD. The adapter protein Crkl links Cbl to C3G after integrin ligation and enhances cell migration. *J Biol Chem* 274(53):37525–37532, 1999.

Ushach I, Zlotnik A. Biological role of granulocyte macrophage colony-stimulating factor (GM-CSF) and macrophage colony-stimulating factor (M-CSF) on cells of the myeloid lineage. *J Leukoc Biol* 100(3):481–489, 2016.

Valent P. Targeting the JAK2-STAT5 pathway in CML. *Blood* 124(9):1386–1388, 2014.

Van Etten RA. Cycling, stressed-out and nervous: cellular functions of c-Abl. *Trends Cell Biol* 9(5):179–186, 1999.

Velten L, Haas SF, Raffel S, Blaszkiewicz S, Islam S, Hennig BP, Hirche C, Lutz C, Buss EC, Nowak D, Boch T, Hofmann W-K, Ho AD, Huber W, Trumpp A, Essers MAG, Steinmetz LM. Human haematopoietic stem cell lineage commitment is a continuous process. *Nat Cell Biol* 19(4):271–281, 2017.

Verfaillie CM, McCarthy JB, McGlave PB. Mechanisms underlying abnormal trafficking of malignant progenitors in chronic myelogenous leukemia. Decreased adhesion to stroma and fibronectin but increased adhesion to the basement membrane components laminin and collagen type IV. *J Clin Invest* 90(4):1232–1241, 1992.

Verma A, Goel A, Koner N, Gunasekaran G, Radha V. Development and tissue specific expression of RAPGEF1 (C3G) transcripts having exons encoding disordered segments with predicted regulatory function. *Mol Biol Rep* 51(1):907, 2024.

Vermes I, Haanen C, Steffens-Nakken H, Reutelingsperger C. A novel assay for apoptosis: Flow cytometric detection of phosphatidylserine expression on early apoptotic cells using fluorescein labelled Annexine V. *J Immunol Methods* 184(1):39–51, 1995.

Vetrie D, Helgason GV, Copland M. The leukaemia stem cell: similarities, differences and clinical prospects in CML and AML. *Nat Rev Cancer* 20(3):158–173, 2020.

Vishnu VV, Muralikrishna Bh, Verma A, Nayak SC, Sowpati DT, Radha V, Shekar PC. C3G Regulates STAT3, ERK, Adhesion Signaling, and Is Essential for Differentiation of Embryonic Stem Cells. *Stem Cell Rev Rep* 17(4):1465–1477, 2021.

Voncken JW, van Schaick H, Kaartinen V, Deemer K, Coates T, Landing B, Pattengale P, Dorseuil O, Bokoch GM, Groffen J. Increased neutrophil respiratory burst in bcr-null mutants. *Cell* 80(5):719–728, 1995.

Voss AK, Krebs DL, Thomas T. C3G regulates the size of the cerebral cortex neural precursor population. *EMBO J* 25(15):3652–3663, 2006.

Vossler MR, Yao H, York RD, Pan M-G, Rim CS, Stork PJS. cAMP Activates MAP Kinase and Elk-1 through a B-Raf- and Rap1-Dependent Pathway. *Cell* 89(1):73–82, 1997.

Vuelta E, Ordoñez JL, Alonso-Pérez V, Méndez L, Hernández-Carabias P, Saldaña R, Sevilla J, Sebastián E, Muntión S, Sánchez-Guijo F, Hernández-Rivas JM, García-Tuñón I, Sánchez-Martín M. CRISPR-Cas9 Technology as a Tool to Target Gene Drivers in Cancer: Proof of Concept and New Opportunities to Treat Chronic Myeloid Leukemia. *CRISPR J* 4(4):519–535, 2021.

Wada Y, Kubota H, Maeda M, Taniwaki M, Hattori M, Imamura S, Iwai K, Minato N. Mitogen-Inducible*SIPA1*Is Mapped to the Conserved Syntenic Groups of Chromosome 19 in Mouse and Chromosome 11q13.3 Centromeric to*BCL1*in Human. *Genomics* 39(1):66–73, 1997.

Walter MJ. Antecedent CHIP in CML? *Blood* 129(1):3–4, 2017.

Wang S-F, Aoki M, Nakashima Y, Shinozuka Y, Tanaka H, Taniwaki M, Hattori M, Minato N. Development of Notch-dependent T-cell leukemia by deregulated Rap1 signaling. *Blood* 111(5):2878–2886, 2008.

Wang Z, Dillon TJ, Pokala V, Mishra S, Labudda K, Hunter B, Stork PJS. Rap1-Mediated Activation of Extracellular Signal-Regulated Kinases by Cyclic AMP Is Dependent on the Mode of Rap1 Activation. *Mol Cell Biol* 26(6):2130–2145, 2006.

Warmuth M, Bergmann M, Prieß A, Häuslmann K, Emmerich B, Hallek M. The Src Family Kinase Hck Interacts with Bcr-Abl by a Kinase-independent Mechanism and Phosphorylates the Grb2-binding Site of Bcr. *J Biol Chem* 272(52):33260–33270, 1997.

Warsch W, Kollmann K, Eckelhart E, Fajmann S, Cerny-Reiterer S, Hölbl A, Gleixner KV, Dworzak M, Mayerhofer M, Hoermann G, Herrmann H, Sillaber C, Egger G, Valent P, Moriggl R, Sexl V. High STAT5 levels mediate imatinib resistance and indicate disease progression in chronic myeloid leukemia. *Blood* 117(12):3409–3420, 2011.

Weerkamp F, Dekking E, Ng YY, van der Velden VHJ, Wai H, Böttcher S, Brüggemann M, van der Sluijs AJ, Koning A, Boeckx N, Van Poecke N, Lucio P, Mendonça A, Sedek L, Szczepański T, Kalina T, Kovac M, Hoogeveen PG, Flores-Montero J, Orfao A, et al. Flow cytometric immunobead assay for the detection of BCR–ABL fusion proteins in leukemia patients. *Leukemia* 23(6):1106–1117, 2009.

Weisberg E, Manley PW, Breitenstein W, Brüggen J, Cowan-Jacob SW, Ray A, Huntly B, Fabbro D, Fendrich G, Hall-Meyers E, Kung AL, Mestan J, Daley GQ, Callahan L, Catley L, Cavazza C, Mohammed A, Neuberg D, Wright RD, Gilliland DG, et al. Characterization of AMN107, a selective inhibitor of native and mutant Bcr-Abl. *Cancer Cell* 7(2):129–141, 2005.

Westerberg LJS, Dedic B, Näslund E, Thorell A, Spalding KL. Superior normalization using total protein for western blot analysis of human adipocytes. *PLoS One* 20(7):e0328136, 2025.

White HE, Salmon M, Albano F, Andersen CSA, Balabanov S, Balatzenko G, Barbany G, Cayuela J-M, Cerveira N, Cochaux P, Colomer D, Coriu D, Diamond J, Dietz C, Dulucq S, Engvall M, Franke GN, Gineikiene-Valentine E, Gniot M, Gómez-Casares MT, et al. Standardization of molecular monitoring of CML: results and recommendations from the European treatment and outcome study. *Leukemia* 36(7):1834–1842, 2022.

Wiese W, Barczuk J, Racinska O, Siwecka N, Rozpedek-Kaminska W, Slupianek A, Sierpinski R, Majsterek I. PI3K/Akt/mTOR Signaling Pathway in Blood Malignancies—New Therapeutic Possibilities. *Cancers (Basel)* 15(21):5297, 2023.

Wolff JH, Mikkelsen JG. Delivering genes with human immunodeficiency virus-derived vehicles: still state-of-the-art after 25 years. *J Biomed Sci* 29(1):79, 2022.

Woodring PJ, Hunter T, Wang JYJ. Regulation of F-actin-dependent processes by the Abl family of tyrosine kinases. *J Cell Sci* 116(13):2613–2626, 2003.

Wylie AA, Schoepfer J, Jahnke W, Cowan-Jacob SW, Loo A, Furet P, Marzinzik AL, Pelle X, Donovan J, Zhu W, Buonamici S, Hassan AQ, Lombardo F, Iyer V, Palmer M, Berellini G, Dodd S, Thohan S, Bitter H, Branford S, et al. The allosteric inhibitor ABL001 enables dual targeting of BCR–ABL1. *Nature* 543(7647):733–737, 2017.

Xiao P, Dolinska M, Sandhow L, Kondo M, Johansson A-S, Bouderlique T, Zhao Y, Li X, Dimitriou M, Rassidakis GZ, Hellström-Lindberg E, Minato N, Walfridsson J, Scadden DT, Sigvardsson M, Qian H. Sipa1 deficiency–induced bone marrow niche alterations lead to the initiation of myeloproliferative neoplasm. *Blood Adv* 2(5):534–548, 2018.

Xie S, Wang Y, Liu J, Sun T, Wilson MB, Smithgall TE, Arlinghaus RB. Involvement of Jak2 tyrosine phosphorylation in Bcr-Abl transformation. *Oncogene* 20(43):6188–6195, 2001.

Xu Y, Ikeda S, Sumida K, Yamamoto R, Tanaka H, Minato N. Sipa1 deficiency unleashes a host-immune mechanism eradicating chronic myelogenous leukemia-initiating cells. *Nat Commun* 9:914, 2018.

Yamamoto R, Morita Y, Ooehara J, Hamanaka S, Onodera M, Rudolph KL, Ema H, Nakauchi H. Clonal analysis unveils self-renewing lineage-restricted progenitors generated directly from hematopoietic stem cells. *Cell* 154(5):1112–1126, 2013.

Yamashita M, Dellorusso PV, Olson OC, Passegué E. Dysregulated haematopoietic stem cell behaviour in myeloid leukaemogenesis. *Nat Rev Cancer* 20(7):365–382, 2020.

Yang H, Zhou H, Huang Z, Tao K, Huang N, Peng Z, Feng W. Induction of CML-specific immune response through cross-presentation triggered by CTP-mediated BCR-ABL-derived peptides. *Cancer Lett* 482:44–55, 2020.

Ye D, Wolff N, Li L, Zhang S, Ilaria RL. STAT5 signaling is required for the efficient induction and maintenance of CML in mice. *Blood* 107(12):4917–4925, 2006.

Zembruski NCL, Stache V, Haefeli WE, Weiss J. 7-Aminoactinomycin D for apoptosis staining in flow cytometry. *Anal Biochem* 429(1):79–81, 2012.

Zhai B, Huo H, Liao K. C3G, a Guanine Nucleotide Exchange Factor Bound to Adapter Molecule c-Crk, Has Two Alternative Splicing Forms. *Biochem Biophys Res Commun* 286(1):61–66, 2001.

Zhang C, Chen S, Bao J, Zhang Y, Huang B, Jia X, Chen M, Wan J-B, Su H, Wang Y, He C. Low Doses of Camptothecin Induced Hormetic and Neuroprotective Effects in PC12 Cells. *Dose Response* 13(2):1559325815592606, 2015.

Zhang H, Nguyen-Jackson H, Panopoulos AD, Li HS, Murray PJ, Watowich SS. STAT3 controls myeloid progenitor growth during emergency granulopoiesis. *Blood* 116(14):2462–2471, 2010.

Zhang M, Meng Y, Ying Y, Zhou P, Zhang S, Fang Y, Yao Y, Li D. Selective activation of STAT3 and STAT5 dictates the fate of myeloid progenitor cells. *Cell Death Discov* 9(1):274, 2023.

Zjablovskaja P, Danek P, Kardosova M, Alberich-Jorda M. Proliferation and Differentiation of Murine Myeloid Precursor 32D/G-CSF-R Cells. *J Vis Exp*(132):57033, 2018.

Annexes

ANNEXES

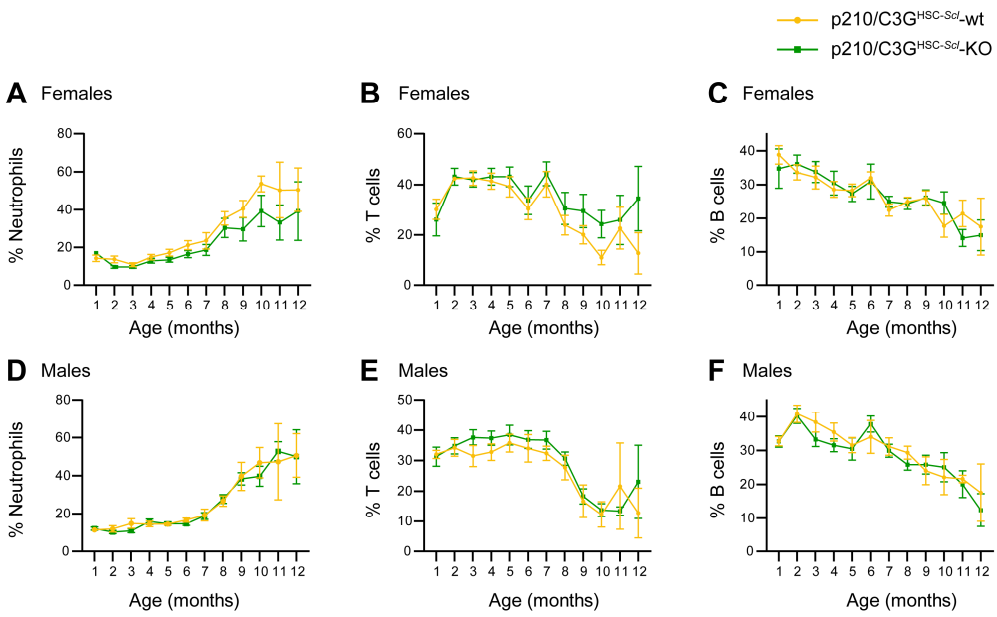

Figure 50. Sex-dependent differences in hematological populations are more evident in p210/C3G$^{HSC\text{-}Scl}$-KO female mice. XY plots show the mean value ± SEM of the percentage of total PB leukocytes corresponding to (**A, D**) neutrophils ($Gr1^+Mac1^+$), (**B, E**) T cells ($CD3^+$), and (**C, F**) B cells ($B220^+$) over a 1-year monitoring period in p210 (**A–C**) female and (**D–F**) male mice. The PB sample collected at month 1 was obtained prior to tamoxifen administration. Statistical analysis was performed using two-way ANOVA followed by a multiple-comparison test.

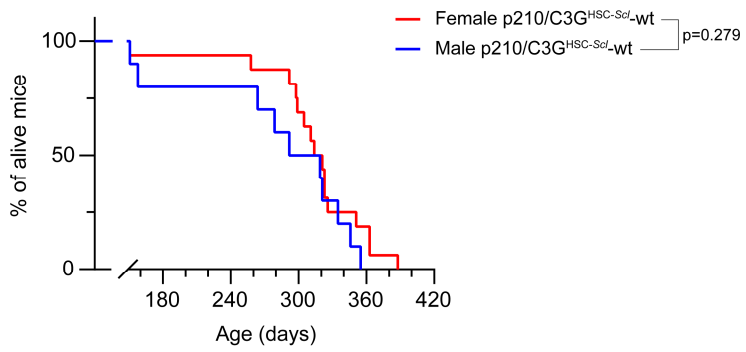

Figure 51. Female and male p210/C3G$^{HSC\text{-}Scl}$-wt mice display similar overall survival in chronic myeloid leukemia (CML). Kaplan-Meyer plot represents the overall survival all p210/C3G$^{HSC\text{-}Scl}$-wt mice over the 14-month duration of the experiment. Statistical analysis was performed using the log-rank test.

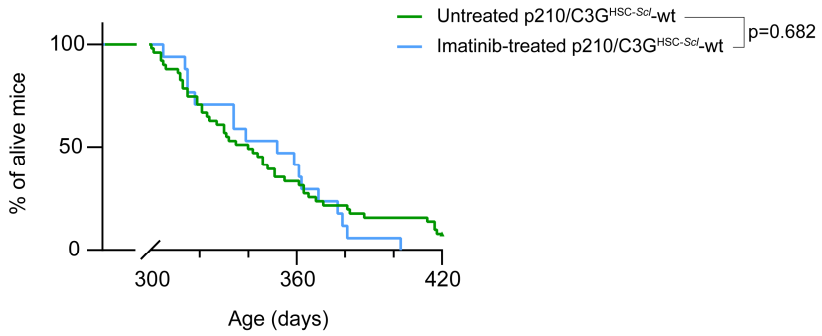

Figure 52. Imatinib-treated p210/C3G$^{HSC\text{-}Scl}$-wt mice display similar overall survival to that of untreated mice. Kaplan-Meyer plot represents the overall survival of monitored p210/C3G$^{HSC\text{-}Scl}$-wt mice compared to imatinib-treated p210/C3G$^{HSC\text{-}Scl}$-wt mice. Only mice older than 300 days old are included in the plot. Statistical analysis was performed using the log-rank test.

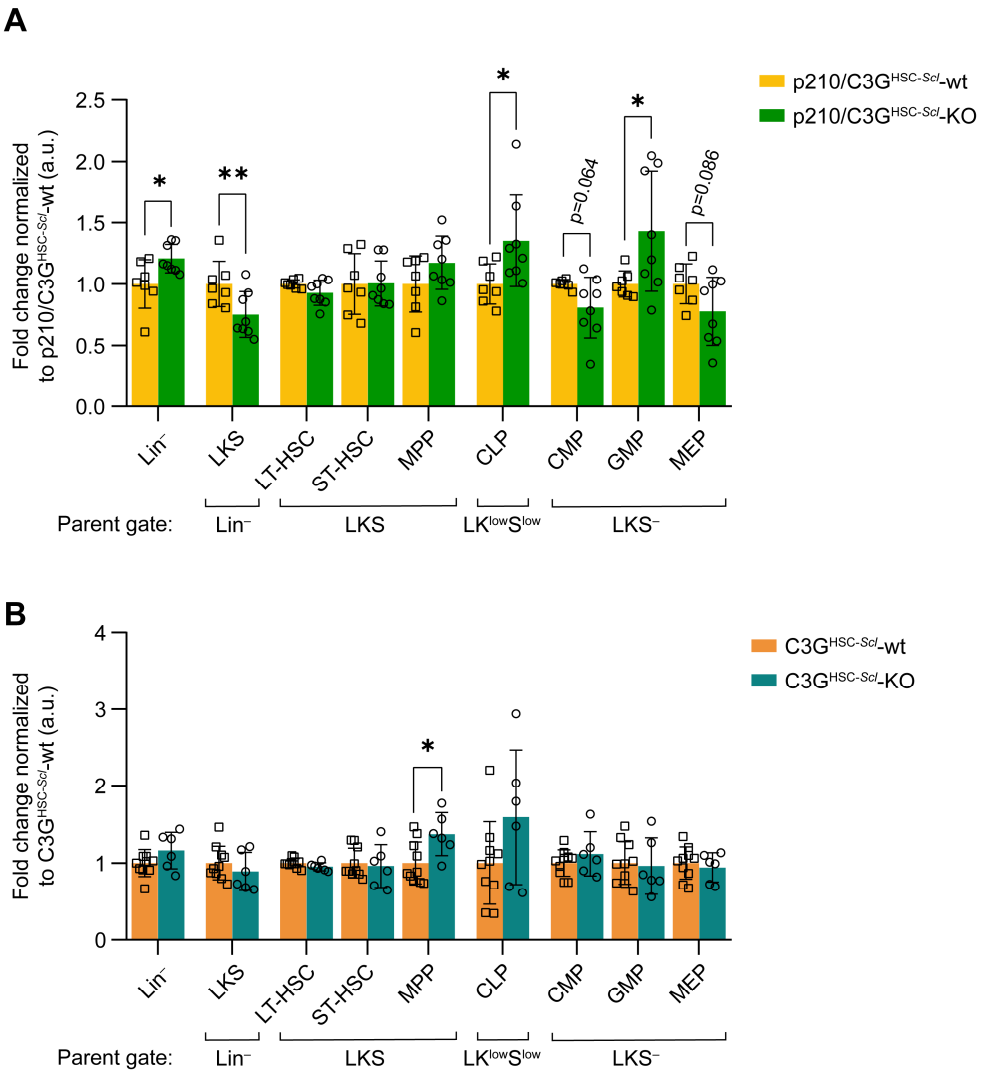

Figure 53. Normalized values of hematopoietic stem and progenitor cell (HSPC) proportions in the bone marrow (BM) of p210 and non-p210 mice. (**A**) Bar plots show the mean ± SD of the percentage of each p210/C3G$^{HSC\text{-}Scl}$-KO HSPC subpopulation within the parental gate, normalized to p210/C3G$^{HSC\text{-}Scl}$-wt values. (**B**) Bar plots show the mean ± SD of the percentage of each C3G$^{HSC\text{-}Scl}$-KO HSPC subpopulation within the parental gate, normalized to C3G$^{HSC\text{-}Scl}$-wt values. Parental gating markers are indicated below. Only 6-month-old mice were analyzed. Statistical analysis was performed using an unpaired t-test. *$p \leq 0.05$, **$p \leq 0.01$.

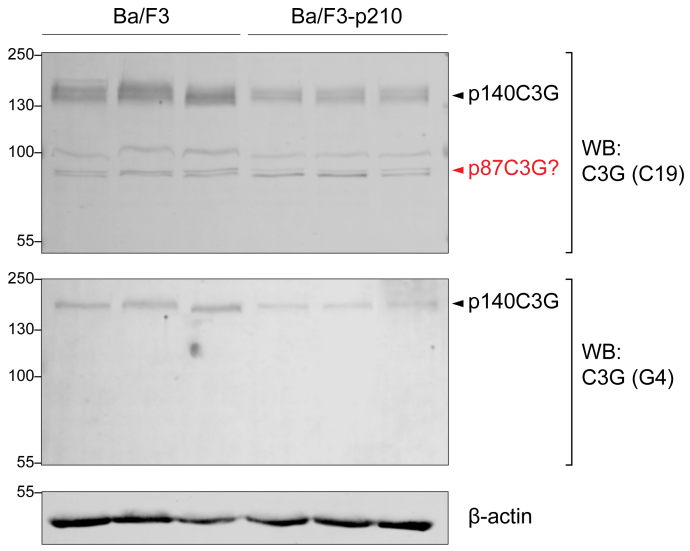

Figure 54. p87C3G is not clearly visible under our experimental conditions. Analysis of three independent lysates from Ba/F3 and Ba/F3-p210 cells. Immunoblotting of C3G was performed using the C19 antibody (C-terminal) and the G4 antibody (N-terminal). Since p87C3G lacks part of the N-terminal domain, it is expected to be detected by C19 but not by G4. A faint band pattern is observed at ~80-90 kDa in the C19-incubated membrane; however, given previous reports indicating that the p87 form is usually expressed at higher levels than p140C3G (Gutiérrez-Berzal *et al.*, 2006), we cannot definitively assign this band to p87C3G. As expected, p140C3G is detectable with both antibodies. β-actin was used as a loading control. Molecular weights of the protein marker ladder are indicated. WB: western blot.

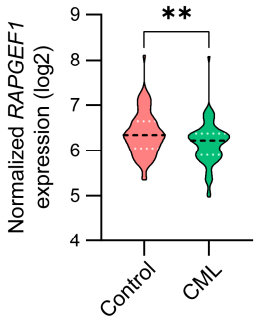

Figure 55. *RAPGEF1* (C3G) expression is reduced in chronic myeloid leukemia (CML) patients compared with healthy individuals. Violin plots show normalized $\log_2$ gene expression levels in BM cells isolated from CML patients and healthy controls. Data were obtained from the BloodSpot 3.0 database (Gíslason *et al.*, 2024), using samples from the GSE13159 dataset ("Microarray Innovations in LEukemia (MILE) study: Stage 1"). Statistical analysis was performed using an unpaired t-test. **$p \leq 0.01$.

ABBREVIATIONS

5-FU	5-Fluorouracil
ABL1	Abelson murine leukemia viral oncogene homolog 1
ACK	Ammonium-Chloride-Potassium
AIR	Autoinhibitory region
AKT	Stock A strain K thymoma
ALL	Acute lymphoid leukemia
Allo-HSCT	Allogeneic HSC transplantation
AML	Acute myeloid leukemia
AMP	Adenosine monophosphate
AMPK	AMP-activated protein kinase
ANOVA	ANalysis Of VAriance
AP	Accelerated phase
APC	Allophycocyanin
ATP	Adenosine triphosphate
BCL-2	B-cell lymphoma 2
BCR	Breakpoint cluster region
BM	Bone marrow
BMA	BM adipocytes
BMT	Bone marrow transplantation
BP	Blast crisis phase
bp	Base pair
BSA	Bovine serum albumin
BV	Brilliant Violet
C3G	Crk SH3-binding GNRP
CAR-T	Chimeric antigen receptor T-cell
Cas9	CRISPR-associated protein 9
CBA	Chromosome banding analysis
c-Cbl	Cellular homolog of casitas B-lineage lymphoma
CCyR	Complete cytogenetic response
cDC	Conventional dendritic cell
Cdc25	Cell division cycle 25
Cdc25HD	Cdc25-homology domain
CHIP	Clonal hematopoiesis of indeterminate potential
CHR	Complete hematological response
c-Kit	Cellular homolog of Kit (Kitten)
CLL	Chronic lymphoid leukemia
CM	Conditioned medium
CML	Chronic myeloid leukemia
CNL	Chronic neutrophilic leukemia
CP	Chronic phase
CRISPR	Clustered regularly interspaced short palindromic repeats
Crk	Chicken tumor virus number 10 (CT10) regulator of kinase

Cy	Cyanine
CyR	Cytogenetic response
DLBCL	Diffuse large B-cell lymphoma
DMR	Deep molecular response
DMSO	Dimethyl sulfoxide
DNA	Deoxyribonucleic acid
EBD	E-cadherin binding domain
EDTA	Ethylenediaminetetraacetic acid
ER	Estrogen receptor
ERK	Extracellular signal-regulated kinase
ET	Essential thrombocythemia
FA	Focal adhesion
FBS	Fetal bovine serum
FcγR	Fc gamma receptor
FDA	US Food and Drug Administration
FISH	Fluorescence in situ hibridation
FITC	Fluorescein isothiocyanate
Flox	Flanked by LoxP
fMLP	Formyl-Met-Leu-Phe
Gab2	Grb2-associated binding protein 2
GAP	GTPase-activating protein
G-CSF	Granulocyte colony-stimulating factor
G-CSF-R	G-CSF receptor
GEF	Guanine nucleotide exchange factor
GFP	Green fluorescent protein
GM-CSF	Granulocyte-macrophage colony-stimulating factor
GNRP	Guanine nucleotide-releasing protein
Grb2	Growth factor receptor-bound protein 2
Gr1	Granulocyte-differentiation antigen-1
GST	Glutathione-S-transferase
GTP	Guanosine triphosphate
HPC	Hematopoietic progenitor cell
HSC	Hematopoietic stem cell
HSPC	Hematopoietic stem and progenitor cell
i.p.	Intraperitoneal
IC_{50}	Half maximal inhibitory concentration
IFN	Interferon
IFU	Infectious units
IL	Interleukin
IL-7Rα	IL-7 receptor α
IS	International scale
JAK	Janus kinase
kb	Kilobase
kDa	Kilodalton
KO	Knockout

LSC	Leukemic stem cell
Mac-1	Macrophage antigen-1
MAPK	Mitogen-activated protein kinase
M-CSF	Macrophage colony-stimulating factor
MEK	MAPK/ERK kinase
mESC	Mouse embryonic stem cells
MK	Megakaryocyte
MMR	Major molecular response
MOI	Multiplicity of infection
MPN	Myeloproliferative neoplasm
MR	Molecular response
mRNA	Messenger RNA
mTOR	Mammalian target of rapamycin
NK	Natural killer
NTD	N-terminal domain
o/n	Overnight
p-	Phosphorylated
PB	Peripheral blood
PBS	Phosphate-buffered saline
PCR	Polymerase chain reaction
PCyR	Partial cytogenetic response
pDC	Plasmacytoid dendritic cell
PE	Phycoerythrin
PerCP	Peridinin-chlorophyll-protein
Ph	Philadelphia
PI	Propidium iodide
PI3K	Phosphoinositide 3-kinase
PKC	Protein kinase C
PLA	Platelet-leukocyte aggregate
PMF	Primary myelofibrosis
PMSF	Phenylmethylsulfonyl fluoride
PP2A	Protein phosphatase 2A
PROTAC	Proteolysis-targeting chimera
PV	Polycythemia vera
Raf	Rapidly accelerated fibrosarcoma
Rap	Ras-associated protein
Ras	Rat sarcoma
RBD	Ras binding domain
REM	Ras exchanger motif
RNA	Ribonucleic acid
ROS	Reactive oxygen species
RT	Room temperature
RT-qPCR	Reverse transcription-quantitative PCR
Sca1	Stem cell antigen 1
SD	Standard deviation

SDS	Sodium dodecyl sulfate
SEM	Standard error of the mean
SH	Src-homology
shRNA	Short hairpin RNA
siRNA	Small-interfering RNA
SLAM	Signaling lymphocyte activation molecule
SOCS	Suppressors of cytokine signaling
SOS	Son of sevenless
Src	Rous sarcoma virus
STAMP	Specifically targeting the ABL myristoyl pocket
STAT	Signal transducer and activator of transcription
TAM	Tamoxifen
TFR	Treatment-free remission
TKI	Tyrosine kinase inhibitor
US	United States
UV	Ultraviolet
WBC	White blood cell
Wnt	Wingless/Int-1
WT	Wild type

LIST OF FIGURES

INTRODUCTION

METHODS

RESULTS

DISCUSSION

ANNEXES

LIST OF TABLES

INTRODUCTION

METHODS